



HAL
open science

La souris humanisée : modèle d'étude de l'immunothérapie anti-cancer

Philippe De La Rochère

► **To cite this version:**

Philippe De La Rochère. La souris humanisée : modèle d'étude de l'immunothérapie anti-cancer. Immunologie. Université Sorbonne Paris Cité, 2018. Français. NNT : 2018USPCB068 . tel-02510742

HAL Id: tel-02510742

<https://theses.hal.science/tel-02510742>

Submitted on 18 Mar 2020

HAL is a multi-disciplinary open access archive for the deposit and dissemination of scientific research documents, whether they are published or not. The documents may come from teaching and research institutions in France or abroad, or from public or private research centers.

L'archive ouverte pluridisciplinaire **HAL**, est destinée au dépôt et à la diffusion de documents scientifiques de niveau recherche, publiés ou non, émanant des établissements d'enseignement et de recherche français ou étrangers, des laboratoires publics ou privés.



Thèse de doctorat de l'Université Sorbonne Paris Cité

Préparée à l'Université Paris Descartes

Ecole doctorale BioSPC-ED157

Unité INSERM 932/Equipe SIRIC TRANSIM

La souris humanisée : modèle d'étude de
l'immunothérapie anti-cancer

Par Philippe De La Rochère

Thèse de doctorat d'immunologie

Dirigée par Eliane Piaggio

Présentée et soutenue publiquement, à Paris, le 27/09/18

Jury :

Rapporteur: Dr. Carole GUILLONNEAU

Rapporteur: Dr. Gilles MARODON

Examineur: Dr. Corinne TANCHOT

Examineur: Dr. Nabila SEDDIKI

Examineur: Dr. Sergio ROMAN-ROMAN

Directeur de thèse: Dr. Eliane PIAGGIO

Sommaire

REMERCIEMENTS	4
ABREVIATIONS	7
RESUME	11
PREAMBULE	13
INTRODUCTION	14
1. DEVELOPPEMENT DES CANCERS	15
1.1. ONCOGENESE	15
1.2. ETAPES CLES DU DEVELOPPEMENT DU CANCER	16
1.2.1. CAPACITE DE REPLICATION ILLIMITEE : ROLE DE LA SENESCENCE DANS LE PROCESSUS TUMORAL	16
1.2.2. VASCULARISATION	17
1.2.3. INVASION TISSULAIRE ET METASTASE	19
1.2.4. MECANISMES D'ECHAPPEMENT	20
2. INTERACTION ENTRE CANCER ET SYSTEME IMMUNITAIRE : LA BASE DE L'IMMUNOTHERAPIE	22
2.1. IGNORANCE	22
2.2. TOLERANCE	23
2.3. IMMUNOEDITION	23
2.3.1. ELIMINATION	24
2.3.2. EQUILIBRE	24
2.4. THERAPIES MODULANT L'INTERACTION CANCER-SYSTEME IMMUNITAIRE	25
2.4.1. ANTIGENES TUMORAUX ET PRESENTATION ANTIGENIQUE	26
2.4.2. PRIMING ET ACTIVATION DES LYMPHOCYTES T	29
2.4.3. MIGRATION DES LYMPHOCYTES T ET INFILTRATION DES TUMEURS	33
2.4.4. RECONNAISSANCE ET DESTRUCTION DES CELLULES TUMORALES	35
3. ETAT DES LIEUX DES THERAPIES DU CANCER : PLACE DE L'IMMUNOTHERAPIE	37
3.1. CYTOKINES	39
3.2. VACCINS	41
3.3. THERAPIES CIBLEES	43
3.4. THERAPIES CELLULAIRES	45
3.5. VIRUS ONCOLYTIQUES	48
3.6. ANTICORPS REGULANT DES POINTS DE CONTROLE DU SYSTEME IMMUNITAIRE	49
4. MODELES MURINS D'ETUDES EN IMMUNO-ONCOLOGIE	55
4.1. MODELES SYNGENIQUES	55
4.2. MODELES DE SOURIS HUMANISEES	57
4.2.1. SOURIS IMMUNODEFICIENTES	57
4.2.2. HUMANISATION DES SOURIS	60
4.2.2.1. PBMC : MODELE HU-PBL-SCID	62
4.2.2.2. CELLULES SOUCHES CD34 ⁺ : MODELES HU-SRC-SCID ET BLT	64
4.2.3. TUMEUR D'ORIGINE HUMAINE : LIGNEE CELLULAIRE ET PDX	69
4.2.4. NOUVEAUX DEVELOPPEMENTS DANS LES MODELES DE SOURIS HUMANISEES	73

4.2.4.1.	PREPARATION DE LA NICHE POUR LA PRISE DE GREFFE DES CSH	74
4.2.4.2.	CYTOKINES ET COMPATIBILITE STROMALE	75
4.2.4.3.	MANIPULATION DU CMH	77
4.2.4.4.	HUMANISATION DES IMMUNE CHECKPOINTS DANS DES SOURIS IMMUNOCOMPETENTES	78
4.2.5.	EVALUATION PRECLINIQUE DANS LES MODELES HUMANISES	80
4.2.5.1.	THERAPIES CELLULAIRES	82
4.2.5.2.	INHIBITEURS DE CHECKPOINTS IMMUNITAIRES	83
4.2.5.3.	AUTRES IMMUNOTHERAPIES BASEES SUR DES ANTICORPS	84
4.2.5.4.	THERAPIE GENIQUE	85
4.2.5.5.	THERAPIES BASEES SUR LES CYTOKINES	86
RESULTATS		90
ARTICLE I		91
ARTICLE II		147
DISCUSSION		179
PERSPECTIVES		185
BIBLIOGRAPHIE		191
ANNEXES		212

Remerciements

La forme de mes remerciements va être à l'image de mon parcours scientifique long de 13 années : un inventaire à la Prévert qui je l'espère n'oubliera personne mais je m'excuse par avance auprès de celle ou celui que j'omettrais.

Je remercie en premier lieu les membres de mon jury le Dr. Carole Guillonnet et le Dr. Gilles Marodon qui ont accepté d'être les rapporteurs de mon travail de thèse et qui, par leurs commentaires pertinents, ont permis d'améliorer mon manuscrit. Je remercie, également, le Dr. Corinne Tanchot, le Dr. Nabila Seddiki et le Dr. Sergio Roman-Roman pour avoir pris de leur temps pour être examinateurs de mon travail.

Je remercie bien évidemment le Dr. Eliane Piaggio qui a su me convaincre de commencer l'aventure doctorale à 34 ans, avec deux enfants. Ton énergie, ta motivation, ton amour de la science et ton implication auprès de tes étudiants m'ont accompagné au cours de ces 4 années et m'ont permis, je l'espère, de progresser dans mon travail scientifique. J'espère que tu arriveras aux buts que tu t'es fixée et je te souhaite le meilleur pour toi et ta famille.

Merci à l'Institut Curie et Sebastian Amigorena de m'avoir accueilli au sein de leur laboratoire pendant quasiment 10 ans. Je mesure la chance d'avoir pu travailler au sein d'une structure disposant de tous les moyens humains, techniques et financiers pour faire de la « bonne » science.

Commence ici un inventaire qui va suivre la chronologie de ma carrière :

Merci à Nuala de m'avoir pris avec toi pour débiter ma carrière en M2. Ce fut bref mais les 6 mois passés sous ta direction m'ont permis de comprendre que je voulais faire ce métier et m'ont permis de rencontrer James qui, même si on ne se voit plus beaucoup, est un ami avec qui ce fut super agréable de travailler malgré son acointance avec le PSG....

Merci à Michèle de m'avoir proposé de travailler avec toi alors que je n'avais rien. Travailler avec toi fut un apprentissage pour moi qui m'est encore utile aujourd'hui.

Merci à tous les collègues de l'IUH de l'hôpital Saint-Louis qui ont égayé mon travail quotidien : Philippe et Pyramide, Jérôme et l'ASM, Nicolas et sa « bonne » humeur, Emeline et son autre bonne humeur ainsi que tous les gens que j'oublie.

Arrivé au chapitre Institut Curie, je remercie Olivier Lantz de m'avoir accueilli dans son équipe et d'avoir réussi à me garder à l'Institut.

Un grand grand grand grand merci aux deux personnes suivantes qui ont fait que mon passage dans ce laboratoire a été un plaisir et qui ont fait que venir bosser n'était pas que ça : Christine et Jordan. Raconter nos vies à l'animalerie, à la paillasse, au bureau ou en mangeant va me manquer. Vous êtes deux personnes gentilles (non, ce n'est pas une insulte !!!), bienveillantes, serviables (non, ce n'est pas un défaut !!!) et je ne demande rien d'autre que de travailler encore avec des personnes comme vous (humainement et professionnellement). Je suis triste de vous quitter et vous souhaite plus que le meilleur dans vos vies personnelles.

Merci à la quinquana la plus dynamique que je connaisse, qui a une vie de roman photo et l'insouciance des ados : Sophie. Réussir à te fourrer dans des situations pas possibles m'a égoïstement réjoui mais j'envie ton entrain et ton énergie. Ne lâche rien et vie ta vie.

Merci à celles qui m'ont énormément aidé pendant ma thèse : Marine et Mélanie. Vous avez toutes les deux des tempéraments différents mais travailler avec vous a toujours été agréable. J'espère que travailler avec moi n'a pas été trop pénible... Marine, j'espère que tu vas enfin te barrer de chez papa, il a le droit à sa liberté le pauvre et fout la paix à tes mecs !!! Mélanie, j'espère pour toi ne plus te voir rapidement et peut être un jour tu me raconteras quelque chose de croustillant que je me ferai un plaisir de raconter à tout le monde...

Merci à la nation Argentine : vous nous avez permis d'être champion du monde et vous nous avez apporté ma copine de thèse, Pamela (trop cool) mais aussi Letitia (trop princesse), Nicolas (trop Gordito), Jimena (trop de bisous) et vous acceptez même les brésiliens comme Rodrigo (trop de bébé)...

Merci à tous ceux qui ont fait que la vie est au labo est cool : Virginie (encore un qui part mais tu es habituée maintenant, non?), Caroline (tu es la plus fashion des blondes vénitiennes que je connaisse, tu me manques), Adèle (j'espère que tu ne

regrettes pas ta thèse), Anais (révolte toi mais pas trop fort sinon tu vas tomber dans les pommes...), Ruby (j'espère que tous les problèmes sont derrière toi et que tu profiteras de la vie avec ton bébé et ton mari au maximum).

Merci à tous les membres de l'U932 et de l'Institut Curie qui ont partagé des moments avec moi ; vous êtes trop nombreux pour tous vous citer.

Evidemment je finis par ma famille qui est la source de toutes mes motivations. Merci à mes parents qui m'ont montré comment être une bonne personne, à mes frères qui seront à jamais ceux que j'aimerais toujours embêter.

Tout ce que je fais est en pensant aux trois personnes les plus importantes de ma vie; Nadia, Paul et Juliette, j'espère que notre vie sera pleine d'un bonheur commun et je ne voudrai jamais autre chose que votre amour.

Abréviations

A

AAV: Adeno-associated virus

ACT: Adoptive cell transfer

ADCC: Antigen-dependent cell-mediated cytotoxicity

APC: Antigen-presenting cells

B

BCG: Bacille Calmette-Guérin

BLT : Bone marrow, liver, thymus

BRG : BALB/c Rag2^{-/-} IL-2R γ c^{-/-}

C

CAR-T: Chimeric antigen receptor T cells

cDC: Conventional dendritic cell

CSH: Cellules souches hématopoïétiques

CTA: Cancer testis antigen

CTLA-4: Cytotoxic T-lymphocyte associated protein 4

D

DAMP: Damage-associated molecular pattern

DARPin: Designed ankyrin repeat proteins

DC: Dendritic cell

E

EGF: Epidermal growth factor

EGFR: Epidermal growth factor receptor

F

FDA: Federal Drug Administration

Flt3: Fms-like tyrosine kinase 3

G

GEMM: Genetically engineered mouse model

GITR: Glucocorticoid-induced TNFR family related gene

GM-CSF: Granulocyte macrophage colony-stimulating factor

GvHD: Graft versus Host Disease

GvT: Graft versus Tumor

H

HER2: Human epidermal growth factor receptor 2

HIF: Hypoxia inducible factor

HIS: Human immunocompetent system

HLA: Human leucocyte antigen

Hu-PBL: Human peripheral blood leucocyte

Hu-SRC: Human scid repopultain cells

I

ICD: Induce cell death

ICOS: Inducible T-cell costimulator

IDO: Indoleamine 2,3-dioxygenase

IFN- γ : Interferon- γ

IL: Interleukin

IL2RA: Interleukin-2 receptor alpha

i.p.: Intraperitoneally

IRAE: Immune related adverse event

i.t.: Intratracheally

i.v.: intravenously

L

LAG-3: Lymphocyte-activation gene 3

M

MDSC: Myeloid-derived suppressor cell

MHC: Major histocompatibility complex

MISTRG: C;129S4-*Rag2*^{tm1.1Flv} *Csf1*^{tm1(CSF1)Flv} *Csf2/Il3*^{tm1.1(CSF2,IL3)Flv} *Thpo*^{tm1.1(TPO)Flv}
Il2rg^{tm1.1Flv} Tg(SIRPA)1Flv/J

N

NK: cellules Natural killer

NOD-Scid: NOD.CB17-*Prkdc*^{scid}/J **NOG:** NOD.Cg-*Prkdc*^{scid} *Il2rg*^{tm1Sug}/JicTac

NOG: NOD.Cg-*Prkdc*^{scid} *Il2rg*^{tm1Sug}/JicTac

NOG-EXL: NOD.Cg-*Prkdc*^{scid} *Il2rg*^{tm1Sug} Tg(SV40/HTLV-IL3,CSF2)10-7Jic/JicTac

NSCLC: Non-small cell lung cancer

NSG: NOD.Cg-*Prkdc*^{scid} *Il2rg*^{tm1Wjl}/SzJ

NSG-SGM3: NOD.Cg-*Prkdc*^{scid} *Il2rg*^{tm1Wjl} Tg(CMV-IL3,CSF2,KITLG)1Eav/MloySzJ

NSGW41: NOD.Cg-*Kit*^{W-41J} *Prkdc*^{scid} *Il2rg*^{tm1Wjl}/WaskJ

P

PAP: Phosphatase acide prostatique

PBMC: Peripheral blood mononuclear cell

PD1: Programmed cell death protein 1

PD-L1: Programmed cell death-ligand 1

PDX: Patient derived xenograft

PI3 kinase: Phosphoinositide 3-kinase

pTreg: Peripheral Treg

R

RAG: Recombination-activating genes

S

SASP: Senescence-associated secretory phenotype

SCF: Stem cell factor

SCID: Severe combined immunodeficient

Sirp α : Signal regulatory protein α

T

TAA: Tumor-associated antigen

TAM: Tumor-associated macrophage

TCR: T cell receptor

TEM: Transition épithélio-mésenchymateuse

TIL: Tumor-infiltrating lymphocyte

TLR: Toll-like receptor

TNF- α : Tumor necrosis factor- α

TPO: Thrombopoïétine

Treg cell: Regulatory T cell

TSA: Tumor-specific antigen

V

VEGF: Vascular endothelial growth factor

VIH: Virus de l'immunodéficence humaine

VLS: Vascular leak syndrome

Résumé

Actuellement l'immunothérapie révolutionne le traitement du cancer, en basculant la stratégie de traitement du ciblage de la tumeur vers le ciblage du système immunitaire. Le blocage des points de contrôle immunitaire avec des anticorps anti-CTLA-4, anti-PD1 et anti-PD-L1 a donné des résultats cliniques impressionnants, mais le taux de réponse reste faible. Il est donc essentiel de mieux comprendre leurs mécanismes d'action, d'identifier les biomarqueurs de réponse et de toxicité, et d'évaluer des combinaisons thérapeutiques. De telles études mécanistiques et précliniques nécessitent d'optimiser des modèles murins adaptés. A ces fins, mon travail de thèse a consisté à mettre en place des modèles de souris humanisées dans lesquels des souris immunodéficientes sont greffées avec des cellules tumorales et immunitaires humaines afin d'étudier des approches d'immunothérapie, en monothérapie ou en combinaison avec d'autres traitements. Nous avons évalué la prise de greffe de lignées cellulaires tumorales et de xénogreffes dérivées de patients (PDX), dans différentes souris receveuses reconstituées, soit avec des cellules souches hématopoïétiques (CSH) de sang de cordon ombilical, soit avec des cellules mononuclées du sang humain (PBMC). Nous avons observé que l'injection de CSH génère plusieurs sous populations de cellules immunitaires (cellules myéloïdes, lymphocytes T et B, cellules NK), détectables à partir de 4 semaines ; tandis que l'injection de PBMC génère principalement des lymphocytes T, détectables à partir de 1 semaine. Dans ce dernier modèle, la reconstitution lymphocytaire est associée à un effet anti-tumoral, mais est aussi accompagnée du développement de la maladie du greffon contre l'hôte. Les deux modèles présentent des avantages et des inconvénients pour l'évaluation des immunothérapies du cancer, qui sont discutés dans ma thèse. En utilisant ces modèles, nous avons évalué l'effet thérapeutique d'un anticorps anti-PD1, utilisé en clinique, sur des lignées de cellules tumorales ou sur des PDX de différents types de tumeurs. Nous avons observé une hétérogénéité dans la réponse au traitement, reflétant l'observation clinique des patients répondeurs et non-répondeurs. Nous avons par ailleurs évalué l'efficacité d'une immunothérapie innovante : les complexes IL-2/anti-IL-2. Nous avons observé une réponse aux

traitements dans des PDX de poumons. Finalement, afin d'évaluer l'intérêt des souris humanisées pour l'étude des combinaisons thérapeutiques, nous avons testé une thérapie anti-PD1 associée avec une thérapie ciblée dans le cancer de la vessie. Nos résultats, identifiant les atouts et les limitations des souris humanisées, démontrent la pertinence de ces nouveaux modèles pour l'évaluation des thérapies en immunoncologie et ouvrent des perspectives dans l'étude des combinaisons thérapeutiques.

Préambule

Cancer : Terme générique désignant une tumeur maligne constituée de cellules proliférant anormalement, qui peuvent envahir les tissus voisins et donner lieu, à distance, à des métastases. Cette définition, quoiqu'incomplète, pose les bases des connaissances partagées par un grand nombre d'être humain sur cette maladie. Cette maladie protéiforme, multi-organe, à pronostique varié est une des causes majeures de mortalité dans le monde avec plus de 14 millions de nouveaux cas chaque année et 8 millions de décès [1]. Le traitement des cancers est un enjeu majeur de santé publique notamment en France qui a vu les pouvoirs publics fixer 4 priorités dans le cas du Plan cancer (2014-2019) : 1. Guérir plus de malade, 2. Donner plus de moyens à la recherche fondamentale et à la recherche clinique, 3. Améliorer la vie des malades pendant et après le cancer et 4. Faire de la prévention une priorité. Ce 3^{ème} plan, à qui a été alloué 1,5 milliards d'euros a donc pour vocation de faire la part belle à la recherche.

Dans ce cadre, l'utilisation de notre propre système immunitaire pour traiter le cancer est une révolution majeure dans le traitement du cancer depuis ces 10 dernières années. Ce concept, appelé immunothérapie, est la thématique principale de l'équipe TransIm (Translational Immunotherapy) dont je fais parti.

Mon travail de thèse a consisté à développer des modèles de souris humanisées afin de pourvoir aux besoins de modèles précliniques *in vivo* plus proche de l'homme mais aussi de comprendre les mécanismes mis en jeu dans le cas de l'immunothérapie anti-cancer.

A travers mon travail, je vais vous montrer l'utilité de ces modèles pour l'évaluation de l'immunothérapie anti-cancer mais aussi leurs limites.

Introduction

1. Développement des cancers

1.1. Oncogenèse

L'oncogenèse ou conversion d'une cellule normale en cellule tumorale est un mécanisme complexe dont la compréhension a beaucoup progressé depuis les années 1970. Le développement de la génétique moléculaire a permis la découverte des oncogènes [2,3]. Les oncogènes cellulaires sont des séquences génomiques dont l'expression a pour conséquence une prolifération anormale des cellules et l'apparition de cancers. Ces oncogènes sont présents dans l'ensemble des types de tumeur et sont multiples. Les oncogènes proviennent, à l'origine, de proto-oncogènes dont l'altération, qualitative ou quantitative, entraîne une modification d'expression protéique qui stimule la division cellulaire ou inhibe l'apoptose. Les processus entraînant l'altération des proto-oncogènes peuvent être des mutations, des amplifications géniques ou des translocations. Deux autres catégories de gènes sont associés au processus oncogénique : les gènes suppresseurs de tumeur et les gènes de réparation de l'ADN [4].

Les gènes suppresseurs de tumeurs régulent négativement la prolifération cellulaire. La perte de fonction de ces gènes sur les 2 chromosomes peut entraîner le processus oncogénique. Les gènes suppresseurs de tumeur les plus fréquents sont p53, PTEN ou pRB. Il est remarquable que pour une localisation de cancer (cancer du poumon ou sein ou ovaire...) il existe une multitude d'oncogènes pouvant être impliqué (myc, ras, p53...) mais aussi qu'un oncogène peut être présent dans plusieurs types de cancer différents [5] ou au contraire qu'un processus oncogénique peut être associé spécifiquement à un type particulier de cancer (par exemple la fusion bcr/abl de la leucémie myéloïde chronique). Des mutations dans les gènes de réparation de l'ADN impliquent que les erreurs d'appariement au niveau de l'ADN produites par l'action des polymérases ne sont plus corrigées. Ce mécanisme de réparation des mésappariements (Mismatch repair) est défectueux lorsque les gènes de réparation de l'ADN sont mutés et entraîne une instabilité des microsatellites provoquant des cancers [6].

1.2. Etapes clés du développement du cancer

Le processus oncogénique entraîne l'apparition d'un phénomène anormal au niveau cellulaire mais n'explique pas l'apparition de tumeur qui est une multiplication anormale de ces cellules. La façon dont ce processus se forme est complexe. Hanahan et Weinberg ont décrit les étapes clés dans le développement du cancer, dans deux revues en 2000 et 2011, un concept appelé « Hallmark of cancer » [7,8]. Les cellules cancéreuses ont besoin d'acquérir quatre grandes capacités pour poursuivre leur processus de transformation tumorale : capacité de réplication illimitée, d'angiogenèse, d'invasion tissulaire et métastatique et enfin elles doivent posséder des mécanismes d'échappement au contrôle de la prolifération anormale.

1.2.1. Capacité de réplication illimitée : rôle de la sénescence dans le processus tumoral

La notion d'immortalisation, liée aux cellules cancéreuses, est un concept admis depuis longtemps notamment par l'établissement de lignée tumorale cultivée *in vitro*. En effet depuis 1948 [9], dans un modèle de lignée d'origine animale et depuis 1953 avec l'établissement de la lignée HeLa [10] d'origine humaine, nous savons que les cellules cancéreuses possèdent ce pouvoir de réplication illimitée. Les cellules, dites normales, ont une capacité limitée de division et entrent rapidement en sénescence après un certain nombre de divisions ou pour celles arrivant à passer outre cet état de sénescence, elles entrent en phase de crise et meurent. Le nombre de divisions avant la mort cellulaire est variable selon le type cellulaire mais se situe aux alentours de 50, selon la limite de Hayflick [11].

Les cellules cancéreuses réussissent à passer à travers ces étapes, notamment grâce à l'action d'une enzyme ; la télomérase [12]. En effet, à chaque réplication l'extrémité des chromosomes, appelées télomères, se raccourcissent et cette perte répétée

entraîne une perte d'information génétique portée par des gènes proches des télomères qui explique la mort des cellules. La télomérase est une reverse-transcriptase qui synthétise des répétitions télomériques (TTAGGG) de novo aux extrémités des chromosomes à chaque réplication cellulaire. Cette télomérase est fortement exprimée dans les cellules cancéreuses et induit une résistance aux phénomènes de sénescence/apoptose [13].

Un autre phénomène lié à la sénescence entre en jeu dans la progression tumorale. En effet, la sénescence des cellules du micro-environnement tumoral peut avoir des effets anti- ou pro-tumoraux [14]. Le phénotype sécrétoire associé à la sénescence (SASP), contenant des facteurs solubles, des protéines insolubles ou des protéases relarguées par les cellules sénescents, joue un rôle dans la progression tumorale. Les effets pro-tumoraux majeurs du SASP sont d'induire la prolifération des cellules épithéliales stimulant la croissance tumorale ou de favoriser la motilité cellulaire. Ce phénomène a été observé dans une grande variété de tissus ; sein [15], peau [16], prostate [15], pancréas [17] ou muqueuse oropharyngée [18].

1.2.2. Vascularisation

Les tumeurs ne peuvent croître ou métastaser au-delà de 2-3 mm³ sans vascularisation [19]. En effet, comme n'importe quel tissu sain, les tumeurs ont besoin d'apport de nutriments et d'oxygène tout autant que d'évacuer leurs déchets. Un des mécanismes permettant à la tumeur de développer sa propre vascularisation est l'angiogenèse qui est le développement de vaisseaux capillaires à partir de capillaires préexistants. Ce phénomène rare et transitoire chez l'adulte (cicatrisation, cycle menstruel féminin) est initié par un changement dans la balance de facteurs pro- et anti-angiogéniques vers une phase positive pour la vascularisation. Ce phénomène, appelé « switch angiogénique », est crucial dans la croissance tumorale [20,21]. Plusieurs mécanismes entrent en jeu pour promouvoir cette angiogenèse tumorale et le plus important est l'hypoxie. Les cellules endothéliales possèdent des mécanismes de sensibilité à l'oxygène notamment les facteurs de transcription

inductibles par hypoxie (HIF) [22], régulant l'angiogenèse mais aussi la survie cellulaire ou l'inflammation. Le niveau d'expression des HIF est plus élevé dans beaucoup de cancer avec un faible pronostic [23,24]. Cette hypoxie, liée à un fort niveau d'expression des HIF, est une des causes de l'expression du VEGF (vascular endothelial growth factor) qui contrôle l'induction positive du switch angiogénique [25,26]. En effet, le VEGF, dont l'expression peut aussi être une conséquence oncogénique, induit l'angiogenèse par effet direct sur les cellules endothéliales [27] et, tout comme les HIF, est fortement exprimé dans un grand nombre de tumeur [28]. Cependant, l'angiogenèse tumorale chroniquement activée produit un réseau vasculaire anormal, anarchique qui induit un flot sanguin erratique mais aussi l'apparition de zones non accessibles à certaines thérapies.

Plusieurs autres modes de vascularisation des tumeurs existent, autre que l'angiogenèse.

Tout d'abord, la cooptation vasculaire est le phénomène par lequel la tumeur détourne des vaisseaux préexistants pour son propre apport sanguin [29]. La cooptation vasculaire est localisée en périphérie de la tumeur et les traitements anti-angiogéniques semblent être moins efficaces sur les tumeurs présentant cette vascularisation, du fait d'une moindre accessibilité des traitements [30].

La croissance micro vasculaire "intussusceptive" (IMG ou angiogenèse par scission) est un mécanisme consistant en l'insertion répétée de nouveaux piliers de tissus transcapillaires minces, qui augmentent ensuite en taille, permettant ainsi au réseau capillaire de se développer par la scission du capillaire préexistant en deux nouveaux vaisseaux. Ce mécanisme est présent dans certaines tumeurs [31,32] et semblerait impliqué dans un processus de vascularisation des régions plus centrales des tumeurs en l'absence de VEGF.

Le mimétisme vasculaire est la capacité plastique, de certaines cellules tumorales agressives, à exprimer un phénotype de cellules souches pour former un réseau vasculaire de novo. Il a été découvert dans le mélanome uvéal [33] mais est présent dans une majorité des cancers et est associé à un pronostic vital faible [34].

1.2.3. Invasion tissulaire et métastase

La capacité des tumeurs à envahir les tissus périphériques et à métastaser est une de leurs caractéristiques fondamentales : le développement de métastases est la principale cause de décès chez la plupart des patients atteints de cancer. Les métastases sont des cellules cancéreuses qui se sont détachées d'une tumeur primaire et qui ont migré par les vaisseaux lymphatiques ou les vaisseaux sanguins dans une autre partie du corps où elles se sont installées. Le processus par lequel les cellules tumorales envahissent les tissus par métastase est appelé la cascade invasion-métastase [35] qui est composée de la série d'étapes suivantes : envahissement local de la matrice extracellulaire, intravasation, survie dans la circulation sanguine, extravasation dans l'organe cible, adaptation à l'organe pour la formation des micrométastases puis colonisation macrométastatique.

Un des mécanismes expliquant ce processus métastatique est l'acquisition par certaines cellules cancéreuses (carcinome) d'un certain nombre de caractéristiques de cellules mésenchymateuses : c'est la transition épithélio-mésenchymateuse (TEM). Il a en effet été montré que l'activation de la TEM, par l'expression forcée de facteurs de transcription liés à la TEM (SLUG, SNAIL), augmente le processus métastatique dans des tumeurs de sein humaines implantées orthotopiquement dans un modèle murin [36–38]. Ce processus métastatique est notamment favorisé par l'inactivation ou la régulation négative de la cadhérine E, molécule d'adhésion intercellulaire, dans les carcinomes humains [39,40]. La perte de jonction intercellulaire, liée à la perte de la cadhérine E, peut être aussi amplifiée par l'acquisition d'autres molécules d'adhésion, davantage liées à la migration cellulaire, telle que la cadhérine N [41,42].

Le rôle du stroma dans la stimulation du processus métastatique a déjà partiellement été mis en évidence. Plusieurs acteurs peuvent jouer un rôle comme les cellules souches mésenchymateuses qui en sécrétant la chimiokine CCL5 stimulent l'invasion tissulaire [43]. Les macrophages peuvent aussi faciliter le processus métastatique en sécrétant des métalloprotéinases matricielles qui dégradent le microenvironnement tumoral et favorise l'invasion mais aussi la survie cellulaire et l'angiogenèse [44,45].

D'autre part, les macrophages sont capables de sécréter d'autres molécules promouvant l'invasion des cellules tumorales en réponse à des signaux tumoraux : les cathepsines B et S en réponse à une sécrétion d'IL-4 des cellules tumorales [46] ou l'EGF (epidermal growth factor) en réponse à une sécrétion de CSF-1 des cellules tumorales (cytokine pro-macrophagique) [47]. Par ailleurs, l'expression de l'IL-34 par les cellules cancéreuses promeut la progression tumorale et la formation de métastases par le recrutement de macrophages associés aux tumeurs [48].

Le processus métastatique se termine, comme décrit précédemment, par la colonisation du tissu distant de la tumeur primaire. Cette étape peut requérir un temps d'adaptation au nouvel environnement tumoral. Ce temps de dormance peut avoir plusieurs causes : la sécrétion de facteurs de suppression par la tumeur primaire [49,50], une incapacité à activer une angiogenèse tumorale au site métastatique [51], un faible accès aux nutriments [52] ou l'action anti-tumoral du système immunitaire [53].

1.2.4. Mécanismes d'échappement

En plus de leurs capacités de développement, les cellules cancéreuses sont capables d'échapper à leur destruction. Voici quelques-uns des mécanismes d'échappement mis en œuvre par les cellules tumorales.

Les cellules cancéreuses peuvent moduler l'expression des facteurs de croissance leur étant bénéfiques. Elles peuvent sécréter des facteurs de croissance, ayant une action autocrine ou une action sur les cellules de leur stroma. Elles peuvent aussi augmenter à leur surface le niveau d'expression des récepteurs à ces facteurs de croissance afin les rendre hyper-réactifs [54,55].

Les tumeurs peuvent perdre les mécanismes de régulation (boucle d'inhibition) de la prolifération cellulaire. Par exemple, la perte de régulation de la voie de la PI3-kinase a pour conséquence une augmentation de la prolifération cellulaire. Les tumeurs mutées pour PTEN et mTOR sont des exemples de ce phénomène [56,57]. Les gènes suppresseurs de tumeur jouent un rôle prépondérant dans ce contrôle de la

prolifération et il a été montré que l'inactivation de certains gènes suppresseurs de tumeur (pRB : protéine du rétinoblastome, p53) était couramment observée dans un grand nombre de cancer [58,59]. Cette prolifération incontrôlée pourrait être contrebalancée par l'inhibition de contact. Une concentration cellulaire excessive entraîne des contacts cellulaires trop denses et un arrêt de la prolifération dans le cas de cellules normales. Dans le cas des cellules cancéreuses, cette inhibition de contact est réduite voire absente [60].

Les cellules tumorales, hautement anormales, présentant un niveau de stress élevé ainsi que des dégâts au niveau de l'ADN, devraient enclencher spontanément un programme de mort cellulaire. L'entrée d'une cellule dans ce programme est la résultante d'une balance entre des signaux positifs et négatifs pour l'induction de l'apoptose. Les cellules cancéreuses peuvent faire pencher cette balance à leur profit en synthétisant des protéines anti-apoptotiques (Bcl-2) [61] ou de survie (Igf1/2) [62] mais aussi en diminuant la synthèse de protéines pro-apoptotiques (Bax) [63].

Un axe majeur d'échappement des tumeurs est également leur capacité à échapper au contrôle du système immunitaire. Cette particularité, sur laquelle je reviendrai ultérieurement dans ce manuscrit, est le point de départ de mon travail de thèse.

2. Interaction entre cancer et système immunitaire : la base de l'immunothérapie

Le concept de l'immunosurveillance, définie comme la capacité du système immunitaire à détecter et éliminer les tumeurs naissantes, est largement débattu depuis son introduction par Paul Ehrlich en 1909 [64]. En effet, l'instabilité génétique, propre aux cellules tumorales, induit l'expression nouvelle d'antigènes associés aux tumeurs (TAA) qui devraient être reconnus par le système immunitaire entraînant la destruction de ces cellules. La non-destruction des cellules tumorales, exprimant des TAA, suggèrent que les tumeurs échappent à la détection par le système immunitaire. Plusieurs mécanismes d'interaction entre les tumeurs et le système immunitaire permettent d'expliquer le phénomène d'échappement. La meilleure compréhension de ces mécanismes permettra de trouver de nouvelles thérapies anti-cancer tournées vers l'utilisation du système immunitaire.

2.1. Ignorance

Une condition nécessaire à une réponse immunitaire anti-tumorale spécifique est l'expression par les tumeurs de TAA. Cependant, cette expression n'est pas toujours suffisante pour induire une réponse immunitaire [65]. Le « priming » est la première rencontre des lymphocytes T naïfs avec leur antigène spécifique, présenté par les cellules présentatrices de l'antigène. Ce priming entraîne leur différenciation en cellules T effectrices, motrices de la réponse immune adaptative. Zinkernagel propose que l'absence de réponse anti-tumorale est liée à l'absence de priming des cellules T [66] c'est à dire à l'ignorance des cellules tumorales par le système immunitaire. En effet, la greffe d'un petit fragment de sarcome n'entraîne pas de réponse immunitaire au contraire de l'injection d'une suspension cellulaire, représentant la même quantité de cellules tumorales. La migration des cellules tumorales provenant de l'injection de la suspension cellulaire vers les organes

lymphoïdes serait la clé de ce priming des cellules T, alors que l'injection du fragment de sarcome n'entraîne pas de migration des cellules tumorales suffisante pour initier ce priming. Une réponse immunitaire faible ou limitée dans le temps, dû à un apport faible de TAA, ne suffit pas à provoquer le rejet de la tumeur, tandis que des réponses T fortes et prolongées peuvent aboutir à un rejet complet. La réponse immunitaire contre les TAA apparaît alors lorsqu'une masse tumorale critique est atteinte. Cependant, malgré une réponse effectrice des lymphocytes T, celle-ci arrive trop tardivement pour contrôler la croissance tumorale.

2.2. Tolérance

Le concept de tolérance du système immunitaire vis à vis des cellules cancéreuses implique une absence des signaux de dangers tissulaire et cellulaire lors de la croissance tumorale. Dans ce modèle, les lymphocytes T spécifiques des antigènes de la tumeur sont inhibés car la tumeur, qui est un tissu en construction, n'envoie pas de signaux de stress ou de danger aux « patrouilleurs » du système immunitaire [67]. Cette hypothèse est renforcée par l'observation que l'apport exogène de signaux de danger permet l'activation des réponses immunitaires anti-tumorales, ayant pour conséquence le rejet de la tumeur. Il a notamment été montré que les chimiothérapies induisant une mort immunogénique, telles que la doxorubicine, permettait la sécrétion de facteur, tel que HMGB1, qui stimule la réponse immunitaire anti-cancer [68]. Egalement, l'injection du Bacille Calmette-Guérin (BCG), chez des patients atteints de cancer de la vessie, montre une protection contre une récurrence [69].

2.3. Immunoédition

Malgré les théories de l'ignorance et de la tolérance, plusieurs observations montrent un rôle majeur du système immunitaire dans le contrôle des tumeurs. Tout d'abord,

dans des modèles de souris, il a été montré que les lymphocytes T et l'IFN- γ collaborent pour contrer le développement de sarcomes induits par les carcinogènes [70]. De plus, les souris immunodéficientes pour l'IFN- γ ou la perforine sont plus enclines à développer des tumeurs spontanées [71,72]. Chez l'homme, il a été montré que des patients immunodéprimés (HIV positif ou sous traitement immunosuppresseur) ont une augmentation significative de leur incidence à développer un cancer [73].

Les tumeurs peuvent cependant aussi échapper à l'immunoédition en favorisant l'émergence de clones cellulaires peu immunogéniques [64]. L'immunoédition est ainsi composée de trois phases distinctes : 1) l'élimination, 2) l'équilibre et 3) l'échappement.

2.3.1. Elimination

Cette phase d'élimination correspond à l'immunosurveillance, mécanisme par lequel les cellules immunitaires jouent leur rôle de sentinelle anti-cellules cancéreuses. Cette phase met en jeu à la fois l'immunité innée et adaptative. Cette coopération commencerait par l'activation de l'immunité innée, via les cellules dendritiques et les cellules Natural Killer (NK), grâce à la sécrétion par la tumeur de médiateurs de la réponse innée [74,75] ou par l'expression de récepteurs spécifiques de l'immunité innée tel que MICA, ligand de NKG2D (récepteur des cellules NK), à la surface des cellules tumorales [76]. Le processus d'élimination peut être complet mais il peut y avoir des échecs et les tumeurs rentrent soit dans la phase d'équilibre soit dans la phase d'échappement.

2.3.2. Equilibre

Au cours de cette phase, qui peut être très longue [77], il existe un équilibre entre l'élimination d'un certain nombre de cellules tumorales et l'apparition de nouvelles

cellules tumorales. Robert Schreiber a montré dans un modèle de sarcome induit que le système immunitaire adaptatif était capable de maintenir cet équilibre, et alors qu'en son absence, les cellules tumorales étaient capables de proliférer [78]. L'apparition ou la survie de certains clones cellulaires, au cours de cette phase d'équilibre, est un phénomène central de l'histoire du cancer. Cette immunoédition sélectionne des clones qui peuvent être résistants au système immunitaire et entraîne leur entrée dans la phase d'échappement. Un ensemble de mécanismes entre en jeu pour échapper au système immunitaire, c'est la troisième phase de l'immunoédition : l'échappement. Dans le prochain chapitre, j'expliquerai comment le système immunitaire utilise ces mécanismes d'échappement et comment les récents développements de l'immunothérapie arrivent à les outrepasser.

2.4. Thérapies modulant l'interaction cancer-système immunitaire

Il existe une série d'étapes cruciales dans la lutte contre le cancer par le système immunitaire, résumée ci-dessous par Chen et Mellman **Figure 1** [79]. Ce cycle cancer-immunité est composé de sept étapes : relargage d'antigènes tumoraux, présentation antigénique, priming et activation des lymphocytes T, migration vers la tumeur des lymphocytes T spécifiques, infiltration de ces lymphocytes dans la tumeur, reconnaissance des cellules tumorales par les lymphocytes et finalement la mort des cellules tumorales. Il a été montré que de nombreux mécanismes d'échappement au contrôle du système immunitaire par les cellules cancéreuses existaient au cours de ces étapes. Je vais discuter de ces mécanismes d'échappement et comment les nouvelles immunothérapies peuvent ou pourraient outrepasser ces mécanismes.

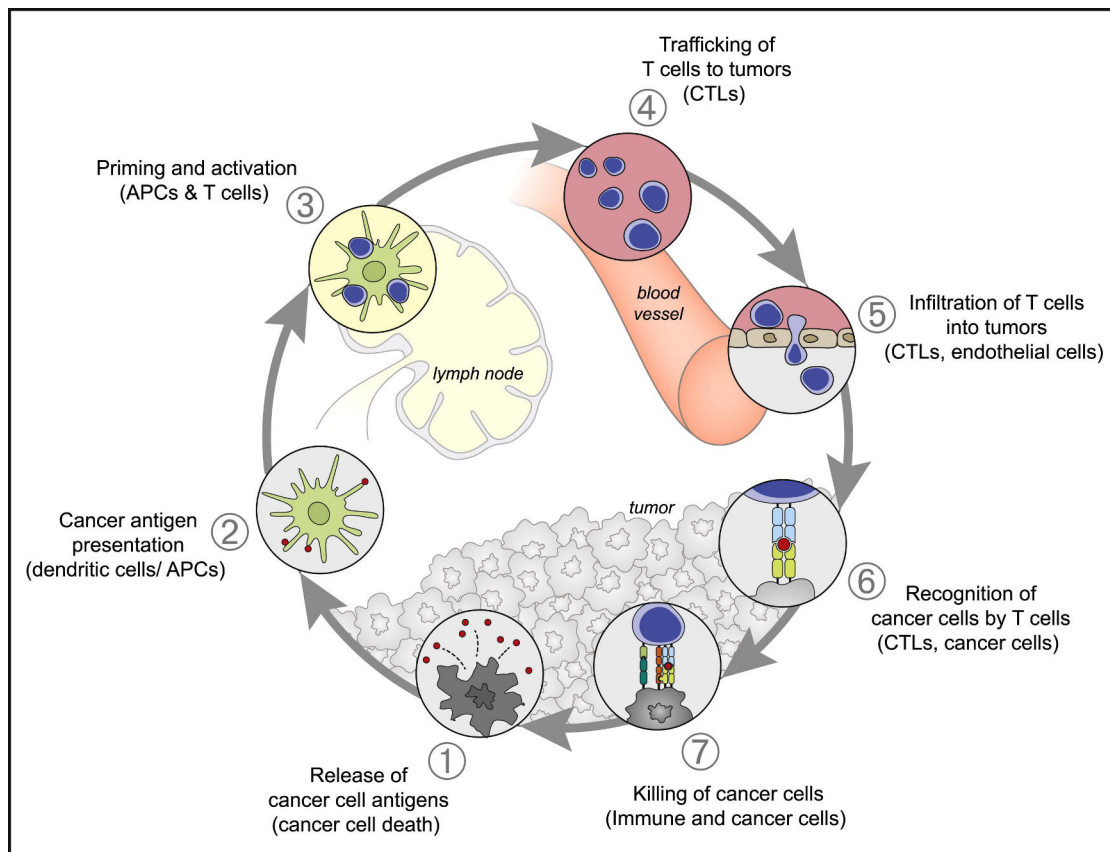


Figure 1 : Le cycle cancer-immunité. Adapté de Chen et Mellman. *Immunity*, 2013. [79]

2.4.1. Antigènes tumoraux et présentation antigénique

Un pré-requis de la régulation du processus cancéreux par le système immunitaire est l'immunogénicité des cellules tumorales. Une étape importante pour la mise en place de la réponse adaptative contre le cancer est la reconnaissance d'antigènes tumoraux par les cellules présentatrices de l'antigène et leur activation, essentielle pour une initiation de cette réponse immunitaire. Cependant, plusieurs écueils se présentent pour empêcher la disponibilité de ces antigènes et leur association aux molécules du complexe majeur d'histocompatibilité (CMH) afin d'être présentés aux lymphocytes T.

Une des stratégies, d'immunothérapie, pour améliorer l'accessibilité aux antigènes tumoraux est la stratégie vaccinale. La stratégie vaccinale consiste à délivrer des antigènes tumoraux de façon exogène pour améliorer la réponse immunitaire anti-

tumeur. Plusieurs catégories d'antigènes tumoraux existent : les **antigènes associés aux tumeurs (TAA)**, les **cancer/testis antigènes (CTA)** et les **antigènes spécifiques des tumeurs (TSA)**. Les TSA, appelés aussi néo-antigènes, sont les seuls à être exprimés uniquement par les cellules tumorales. L'expression des TSA est due à des mutations dans le génome qui sont spécifiques d'une tumeur. Il a été montré que la charge mutationnelle élevée (mesure quantitative des mutations de la tumeur) des tumeurs était corrélée à une meilleure réponse aux immunothérapies [80] et que selon le type de tumeur cette charge mutationnelle est très variable [81] **Figure 2**.

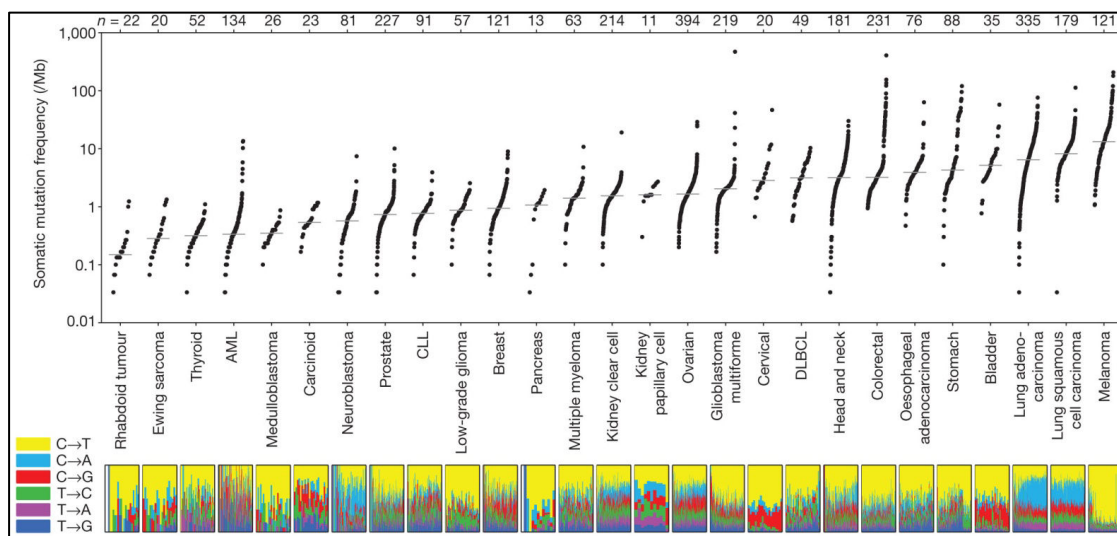


Figure 2 : Fréquence des mutations somatiques dans les différents types de cancer humain. Adapté de Lawrence et al. Nature, 2013 [81].

Peu de stratégies vaccinales, ciblant les antigènes tumoraux, se sont avérées efficaces. Ceci peut s'expliquer par plusieurs raisons : les TAA peuvent être tolérés par le système immunitaire, puisque déjà exprimés par un certain nombre de tissus sains, une baisse ou l'absence d'expression des molécules du CMH à la surface des cellules tumorales ou un environnement cytokinique inadapté [82].

La stratégie vaccinale qui suscite beaucoup d'intérêt serait de cibler la réponse immunitaire contre des néo-antigènes. Ils ne sont, en effet, pas sujet au contrôle des mécanismes de tolérance centrale du système immunitaire et pourrait induire une réponse lymphocytaire T plus conséquente. Cependant, cette stratégie implique une médecine personnalisée car chaque tumeur présente ses propres néo-antigènes.

Sahin et al ont montré l'efficacité de cette méthode en injectant un mélange d'ARN codant pour plusieurs néo-épitopes propre à chaque patient. Ces néo-épitopes ont été identifiés par séquençage de la tumeur de chaque patient. Des réponses cliniques significatives ont été observées chez des patients traités (réponse T CD4⁺ prépondérante) sauf pour un patient dont la tumeur a perdu l'expression en surface du CMH de classe 1, nécessaire à la reconnaissance par les lymphocytes T [83].

Dans le cadre de la présentation antigénique des antigènes tumoraux, des signaux de dégradation (**D**amage-**a**ssociated **m**olecular **p**attern : DAMP) sont aussi indispensables pour activer efficacement le système immunitaire. Ces signaux peuvent être présents dans le milieu extracellulaire des tumeurs après l'induction d'une mort cellulaire immunogénique (**I**mmunogenic **c**ell **d**eath : ICD). Contrairement à certaines formes d'apoptoses, ces ICD sécrètent un ensemble de DAMP qui peuvent stimuler le système immunitaire. Ces ICD peuvent être induites par des traitements spécifiques (chimiothérapie spécifique, radiothérapie). L'activation des voies de signalisation impliquant les DAMPs peut avoir un effet bénéfique dans le traitement du cancer (BCG dans le cancer de la vessie [69], utilisation de la voie de détection d'ADN : cGAS-cGAMP-STING [84]). L'utilisation de chimiothérapies, telles que la doxorubicine, la mitoxantrone, l'oxaliplatine et la bortezomib qui induisent une ICD est aussi une voie intéressante pour activer une réponse immunitaire [85,86]. La mort cellulaire induite par ces chimiothérapies entraîne la production de la calréticuline, de heat-shock protéines et de molécules telles que HMGB1 qui activent les cellules dendritiques (DC) via le Toll-like récepteur de type 4 (TLR4) [87]. **Figure 3.**

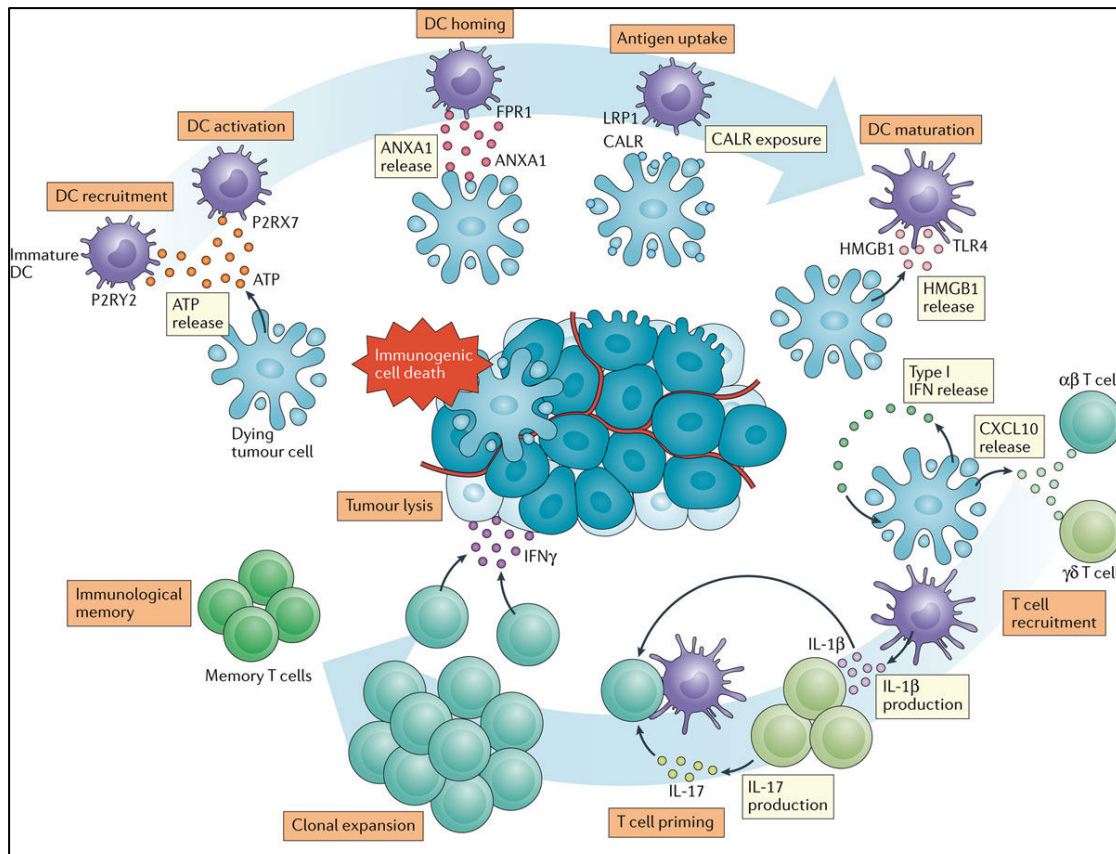


Figure 3: Mécanismes impliquant le système immunitaire dans le cas de l'ICD.
Adapté de Galluzzi et al. Nature reviews Immunology, 2017. [88].

D'autres mécanismes peuvent induire l'ICD tels que l'irradiation [89], la haute pression hydrostatique [90] et la thérapie photodynamique [91].

L'ensemble de ces thérapies ciblant à la fois l'antigénicité (vaccins) et l'activation adjuvante (ICD) permet de contribuer à l'initiation d'une réponse immunitaire anti-tumorale efficace. Les avancées vaccinales majeures seront discutées ultérieurement dans le chapitre dédié à l'état des lieux sur l'immunothérapie chez l'homme.

2.4.2. Priming et activation des lymphocytes T

Les étapes suivants le relargage d'antigènes et à la présentation antigénique sont le priming et l'activation des lymphocytes T. Ce processus s'effectue dans les ganglions lymphatiques drainant la tumeur, grâce à la migration des cellules dendritiques (DC)

dans ces ganglions où elles présentent les antigènes aux lymphocytes T, en association aux molécules du CMH. La première immunothérapie anti-cancer avait pour objectif d'augmenter la réponse immunitaire en augmentant la prolifération et la différenciation des lymphocytes T, grâce à l'administration d'interleukine-2 (IL-2), cytokine clé impliquée dans la prolifération et la survie des lymphocytes T. En 1992, la Food and Drug Administration (FDA) a autorisé le traitement de cancer du rein métastatique par injection d'IL-2 puis l'a approuvé pour le traitement des mélanomes métastatiques en 1998 [92,93]. Toutefois, l'IL-2 exerce à la fois des fonctions stimulatrices et régulatrices au sein du système immunitaire [94]. L'IL-2 agit en se fixant sur ses récepteurs qui peuvent être dimérique (IL-2R β (CD122) et IL-2R γ (γ , CD132)) ou trimérique (IL-2R α (CD25), IL-2R β (CD122) et IL-2R γ (γ , CD132)). Le récepteur trimérique a une affinité 10 à 100 fois plus forte pour l'IL-2 que le récepteur dimérique. Ce récepteur trimérique est exprimé sur les lymphocytes T régulateurs (Treg) et les lymphocytes T activés alors que le récepteur dimérique est exprimé sur les lymphocytes T CD8⁺ et les cellules NK. L'injection d'IL-2 à forte dose pour traiter des cancers est basée sur l'objectif d'activer ces cellules CD8⁺ et NK, ce qui serait impossible avec des doses plus faibles d'IL-2, à cause de son affinité préférentielle au récepteur trimérique. Cependant, l'administration d'IL-2 à haute dose induit des effets indésirables sévères tels que des syndromes de fuite vasculaire (VLS), des œdèmes pulmonaires, de l'hypotension et de la toxicité cardiaque. Ces effets indésirables sont notamment liés à une sur-activation des cellules NK qui sécrètent des cytokines pro-inflammatoires [95].

Une autre façon d'amplifier cette phase d'activation et de priming des lymphocytes T consiste à bloquer leur régulation. Les Treg sont une sous-population de lymphocytes T CD3⁺ qui ont la capacité d'inhiber la prolifération et/ou la fonction des différentes cellules du système immunitaire. Les mécanismes d'inhibition utilisés par les Treg sont 1) la sécrétion de cytokines inhibitrices (TGF β , IL-35, IL-10), 2) la cytolise via les molécules de granzyme et de perforine, 3) la perturbation métabolique via la privation d'IL-2 ou la production d'AMP cyclique ou d'adenosine qui inhibent la fonction effectrice des lymphocytes T et 4) la modulation de la maturation et de la fonction des cellules dendritiques [96]. Ils jouent un rôle essentiel dans cette régulation en prévenant les réponses auto-immunes. Dans le cas des cancers, il est

notamment intéressant de noter qu'une augmentation du nombre de Treg, dans le microenvironnement tumoral des patients, est associée à un mauvais pronostic [97]. Plusieurs mécanismes peuvent expliquer cette présence élevée des Tregs : 1) une migration augmentée des Treg comparée aux lymphocytes effecteurs, [98,99] 2) une expansion locale dans le microenvironnement tumorale [98,100] et 3) une génération de Treg périphériques dans la tumeur ou dans les ganglions drainant ces tumeurs [101,102]. Une des stratégies d'immunothérapie a donc été d'éliminer les Treg, pour limiter leur fonction suppressive, notamment par l'utilisation d'anticorps anti-CTLA-4. L'expression de CTLA-4 sur les lymphocytes T conventionnels est induite par l'activation du récepteur aux cellules T (TCR) et alors qu'elle est constitutivement présente sur les Treg. CTLA-4 est une protéine homologue à CD28 ; les deux peuvent se lier aux molécules de co-stimulation CD80 et CD86, exprimées sur les cellules dendritiques. Alors que la liaison CD28-CD80/86 induit une activation des lymphocytes T, la liaison CTLA-4-CD80/86 induit la transformation des cellules présentatrices de l'antigène vers un profil tolérogène [103]. Comme CTLA-4 a une affinité beaucoup plus élevée que CD28 pour ses ligands communs CD80 et CD86, CTLA-4, constitutivement exprimée par les cellules Treg, peut supplanter la liaison CD28-CD80/86 sur les cellules présentatrices d'antigène, inhibant ainsi la co-stimulation des cellules T conventionnelles [104]. L'utilisation d'anticorps anti-CTLA-4 permet d'outrepasser ce mécanisme d'inhibition. Par ailleurs, l'activation des lymphocytes T entraîne une expression de CTLA-4 à leur surface, entraînant une régulation négative de leur activation. En limitant la signalisation médiée par CD28 pendant la présentation de l'antigène, CTLA-4 réduit les réponses immunitaires aux antigènes tumoraux. Pour toutes ces raisons, l'utilisation d'anticorps anti-CTLA-4 a notamment été testée pour lever les inhibitions du système immunitaire et induire une réponse immunitaire contre des tumeurs murines [105]. D'autres molécules peuvent réguler activement ou négativement cette étape de priming/activation.

OX-40 et 4-1BB, membres de la famille du TNF, sont des protéines de surface exprimées par les lymphocytes T qui agissent en qualité de co-stimulateur après stimulation du TCR. Dans ce contexte, la liaison de 4-1BB ou de OX-40, à leur ligand, augmente la prolifération cellulaire et la production de cytokines [106,107]. Des études ont montré que l'injection d'un anticorps agoniste de 4-1BB, ou de OX-40,

augmentait l'immunité anti-tumorale dans un grand nombre de modèles de tumeurs déjà établis chez la souris [108,109].

Une autre façon de moduler positivement le priming du système immunitaire, autre que le ciblage des lymphocytes T, est de s'intéresser à l'autre composante de cette étape : les cellules présentatrices de l'antigène (APC).

CD40 est exprimée de façon constitutive sur les lymphocytes B et les DC. La liaison avec son ligand, CD40-L, exprimé notamment par les lymphocytes T activés, entraîne une activation des APCs. CD40 semble primordial dans l'activation des DC, et leur permet d'induire une réponse T cytotoxique, en partie grâce à la sécrétion de l'IL-12 [110]. L'utilisation d'un anticorps dirigé contre CD40 a montré des effets bénéfiques dans des lymphomes de souris, corrélés avec une augmentation d'une réponse T CD8⁺ mémoire [111].

Une représentation schématique des interactions entrant en jeu dans la régulation de la réponse immunitaire est présentée **Figure 4**. La composante priming/activation est tout autant représentée que la composante interaction avec le microenvironnement tumoral. Cette dernière composante sera discutée dans un chapitre ultérieur.

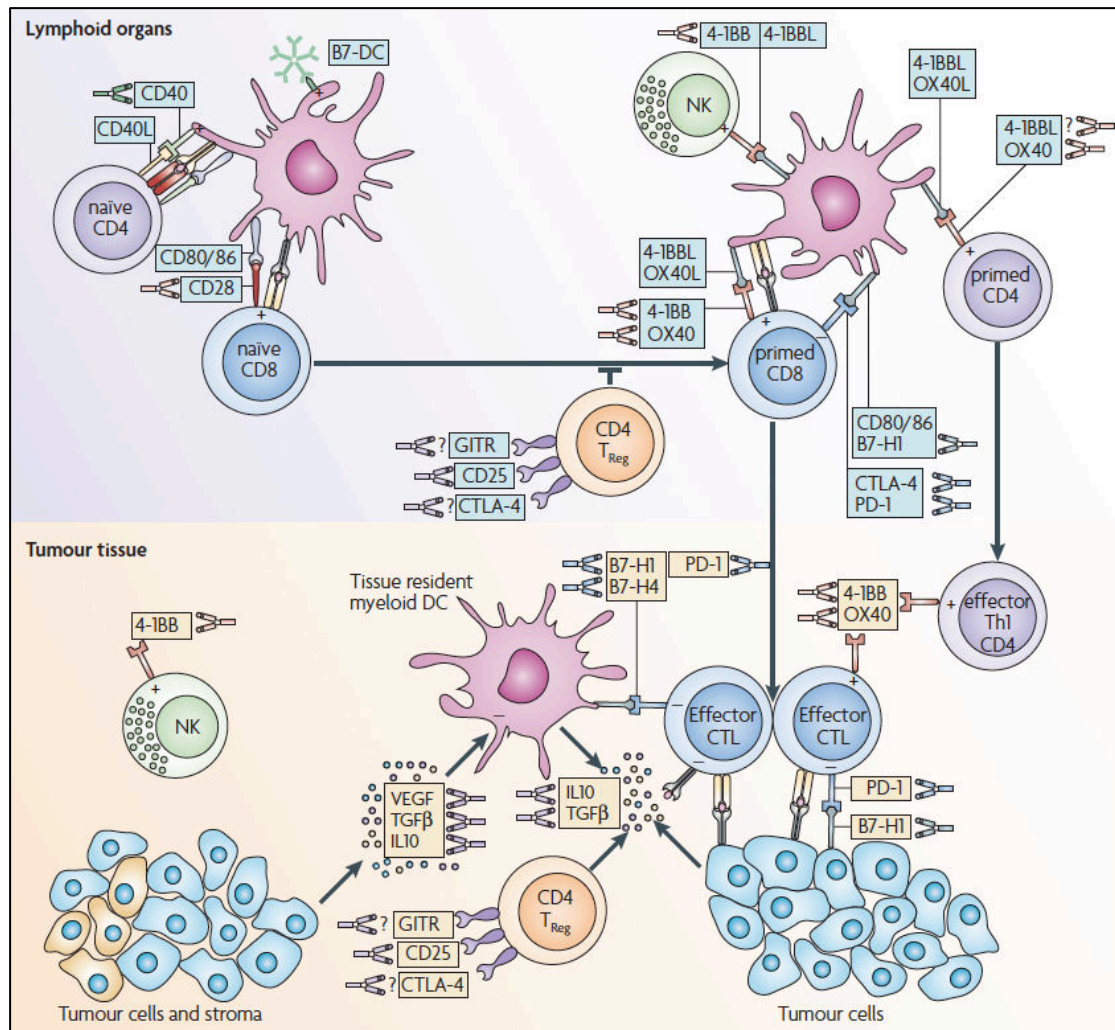


Figure 4 : Représentation schématique des points d'intervention des anticorps thérapeutiques activant la réponse immunitaire. Adapté de Melero et al. Nature reviews Cancer, 2007. [112].

2.4.3. Migration des lymphocytes T et infiltration des tumeurs

La migration et l'infiltration des effecteurs de la réponse immunitaire vers les cellules cancéreuses sont des étapes cruciales dans la lutte entre ces deux systèmes. En général, le niveau d'infiltration tumorale par les lymphocytes T CD8⁺ cytotoxiques prédit, de manière positive, la survie globale dans de nombreux types de cancer [113]. Néanmoins, dans certains types de cancers, comme les cancers du rein métastatiques, une faible infiltration des lymphocytes T CD8⁺ a une valeur pronostic

positive [114]. Ces données peuvent être expliqués par la présence de lymphocytes T CD8⁺ FoxP3⁺, qui ont une fonction régulatrice. Le degré d'infiltration tumorale par des lymphocytes T CD8⁺ a servi à la classification en tumeurs « infiltrées ou chaudes » en opposition aux tumeurs « peu/pas infiltrées ou froides ». Ces tumeurs chaudes ont une prédiction aux traitements anti-PD1 et anti-PD-L1 (discutés ultérieurement) beaucoup plus positives [115,116]. La notion d'immunoscore est basé sur la mesure du niveau d'infiltration de lymphocytes T CD8⁺ dans les différentes régions de tumeurs (centre ou périphérie) [117], et permet de prendre en compte des notions immunologiques dans la réponse aux traitements qui était moins ou pas prises en compte dans les précédentes évaluations biologiques chez les patients. En effet, la gradation des tumeurs était, jusqu'alors, plus basée sur la charge tumorale, l'invasion ganglionnaire et la présence de métastase. Cependant, le devenir clinique des patients est variable même si ils présentent les mêmes signes cliniques [118]. L'utilisation de l'immunoscore, a montré des résultats probants dans la prédiction aux rechutes notamment dans le cancer du colon [119] et du mélanome cutané [120]. Il est donc essentiel, dans le contexte de l'immunothérapie, d'induire une infiltration de cellules T efficace. Le diagnostic du cancer et les traitements qui en découlent changent d'approche.

L'amélioration de la migration des lymphocytes T vers la tumeur est en partie axée sur l'action des chimiokines. Kershaw et al. ont démontré que l'expression de CXCR2 (récepteur de CXCL1 sécrété par les cellules tumorales) dans les cellules T permettait à celles-ci de migrer efficacement vers les cellules tumorales *in vitro* [121]. De leur côté, Di Stasi et al. ont démontré que l'expression de CCR4 sur des cellules avec un récepteur chimérique pour l'antigène CD30 (CAR-T-CD30) améliorait la migration de ces cellules vers le lymphome d'Hodgkin CD30⁺ qui sécrète CCL17, le ligand de CCR4. En outre, le transfert adoptif de cellules T CCR4-CAR-CD30 a entraîné une activité anti-lymphome plus forte dans un modèle de souris xénotreffée en raison de la migration accrue des cellules CAR-T vers le site de la tumeur [122].

Après la migration des lymphocytes T vers le site tumoral, une autre barrière demeure : l'intravasation tumorale. Cette intravasation, discutée précédemment, peut être empêchée notamment par un phénomène appelé « anergie des cellules épithéliales » [123]. Cette anergie entraîne une sous-expression de molécules

d'adhésion telles que ICAM-1 ou VCAM-1 sur les cellules épithéliales. L'absence de ces molécules d'adhésion a pour conséquence une baisse de l'intravasation tumorale des lymphocytes T effecteurs spécifiques des cellules tumorales. Le ciblage du VEGF et de son récepteur, par un anticorps anti-VEGF, surmonte cette anergie en « normalisant » la vascularisation afin de permettre l'infiltration lymphocytaire [124].

2.4.4. Reconnaissance et destruction des cellules tumorales

Après avoir surmonté l'ensemble de ces écueils, les lymphocytes T arrivent au site d'action : la tumeur. Cependant, il existe un ensemble de barrières à franchir. Une de ces barrières est l'inhibition de la réponse T spécifique aux tumeurs par un ensemble de molécules exprimées, après activation, sur les lymphocytes T. Un des mécanismes de régulation négatif passe par la voie de signalisation impliquant PD1 et PD-L1. La liaison de PD1 avec son ligand PD-L1, exprimé par les cellules tumorales et les cellules myéloïdes suppressives (MDSC), inhibe la prolifération des lymphocytes T, la sécrétion de cytokines et leur capacité cytotoxique [125]. De plus chez la souris, l'engagement de PD1 a montré qu'il entraînait une expression de FoxP3, dans les lymphocytes T CD4⁺, et donc l'induction de Treg induit [126]. Il a été aussi montré que l'expression de PD1 sur des macrophages humains et murins inhibait leur potentiel de phagocytose contre les cellules tumorales [127]. Cette voie de régulation du système immunitaire est utilisée par les cellules tumorales et leur microenvironnement pour développer des résistances immunitaires. L'expression de PD-L1 a été retrouvée dans un grand nombre de tumeur notamment les cellules tumorales, les macrophages et sur les lymphocytes infiltrant la tumeur (TIL) [128]. L'injection d'anticorps bloquant l'interaction PD1/PD-L1 a montré des effets bénéfiques dans des modèles de tumeurs de souris [129,130]. D'autres molécules, qui sont exprimées à la surface des cellules T activées, telles que LAG-3, TIM-3 ou TIGIT agissent également comme des inhibiteurs de la réponse immunitaire si ils fixent leur ligand présent sur les cellules tumorales ou sur les MDSC. L'utilisation d'anticorps, bloquant leur interaction avec leur ligand, a permis d'obtenir des effets

positifs dans différents modèles de tumeurs murines [131–133]. Ces molécules sont considérées comme faisant parti des marqueurs de lymphocytes T épuisés. Le concept d'épuisement des lymphocytes T a été décrit pour la première fois lors d'une infection chronique virale chez la souris [134] et semble corrélé avec une forte concentration antigénique [135]. Les lymphocytes T épuisés perdent progressivement leur capacité de prolifération, de production de cytokines et leurs capacités cytotoxiques. Il a été montré que la combinaison de traitement ciblant plusieurs de ces marqueurs dans des modèles de cancer permettait d'obtenir une réponse anti-tumorale [131,132].

Les stratégies impliquant les levées de l'inhibition du système immunitaire, à l'aide d'anticorps bloquants les points de contrôle négatifs, prennent une place prépondérante dans l'essor des nouvelles immunothérapies mais il existe des stratégies permettant d'augmenter davantage leur efficacité en activant les lymphocytes T. ICOS (Inducible T cell co-stimulator) est exprimé par les cellules T activées et son interaction avec son ligand, ICOS-L, entraîne une augmentation de leurs fonctions effectrices, notamment par la production de cytokines, telle que l'IL-10 impliquée dans la régulation des Treg [136]. L'induction de ICOS, par un anticorps agoniste, est un bon candidat d'immunothérapie notamment en combinaison avec un traitement anti-CTLA-4 car les voies d'activation via CTLA-4 semble requérir l'implication d'ICOS [137]. Une autre molécule ciblée dans l'immunothérapie est GITR. GITR est exprimé sur les lymphocytes T activés et sur les Treg de façon constitutive. Il a été montré que la modulation de GITR, par des anticorps agonistes, entraîne une activité anti-tumorale qui peut être attribuée à son rôle co-stimulateur dans les lymphocytes T conventionnels mais aussi à un effet déplétant des Treg intra-tumoraux [138].

La tumeur est aussi capable de priver les lymphocytes T de leurs nutriments, notamment le tryptophane. Cette privation entraîne une baisse de la prolifération lymphocytaire [139]. En effet, l'expression par les tumeurs de l'enzyme IDO (indoleamine-pyrrole-2,3-dioxygenase-1,2), qui catalyse ce tryptophane, est associée à des résistances thérapeutiques [140]. L'utilisation d'inhibiteur d'IDO a montré un effet synergique, pour l'élimination des tumeurs, avec d'autres anticorps modulant le système immunitaire [141,142].

3. Etat des lieux des thérapies du cancer : place de l'immunothérapie

Le traitement du cancer a été un processus évolutif à travers les âges en commençant par la chirurgie (**Figure 5**). L'ablation d'une tumeur a été, pendant longtemps, le seul traitement des tumeurs solides et reste aujourd'hui l'un des traitements principaux. Les progrès significatifs de la chirurgie ont été la découverte de l'anesthésie générale et la découverte de l'asepsie. Les effets indésirables liés à la chirurgie sont communs à tous types de chirurgie : fatigue, douleur cicatricielle, saignement ou infection nosocomiale. De plus, l'ablation ganglionnaire est associée à des effets indésirables dus aux modifications du drainage lymphatique. La chirurgie peut être associée à des chimiothérapies ou des radiothérapies en traitement adjuvant ou néo-adjuvants. Réalisés avant la chirurgie, les traitements néo-adjuvants ont pour objectif de réduire la taille tumorale afin d'en faciliter l'ablation ultérieure. Réalisés après la chirurgie, les traitements adjuvants ont pour objectif d'éliminer les cellules cancéreuses encore présentes localement (radiothérapie) ou présentes dans l'ensemble de l'organisme (chimiothérapie).

La radiothérapie est un traitement locorégional des cancers. L'utilisation de rayons pour détruire les cellules cancéreuses doit beaucoup à Marie Curie et à ses découvertes sur les rayonnements ionisants du polonium et du radium qui furent récompensées par deux prix Nobel. Trois types de radiothérapies existent : la radiothérapie externe (source de rayonnement externe au patient et dirigée vers la masse tumorale à détruire), la curiethérapie (source de rayonnement placée dans le patient au plus proche de la tumeur) et la radiothérapie métabolique (administration orale ou par voie veineuse d'une substance radioactive qui se fixe préférentiellement sur les cellules cancéreuses). Les effets indésirables associés à la radiothérapie sont liés aux principes de la radiation, qui même ciblée, altère les cellules saines environnant la tumeur. Les conséquences peuvent être temporaires ou persistantes et sont situées aux niveaux des zones corporelles irradiées.

La chimiothérapie est un traitement utilisant des molécules chimiques qui agissent directement contre les cellules cancéreuses. Contrairement à la chirurgie et à la

radiothérapie, la chimiothérapie cible l'ensemble des cellules cancéreuses même celles non détectées par examen. Les chimiothérapies agissent sur les cellules qui possèdent un haut niveau de prolifération en les détruisant ou en empêchant leur prolifération. Les effets indésirables associés à la chimiothérapie sont liés à leur action sur toutes les cellules en division. La chimiothérapie agit notamment sur les cellules hématopoïétiques pouvant entraîner une leucopénie, anémie et/ou thrombopénie. De par l'absence de ciblage des cellules tumorales, les chimiothérapies peuvent entraîner des troubles dans divers organes : foie, rein, peau...

Cependant ces approches thérapeutiques, malgré une efficacité notable, ont montré leurs limites : incapacité à éliminer l'ensemble de la charge tumorale notamment à cause des métastases (chirurgie et radiothérapie) et de la résistance aux traitements (radiothérapie et chimiothérapie).

D'autres approches thérapeutiques ont été développées impliquant le système immunitaire.

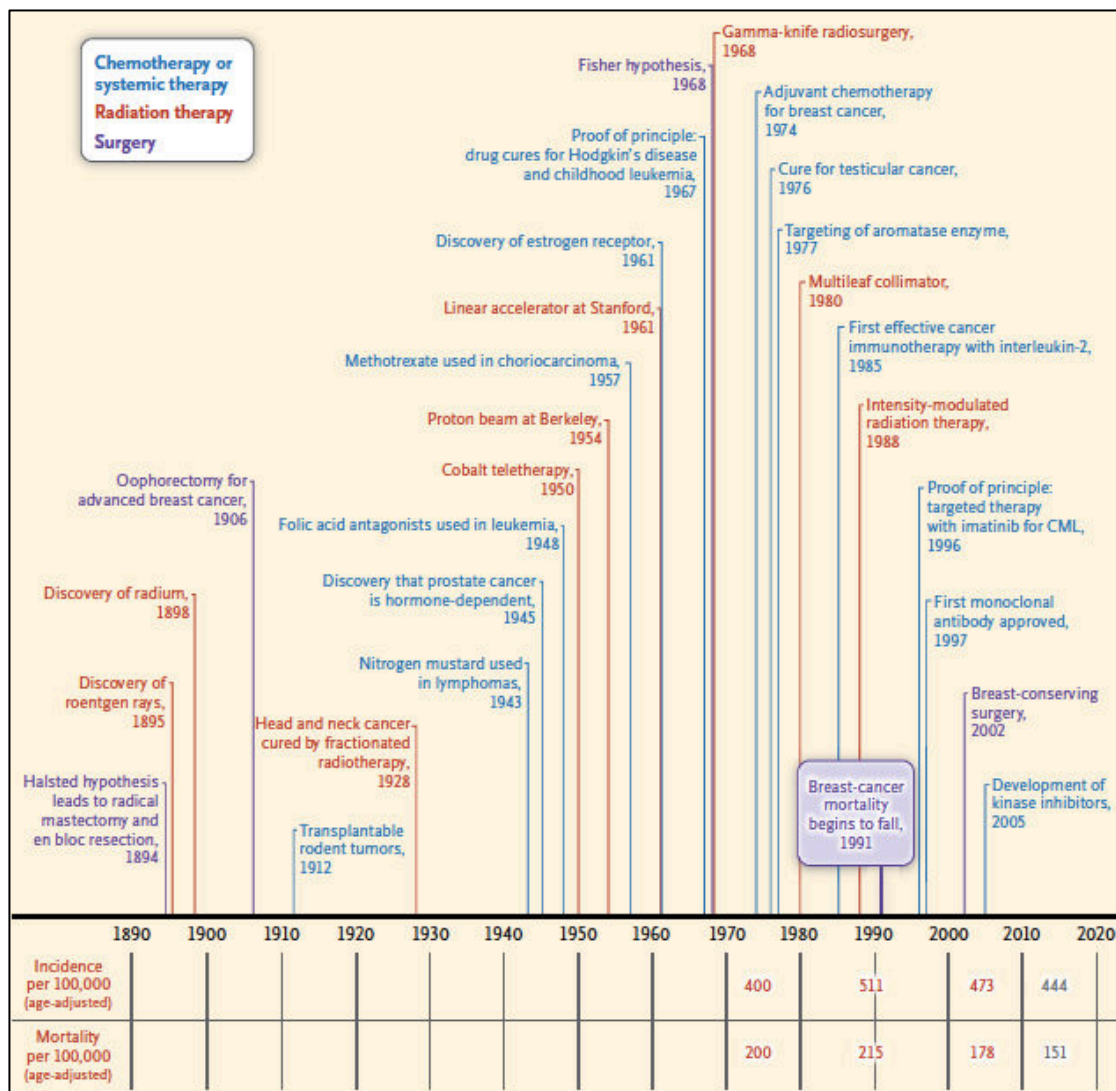


Figure 5 : Chronologie des événements cruciaux dans le traitement du cancer.

Adapté de DeVita et al. *New England Journal of Medicine*. 2012. ref

3.1. Cytokines

L'utilisation de cytokines comme immunothérapie contre le cancer repose sur l'observation que les cytokines sont des acteurs majeurs de la régulation du système immunitaire. Les cytokines peuvent être utilisées comme adjuvant dans les stratégies vaccinales notamment avec l'utilisation du facteur stimulant la formation de colonie granulocytaire (GM-CSF) pour stimuler la réponse innée. Cependant, l'utilisation de cytokines seules a été parmi les premières immunothérapies à obtenir des autorisations de mises sur le marché. L'IFN- α a obtenu cette autorisation en 1986 pour traiter les leucémies à tricholeucocytes et a vu sa posologie étendue à d'autres

cancers hématologiques (sarcome de Kaposi, leucémie myéloïde chronique) [143–145]. L'IFN- α induit l'expression de molécules de CMH I à la surface des cellules tumorales, joue un rôle positif dans la maturation des DC, possède des propriétés anti-angiogéniques et induit l'apoptose des cellules tumorales [146]. Toutefois, cette efficacité est associée à une forte toxicité liée à un syndrome grippal et à des neurotoxicités [147]. L'IL-2 a, de son côté, obtenu son autorisation de mise sur le marché, en 1992, pour traiter les cancers rénaux métastatiques [148] et en 1998 pour les mélanomes [149]. Comme expliqué précédemment, l'utilisation de l'IL-2 à forte dose permet l'activation non seulement des récepteurs de haute affinité à l'IL-2 (présent sur les Tregs) mais aussi les récepteurs à affinité intermédiaire présents à la surface des cellules T CD8⁺ et NK. Cette efficacité a pour conséquence un relargage secondaire de cytokine qui est associée à une forte toxicité incluant hypotension et syndrome de fuite vasculaire [150]. Une stratégie pour garder cette efficacité sans toxicité pourrait être l'utilisation de complexe IL-2/anticorps anti-IL-2, comme décrit précédemment dans les études chez la souris [151,152].

Il a été montré que, lorsque l'IL-2 est complexée avec un anticorps monoclonal anti-IL-2, en fonction de la spécificité fine de l'anticorps, ce complexe peut réorienter de préférence l'action de l'IL-2 vers Treg ou les lymphocytes T CD8⁺ et les cellules NK fondamentales pour former une réponse immunitaire anti-tumorale efficace [151]. De plus, les complexes IL-2 ont une demi-vie plus longue que l'IL-2 ordinaire, et donc une meilleure pharmacodynamique [153]. Un obstacle majeur au traitement à haute dose avec l'IL-2 est la toxicité grave due à l'apparition d'un syndrome de fuite vasculaire. En effet, l'œdème pulmonaire associé à l'IL-2 semble être provoqué par une interaction directe de l'IL-2 avec les récepteurs fonctionnels de l'IL-2 (IL-2R α , CD25) sur les cellules endothéliales pulmonaires *in vivo* [154]. Cet effet secondaire peut également être abrogé par l'utilisation de complexe IL-2 dirigée sur IL-2R $\beta\gamma$, qui devrait éviter l'activation via CD25 sur les cellules endothéliales. Des études récentes sur des modèles murins de cancer ont montré que les complexes IL-2 dirigés sur IL-2R $\beta\gamma$ peut stimuler la réponse antitumorale en induisant une stimulation plus spécifique des cellules T NK et CD8⁺ [155].

D'autres cytokines sont en phase d'évaluation clinique telle que l'IL-12 ; cytokine impliquée dans les réponses immunitaires innée et adaptative ainsi que dans des

processus anti-angiogéniques [156]. Les premiers résultats ont montré une toxicité sévère entraînant la mort de deux patients sur les dix-sept enrôlés dans l'essai clinique.

3.2. Vaccins

La stratégie vaccinale repose sur l'expression par les cellules cancéreuses de TAA. Elle est divisée en deux catégories : les vaccins préventifs et les vaccins thérapeutiques.

Le but des vaccins préventifs est d'empêcher le cancer de se développer. Le Gardasil® et le Cervarix® sont les deux vaccins utilisés contre les cancers viro-induits par le papillomavirus humain (HPV), administrées chez les adolescentes en prévention du cancer du col de l'utérus. Ces vaccins, composés d'une protéine virale de la capsid : L1, a montré des protections efficaces contre l'infection à l'HPV [157]. L'utilisation des vaccins préventifs dans les cancers non-viro-induits est difficilement envisageable car les origines des mutations sont trop différentes d'un patient à l'autre.

Les vaccins thérapeutiques ciblent les tumeurs déjà établies. Le but est d'apporter au système immunitaire des signaux lui permettant d'enclencher une réponse immunitaire spécifique adaptée. Ces signaux sont de deux ordres : un TAA et un adjuvant. Trois types de stratégie vaccinales sont développées : la stratégie utilisant des peptides ou des protéines, la stratégie basée sur l'utilisation des cellules tumorales et la stratégie basée sur l'injection d'APC **Figure 6**. La stratégie peptidique a reposé, en premier lieu, sur l'injection de peptide, dérivé de TAA, restreint au CMH de classe I afin d'activer les lymphocytes T CD8⁺ spécifiques. L'ajout d'adjuvant est nécessaire afin d'induire une réponse immunitaire suffisante, notamment pour l'activation des CPA. Les adjuvants sont des signaux non-antigéniques activant le système immunitaire tels que des ligands de TLR, des signaux de danger tissulaire ou des facteurs de croissance cellulaire. Du fait que les peptides injectés étaient restreints au CMH de classe I, les lymphocytes T CD4⁺ n'étaient pas activés ce qui peut limiter l'action des lymphocytes T CD8⁺. L'utilisation de peptides longs synthétiques contenant des épitopes restreints par les molécules de CMH I et II a été une stratégie pour obtenir une meilleure activation du système immunitaire [158]. Cependant, à ce jour, malgré des résultats encourageants dans les modèles murins, il

n'existe pas de vaccins peptidiques avec des effets cliniques chez l'homme suffisamment positifs pour obtenir d'autorisation de mise sur le marché.

Une autre stratégie vaccinale thérapeutique est l'utilisation des cellules tumorales elle-même. La stratégie est basée sur l'injection de cellules tumorales mortes afin de délivrer des antigènes tumoraux au système immunitaire. Ces cellules peuvent aussi être modifiées pour exprimer des cytokines, recrutant des APC, tel que le facteur stimulant la formation de colonies de macrophages et ce cellules dendritiques GM-CSF [159].

Une stratégie vaccinale efficace chez la souris est l'injection d'ADN codant pour un antigène tumoral couplé ou administré avec des adjuvants [160]. Cependant chez l'homme, l'utilisation d'ADN seul a montré peu d'efficacité avec une faible immunogénicité. L'amélioration des injections, notamment par électroporation *in vivo*, l'ajout de nouveaux adjuvants ou l'utilisation séquentielle d'ADN suivie par un rappel vaccinal basé sur les virus a montré des résultats encourageants [161].

L'unique stratégie vaccinale thérapeutique qui a donné lieu à une autorisation de mise sur le marché par la FDA est celle basée sur l'utilisation des APC. Provenge® est une vaccination basée sur l'injection de cellules dendritiques autologues de patients atteints de cancer de la prostate au stade métastatique. Ces cellules dendritiques sont obtenues par culture *in vitro* de CSH des patients et activées par une protéine de fusion PA2024, composée d'un TAA exprimé par une majorité de cancer de la prostate : la phosphatase acide prostatique (PAP) et du GM-CSF [162]. La survie globale des patients traités par Provenge® est augmentée de quatre mois comparée à la survie des patients ayant reçu un placebo.

De l'ensemble des essais thérapeutiques vaccinaux chez l'homme, bien que des réponses immunitaires soient détectées chez les patients, il semble que l'induction d'une réponse anti-tumorale par un vaccin est insuffisante pour observer des réponses cliniques. La combinaison de ces stratégies vaccinales avec d'autres telles que l'utilisation d'inhibiteurs de point de contrôle fait l'objet d'un grand nombre d'études actuellement.

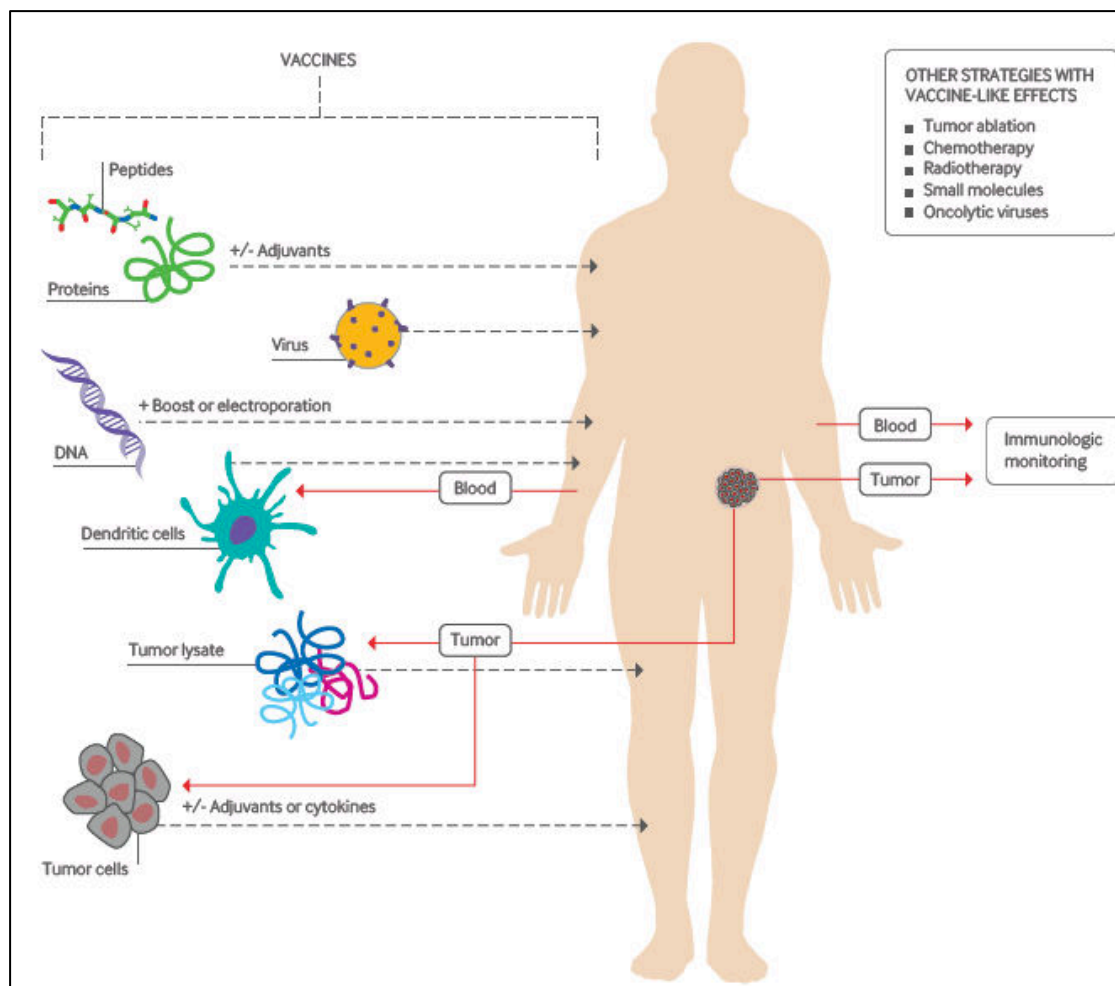


Figure 6 : Approches vaccinales appliquées au cancer. *Adapté de Butterfield. BMJ 2015, [161].*

3.3. Thérapies ciblées

Les thérapies ciblées utilisent des molécules, ciblant les cellules tumorales, qui bloquent la croissance et/ou la dissémination tumorale. Elles diffèrent des chimiothérapies conventionnelles par le ciblage de molécules précises exprimées par des cellules tumorales ; ainsi les thérapies ciblées sont plus des thérapies personnalisées qui demandent un criblage moléculaire des tumeurs afin d'identifier les cibles spécifiques. Il existe différentes stratégies de thérapies ciblées qui agissent via divers mécanismes : blocage d'une voie oncogénique par un anticorps monoclonal inhibant un récepteur surexprimé à la surface des cellules tumorales, anticorps monoclonal induisant la cytotoxicité à médiation cellulaire dépendante des anticorps

(Antibody-Dependent Cell-mediated Cytotoxicity: ADCC), petites molécules pénétrant la membrane cellulaire inhibant la voie de signalisation intracellulaire, anticorps liés à des drogues cytotoxiques, inhibiteurs de transduction du signal et inhibiteurs d'angiogenèse. Un exemple du panel d'utilisation de ces thérapies ciblées est utilisé dans le cas des cancers du sein exprimant le récepteur épidermique humain de type 2 (HER2). La surexpression de la protéine HER2 est présente dans environ 25% des cancers du sein HER2 [163]. Le proto-oncogène *HER2* code pour la glycoprotéine transmembranaire HER2 qui appartient à la famille des récepteurs de facteurs de croissance épidermiques à activité tyrosine kinase, impliqué notamment dans la prolifération cellulaire, la survie et l'invasion tumorale. L'activation d'un récepteur de la famille HER nécessite l'homodimérisation ou l'hétérodimérisation de celui-ci, entraînant une phosphorylation des résidus à activité tyrosine kinase du domaine intracellulaire [164]. La surexpression de HER2 à la surface des cellules tumorales entraîne sa dimérisation, même en absence de ligand, induisant la transduction du signal en intracellulaire et l'activation des deux principales voies de signalisation sous-jacentes : la voie RAS/Raf/Mitogen-activated protein kinase (MAPK) et la voie phosphoinositide 3-kinase (PI3K)/AKT/mTOR. Ces cancers HER2⁺ sont la cible de plusieurs stratégies de thérapies ciblées. Tout d'abord, L'Herceptin[®] et le Perjeta[®] sont des anticorps monoclonaux dirigés contre HER2 et qui induisent à la fois une diminution de la signalisation de HER2 dans les cellules tumorales et une ADCC des cellules tumorales [165]. Le même anticorps, l'Herceptin[®] ou « Trastuzumab », a été couplé à l'emtansine qui est un agent ayant une activité cytotoxique liée à l'inhibition de l'assemblage des microtubules pour former le Kadcylla[®]. Ce procédé permet l'internalisation de la chimiothérapie spécifiquement dans les cellules tumorales cibles présentant une surexpression de HER2 et permet donc d'augmenter l'index thérapeutique de l'emtansine. L'utilisation du Kadcylla[®] en monothérapie ou en combinaison avec l'Herceptin[®] a montré une amélioration de la survie globale pour des patientes porteuses d'un cancer du sein HER2⁺ métastatiques avec des effets indésirables apparaissant plus tardivement que les traitements usuels que sont la capécitabine et le Tykerb[®] [166]. Une autre stratégie, ciblant HER2, est l'utilisation de petites molécules, pénétrant la membrane cellulaire, qui bloquent l'activité tyrosine/kinase de la partie intra-cytoplasmique de HER2 : le Nerlynx[®], le

Tykerb[®], et le Giotrif[®]. Le développement du nombre croissant de ces molécules de thérapies ciblées entraîne une difficulté pour les médecins à choisir la molécule la plus adaptée aux différents types de tumeur ou à leurs stades d'évolution.

D'autres cibles tumorales ont été la source de développement de thérapies ciblées. Un membre de la même famille de récepteur que HER2, le récepteur aux facteurs de croissance épidermiques (EGFR) est sur-exprimé dans une proportion faible, mais significative, de cancers du poumon non à petites cellules (NSCLC). Le Tarceva[®] et l'Iressa[®] sont des petites molécules ayant le même mode d'action que le Tykerb[®] et ses affiliés. Leur utilisation a montré des réponses durables dans les tumeurs mutées pour l'EGFR [167,168]. Le blocage des voies de signalisation dans les cellules tumorales est un axe important de l'utilisation des thérapies ciblées. La voie de signalisation PI3K/AKT/mTOR régule le cycle cellulaire, la prolifération et la survie [169]. Elle est souvent fortement altérée dans les cancers entraînant une sur-activation de la prolifération cellulaire [170]. Des inhibiteurs de cette voie sont utilisés dans des leucémies et des lymphomes : l'Idelalisib[®] et le Copanlisib[®].

Les thérapies ciblées peuvent aussi inhiber l'angiogenèse nécessaire à la croissance tumorale. Le blocage de l'activité du facteur de croissance endothélial vasculaire (VEGF) par des petites molécules de type inhibiteur de tyrosine/kinase (Nexavar[®], Sutent[®]) ou par un anticorps anti-VEGF (Avastin[®]) sont utilisés en clinique dans un nombre croissant de cancer, notamment l'Avastin[®] qui est utilisé dans les cancers du colon, du poumon, du sein, du rein, de l'ovaire et du glioblastome.

3.4. Thérapies cellulaires

Un développement important dans l'immunothérapie anti-cancer est celui du transfert adoptif de cellules T (ACT). Trois formes d'ACT ont été développées : les TIL, les cellules T exprimant un TCR modifié et les cellules exprimant un récepteur antigénique chimérique (CAR-T cells).

Des études *in vitro* ont montré, dans des mélanomes, la présence de TIL capables de reconnaître de façon spécifique des cellules tumorales [171]. Cette étude a ouvert la

voie à la première utilisation de TIL autologues, expandues *in vitro* et injectées au patient, comme outil permettant une régression tumorale chez des patients atteints de mélanomes métastatiques [148]. Malgré un effet anti-tumoral certain, les réponses étaient souvent de courte durée et les TIL, transférés chez les patients, étaient retrouvés dans de faibles proportions dans le sang quelques jours après injection. Une amélioration significative a été apportée en déplaçant les lymphocytes du patient avant le transfert des TIL. Des patients, atteints de mélanome métastatique, ont reçu une chimiothérapie lymphodéplétante (cyclophosphamide et fludarabine) non myéloablatrice suivie d'injection de TIL et d'IL-2. 10 patients sur 13 ont montré des signes de régression tumorale, cependant accompagné de destruction auto-immune de mélanocytes [172] montrant les progrès encore à effectuer dans ce domaine.

Une évolution des thérapies cellulaires a été le développement de lymphocytes T transgéniques soit pour des TCR spécifiques soit pour des CAR. Ces deux stratégies diffèrent par leurs mécanismes de reconnaissance de l'antigène et leur signalisation intracellulaire mais repose sur le même principe : la reconnaissance spécifique d'un antigène tumoral via un récepteur à la surface des cellules T tueuses. Les caractéristiques de ces deux systèmes (résumées dans le **Tableau 1**) présentent une différence majeure : la nécessité pour les lymphocytes T à récepteurs spécifiques de reconnaître les molécules de HLA (Human leucocyte antigen) à la surface des cellules tumorales contrairement aux cellules CAR-T. En effet, les thérapies, ayant utilisé les lymphocytes T à récepteur spécifique modifiés, sont basées sur une reconnaissance spécifique du TCR avec les molécules de HLA-A2 à la surface des cellules tumorales. Les premières thérapies, utilisant ces cellules, ont ciblé un antigène de mélanome métastatique, MART-1 [173]. Par la suite, un TCR, ciblant l'épitope MART1, avec une avidité plus élevée, a été développé dans le but d'obtenir une meilleure reconnaissance des cellules tumorales présentant une expression plus faible de MART-1. Cependant, cette meilleure avidité entraîne une reconnaissance des mélanocytes non tumoraux et donc l'apparition d'effets secondaires néfastes [174]. Cette stratégie cellulaire a longtemps ciblé des antigènes non spécifiques des tumeurs tel que MART-1, MAGE-A3 [175] ou NY-ESO-1 [176], à de rares exceptions près, comme l'utilisation d'un TCR spécifique d'une forme mutée de ERB2 dans le

cancer du canal biliaire [177]. Malgré des résultats encourageants, un des principaux mécanismes d'échappement des cellules tumorales au système immunitaire est la perte d'expression des molécules HLA à leurs surface [178], ce qui rend inefficace l'utilisation de ces lymphocytes T à récepteurs spécifiques modifiés. Par conséquent, le développement des cellules CAR-T est devenu plus important notamment car les cellules CAR-T et leurs récepteurs sont capables de reconnaître des antigènes en absence de reconnaissance HLA [179,180]. Les cellules CAR-T expriment à leur surface un CAR qui combine le domaine de fixation à l'antigène d'intérêt, dérivé de la chaîne variable de l'anticorps, avec le domaine intracellulaire de signalisation du TCR. Des améliorations ont été apportées, dans les dernières générations de cellules CAR-T, notamment par l'ajout de molécules co-stimulatrices (CD27, CD28, CD134, CD137 ou ICOS) **Figure 7** [181].

Actuellement, une seule thérapie utilisant des cellules CAR-T vient d'obtenir l'approbation clinique de la FDA, en 2017. Le Kymriah®, développé par Novartis, cible CD19 dans les lymphomes non-hodgkinien et dans les leucémies lymphoblastiques sévères à cellules B. L'écueil majeur dans l'utilisation des thérapies cellulaires est la toxicité induite (toxicité neurologique, syndrome aigu des cytokines) dûe à l'action des cellules CAR-T ou dûe à l'immunogénicité des séquences utilisées pour synthétiser le CAR [182]. Pour l'instant, les mécanismes mis en œuvre sont peu compris et nécessiteraient certainement des modèles pour les étudier davantage, notamment des modèles animaux.

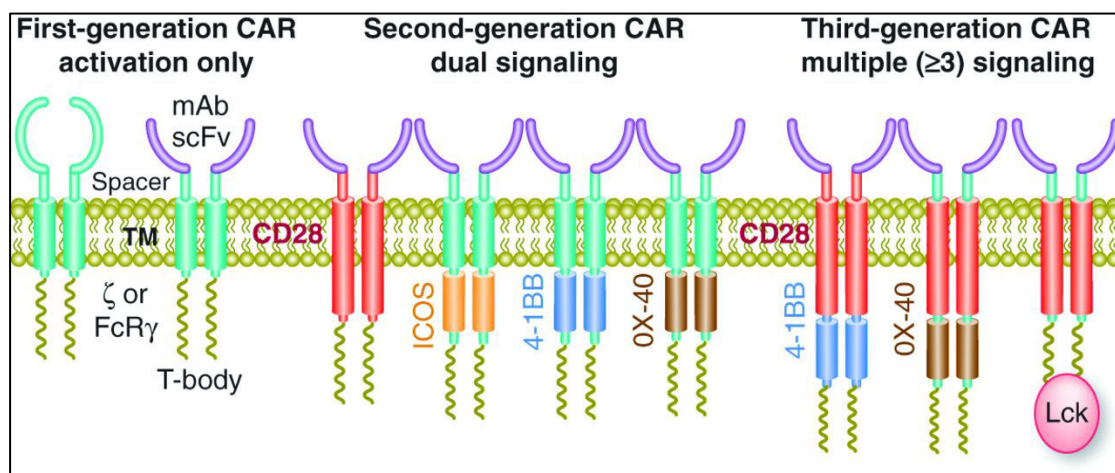


Figure 7 : Evolution des CAR-T. *Adapté de Sadelain et al. Cancer Discovery. 2013. [181].*

Lymphocytes T à récepteur spécifique	Cellules CAR-T
Faible avidité (peut être augmentée)	Avidité contrôlable
Peut cibler l'ensemble des antigènes des cellules cancéreuses	Peut cibler uniquement les antigènes de surface
Reconnaissance des cellules tumorales HLA-dépendante	Reconnaissance des cellules tumorales HLA-indépendante
Survie des cellules injectées tout au long de la vie	Survie longue des cellules injectées (au moins une décennie)
Toxicité « off-target » difficile à prévoir (dépendante de l'antigène, du TCR)	Syndrome de relargage cytokinique sévère et neurotoxicité

Tableau 1 : Différence entre les lymphocytes T à récepteur spécifique et les cellules CAR-T. *Adapté de June et al. Science, 2018. [183].*

3.5. Virus oncolytiques

L'utilisation des virus oncolytiques comme immunothérapie contre le cancer est basée sur la capacité de virus génétiquement, ou non, modifiés de se répliquer sélectivement dans les cellules tumorales et ainsi d'entraîner leur destruction. L'observation que des patients atteints de cancer entraient en rémission suite à une infection virale est ancienne [184]. Les mécanismes à travers lesquels les virus oncolytiques entraînent un rejet tumoral sont mal connus. Cependant, la réplication virale entraîne la mort de la cellule tumorale avec comme conséquence l'initiation d'une réponse immunitaire. En effet, cette mort cellulaire induit un relargage d'antigènes tumoraux qui peuvent servir à promouvoir une réponse immunitaire adaptative. Le seul virus oncolytique à avoir obtenu l'approbation de la FDA, Imlygic®, est un virus *Herpes simplex* de type 1 atténué (HSV-1) produit par délétion fonctionnelle de deux gènes (ICP34.5 et ICP47), encodant aussi pour le GM-CSF,

injecté dans les mélanomes cutanés. L'addition du GM-CSF permet d'attirer les cellules dendritiques au site de mort tumorale et d'induire une réponse T cytotoxique. Le ciblage des cellules tumorales se fait par l'injection des virus oncolytiques en intra-tumoral et par le tropisme des virus pour des protéines de surface qui sont exprimées par les cellules tumorales. **Figure 8.**

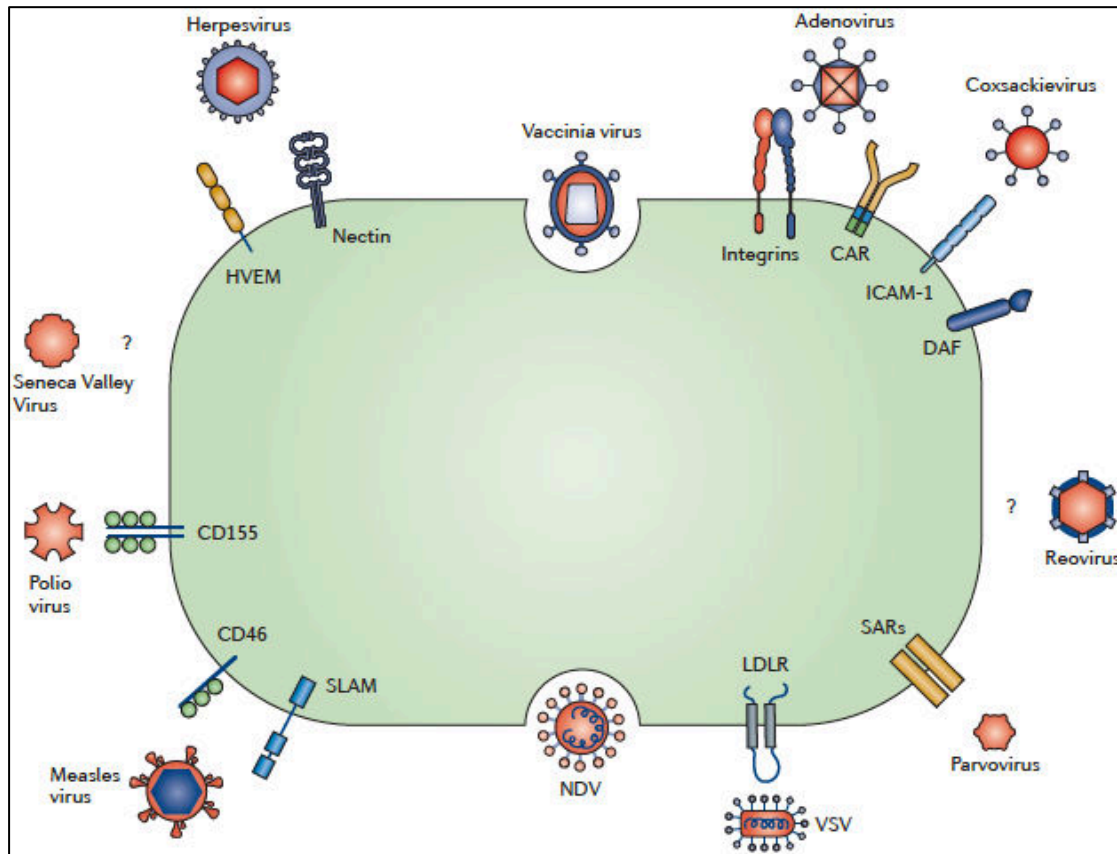


Figure 8 : Mécanismes d'entrée des virus dans les cellules cancéreuses. *Adapté de Kaufman et al. Cancer immunotherapy, 2015. [185].*

3.6. Anticorps régulant des points de contrôle du système immunitaire

L'utilisation d'anticorps monoclonaux ciblant les points de contrôle négatif du système immunitaire a montré un énorme potentiel dans le traitement du cancer. A ce jour, six anticorps bloquants ont l'approbation de la FDA. Ils ciblent soit CTLA-4 : Yervoy® (Bristol-Myers Squibb), soit PD1 : Opdivo® (Bristol-Myers Squibb) et Keytruda® (Merck), soit PD-L1 : Tecentriq® (Genentech/Roche), Bavencio® (Pfizer) et

Imfinzi® (Astrazeneca). Les mécanismes d'action de ces anticorps chez l'homme sont encore mal connus. Des études chez la souris ont montré que les anticorps anti-PD1 avaient une double action en ciblant les lymphocytes T effecteurs et en modifiant le métabolisme glucidique de l'environnement tumoral. Il a notamment été montré qu'une certaine population de lymphocytes T CD8⁺ proliférait après injection d'anticorps anti-PD1. Ces lymphocytes T CD8⁺ expriment CXRC5, CD28 et PD1^{low} [186,187]. Il a, notamment, été montré que les lymphocytes T CD8⁺ proliférant dans le sang, après injection d'anticorps anti-PD1, exprimaient majoritairement CD28 [187]. Ces cellules n'expriment pas des marqueurs de fort épuisement tel que PD1^{high}, Tbet^{low}, Eomes^{high} ou plus particulièrement TIM3 qui a été montré comme étant associé à une résistance clinique aux anti-PD1 [188,189]. D'autre part, il a été montré que le mécanisme par lequel des tumeurs, en consommant le glucose de l'environnement tumoral, inhibent les lymphocytes T est bloqué par l'administration d'anticorps anti-PD1 mais aussi d'anticorps anti-PD-L1 et anti-CTLA-4, chez la souris [190].

Par ailleurs, un ensemble d'anticorps ciblant d'autres points de contrôle du système immunitaire sont actuellement en phase d'évaluation dans des essais cliniques. Ils peuvent moduler la réponse immunitaire soit par une activation cellulaire (4-1BB, ICOS, GITR, CD27, OX40 ou CD40) soit en inhibant des phénomènes régulateurs négatifs (CD70, VISTA, B7-H3, TIM-3, LAG-3, KIRDL). **Tableau 2.**

Cible	Indication tumorale	Nom	N° d'essai clinique
CTLA-4 (bloquant)	Mélanome	Yervoy®	Approbation clinique
PD1 (bloquant)	Mélanome métastatique Poumon (NSCLC) Lymphome d'Hodgkin ORL Carcinome urotheliale métastatique Carcinome hépatocellulaire	Opdivo®	Approbation clinique

	Colorectal avec des aberrations MSI et MMR		
PD1 (bloquant)	Mélanome métastatique Poumon (NSCLC) Lymphome d'Hodgkin ORL Cancer gastrique Carcinome urotheliale métastatique Tumeur solide avec des aberrations MSI et MMR	Keytruda®	Approbation clinique
PD-L1 (bloquant)	Carcinome urotheliale métastatique Poumon (NSCLC)	Tecentriq®	Approbation clinique
PD-L1 (bloquant)	Carcinome des cellules de Merkel Carcinome urotheliale métastatique	Bavencio®	Approbation clinique
PD-L1 (bloquant)	Carcinome urotheliale métastatique	Imfinzi®	Approbation clinique
4-1BB (CD137 agoniste)	Lymphomes multiples Tumeurs solides métastatiques	Utomilumab	NCT01307267 NCT02444793 NCT02315066 NCT02554812
ICOS (CD278 agoniste)	Pas de restriction tissulaire	GSK3359609 JTX-2011	NCT02723955 NCT02904226
GITR (CD357 agoniste)	Mélanome et tumeur solides	TRX518-001 MK-4166	NCT01239134 NCT02628574 NCT02132754
CD70 (bloquant)	Cancer avancé	ARGX-110	NCT01813539 NCT02759250

CD27 (agoniste)	Cancer hématologique et tumeurs solides	Varlilumab	NCT01460134 NCT02335918
OX40 (CD134 agoniste)	Cancer avancé	9B12 MOXR0916 PF-04518600 MEDI6383	NCT01644968 NCT02410512 NCT02219724 NCT02315066 NCT02221960
CD40 (agoniste)	Mélanome Tumeurs solides	CP-870,893 RO7009789	NCT01103635 NCT02304393
VISTA (B7-H5 bloquant)	Cancer avancé et lymphome	CA-170 JNJ-61610588	NCT02812875 NCT02671955
B7-H3 (CD276 bloquant)	Mélanome et poumon (NSCLC)	enoblituzumab	NCT02381314
TIM-3 (bloquant)	Cancer avancé	TSR-022 MBG453	NCT02817633 NCT02608268
LAG-3 (CD223 bloquant)	Cancer avancé Mélanome Cancer avancé	Relatlimab IMP321 LAG525	NCT01968109 NCT02061761 NCT02658981 NCT02676869 NCT02460224
KIR2DL-1,-2,- 3 (bloquant)	Leucémie, lymphome et tumeurs solides	Lirilumab	NCT01714739 NCT02599649 NCT02399917 NCT02481297 NCT01687387

IDO-1,2 (inhibiteur)	Tumeurs solides	1-methyl-d-tryptophan	NCT00567931
			NCT01191216
	Pancréas, mélanome, sein	Indoximod	NCT02077881
			NCT02073123
	Tumeurs solides		NCT01792050
	Tumeurs solides	GDC-0919	NCT02048709
	Mélanome et tumeurs solides	epacadostat	NCT02752074
			NCT02298153
		NCT02318277	

Tableau 2 : Traitements approuvés par la FDA et essais cliniques utilisant des anticorps anti-checkpoints. Adapté de Dempke et al. *European Journal of Cancer*, 2017. [191].

Toutefois, ces anticorps, utilisés en clinique, déséquilibrent le système immunitaire et entraînent le développement de maladies auto-immunes [192] aussi appelées événements indésirables liés au système immunitaire (Immune-related adverse events : IRAEs). Les organes atteints par ces IRAE sont multiples : peau, poumon, foie, système neuronal, articulation notamment et peuvent entraîner l'arrêt des traitements. **Figure 9.** Les IRAE de grades élevés sont observées davantage avec l'injection d'anticorps anti-CTLA-4. Bien que l'injection des stéroïdes permette la régression de ces IRAEs [193], elle peut diminuer tout autant la réponse anti-tumorale.

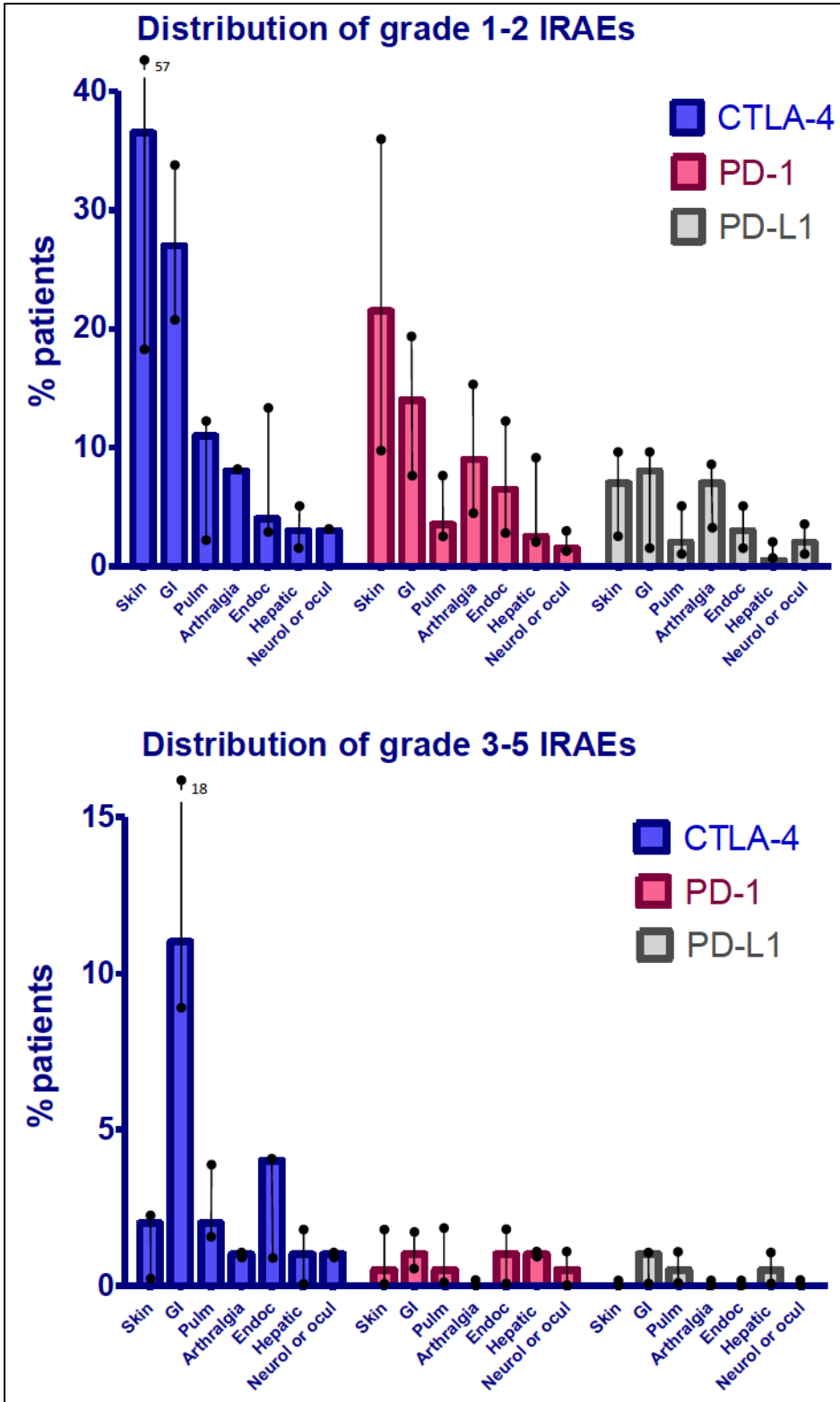


Figure 9 : Répartition tissulaire des IRAE pour tous les types de tumeur confondus selon leur grade en fonction des monothérapies par injection d'anticorps anti-CTLA-4, anti-PD-1 ou anti-PD-L1 (GI : Gastro-intestinal, endoc : endocrine (thyroid dysfunction, hypophysitis)) Adapté de Michot et al. *European Journal of Cancer*, 2016. [192].

4. Modèles murins d'études en immuno-oncologie

Avec l'avènement des immunothérapies, il y a eu un bond significatif, dans les dix dernières années, dans l'efficacité du traitement du cancer avec des taux de survie à long terme sans précédent dans un nombre croissant d'indications [194–198]. Cependant, il existe encore de nombreux patients qui ne répondent pas à ces immunothérapies, ce qui implique qu'il soit nécessaire de mettre l'accent sur l'identification de nouvelles immunothérapies ou de combinaisons qui peuvent prolonger les réponses ou améliorer le taux de patient répondeur. Pour cela, il existe une demande croissante de modèles précliniques toujours plus prédictifs et pertinents afin d'améliorer le développement rationnel de « médicaments immunothérapeutiques », de tester des combinaisons thérapeutiques et de minimiser les échecs dans les essais cliniques.

Les modèles de rongeurs ont longtemps été des outils clés pour mener des recherches biomédicales. Étant donné le besoin de modèles expérimentaux récapitulant la biologie humaine et considérant l'accès restrictif aux modèles de primates non humains pour des raisons éthiques et économiques, les souris représentent l'une des sources de modèles animaux les plus utilisées. Les quatre principales approches, utilisant des modèles de souris, pour évaluer les immunothérapies comprennent aujourd'hui : des modèles de tumeurs chimiquement induites, des modèles de tumeurs de souris syngéniques dans des hôtes pleinement immunocompétents, des modèles de souris génétiquement modifiées (*Genetically Engineered Mouse Model* GEMM), et des modèles de souris dites « humanisées ».

4.1. Modèles syngéniques

Les souris syngéniques ont été et sont encore des modèles utiles dans les études pharmacologiques [199,200] notamment par leur facilité d'utilisation (croissance synchrone et planifiable des tumeurs, modification des lignées). Cependant, elles ont plusieurs inconvénients dans l'évaluation préclinique des immunothérapies. Le premier, qui est partagé par l'ensemble des modèles non-humanisés, est la présence d'un système immunitaire murin et non humain. De plus, la plupart de ces lignées ont

été générées à partir de tumeurs chimiquement induites par l'injection de carcinogènes impliquant la formation d'altération génétique multiple qui ne reflètent que peu les tumeurs humaines. Par ailleurs, ces tumeurs ont souvent une croissance *in vivo* rapide ce qui encore ne reflètent pas la maladie chez l'homme et n'octroie qu'un court laps de temps pour évaluer l'efficacité des traitements.

Les souris GEMM sont des souris porteuses des mutations alléliques dans les voies d'activation oncogénique. Elles possèdent aussi, un système immunitaire murin mais elles outrepassent certains problèmes rencontrés chez les souris syngéniques. L'apparition et le développement de la tumeur résultent de processus oncogénique plus proche de la pathologie humaine. Par ailleurs, le développement des GEMM a permis d'avoir une expression inductible de ces processus oncogéniques dans les tissus d'intérêt [201]. Il existe des modèles de souris ayant une initiation et une progression tumorale plus proche de ce qui se passe chez l'homme. L'équipe de Tyler Jacks a, notamment, développé un modèle de souris dans lequel l'activation de l'oncogène Kras et la perte de fonction du gène suppresseur de tumeur, p53, sont conditionnées à l'injection d'un lentivirus codant pour la recombinaise Cre. L'inoculation intratrachéale permet un développement de tumeurs pulmonaires en 3 à 4 mois [202]. Ce développement tumoral, plus proche de la physiologie observée chez l'homme dans les tumeurs de poumon non à petites cellules a permis de comprendre certains mécanismes de tolérance. En effet, l'expression d'un néo-antigène, à travers tout le processus tumoral, malgré sa présence dans les ganglions drainant la tumeur, induit la tolérance des lymphocytes T CD4⁺ associée à une anergie de ces cellules et à une conversion des lymphocytes T spécifiques des néo-antigène en pTreg (Treg induit en périphérie) [203]. A l'opposé, l'expression de ce même néo-antigène dans une lignée cellulaire injectée dans des souris, est suffisante pour induire une réponse T spécifique amenant à une migration de ces lymphocytes vers la tumeur où ils sécrètent de l'IFN- γ [204]. La comparaison de l'immunogénicité dans ces deux modèles montre bien la difficulté pour appréhender les relations entre le système immunitaire et la tumeur, même dans un environnement entièrement murin. L'utilisation de ces modèles, reflétant de façon plus physiologique, l'apparition des tumeurs est une voie intéressante. La difficulté de travailler avec ces modèles réside, cependant, dans l'hétérogénéité de leur apparition et de leur croissance.

Malgré l'utilité de ces modèles, la problématique liée à la présence d'un système immunitaire murin demeure. Pour résoudre cette limitation, des modèles de souris humanisées qui reproduisent les échanges entre les cellules immunitaires et tumorales, toutes deux d'origine humaine, ont été développés. Les modèles de souris humanisées sont composés de trois éléments : 1) des souris hôtes immunodéficientes, 2) des cellules immunitaires d'origine humaine, et 3) des cellules tumorales d'origine humaine. Les souris immunodéficientes offrent une opportunité unique de reconstituer, au moins partiellement, un système immunitaire humain associé à des tumeurs humaines, sans qu'elles ne soient rejetées, pour caractériser les nouvelles avancées thérapeutiques, médiées par le système immunitaire, dans un cadre physiologiquement plus pertinent.

4.2. Modèles de souris humanisées

4.2.1. Souris immunodéficientes

Depuis les années 1980, la découverte de souris mutées *scid* [205] (immunodéfiance combinée sévère : severe combined immunodeficiency) et leur capacité à héberger des cellules mononuclées du sang périphérique (Peripheral Blood Mononuclear Cell : PBMC) [206], des tissus hématopoïétiques fœtaux [207] ou des cellules souches hématopoïétiques (CSH) [208], les souris immunodéficientes sont devenues de plus en plus sophistiquées. L'étude de l'hématopoïèse a bénéficié de modèles utilisant des souris immunodéficientes, tout comme l'évaluation de traitement contre des maladies infectieuses (VIH [209], hépatite C [210], EBV [211], *Salmonella enterica* Typhi [212]), l'auto-immunité [213] et la GvHD (réaction du greffon contre l'hôte : Graft versus Host Disease) [214,215]. Néanmoins, pour évaluer l'immunothérapie du cancer, une complication survient, car les modèles doivent simultanément tolérer la transplantation de tumeurs humaines et de cellules immunitaires humaines. Le premier modèle permettant la transplantation de tumeurs humaines était la souris nude, dépourvue de lymphocytes T [216]. Mais depuis lors, il est devenu clair que plus les souris sont immunodéficientes, meilleure est l'efficacité de la prise de greffe, en particulier en l'absence d'activité des cellules NK [217]. Parallèlement à l'efficacité supérieure de la prise de greffe de tumeur

humaine chez des souris immunodéficientes, leur capacité à permettre la reconstitution de cellules immunitaires humaines devient cruciale pour les études d'immunothérapie. Fondamentalement, l'injection de cellules hématopoïétiques humaines dans un contexte immunocompétent murin entraîne un rejet complet et immédiat des cellules humaines. Cette xénoréactivité est due à la reconnaissance des cellules humaines par les systèmes immunitaires inné et adaptatif de la souris. La première étape pour éviter la xénoréactivité fût la génération de souris dépourvues de lymphocytes T et de lymphocytes B en raison de mutations dans des gènes impliqués dans le système immunitaire : 1) la mutation du gène *Prkdc* (*Scid*) qui affecte la réparation de l'ADN [205], et 2) et la mutation *Rag* (gène activant la recombinaison : *Recombination-activating gene*) [218]. Les gènes *Rag* (*Rag-1* et *Rag-2*) sont impliqués dans la recombinaison V(D)J qui génère les récepteurs spécifiques d'antigène des lymphocytes T (TCR) et des lymphocytes B (BCR). L'absence de recombinaison conduit à un blocage du développement et de la survie des cellules T et B. Les deux souris déficientes *Rag-1* ou *Rag-2* existent [219], la souris mutée *Rag-2* étant la plus largement utilisée dans les modèles immunodéficients [220,221]. La conception de ces souris, défectueuses pour l'immunité murine adaptative, permet la reconstitution hématopoïétique humaine, mais avec des niveaux de greffe faibles et variables [222,223]. Néanmoins, la problématique de la qualité et de la quantité de reconstitution est cruciale dans le domaine de l'immunothérapie anticancéreuse car des cellules T, B, NK et/ou myéloïdes humaines fonctionnelles sont nécessaires pour comprendre l'efficacité thérapeutique des médicaments immunomodulateurs.

En comparant les efficacités de reconstitution immunitaire humaine dans les différentes souches de souris, la mutation *Scid* sur le fond NOD (Non Obese Diabetic) a montré un net avantage. La différence observée est due aux défauts accumulés dans les cellules NK, l'activité des macrophages et dans le système du complément, permettant une reconstitution immunitaire humaine au moins 5 fois supérieure à celle des souris *Scid* CB-17 originales [224]. Il est devenu évident que la population immunitaire restante chez les souris hôtes partiellement immunodéficientes jouait toujours un rôle dans le rejet de la xénogreffe humaine. Par conséquent, l'étape suivante dans l'amélioration significative de la qualité et des niveaux de la reconstitution du système immunitaire humain a été réalisée en désactivant la chaîne

γ commune du récepteur de l'IL-2 [225–227] (IL-2R γ_c , partagée par les récepteurs de l'IL-2, IL-4, IL-7, IL-9, IL-15 et IL-21 [228]), conduisant à l'absence de cellules NK murines. La combinaison de la mutation Scid ou Rag KO avec l'IL-2R γ_c KO a donné naissance à la «nouvelle génération» de modèles de souris sévèrement immunodéprimés, à savoir les souris NSG (NOD.Cg-Prkdc^{scid} Il2rg^{tm1Wjl}/SzJ) [225], NOG (NOD.Cg-Prkdc^{scid} Il2rg^{tm1Sug}/JicTac) [226] et BRG (BALB/c Rag2^{-/-} IL-2R γ_c ^{-/-}) [227]. Les souris NOG et NSG diffèrent, principalement, par la nature de la délétion de la chaîne γ commune du récepteur de l'IL-2 (IL-2R γ_c) qui est totale dans les souris NSG alors que les souris NOG ne présentent qu'une délétion de la queue cytoplasmique de la molécule.

De manière intéressante, les souris C57BL/6 Rag KO et IL-2R γ_c KO étaient encore capables de rejeter des cellules humaines xénogreffées [227,229,230], mettant en évidence qu'il existe d'autres mécanismes impliqués dans le rejet immunitaire des cellules humaines dans ce contexte génétique particulier. Le travail de Takenaka en 2007 [230], a permis de comprendre le mécanisme impliqué dans ce phénomène. Ses travaux ont montré que le fond génétique de la souris NOD, mais pas celui de la C57BL/6 (ou de la BALB/c), code pour un allèle de Sirp α particulièrement tolérant pour la molécule CD47 humaine [230–234]. En effet, le gène Sirp α est essentiellement exprimé dans les cellules myéloïdes et les neurones [235] et code pour une protéine transmembranaire de la superfamille des immunoglobulines inhibitrices (CD172a) qui agit comme un signal «ne pas manger» en interagissant avec son ligand apparenté ; la molécule CD47 exprimée de façon ubiquitaire sur les cellules. Cette interaction entre le Sirp α de la NOD et le CD47 humain empêche donc la phagocytose des cellules immunitaires humaines par les cellules myéloïdes murines.

Ces découvertes ont conduit au développement de la « prochaine génération » de souris immunisées dites HIS (Human Immune System) dans lesquelles, le transfert de l'allèle NOD.Sirp α (Balb/c Rag2^{-/-} IL-2R γ_c ^{-/-} NOD.Sirp α : BRGS) [233] ou même un gène Sirp α humain (SRG) [221] dans le même fond génétique, ont augmenté leur tolérance à la xénogreffe de cellules souches hématopoïétiques humaines et justifié, au moins partiellement, la différence observée entre les C57BL/6 et les autres fonds génétiques de souris. Ces nouvelles souris HIS se sont révélées robustes dans leurs

niveaux de reconstitution, la reproductibilité de la reconstitution, et ont permis les premières études sur les thérapies immuno-oncologiques, qui ont néanmoins mis en évidence que toutes ces souris HIS présentaient encore un défaut important. En effet, la reconstitution immunitaire n'était pas optimale puisque le compartiment myéloïde du système humain était largement sous-représenté.

Je vais tout d'abord décrire les principales approches utilisées pour la reconstitution des cellules immunitaires chez ces souris, puis discuter des nouveaux développements de souris humanisées visant à améliorer la reconstitution hématopoïétique chez les souris hôtes.

4.2.2. Humanisation des souris

Deux sources majeures de cellules immunitaires humaines sont actuellement utilisées pour l'établissement d'un système immunitaire humain fonctionnel chez des souris immunodéficientes : i) des PBMCs ou ii) des cellules souches hématopoïétiques humaines CD34⁺ ; qui sont généralement utilisées dans trois types de modèles : les souris Hu-PBL-scid (Peripheral Blood Lymphocyte : lymphocytes du sang périphérique), les souris Hu-SCR-scid (Cellule Scid-Repopulante) et les souris BLT (Bone marrow, Liver, Thymus ; moelle osseuse, foie, thymus), décrits en détails ci-dessous (**Figure 10**). Comme pour tous les modèles, chacune de ces approches a ses avantages et ses limites.

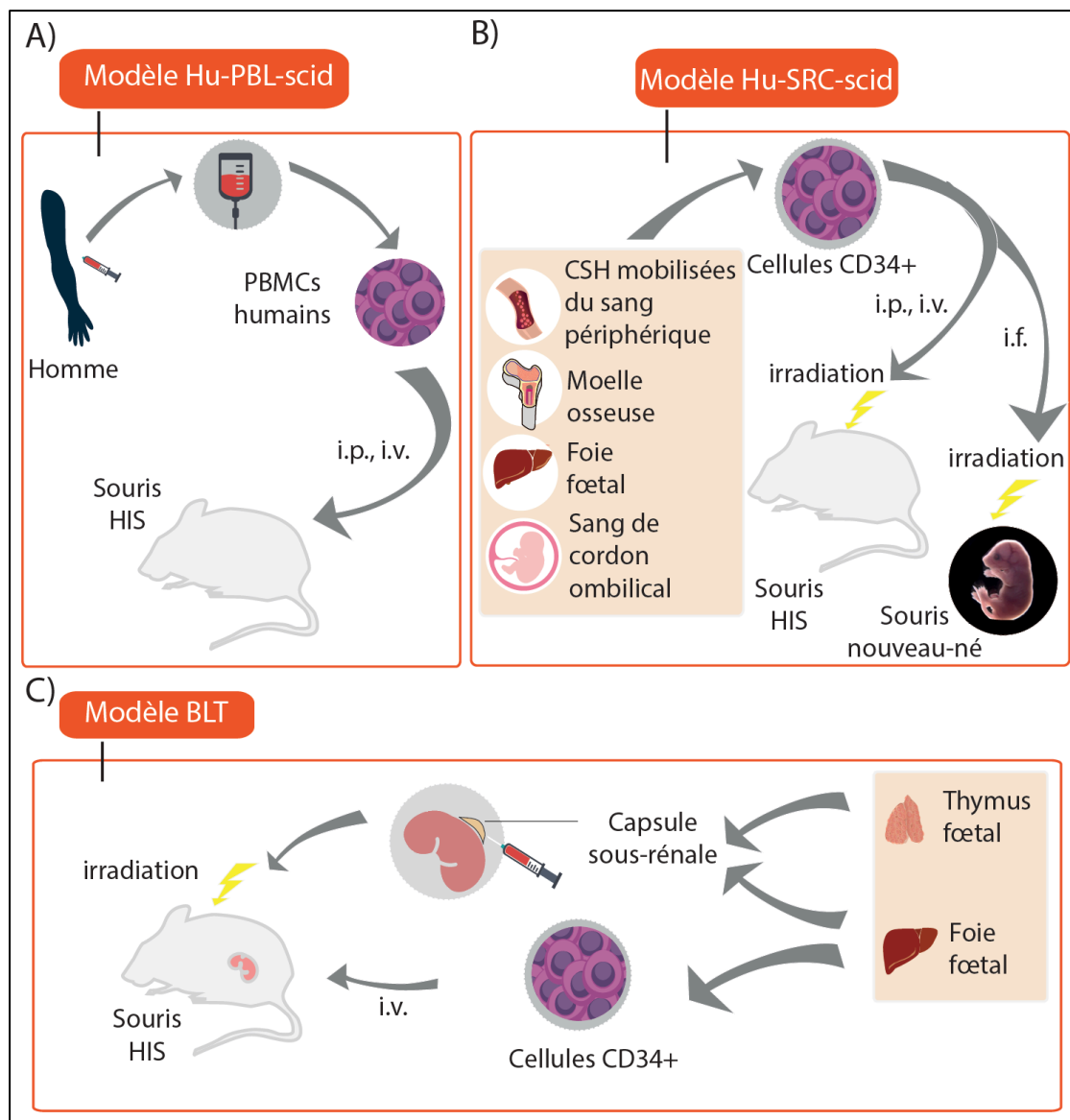


Figure 10 : Schéma des modèles de souris humanisées Hu-PBL-scid, Hu-SRC-scid et BLT A) Modèle Hu-PBL-scid : Les PBMCs sont injectées par voie intraveineuse (i.v.) ou intrapéritonéale (i.p.) dans une souris adulte immunodéficiente. B) Modèle Hu-SRC-scid : Des cellules souches hématopoïétiques provenant de mobilisation dans le sang par G-CSF, de moelle osseuse, de foie fœtal ou de cordon ombilical sont injectées par voie i.v., i.p., ou intra-fémorale (i.f.) dans des souris immunodéficientes nouvellement nées ou adultes après irradiation sublétale. C) Modèle BLT : Une partie de foie et thymus fœtal est implanté sous la capsule rénale dans une souris immunodéficiente. En parallèle, sont injectées des cellules souches hématopoïétiques provenant du même foie fœtal. *Adapté de De La Rochère et al. Trends in Immunology, 2018.*

4.2.2.1. PBMC : modèle Hu-PBL-scid

La version la plus simple et économique de l'humanisation est la greffe de leucocytes déjà différenciés chez des souris immunodéficientes, modèle connu sous le nom de Hu-PBL-scid. Cette approche a été décrite pour la première fois en 1988 en utilisant des souris CB17-scid [206] et a depuis été largement utilisée pour l'étude des réponses immunitaires humaines dans l'auto-immunité et les maladies infectieuses. La procédure la plus simple pour l'isolement des leucocytes humains se fait à partir de sang (PBMC), bien que les leucocytes matures puissent également être isolés de la rate ou des ganglions lymphatiques [236,237]. Idéalement pour les études immuno-oncologiques, les souris humanisées doivent être greffées avec des PBMC et une tumeur provenant du même patient. Cependant, cela est rarement possible en raison de l'obstacle de l'obtention simultanée des deux tissus. Ainsi, la majorité des protocoles sont basés sur l'injection de PBMC provenant de donneurs sains, qui n'ont pas le même CMH (complexe majeur d'histocompatibilité) que la greffe tumorale. Bien que cela soit pratique, les variations intrinsèques dues à l'allogénicité et à l'expérience immunitaire de chaque donneur de PBMC sont difficiles à contrôler [236,238].

Les PBMCs peuvent être injectées par voie intrapéritonéale (i.p.), par voie intraveineuse (i.v.) ou même intraspléniquement dans des souris adultes [236,239]. Néanmoins, la voie i.v. est la méthode couramment utilisée pour la prise de greffe de PBMC (par voie veineuse ou rétro-orbitale) car elle a donné de bons résultats sur la cinétique, la quantité et la capacité fonctionnelle des cellules greffées [238,240].

Au sein de l'inoculum de PBMC, outre les leucocytes humains matures, il y a quelques cellules souches hématopoïétiques mais elles ne parviennent pas à coloniser l'hôte murin en raison de l'absence d'un microenvironnement approprié pour leur développement. Ainsi, la sous-population immunitaire principale qui reste fonctionnelle chez l'hôte murin après la prise de PBMC est constituée de lymphocytes T, probablement en raison de la capacité de prolifération homéostatique intrinsèque des cellules T et de leur xéno-réactivité vis-à-vis de l'hôte murin. Ainsi, l'injection d'environ 20×10^6 de PBMC, dans une souris NSG, entraîne typiquement jusqu'à 50%

de cellules CD45⁺ humaines dans le sang périphérique de la souris hôte après 4 semaines de prise de greffe. La plupart de ces cellules CD45⁺ humaines (environ 80-95%) sont des cellules T CD3⁺ avec un phénotype CD45RO⁺ activé/mémoire et un rapport CD4 :CD8 autour de 1, qui est maintenu 4-6 semaines après l'injection de PBMC [236,239]. Seuls de très faibles taux de cellules B et de cellules myéloïdes humaines sont observés, très probablement en raison du manque de cytokines humaines nécessaires à leur survie [241,242].

Environ quatre semaines après l'injection de PBMC, des cellules CD45⁺ humaines apparaissent dans d'autres tissus lymphoïdes tels que la rate, les ganglions lymphatiques et le foie [239]. Néanmoins, les profils de distribution des cellules T CD4⁺ et CD8⁺ seront différents dans ces organes. En effet, la sous-population la plus importante dans la pulpe rouge de la rate est constituée de lymphocytes T CD8⁺ alors que les cellules T CD4⁺ sont plus proéminentes dans la pulpe blanche de la rate ; et peu de lymphocytes B peuvent être détectés dans les ganglions lymphatiques et la rate [239]. Fait intéressant, de faibles, mais détectables, taux de cytokines humaines IL-1 β , GM-CSF, IFN- γ , IL-10, IL-2 et IL-5 ont été détectés dans le plasma de souris reconstituées avec des PBMC humaines, ce qui peut contribuer à la survie des cellules humaines [243].

La principale limitation de la prise de greffe de PBMC humaines dans ces modèles est qu'elle conduit invariablement à la maladie létale du greffon contre l'hôte (Graft versus Host Disease : GvHD), puisque les lymphocytes T humains greffés réagiront contre les cellules exprimant les molécules murines du CMH [206,226,242]. Le développement de la GvHD peut être suivi par plusieurs paramètres en pesant notamment régulièrement les souris [244] ; une perte de plus de 10% du poids corporel indiquant l'apparition de GvHD clinique mais un ensemble de critère est à évaluer (**Tableau 3**). Certaines études ont rapporté que l'apparition de la GvHD est directement corrélée avec le degré de prise de greffe de cellules T humaines, et que l'irradiation sous-létale de la souris hôte, précédant l'injection de PBMC, accélère son apparition [242]. Ces résultats indiquent que la fenêtre d'observation thérapeutique est limitée à quelques semaines (généralement 4 à 6 semaines après l'injection de PBMC) avant l'apparition de signes cliniques évidents de GvHD [226,242]. Fait

intéressant, les lymphocytes T CD4⁺ semblent jouer un rôle majeur dans l'induction de la GvHD chez les souris Hu-PBL-scid, car la déplétion des lymphocytes CD4⁺ des PBMC avant l'injection allège les symptômes cliniques et prolonge la survie des souris [245].

Critère	Grade 0	Grade 1	Grade 2
Perte de poids	<10%	>10% et <25%	>25%
Posture	Normale	Voutée uniquement au repos	Sévèrement voutée Mouvement contraint
Activité	Normale	Moyennement diminuée	Nulle sauf stimulation
Texture du pelage	Normale	Moyennement ébouriffée	Sévèrement hirsute Sans toilettage
Aspect cutané	Normal	Desquamation au niveau des pattes et de la queue	Zones dépoilées

Tableau 3 : Évaluation clinique de la GvHD chez les animaux injectés avec des PBMC. Adapté de Cooke et al. Blood, 1996. [244].

Une autre faiblesse de ce modèle est la reconstitution limitée des cellules myéloïdes et des lymphocytes B humains. Les efforts actuellement en cours pour identifier des procédés permettant améliorer la reconstitution d'autres types de cellules immunitaires que les lymphocytes T sont décrits ultérieurement.

4.2.2.2. Cellules souches CD34⁺ : modèles Hu-SRC-scid et BLT

Une autre approche pour la mise en place d'un système immunitaire humain consiste à injecter des cellules souches hématopoïétiques (CSH) humaines CD34⁺ chez des souris receveuses immunodéficientes nouveau-nées ou adultes [208]. Ce modèle est appelé Hu-SRC-scid. Le succès de la prise de greffe est très variable, en fonction de plusieurs facteurs, y compris la source de CSH, la voie d'injection, la souche et le sexe de la souris receveuse. Une exigence particulière de cette approche est l'irradiation

sublétale (100-400 cGy en fonction des souches et de l'âge) des souris hôtes afin de réduire le nombre de cellules souches hématopoïétiques de souris et ainsi faciliter une prise de greffe de CSH humaines optimale. Certains auteurs ont rapporté des alternatives pour l'irradiation, comme le traitement des souris avec des agents chimiothérapeutiques, tel que le busulfan [246,247] ou par la délétion sélective des cellules progénitrices de la souris par l'administration d'ACK2, un anticorps qui bloque la fonction de c-kit, ce qui conduit à l'élimination transitoire de plus de 98% des CSH endogènes chez des souris immunodéficientes [248]. Les CSH CD34⁺ peuvent être isolées à partir de différentes sources : sang de cordon ombilical humain [225,227], moelle osseuse adulte [249], sang après mobilisation par facteur de croissance (G-CSF) de CSH [250] ou fœtus [249,251]. En pratique, les CSH sont isolées par séparation sur Ficoll et ensuite purifiées par des billes de sélection magnétique anti-CD34⁺ humain. Certains auteurs ont rapporté que la reconstitution immunitaire était similaire entre les CD34⁺ obtenus à partir du sang de cordon ombilical ou de foie fœtal humain [251]. La source la plus abondante de CD34⁺ humain est celle des CSH adultes, mais la qualité de la reconstitution varie en fonction de l'âge du donneur et d'autres facteurs cliniques. Actuellement, le sang de cordon ombilical humain est la source la plus accessible de CSH humaines avec une efficacité notable pour la reconstitution immunitaire [249,251,252]. Le foie fœtal a également été largement utilisé pour fabriquer ce qu'on appelle le « modèle BLT » puisqu'un grand nombre de cellules CD34⁺ peut être obtenu à partir d'un seul échantillon de foie. Ce modèle est généré par la transplantation, de fragment du foie et du thymus fœtaux humains, dans la capsule sous-rénale chez des souris immunodéficientes adultes, qui reçoivent également par voie intraveineuse des CSH autologues CD34⁺ provenant du même foie fœtal [253]. Bien que moins efficace que l'injection chez le nouveau-né, l'injection dans les souris adultes est plus fréquemment utilisée en raison de sa facilité.

Différentes voies d'injection de cellules CD34⁺ peuvent être choisies, en fonction de l'âge des souris à humaniser. Chez les souris adultes, les cellules CD34⁺ sont couramment injectées par voie intraveineuse ou intrafémorale, alors que chez les souris nouveau-nées, les cellules souches peuvent être injectées par voie intraveineuse (veine faciale), intracardiaque ou intrahépatique. Chez les souris

nouveau-nées, Brehm et al. ont rapporté que la voie d'injection n'a pas influencé les résultats de la prise de greffe de CD34⁺ [214] et, chez les souris adultes, Werner-Klein et al. ont démontré qu'il n'y avait pas de différence dans la capacité de reconstitution entre les cellules du cordon ombilical injectées par voie intrafémorale, intrahépatique ou intraveineuse [254]. L'utilisation de souris nouveau-nées ou jeunes (jusqu'à 4 semaines) pour la prise de greffe de CD34⁺, permet un développement accéléré des cellules T et une prise de greffe plus efficace par rapport aux souris adultes [214]. Deux possibilités ont été proposées pour expliquer cette constatation. Une possibilité est que les souris adultes présentent une involution thymique et donc, une architecture thymique altérée sévère entraînant une baisse de l'efficacité du développement des cellules T [225,229,250]. La deuxième possibilité est que les souris nouveau-nées ont un système immunitaire inné moins actif, ce qui favorise un bon développement des lymphocytes T humains [229].

Certains auteurs ont rapporté l'impact du sexe sur la prise de greffe, les souris NSG femelles permettant une greffe plus efficace des cellules CD34⁺ par rapport aux souris mâles NSG [255,256]. Une autre étude a montré des résultats similaires, mais ces auteurs ont rapporté que la production de lymphocytes T naïfs du thymus était plus élevée chez les femelles, alors que l'activation périphérique et l'expansion des lymphocytes T mémoires étaient plus importantes chez les mâles [257].

En général, dans le modèle Hu-SRC-scid, toutes les lignées hématopoïétiques humaines peuvent se développer, bien qu'à des degrés divers [214,225,226]. Les analyses phénotypiques de la population lymphoïde suivant la prise de greffe de CSH ont révélé que la majorité des lymphocytes T étaient constitués de cellules T CD4⁺ fonctionnelles avec un phénotype mémoire CD45RA⁻CD27⁺ [258] et de cellules NK avec une altération fonctionnelle (phénotype hyperactivé, sous-expression de KIRs, défaut de transduction de signaux activateurs) [258,259]. Néanmoins, une certaine controverse subsiste sur la fonctionnalité de ces cellules T humaines notamment en réponse à des antigènes spécifiques [227,259,260]. Des améliorations à ce problème seront discutées ultérieurement. D'un autre côté, la différenciation de la lignée myélo-monocytaire semble être altérée et les monocytes qui se développent sont phénotypiquement immatures [261]. Enfin, certaines études indiquent que la

majorité des cellules B humaines qui se développent sont des cellules B CD5⁺ immatures [258,259,262].

Une des limitations au modèle Hu-SRC-scid est que les cellules T humaines sont éduquées dans le thymus de la souris, et par conséquent leurs TCR sont restreints aux molécules murines du CMH, et ne parviennent donc pas à interagir productivement avec les cellules humaines présentant l'antigène [260]. Bien que le thymus de la souris favorise le développement des lymphocytes T humains, la question de la restriction du CMH n'est toujours pas claire. Halkias et al ont montré que les thymocytes humains ont un comportement similaire dans les environnements thymiques chez la souris et l'homme et qu'ils interagissent avec les cellules hématopoïétiques humaines ainsi qu'avec le tissu thymique de la souris chez les souris HIS [263]. De plus, Watanabe et al. [259] ont montré que l'environnement thymique de la souris est essentiel pour le développement des cellules T humaines (même si l'absence de I-Ab chez la souris ne supprime pas entièrement la production de lymphocytes T), suggérant que le répertoire TCR CD4⁺ humain est probablement restreint par les molécules HLA de classe II ainsi que par le CMH murin.

Au contraire, le modèle BLT, dans lequel le foie et le thymus fœtaux humains transplantés fournissent un microenvironnement thymique humain, favorise le développement des lymphocytes T humains et leur sélection sur les molécules humaines du CMH. Cependant, une sélection positive dans le thymus se produit exclusivement sur les cellules humaines, et les cellules T, ayant une affinité pour le CMH de souris, ne sont pas éliminées, avec pour conséquence une incidence plus élevée de GvHD que dans d'autres modèles greffés avec des CD34⁺. Néanmoins, le modèle BLT est devenu le modèle de choix pour les études sur le VIH [264].

Globalement, les techniques d'humanisation du système immunitaire chez les souris immunodéficientes précédemment décrites ne sont pas totalement satisfaisantes, car les différentes populations immunitaires se greffent à des degrés divers, sont influencées par la reconnaissance des xéno-antigènes, se développent dans un microenvironnement dépourvu de cytokines et de facteurs de croissance humains appropriés, peuvent montrer des traits d'activation non spécifique et une fonction altérée. Pourtant, ces modèles constituent un grand progrès, permettant pour la première fois l'évaluation des immunothérapies en utilisant les mêmes médicaments

que ceux utilisés chez l'homme. Le tableau ci-dessous (**Tableau 4**) compare les différentes caractéristiques des modèles HU-PBMC-scid et Hu-SRC-scid.

	Hu-PBL-scid	Hu-SRC-scid
Source des cellules immunitaires humaines	- Sang périphérique	- Sang de cordon - Moelle osseuse - Cellules du sang périphérique mobilisées - Foie fœtal
Voie d'injection	IP/IV/IS	IV/IF (Adulte) IV/IC/IH (nouveau-né)
Souche de souris	NSG/NOG	NSG/NOG
Pré-conditionnement	Aucun	Irradiation sublétales
Reconstitution immunitaire (sélection, sous-types de cellules, qualité)	Lymphocytes humains différenciés (majoritairement des cellules T). Phénotype activé	Tous les types de cellules hématopoïétiques.
Délai pour la reconstitution	Court (3-5 jours)	Long (3-4 semaines)
Délai d'apparition de la GvHD	4-6 semaines	> 2 mois
Coût	\$	\$\$\$
Complexité technique	Simple	Complexe

Tableau 4. Comparaison de l'humanisation des souris immunodéficientes par des cellules immunes provenant de PBMC ou CSH. Adapté de De La Rochère et al. Trends in Immunology, 2018.

Les dernières avancées, permettant de résoudre une partie des problèmes soulevés précédemment, seront présentées ultérieurement.

4.2.3. Tumeur d'origine humaine : lignée cellulaire et PDX

Une composante essentielle des souris humanisées, utilisées dans l'évaluation de l'immunothérapie anti-cancer, est bien évidemment la source des cellules tumorales. Les souris hôtes immunodéficientes peuvent être greffées avec des lignées cellulaires tumorales humaines ou avec des PDX (Xénogreffes Dérivées du Patient).

Les lignées cellulaires présentent les avantages de la reproductibilité intra- et inter-expérience, d'un taux de prise de greffe très élevé et d'une source inépuisable de matériel tumoral. Cependant, la culture *in vitro* entraîne des mutations et des sélections clonales ne reflétant que peu les tumeurs primaires d'un point de vue moléculaires [265].

Les PDXs sont des fragments de tumeur de patient greffés directement dans des souris immunodéficientes. Le taux de prise de greffe est variable selon les types de tumeur et varie de 10% (tumeur de la prostate, cancer du sein) à 74% (métastases cérébrales de tumeur de poumon non à petites cellules) [266]. Ce taux de prise de greffe est lié à l'observation que l'efficacité de la prise tumorale de la PDX est un facteur de mauvais pronostic pour la survie des patients [267]. Après cette première prise de greffe, des transplantations successives dans des nouvelles souris sont effectuées afin de maintenir la PDX. Ces PDXs peuvent être implantées en orthotopique (lieu d'implantation similaire à celui d'origine de la tumeur, PDOX : Patient derived orthotopic xenograft), en sous-cutanée ou en intrascapulaire. (**Figure 11**)

Ces modèles diffèrent par de nombreux aspects. Par conséquent, le choix des modèles de tumeurs devrait dépendre des objectifs de recherche en tenant compte des paramètres mentionnés ci-dessous (**Tableau 5**). Un point crucial, dans le choix du modèle, est la nature des traitements testés et leur spécificité tumorale. Considérant tous ces points, et en vue de tester des immunothérapies anti-tumorales, les souris immunodéficientes greffées avec des lignées cellulaires tumorales humaines ou des

PDX sont les outils précliniques pertinents pour l'évaluation des immunothérapies anti-tumorales.

	Critères	Lignées cellulaires	PDXs
Moléculaires	Stroma ¹	Souris	Souris
	Représentativité des cancers humains	Intermédiaire	Haute
	Stabilité des cellules tumorales	Faible	Haute
	Preuve de concept de thérapies anti-cancer	Adaptée	Adaptée
	Screening thérapeutique (incluant les combinaisons de traitements)	Intermédiaire	Haute
	Corrélation thérapeutique avec l'efficacité clinique	Intermédiaire	Haute
Expérimentaux	Voie de transplantation (SC, IV, orthotopique, intraductale, intrascapulaire) ²	Aisées	Aisées
	Procédures expérimentales ³	Aisées	Aisées
	Cinétique de croissance tumorale	Homogène et rapide	Variable
	Approche Avatar	Non pertinent	Approprié

Tableau 5 : Principaux critères de comparaison entre les lignées cellulaires et les PDX. Adapté de De La Rochère et al. *Trends in Immunology*, 2018.

¹ Le stroma inclue les cellules endothéliales, les cellules immunitaires et les fibroblastes.

² Pas de réelles différences observées entre les lignées cellulaires et les PDX dans leur capacité à être transplantées notamment en raison de la possible dissociation des PDX avant greffe.

³ Greffe de la tumeur, mesure de la taille tumorale, administration des traitements, analyse statistique.

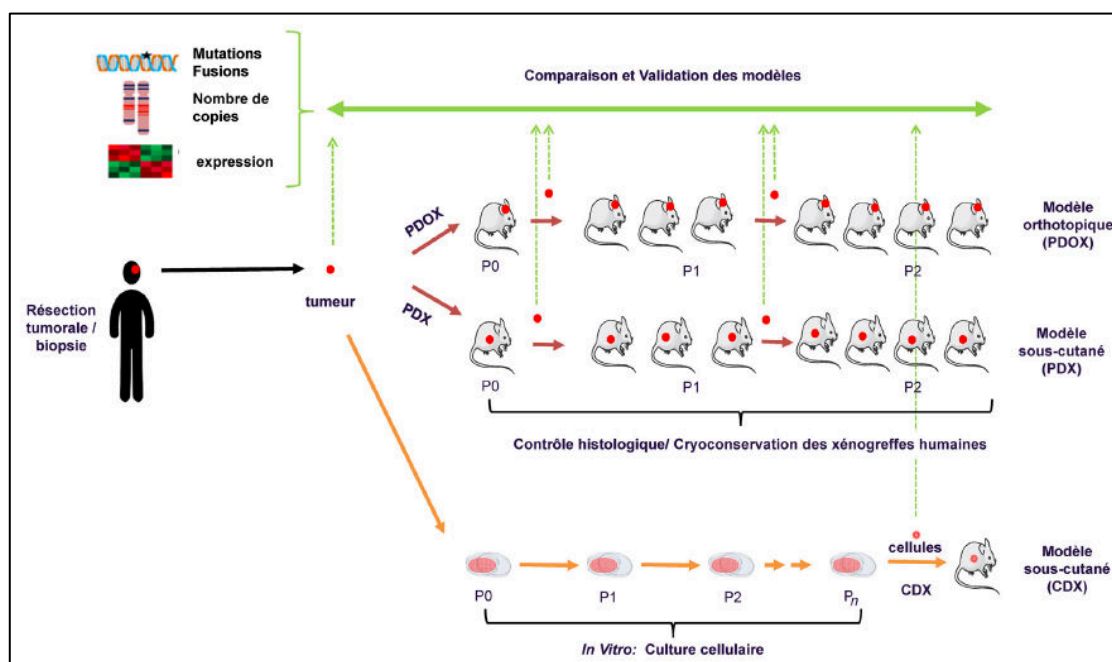


Figure 11 : Méthodologie pour développer des CDX/PDX/PDOX (exemple pour une tumeur cérébrale). La caractérisation des modèles se fait par diverses méthodes (immunohistochimie, exome, RNAseq, puces...) au cours du passage (P1 à Pn) et est comparée aux résultats de la tumeur primaire. *Adapté de Surdez et al. Revue d'oncologie hématologie pédiatrique, 2016. [268].*

Les cancers humains, dans chaque sous-type spécifique à un organe, sont très hétérogènes. Si peu d'altérations moléculaires sont capables de discriminer des sous-catégories dans chaque type de cancer, il est maintenant clair que ces classifications ne représentent pas l'intégralité de l'hétérogénéité des tumeurs. Ceci est démontré par l'incidence élevée des mutations somatiques [81] et des altérations du nombre de copies [269] observées dans les cancers humains, ces deux anomalies ne représentant que deux aspects des caractéristiques moléculaires de la tumeur.

Il a été montré que les profils génomiques sont bien conservés entre les tumeurs des patients et les PDX correspondantes, ainsi qu'entre la même PDX provenant de passages *in vivo* différents et consécutifs [270–272]. De même, la stabilité génomique des PDX est meilleure que celle des lignées cellulaires tumorales humaines.

L'utilisation d'un ensemble de PDX affichant une hétérogénéité pertinente, à la manière d'un essai clinique, est un outil utile pour effectuer des criblages thérapeutiques *in vivo*, comme rapporté par Gao et ses collègues [273]. Une telle approche, qui diminue le nombre de souris à utiliser, est capable de (i) valider que les thérapies ciblées sont, ou non, spécifiques de la cible moléculaire et bénéfiques pour un sous-type de tumeurs et (ii) d'identifier le meilleur traitement ou une combinaison de traitements parmi plusieurs stratégies testées dans un large panel de PDX. L'avantage de cette approche est également lié à la valeur prédictive élevée des PDX pour les réponses thérapeutiques chez les patients cancéreux, avec une valeur prédictive positive et négative de 85% et 91%, respectivement [274], quel que soit le type de tumeur testée. Enfin, les PDX permettraient une prise en charge thérapeutique personnalisée des patients atteints de cancer selon l'approche dite « Avatar ». Le principe de l'approche « Avatar » consiste à greffer la tumeur d'un patient sur des souris immunodéprimées. Après la croissance *in vivo* de la tumeur et au cours des passages précoces est réalisée la caractérisation moléculaire de la tumeur. Ainsi l'efficacité des traitements (monothérapies et/ou combinaisons) est testée sur des passages précoces de cette PDX. Les résultats d'efficacité dans le modèle « Avatar » permettent alors, dans un deuxième temps, de choisir le meilleur traitement au patient dont est issu la PDX (**Figure 12**). Une telle approche a été développée chez des patients atteints de cancer du pancréas, montrant qu'il était possible de revenir vers les patients dans environ 75% des cas, avec une concordance élevée entre l'efficacité préclinique et clinique du médicament testé [275]. L'utilisation de l'approche « Avatar » a également été testée sur des PDX provenant de patientes atteintes de cancer de l'ovaire avec des pistes thérapeutiques prometteuses (interaction entre les voies EGFR et IGF-R) [276]. Cette approche « Avatar », utilisée jusqu'ici pour évaluer des thérapies ciblées, pourrait dans un futur proche être améliorée par l'adjonction de la composante immunitaire du patient et ainsi évaluer l'efficacité des immunothérapies.

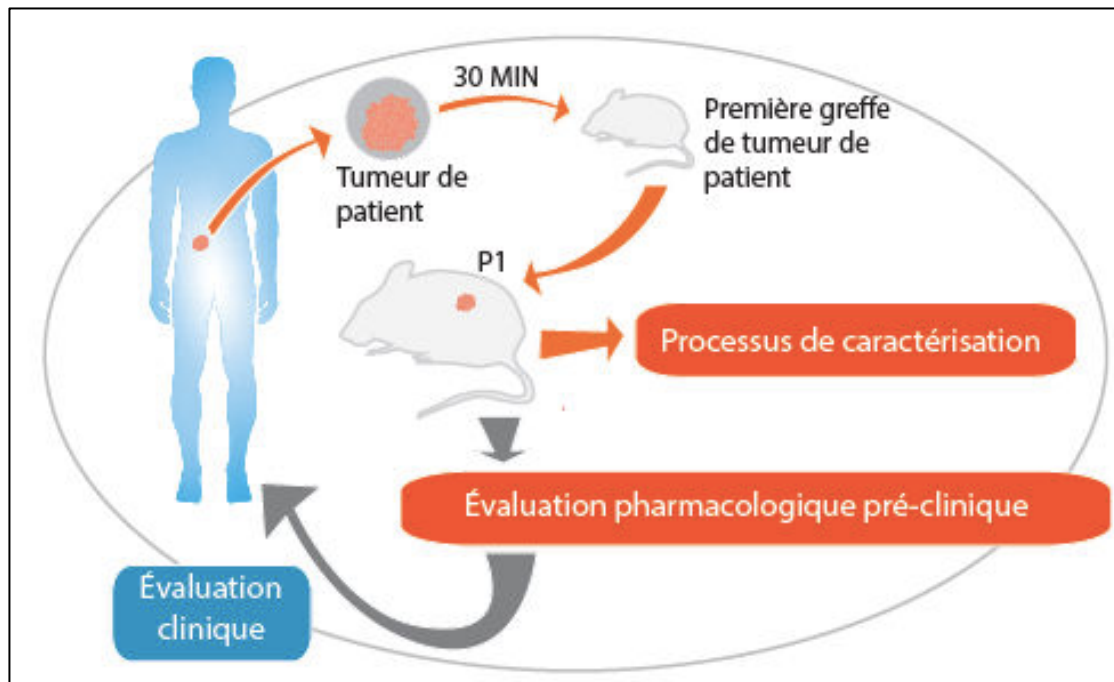


Figure 12 : L'approche « Avatar ». Un fragment tumoral de patient, fraîchement prélevé, est directement greffé sur des souris immunodéprimées. Dès le 1^{er} passage sur souris, cette PDX est caractérisée *in vitro* et en parallèle est utilisée pour l'évaluation des thérapies. Les réponses de la PDX aux traitements sont analysées puis transposées en clinique afin de proposer une thérapie adaptée à chaque patient. *Adapté de De La Rochère et al. Trends in Immunology, 2018.*

4.2.4. Nouveaux développements dans les modèles de souris humanisées

Pour l'évaluation de l'immunothérapie du cancer, le modèle de souris humanisée idéal devrait permettre la reconstitution complète des compartiments myéloïdes et lymphoïdes pendant un laps de temps suffisant pour l'administration du ou des traitements. Cependant, les modèles décrits précédemment sont limités dans leur capacité à donner naissance à des populations de cellules myéloïdes, NK et B fonctionnelles. Différentes approches ont été développées pour résoudre ce problème et sont résumées dans le **Tableau 6** en fin de chapitre.

4.2.4.1. Préparation de la niche pour la prise de greffe des CSH

Des niveaux élevés de chimérisme humain chez les souris HIS nécessitent un conditionnement myéloablatif des souris hôtes lorsque ce sont des CSH humaines qui sont injectées. Ainsi, les modèles de souris HIS précédemment discutés sont généralement pré-conditionnés par l'irradiation sublétales [250,255], ce qui crée l'espace requis dans la niche des cellules souches de l'hôte pour la prise de greffe de cellules souches humaines. Il est à noter que la susceptibilité à l'irradiation dépend de la souche. Par exemple, les souris NRG (NOD.Cg-*Rag1*^{tm1Mom} *Il2rg*^{tm1Wjl}/SzJ) montrent une radio-sensibilité plus faible que les souris NSG [277], ce qui s'explique par le fait que la mutation scid prédispose à une sensibilité plus élevée aux dommages à l'ADN induits par les rayonnements que les souris *Rag1* KO ou *Rag2* KO. Des avancées récentes ont identifié des souris mutantes de *c-kit* (CD117) en tant qu'hôtes appropriés pour la prise de greffe de CSH humaines sans nécessiter d'irradiation préalable. De plus, ces souris favorisent un meilleur développement myéloïde. Comme *c-kit* est impliqué dans la maintenance et la différenciation des CSH, les souris porteuses de la mutation w41 dans *KIT* (souris NSGW41) ont un nombre réduit de CSH murines, ce qui se traduit par une compétition plus faible à long terme entre les cellules souches humaines et murines et une meilleure prise de greffe de CSH humaines transplantées [278–280]. Il est intéressant de noter que les souris NSGW41 ont également montré un développement plus efficace des plaquettes et des cellules érythroïdes d'origine humaine [279], ce qui pourrait rendre ces souris capables d'évaluer l'activité plaquettaire dans le cadre de la tumeur, activité qui a été montrée comme pro-tumorale notamment en favorisant le processus métastatique [281,282]. Les cellules dendritiques, qui présentent une altération de la reconstitution chez les souris HIS, jouent un rôle crucial dans la coordination des réponses immunitaires adaptatives et innées. La signalisation de *Flt3* (tyrosine kinase 3 de type *Fms*) est essentielle pour le développement des DC conventionnelles (cDC) et des DC plasmacytoïdes (pDC). Par conséquent, le gène *Flt3* a été délété chez les souris hôtes en même temps que le ligand humain *Flt3L* injecté, améliorant le développement des DC humaines au détriment de l'homologue murin [283]. La souris BRGF (Balb/c *Rag2*-

IL-2R γ ^{-/-} *Flt3*^{-/-}) humanisée résultante présente en effet un bien meilleur développement des monocytes et de DC humains par rapport à sa souche parentale BRG. De plus, l'amélioration de l'homéostasie des DC entraîne une augmentation du nombre de cellules NK et T humaines. Le transfert du Flt3 KO sur la souche BRGS a encore augmenté les niveaux de reconstitution des cellules NK et a même permis l'étude du développement des ILC (Innate lymphoid cells) humaines [284].

4.2.4.2. Cytokines et compatibilité stromale

Il est connu que les macrophages associés aux tumeurs (TAM), les cellules suppressives dérivées des myéloïdes (MDSC) et les neutrophiles jouent également un rôle important dans le contrôle de la progression du cancer [285,286]. Ces populations cellulaires sont également sous-représentées [287] ou présentent des défauts de maturation et de fonction chez les souris HIS [261]. Pour améliorer la reconstitution de ces cellules chez les souris HIS, l'une des stratégies est basée sur l'injection exogène des cytokines humaines clés qui ne sont pas actives entre les espèces. L'une des premières approches testées a été l'injection hydrodynamique de plasmides codant pour les cytokines humaines IL-4, GM-CSF et Flt3 ligand ou M-CSF [288]. Ces injections ont augmenté le nombre de DC humaines et de monocytes/macrophages chez les souris humanisées. L'étape suivante a été la conception de souris modifiées pour exprimer le SCF humain, le GM-CSF, l'IL-3, la TPO ou le Sirp α (de souris NOD ou humain) dans différentes souches de souris. Dans le contexte NOD, les souris NSG ont été modifiées pour exprimer le hSCF (c-kit ligand), le hGM-CSF et l'hIL-3 (dite NSG SGM3), codés par des constructions d'ADNc qui s'intègrent de façon aléatoire et exprimés sous le contrôle du promoteur CMV [289,290]. Les souris NOG ont été modifiées pour exprimer le hGM-CSF et l'hIL-3 (dite NOG-EXL) de façon ubiquitaire sous le contrôle du promoteur SR α [291]. De plus, les cytokines hIL-3 et hGM-CSF ont été introduites dans le contexte BRG [292]. L'ensemble de ces stratégies a montré des augmentations significatives du nombre

de cellules myéloïdes et de la fonction des macrophages par rapport aux souches parentales après injection de CD34⁺.

Parallèlement, les souris BRG ont été modifiées pour exprimer la hTPO, ce qui a entraîné une augmentation de la prise de greffe de cellules souches hématopoïétiques humaines et un meilleur développement des populations myéloïdes [293]. Par la suite, les souris BRG-hTPO ont été modifiées pour exprimer le Sirp α humain, l'hIL-3 et le hM-CSF, donnant naissance aux souris MISTRG (M-CSF, IL-3, Sirp α , TPO, Rag2^{-/-} IL-2r γ c^{-/-}) [294]. Les souris MISTRG supportent des niveaux supérieurs de développement de cellules myéloïdes, une différenciation accrue des monocytes, des cellules dendritiques et des macrophages, et un nombre plus élevé de cellules NK. Cependant ces souris : i) développent une anémie, par une augmentation de la phagocytose des érythrocytes néo-formés de souris par les cellules myéloïdes humaines [294], ii) ont une durée de vie courte et iii) épuisent la greffe de cellules immunitaires humaines 3-4 mois après la transplantation.

Un autre acteur clé de la réponse immunitaire anti-tumorale ; la cellule NK [295] est très peu représentée chez les souris HIS. Une supplémentation en IL-2 et/ou en IL-15 a été tentée pour augmenter la reconstitution des cellules NK [296]. Katano et ses collègues ont développé une souche de souris exprimant l'IL-2 humaine (Hu-HSC NOG-IL2 Tg), qui a favorisé la différenciation des cellules NK humaines [297]. De même, l'injection d'un vecteur d'ADN codant pour l'IL-15 [288] ou l'administration d'IL-15/IL-15R α [298] a augmenté la présence de cellules NK humaines chez des souris immunodéficientes. De manière intéressante, les souris MISTRG, développées par le groupe de Flavell, permettent une meilleure reconstitution des populations myéloïdes, et comme les cellules myéloïdes produisent l'IL-15 humaine, ces souris montrent également une augmentation de la reconstitution des cellules NK [294]. Cependant, comme expliqué précédemment, les souris MISTRG sont anémiques. Par conséquent, la même équipe a généré des souris Balb/c Rag2^{-/-} IL-2r γ c^{-/-} modifiées pour exprimer le Sirp α ^h et l'IL-15^h (SRG-15) [299], souris qui ont montré un développement et une fonction améliorés des cellules NK, cellules T CD8⁺ et ILC résidant dans les tissus. De même, Katano et ses collègues ont développé une souris alternative permettant la greffe à long terme de cellules NK humaines : les souris IL-15-NOG, où les cellules NK peuvent être étudiées pendant 3 mois, comparées à 2

semaines chez les souris NOG d'origine [300,301]. Bien que ce modèle ait ses propres limites (des niveaux plus élevés de hIL-15 dans le sang comparable à ceux trouvés chez les patients lympho-déplétés ainsi qu'une sénescence des NK), avec les souris SRG-15, ils fournissent un outil amélioré pour étudier les mécanismes impliquant les NK dans l'immunothérapie des cancers.

De manière intéressante, il a été récemment montré que le transfert adoptif de cellules NK, dérivées de sang de cordon humain, dans des souris humanisées reconstituées avec des cellules immunes de sang de cordon humain autologue peuvent survivre sans l'administration de cytokines exogènes [302].

4.2.4.3. Manipulation du CMH

Pour limiter la xéno-GvHD, qui peut être aiguë chez les souris Hu-PBL-scid [242], ou chronique chez les souris Hu-SRC-scid [303], différentes stratégies ont été développées, basées sur la manipulation génétique des molécules du CMH. En effet, l'administration de PBMC chez des souris NSG dépourvues de molécules murines du CMH de classe I et/ou de classe II, telles que des NSG- β 2m KO, un composant structurel de la molécule MHC classe I [242] ou des NOG dépourvues des molécules de classe I et classe II du CMH de souris [304], a conduit à la prise de greffe des cellules immunitaires humaines et a permis de limiter la xéno-GvHD.

Dans le cas des souris Hu-SRC-scid, la discordance entre les CMH humaines et murines, en plus d'induire la GvHD, entraîne un dysfonctionnement dans la fonction des lymphocytes T, car les lymphocytes T humains en développement sont sélectionnés sur les antigènes présentés par le CMH de souris et ne reconnaîtront donc pas les antigènes présentés par les molécules HLA [259].

Fait intéressant, la perfusion de CSH dans des souris NSG transgéniques pour les molécules de classe I et la β 2m humaines (NSG-HLA-A2 / HHD) a permis la génération de cellules T HLA-restreintes fonctionnelles [305]. En outre, la transplantation de CSH appariées pour HLA-DR dans des souris NOD.Rag1KO.IL2R γ CKO transgéniques pour la molécule HLA de classe II HLA-DR4, induit une forte reconstitution des lymphocytes T

et B [306]. De plus, ces souris sont capables de produire toutes les sous-classes d'immunoglobulines spécifiques de l'antigène lors de la vaccination, révélant ainsi le rôle essentiel des molécules HLA de classe II dans le développement de lymphocytes T fonctionnels capables de garantir la commutation des immunoglobulines. Une observation similaire a été faite chez des souris NOG transgéniques pour la molécule HLA-DR4 [307]. Plus récemment, le groupe de Lone a généré une souris combinant à la fois une déficience en CMH murin de classe I et II avec une expression transgénique des molécules HLA de classe I et II appelée «HUMAMICE» (HLA-2^{+/+}/DR1^{+/+}/H-2-β2m^{-/-}/Iaβ^{-/-}/Rag2^{-/-}/IL2Ry^c^{-/-}/perf^{-/-}) [308]. Cette souris ne possède pas de cellules T et B due à la mutation Rag, pas de cellules NK dues à la mutation IL2Ry_c et aucune activité cytolytique résiduelle due à la délétion de la perforine. Les PBMC HLA-appariées, injectées dans les souris HUMAMICE, génèrent un système immunitaire humain fonctionnel, capable de produire des anticorps. Cependant, comme ces souris expriment la molécule Sirpα de la C57BL/6 ceci conduit potentiellement à une prise de greffe sous-optimale des cellules hématopoïétiques humaines, la génération de souris HUMAMICE portant le Sirpα humain serait une amélioration notable.

4.2.4.4. Humanisation des immune checkpoints dans des souris immunocompétentes

Une approche alternative à l'utilisation de souris HIS pour l'étude des mécanismes d'action, de la résistance et de la toxicité des immunothérapies à base d'anticorps anti-checkpoints, a été le développement de souris immunocompétentes C57BL/6 ou Balb/c exprimant des checkpoints humains [309–311]. Ces souris génétiquement modifiées peuvent exprimer jusqu'à deux gènes humains codant pour des checkpoints (PD-L1, CD47, BTLA, CD137, TIM3, LAG-3, ICOS, GITR, OX40, OX40L...). Elles ont été notamment utiles pour comprendre les mécanismes de l'auto-immunité induite par les anticorps anti-CTLA-4 [309], et pour caractériser un anticorps anti-PD-1 candidat pour la clinique [310] dans un environnement immunitaire cependant

entièrement murin.

	Nom des souris	Souche de souris	Protéine impliquée	Effets	réfs
Niche	NSGW41	NSG	c-kit ^m	Améliore l'hématopoïèse et la formation plaquettaire. Améliore la prise de greffe de CSH.	[279]
	BRGF	BRG	FLT3 ^m	Améliore le développement monocyte/DC. Permet l'étude des ILC.	[283,284]
Cytokine	NSG-SGM3	NSG	SCF ^h GM-CSF ^h IL-3 ^h	Améliore la différenciation des macrophages et DC.	[290]
	NOG-EXL	NOG	GM-CSF ^h IL-3 ^h	Améliore la différenciation des macrophages et DC.	[291]
	BRG hIL-3 hGM-CSF	BRG	GM-CSF ^h IL-3 ^h	Améliore la différenciation des macrophages et DC. Remplacement des macrophages alvéolaires murins par des macrophages humains.	[292]
	MISTRG	BRG	GM-CSF ^h IL-3 ^h M-CSF ^h TPO ^h Sirpα ^{NOD}	Améliore la différenciation des macrophages et DC. Améliore le développement NK. Anémie.	[294]
	NOG-IL2 Tg	NOG	IL-2 ^h	Améliore le développement de NK matures et fonctionnels.	[297]
	SRG-15	BRG	IL-15 ^h Sirpα ^h	Améliore le développement de NK circulant et résidant dans les tissus.	[299]

				Evaluation de l'ADCC	
	IL-15 NOG	NOG	IL-15 ^h	Améliore le développement de NK circulant et résidant dans les tissus. Evaluation de l'ADCC	[300]
Modifications du CMH	NSG β2m KO	NSG	β2m ^{-/-m}	Baisse de la xeno-GvHD	[242]
	NSG HLA-A2	NSG	HLA-A2 ^h	Réponse spécifique au virus de la dengue restreinte au HLA.	[305]
	NSG HLA-DR	NOG	HLA-DR4 ^h I-Ab ^{-/-}	Commutation de classe isotypique.	[307]
	Humamice	C57BL/6	HLA-A2 ^{+/+h} DR1 ^{+/+h} H-2-β2m ^{-/-m} Iaβ ^{-/-m} Rag2 ^{-/-m} IL2ry ^{-/-m} Perf ^{-/-m}	Baisse de la GvHD. Réponse T et B contre le virus de l'hépatite B.	[308]
Checkpoint immunitaire	huCTLA-4	C57BL/6	CTLA-4 ^h	Évaluation des Ac anti-CTLA-4 humains.	[309]
	huPD1	C57BL/6	PD1 ^h	Évaluation des Ac anti-PD1 humains.	[310]

Tableau 6 : Dernières générations de souris modifiées génétiquement

m : murin , h : humain. *Adapté de De La Rochère et al. Trends in Immunology, 2018.*

4.2.5. Evaluation préclinique dans les modèles humanisés

Les souris Hu-PBL-scid et Hu-SRC-scid ont été utilisées comme modèles précliniques pour caractériser les réponses immunitaires *in vivo* dans des modèles d'infection, de transplantation, d'auto-immunité et de cancer. Les applications en dehors du

domaine du cancer seront brièvement décrites, l'utilisation des souris HIS sera ensuite détaillée pour l'évaluation des thérapies anti-cancéreuses. Ainsi en dehors des applications anti-cancéreuses, les souris humanisées ont été largement utilisées dans l'étude des infections rétrovirales [312], et en particulier dans la recherche sur le VIH-1. Dans les nouveaux modèles humanisés améliorés [313], il est clairement possible d'établir l'infection par le VIH-1 par inoculation par voie intrapéritonéale, intraveineuse ou au niveau des muqueuses, et d'observer ensuite la réplication virale et la déplétion des lymphocytes T CD4⁺. Par conséquent, la pathogenèse immunitaire de l'infection par le VIH-1 peut être examinée en détail, ainsi que l'efficacité des nouvelles thérapies anti-rétrovirales [314–316]. De même, les souris HIS ont été utilisées pour l'étude des infections par d'autres virus humains (virus de la dengue, virus Epstein Barr, influenza, herpèsvirus associé au sarcome de Kaposi, virus Ebola et hantavirus, virus de l'hépatite B), par des bactéries (fièvre typhoïde, *Mycobacterium tuberculosis*), et par des parasites (paludisme) [317,318]. Un autre domaine d'application des souris HIS est la transplantation, dans le but de prévenir le rejet des allogreffes. Des résultats intéressants ont été observés après une transplantation artérielle [319]. De plus, dans un modèle d'allo-GvHD humaine, décrite chez la souris NSG, il a été démontré l'efficacité des Treg CD8⁺ pour contrôler cette GvHD [320]. Par ailleurs, les souris HIS sont utilisées pour étudier les maladies auto-immunes, en particulier le diabète de type 1, le lupus érythémateux disséminé, l'arthrite, la colite ulcéreuse, la dermatite atopique, les vascularites, ainsi que les pathologies allergiques [318]. Des souris humanisées ont également été utilisées comme modèle robuste pour l'étude de la GvHD humaine [215], et pour évaluer l'action spécifique d'anticorps anti-CTLA-4 sur des lymphocytes T humains [321]. Enfin, les souris Hu-SRC-scid ont été largement utilisées pour l'étude de l'hématopoïèse humaine [322].

Dans le domaine de l'immunothérapie anti-cancéreuse, les souris humanisées représentent l'un des modèles pré-cliniques les plus attractifs pour le criblage d'approches thérapeutiques incluant l'immunothérapie cellulaire, les inhibiteurs de point de contrôle immunitaire, la thérapie génique ou encore l'utilisation de cytokines. L'évaluation des immunothérapies, dans le contexte du cancer, effectuée

dans les souris HIS, est discutée dans les chapitres suivants, et résumée dans le **Tableau 7**.

4.2.5.1. Thérapies cellulaires

Les progrès récents dans l'utilisation des souris humanisées ont fourni de nouvelles possibilités pour évaluer l'efficacité des cellules CAR-T. Il convient de noter que notamment, après plusieurs études précliniques, la FDA a approuvé en septembre 2017 le premier traitement CAR-T de la leucémie lymphoblastique aiguë des cellules B chez les enfants et les jeunes adultes. L'une des premières études dans ce domaine date de 2010, dans lequel des cellules CAR-T conçues pour reconnaître la mésothéline, un antigène fortement exprimé sur des cellules de mésothéliome, ont montré des effets anti-tumoraux puissants sur le mésothéliome malin dans des souris Hu-PBL-scid [323]. En outre, des cellules CAR-T ciblant un antigène de cellules souches de la prostate (PSCA) ont montré une activité anti-tumorale significative dans un modèle murin Hu-PBL-scid de cancer du pancréas [324]. Plus récemment, une étude préclinique avec des cellules CD4⁺ CAR-T, spécifique de la mésothéline, équipées d'un domaine de signalisation intracellulaire de ICOS a montré une forte activité anti-tumorale contre une xénogreffe de cancer du poumon dans des souris NSG [325]. L'efficacité et la fonction des autres cellules CAR-T ont également été testées dans ces modèles, y compris les cellules CAR-T dirigées contre ROR1 (récepteur tyrosine kinase récepteur orphelin 1) dans le lymphome du manteau [326], CD44 (isoforme 6) et CD33/CD123 dans la leucémie myéloïde aiguë [327,328] et le myélome multiple [329], CD27 et CD28 dans le cancer de l'ovaire [330], CD19 dans l'aplasie des cellules B [331] ou CD30 dans le lymphome [332]. Les cellules CAR-T ont également démontré leur potentiel à cibler et à éliminer des cellules souches cancéreuses de gliome par le biais du récepteur à l'IL-13 [333]. Cependant, bien que la thérapie CAR-T ait obtenu des résultats très prometteurs dans des essais précliniques et cliniques, des rapports d'événements indésirables graves tels qu'une toxicité non tumorale, un syndrome de libération de cytokine ou une neurotoxicité

ont également été observés chez l'homme. Le développement de modèles murins humanisés plus sophistiqués devrait aider à fournir une thérapie CAR-T plus sûre et plus efficace.

Un autre volet de la thérapie cellulaire anti-cancer est basé sur l'utilisation des cellules NK. Bien que plusieurs études aient clairement démontré le rôle actif des cellules NK dans la surveillance immunitaire contre le cancer, seules quelques études précliniques ont été réalisées dans ce domaine, et le modèle Hu-SRC-scid représente une plate-forme puissante pour explorer le rôle pivot des cellules NK [334]. Des progrès récents ont été obtenus en stimulant l'activité anti-tumorale des cellules NK et NKT dans des modèles *in vivo* de glioblastome, de cancer de l'ovaire, colorectal et pancréatique [335–338]. D'autre part, l'utilisation d'un modèle humanisé a permis de démontrer l'efficacité anti-tumorale du transfert adoptif *in vivo* de cellules NK allogéniques dans le traitement du cancer colorectal [337]. Actuellement, la thérapie cellulaire NK impliquant des modèles humanisés de cancer du pancréas a montré des preuves précliniques que les cellules NK activées ciblent préférentiellement les cellules souches cancéreuses mettant en évidence la potentielle application clinique de l'immunothérapie NK comme approche pour traiter des tumeurs solides réfractaires [339].

Une autre approche étudiant l'immunothérapie cellulaire dans des modèles humanisés a montré que la réactivation des cellules dendritiques plasmacytoïdes par des agonistes des récepteurs Toll-like (TLR-7) augmentait les réponses anti-tumorales au mélanome [340].

4.2.5.2. Inhibiteurs de checkpoints immunitaires

Parmi les nouvelles immunothérapies émergentes, les inhibiteurs de point de contrôle immunitaire (checkpoint) ont particulièrement démontré des avantages cliniques impressionnants. Beaucoup de ces agents ont été explorés en utilisant des souris humanisées, ce qui peut offrir l'opportunité d'évaluer les anticorps utilisables chez l'homme avant les essais cliniques humains. Fisher et ses collègues ont testé

l'efficacité anti-tumorale d'un anticorps anti-CD137 suite à une xénogreffe de lignée cellulaire de carcinome de la prostate (PC3) dans une souris Hu-PBL-scid [341]. Par la suite, Sanmamed et ses collègues ont rapporté qu'une combinaison d'un anticorps anti-hCD137 (urelumab) et d'un anticorps anti-PD1 (nivolumab) inhibait la croissance tumorale et augmentait la production d'IFN- γ dans un modèle de cellules colorectales HT-29 humaines [245]. De plus, Ashizawa et al. [295] ont rapporté une réduction de la croissance tumorale, en utilisant un anticorps anti-PD1, dans des modèles murins Hu-PBL-scid de lymphomes et de glioblastomes. Shi-Dong Ma et ses collègues ont démontré que le traitement des souris NSG humanisées par des CSHs provenant de cordon ombilical, infectées par EBV, avec la combinaison d'anticorps bloquants CTLA4/PD1 diminuait de manière significative la taille des tumeurs et augmentait la survie de la souris [343]. Récemment, en utilisant un modèle murin Hu-PBL-scid orthotopique de mésothéliome pleural, certains auteurs ont démontré que la combinaison du blocage du point de contrôle PD-1 peut être une stratégie efficace pour améliorer la puissance des thérapies de cellules CAR-T [344].

4.2.5.3. Autres immunothérapies basées sur des anticorps

Actuellement, une multitude de nouvelles stratégies thérapeutiques anti-tumorales à base d'anticorps ont été évaluées dans des modèles précliniques impliquant des souris humanisées notamment via un mécanisme d'ADCC. Ito et ses collègues ont démontré que KM2760, un anticorps anti-CCR4 est capable d'induire un effet anti-tumoral par ADCC, via les NK, chez des patients adultes atteints de leucémie/lymphome [345]. Plus tard, le groupe de Katano a observé des résultats similaires avec le même anticorps dans une lignée cellulaire de lymphome de Hodgkin [297]. En outre, des approches thérapeutiques dans des modèles humanisés ciblant l'anhydrase carbonique (CA) IX, une protéine exprimée sur des cellules de carcinome rénaux, ont entraîné une inhibition de la croissance tumorale [346]. En 2017, Wege et al. ont évalué l'effet bénéfique du renforcement potentiel du trastuzumab (anticorps monoclonal recombinant spécifique des récepteurs

HER2/neu) en association avec l'IL-15 dans des modèles humanisés du cancer du sein [347].

Bien que les souris Hu-PBL-scid soient le modèle le plus couramment utilisé pour évaluer les approches immunothérapeutiques, le modèle Hu-SRC-scid a également été utilisé. Ainsi, des études précliniques récentes ont montré l'efficacité de l'anticorps anti-CD52 (alemtuzumab) dans un modèle Hu-SRC-scid de la leucémie à cellules B réfractaires et du lymphome [348,349]. En outre, Mahne et ses collaborateurs ont observé dans un modèle Hu-SRC-scid traité avec un anticorps anti-GITR, une fréquence réduite de Tregs et une augmentation des lymphocytes T CD8⁺ corrélées avec l'inhibition de la croissance tumorale [350].

Plus récemment, des anticorps bi-spécifiques, ciblant à la fois les lymphocytes T et un antigène tumoral, ont été évalués dans des modèles précliniques humanisés. Goldenberg et ses collègues ont observé dans un modèle de carcinome du colon que l'anticorps bi-spécifique EpCAM/CD3 induisait une réduction tumorale médiée par le recrutement de cellules CD3⁺ à la tumeur humaine [351]. En outre, REGN1979, un anticorps bi-spécifique entièrement humain ciblant à la fois CD20 sur les cellules B et CD3 sur les cellules T a montré une puissante activité anti-lymphome dans les souris NSG humanisées par des PBMC [352]. Récemment, Sahin et ses collègues ont observé un effet thérapeutique significatif de deux anticorps bi-spécifiques (anti-CD3/CLDN6 et anti-CD3/EpCAM) dans des souris Hu-PBL-scid greffées avec une lignée cellulaire de carcinome de l'ovaire [353]. En 2016, un nouvel anticorps bispécifique, ciblant à la fois l'antigène carcino-embryonnaire (CEA TCB) et le CD3, a été testé chez des souris humanisées, montrant une activité anti-tumorale puissante dans des tumeurs solides mal infiltrées [354].

4.2.5.4. Thérapie génique

La thérapie génique avec des virus adéno-associés recombinants (AAV), qui permettent l'expression à long terme de transgènes ayant des effets thérapeutiques, a démontré une large application pour le traitement de maladies génétiques et est

actuellement également testée pour le cancer. Les souris humanisées ont un fort potentiel pour tester l'efficacité biologique des vecteurs AAV sur les cellules et les tissus humains. Ainsi, Münch et ses collaborateurs ont observé qu'une seule administration intraveineuse de vecteur AAV présentant des DARPin spécifiques de Her2/neu était efficace pour réduire la masse tumorale mammaire et prolonger la survie plus longtemps que le trastuzumab dans les souris HIS [355].

4.2.5.5. Thérapies basées sur les cytokines

L'administration de cytokines pro-inflammatoires est une stratégie couramment utilisée visant à stimuler la fonction anti-tumorale des cellules immunitaires effectrices. En utilisant des souris HIS, il a été observé que les immunothérapies à base d'IL-15 peuvent stimuler la survie et la fonction des cellules NK, conduisant à un contrôle significatif de la croissance tumorale incluant le cancer du sein et les leucémies [347,356,357]. Il est à noter que Wege AK et al. ont montré que l'administration concomitante de trastuzumab et d'IL-15 provoquait l'éradication des tumeurs mammaires, mais entraînant en parallèle des effets secondaires fatals associés à une hyper-activation des lymphocytes T [347]. En plus de l'IL-15, d'autres voies impliquant des interleukines ont été testées dans les souris HIS telles que l'IL-2, l'IL-12, l'IL-6 ou l'IL-7 avec des résultats intéressants [358–361]. En particulier, l'administration d'une dose élevée d'IL-2, l'une des premières immunothérapies anticancéreuses approuvées par la FDA, à des souris BRGS a reproduit la toxicité humaine et mis en évidence le rôle des cellules Treg dans le maintien de la tolérance immunitaire [358]. En outre, Durost et ses collègues ont évalué l'effet d'un vecteur AAV exprimant l'IL-2 humaine dans une souris BLT et ont montré une augmentation significative du nombre de cellules Tregs et NK humaines fonctionnelles, comme observé dans les essais cliniques après administration d'IL-2 [362].

Globalement, bien que différents composants du système immunitaire présents dans

les modèles humanisés montrent quelques défauts de maturation et/ou de fonction, des études précliniques chez ces souris ont permis de mieux comprendre l'interaction entre les cellules immunitaires et cancéreuses humaines et leurs réponses aux approches thérapeutiques humaines.

Type de xélogreffe de tumeur	Origine de la tumeur	Origine des cellules immunitaires	Souche de souris	Approche thérapeutique	Refs
Mésothéliome	Tumeur primaire	PBMC	NOD-scid	Cellules CAR-T (cible : mésothéline)	[323]
Pancréas	Tumeur primaire	PBMC	NSG	Cellules CAR-T (cible : PSCA)	[324]
Poumon	Lignée cellulaire	PBMC	NSG	Cellules CAR-T (cible : mésothéline)	[325]
Ovaire	Tumeur primaire	PBMC	NSG	Cellules CAR-T (cible : récepteur au folate/CD19)	[330]
Aplasie à cellules B	Lignée cellulaire	CSH	NSG	Cellules CAR-T (cible : CD19)	[331]
Leucémie aigüe myéloblastique	Lignée cellulaire	CSH	NSG	Cellules CAR-T (cible : CD123)	[327]
Lymphome	Lignée cellulaire	CSH	Rag KO	Cellules CAR-T (cible : CD30)	[332]
Leucémie aigüe myéloblastique	Tumeur primaire/Lignée cellulaire	CSH	NSG	Cellules CAR-T (cible : CD33/CD123)	[328]
Gliome	Lignée cellulaire	PBMC	NSG	Cellules CAR-T (cible : IL13-zetakine)	[333]
Ovaire	Lignée cellulaire	PBMC	NSG	Cellules NK	[336,338]
Glioblastome	Tumeur	PBMC	NSG	Cellules NK	[335]

	primaire				
Cancer colorectal	Lignée cellulaire	CSH	BRGS	Cellules NK	[337]
Pancréas	Lignée cellulaire	PBMC	NSG	Cellules NK	[358]
Leucémie/lymphome	Tumeur primaire	PBMC	NOG	Ac anti-CCR4	[345]
Lymphome d'Hodgkin	Lignée cellulaire	CSH	NOG	Ac anti-CCR4	[297]
Leucémie	Tumeur primaire	CSH	NSG	Ac anti-CD52	[348]
Lymphome	Tumeur primaire	CSH	NSG	Ac anti-CD52	[349]
Carcinome du colon	Lignée cellulaire	CSH	NSG	Ac anti EpCAM/CD3	[351]
Lymphome	Lignée cellulaire	PBMC	NSG	Ac bispécifique (REGN1979)	[352]
Ovaire	Lignée cellulaire	PBMC	NSG	Ac bispécifique (anti-CD3/CLDN6 et anti-CD3/EpCAM)	[353]
Prostate	Lignée cellulaire	PBMC	NSG	Ac anti-CD137	[341]
Carcinome gastrique et carcinome du colon	Tumeur primaire	PBMC	Rag KO	Ac anti-CD137/Anti-PD1	[245]
Lymphome/Glioblastome	Lignée cellulaire	PBMC	NOG	Ac anti-PD1	[342]
Sein	Lignée cellulaire	PBMC	NSG	Thérapie génique	[355]
Mélanome	Lignée cellulaire	CSH	NSG	Ac anti-GITR	[350]
Lymphome B	Lignée cellulaire	CSH	NSG	Ac anti-CTLA4/PD1	[343]

Leucémie	Lignée cellulaire	CSH	NSG	IL-15	[356]
Sein	Lignée cellulaire	CSH	NSG	IL-15 + trastuzumab	[347]
Mélanome	Tumeur primaire	CSH	NSG	Agoniste de TLR-7	[340]
Carcinome des cellules rénales	Lignée cellulaire	PBMC	NSG	Ac anti-Carbonic anhydrase IX	[346]

Tableau 7. Études précliniques utilisant des modèles de souris humanisées pour l'immunothérapie du cancer. Adapté de De La Rochère et al. Trends in Immunology, 2018.

Résultats

Les résultats présentés dans ce manuscrit se présentent sous la forme de deux articles prêts à être soumis aux publications scientifiques pour révision.

L'article I s'est, en premier lieu, focalisé sur la description de l'établissement des modèles de souris humanisées, avec notamment la comparaison des reconstitutions immunitaires obtenues après injection de PBMC ou de cellules souches hématopoïétiques dans des souris immunodéficientes. Nous avons, ensuite étudié, les interactions entre la tumeur et les cellules immunitaires en absence de traitement. Nous avons, au final, évalué la pertinence de ces modèles dans l'évaluation d'immunothérapies, (Nivolumab et complexe IL-2/anticorps anti-IL-2) dans des modèles de souris porteuse de tumeurs issues de lignées cellulaires de tumeur de sein (MDA-MB231) et issues de PDX de poumons. Nous montrons que les modèles Hu-PBL font partis des modèles utiles pour évaluer l'efficacité d'immunothérapies, ciblant les lymphocytes.

L'article II s'est appuyé sur les résultats obtenus dans l'article I pour étudier les interactions entre le système immunitaire et des lignées de tumeur de vessie mutées ou non pour la voie de signalisation de la PI3 kinase. Nous montrons que les lignées mutées pour la PI3 kinase présentent une signature immunologique plus faible que les tumeurs non mutées. L'utilisation du modèle Hu-PBL montre que l'utilisation d'un inhibiteur de la PI3 kinase, le BKM120, dans une tumeur mutée retarde la croissance tumorale. Cette inhibition est accompagnée d'une augmentation de l'infiltration tumorale de cellules HuCD45⁺ en comparaison des tumeurs non traitées.

Article I

A comprehensive analysis of humanized mouse models for the study of cancer immunotherapies

De La Rochere Philippe^{1*}, Loumagne Laure^{2*}, Melanie Rathaux¹, Dubois Marine¹, Nemati Fariba³, Sedlik Christine¹, Decaudin Didier³, Georges Azar², Sidhu Sukhvinder², Piaggio Eliane¹

¹ INSERM U932, and SiRIC Translational Immunotherapy Team, Translational Research Department, Institut Curie, PSL Research University, Paris F-75005, France.

² Sanofi Oncology, 1 Impasse des Ateliers, Vitry Sur Seine, France.

³ Laboratory of Preclinical Investigation, Translational Research Department, and Department of Medical Oncology, Institut Curie, PSL Research University, Paris F-75005, France.

* equal author contribution

Correspondence: Eliane Piaggio INSERM U932, Institut Curie, 26, rue d'Ulm, 75005 Paris, France. Phone: 33 1 56 24 58 05; Fax: 33 1 44 07 07 85; E-mail: eliane.piaggio@curie.fr

Running title:

Disclosure of Potential Conflicts of Interest: No potential conflicts of interest were disclosed.

Abstract

Immunotherapy with anti-checkpoint antibodies has given impressive clinical results and manageable safety profiles, but only in a small fraction of patients and tumor subtypes. Humanized mouse models (HIS), which recapitulate many aspects of the crosstalk between human immune and tumor, represent a promising tool to understand anti-tumor immunity and to perform pre-clinical evaluation of onco-immunotherapies, including combinations. Here we analyzed the different components of HIS mice, including the quality of immune cell engraftment of PBMCs in HIS mice and its consequence on GvHD development, the impact of the immunodeficient host mice strain on the engraftment of human (Hu)-CD34⁺ hematopoietic stem cells (HSC), the cross-talk between human T cells and tumors originating from human cell lines or PDXs from breast and lung origin, and we assessed the therapeutic efficacy of Nivolumab as monodrug or in combination with an IL-2-based immunotherapy. Our data revealed the assets and limitations of these models and constitute a resource for the design of pre-clinical immuno-oncology strategies and a guide for future development of improved HIS models with heightened translational power.

Introduction

The blockade of immune checkpoints with antibodies (Ab) anti-CTLA-4, anti-PD1 and anti-PD-L1, has given impressive clinical results and manageable safety profiles, positioning immunotherapy as a promising therapeutic strategy to treat cancer ¹⁻⁴. However, to implement these novel immunotherapies, it is essential to gain knowledge on their mechanism of action, identify prognostic and predictive biomarkers of response and toxicity, and prioritize the test of therapeutic approaches based on the combination of Abs with other immunotherapies (such as bi-specific antibodies, cytokines, vaccination, dendritic cell stimulation or Treg elimination) or with radiotherapy or chemotherapy. Thus, there is an unmet need to develop more translatable *in vivo* mouse tumor models. These models should be fundamental to elucidate the role of immunity in tumor pathogenesis and to carry out pre-clinical evaluation of novel immunotherapies, mainly combination ones. Ultimately, translational research should help to implement patient-tailored therapies.

The major approaches to assess cancer immunotherapies in preclinical studies today include syngeneic mouse tumor models and genetically engineered mouse models (GEMMs) both in fully immune-competent hosts, as well as humanized mouse models ⁵. While the first two approaches have been intensively used to bridge cancer biology and translational research, one major inconvenient is that they rely on the mouse immune system that does not fully recapitulate the human counterpart ⁶. Moreover, these models do not allow neither the evaluation of the same therapeutic antibodies or drugs used in the clinic that are directed to human targets, not the direct study of the human immune populations. Therefore, humanized mouse models that can reconstitute a functional human immune system and that can be engrafted with human tumors (cell lines or patient-derived xenografts (PDXs)) are essential tools to characterize immunomodulatory compounds in a more physiologically relevant setting.

In humanized mouse models, immunodeficient host mice are grafted with human immune cells and with tumor of human origin ⁷. Mainly, two different sources of human immune cells are used: hematopoietic stem cells (HSC) (**Hu-CD34+ model**) or human peripheral blood mononuclear cells (PBMCs) (**Hu-PBL** (peripheral blood

lymphocytes) **model**). The HSC approach is based in the injection of CD34+ progenitor cells that have the capacity of self-renewal and the ability to reconstitute for a long term period (several months) almost the full complexity of human immune cells, including T cells, NK cells, DC and monocytes. However, mice develop chronic graft-versus-host- disease (GvHD), and developing immune cells are not completely mature and functional. Recently, several strains of highly immunodeficient mice were engineered to improve human immune cell engraftment after injection of HSC ⁷. Today, there are four main commercially available immunodeficient strains described to sustain CD34+ HSC engraftment to different levels: NSG ⁸, NSG-SGM3 ⁹, NOG ¹⁰ and NOG-EXL ¹¹. The NSG and NOG mice differ in terms of their genetic modifications leading to IL2Rgamma chain deficiency. However both mutations achieve the same functional knock down of IL2R gamma expression leading to a complete lack of T, B and NK cell development in these mice. NSG-SGM3 and NOG-EXL are transgenic for the expression of human cytokines involved in human myeloid cell development to improve reconstitution of these cells (IL-3 and GM-CSF for both strains and KIT-ligand for NSG-SGM3 only). To our knowledge, no side-by-side comparison of human immune cell reconstitution in these mouse models has been performed as today. In the Hu-PBL model, leukocytes are generally obtained from PBMCs from healthy donors. From the initial inoculum, very low number of myeloid and B cells are detected, being the T cells the predominant population that repopulates and survives in the host mice. The main limitation of this model is that it leads to fatal acute xeno-GvHD ^{12,13} (usually 3-5 weeks after PBMCs injection), restricting the use of this model to the evaluation of anti-tumor T cell responses within a relatively short window of experimental observation.

Overall, the main hurdles of humanized mice are associated to i) the presence of murine innate immune cells, such as macrophages, dendritic cells and neutrophils, that negatively influence the engraftment of human hematopoietic cell efficacy, ii) the logistic difficulty to obtain matched donor and tumor samples, iii) the incomplete reconstitution of the human immune response, iv) the development of xenogeneic-GVHD, and v) the high cost. Nevertheless, humanized mice may represent a unique

tool to capture the heterogeneity of patients' response and not least, they could potentially be used to evaluate individualized cancer immunotherapies.

Here we performed a rational and thorough assessment of the different components of HIS mice and their impact on anti-tumor immune responses. More specifically, we evaluated: i) the quality of immune cell engraftment of PBMCs in HIS mice and its consequence on GvHD development, ii) the impact of the immunodeficient host mice strain (NSG, NSG-SGM3, NOG and NOG-EXL) on the engraftment of Hu-CD34+ HSCs, iii) the cross-talk between T cells and different types of human tumors (cell lines or PDXs from breast and lung cancer), and iv) we assessed the therapeutic efficacy of a clinical grade anti-PD1 monoclonal antibody (Nivolumab) as monodrug or in combination with an IL-2-based immunotherapy. Our data evaluating the advantages and limitations of these models constitute a resource for the design of pre-clinical immuno-oncology strategies and a guide for future HIS model developments.

Results

1- Human PBMCs engraftment in Hu-PBL mice: immune cell reconstitution and GvHD development

In the Hu-PBL-NSG mice model, injected human peripheral blood mononuclear cells (PBMC) efficiently engraft, but invariably induce GvHD clinically characterized by weight loss, hunched posture, skin changes and high mortality¹³. In consequence, this model can be useful to study immunotherapies only if a therapeutic window exists before the development of overt GvHD. To that end, we evaluated the consequences of injecting different amounts of PBMCs, to determine the best conditions allowing immune reconstitution with delayed GvHD onset. Administration of fresh or thawed PBMCs attains the same level of reconstitution in NSG mice (data not show), thus human PBMCs containing the indicated amounts of CD3+ T cells (from 1 to 30 x 10⁶) either fresh or thawed, were injected i.v. into non-irradiated NSG mice. Immune reconstitution was immunomonitored in peripheral blood, and we arbitrarily considered that mice were stably reconstituted when at

least of 2% of Hu-CD45+ cells were detected in blood at two different days (**Figure 1A**). GvHD development was monitored by regular recording of weight, and GvHD onset was defined when weight loss was >10 %¹⁴. Results summarized in **Figure 1B** indicate that: i) at least $5 \cdot 10^6$ CD3+ T cell-containing PBMCs have to be injected into NSG mice so as to obtain engraftment of human immune cells in most (>90 %) of the animals. ii) The level of maximal reconstitution, calculated as % of Hu-CD45+ cells in blood, increases with the dose of injected PBMCs, reaching up to around a mean of 50% of human hematopoietic cells in mice injected with the highest tested dose. iii) The frequency of mice that develop evident GvHD is positively correlated with the number of PBMC present in the inoculum, varying between 65 to 100 % in mice receiving from 5 to 30×10^6 initial human CD3+ T cells, and also iv) the higher the amount of Hu-PBMC injected, the earlier the clinical symptoms of GvHD are manifested, with an onset of weight loss > 10% of initial weight being detected as soon as 14 days after the graft of $20\text{-}30 \times 10^6$ PBMCs. v) the onset of GvHD clinical symptoms was observed in most of the mice when the % of Hu-PBMCs in blood reached more than 30 %, although it could be detected at lower reconstitution rates (starting from 10 %).

Given these results, grafting between 5 to 10×10^6 CD3+ T cell-containing PBMCs per NSG mouse seemed to give a good compromise between engraftment rate and GvHD development. **Figure 1C** shows the kinetics of immune cell reconstitution and GvHD development for individual mice of pooled experiments in which mice were grafted with 5 or 10×10^6 CD3+ T cell-containing PBMCs. We observed that injection of 10×10^6 CD3+ T cell- containing PBMCs promoted faster reconstitution than 5×10^6 CD3+ T cell-containing PBMCs, albeit with a slightly shorter delay of GvHD onset (**Figure 1B and C**). Of note, immune cell reconstitution was highly heterogeneous among mice, which can in part be attributed to the fact that PBMCs are obtained from different healthy donors. Consequently, for the following experiments, we decided to inject $5\text{-}10 \times 10^6$ CD3+ T cell-containing PBMCs. Also, to take into consideration the important variation in reconstitution observed among donors, in all the following experiments we included in each experimental group mice injected with one of at least 2 different donors.

Reconstitution analysis showed that injection of 10×10^6 PBMCs allows an engraftment of human immune cells mainly in blood and spleen and poorly in the bone marrow (**Figure 1D**). This engraftment increases over time reaching a maximum of 70% in blood and 80% in spleen but remains around 10% in the bone marrow 41 days post-PBMC injection. As soon as day 7, approximately 90% of the engrafted cells were huCD3⁺ T cells in peripheral blood, spleen and bone marrow. At day 7, blood huCD4⁺ and huCD8⁺ T cells were present at equivalent proportion among Hu-CD45⁺ cells (45% and 29% respectively) whereas from day 28 until the onset of GvHD, the proportion of huCD4⁺ T cells increased to become dominant over huCD8⁺ T cells (64% vs 18% respectively). A similar trend was observed in the spleen. From day 7 to day 41 post-PBMC injection, only a minor proportion of CD3⁺ CD56⁺ cells (4 to 7% of Hu-CD45⁺) were found in the blood and in the spleen and some huB cells (2 to 4% of total Hu-CD45⁺) were found in the bone marrow (**Figure 1D**, and **supplementary Figure 1** (gating strategy used for Hu-PBL and Hu-CD34⁺ NSG mice)).

Overall, our data show that Hu-PBMCs engraft in NSG mice in a dose-dependent time-sustainable way, mainly allowing the development of huCD4⁺ and huCD8⁺ T cells and indicating that this model is adapted to study T cell responses. However, injection of huPBMCs induces GvHD in a dose-dependent way.

2- Phenotypic characterization of engrafted T cells in Hu-PBL mice

Since these humanized mice develop GvHD, we then characterized the kinetic of activation of T cells to assess if this model is appropriate for the evaluation of immunomodulatory drugs activity in vivo. After injection in mice, human T cells very rapidly acquire activation markers and a differentiated state phenotype. This was noticeable by comparing the relative proportions of T cells with a differentiated state or T cell expressing activation markers between humanized-mouse and healthy donor blood T cells (**Figure 2 A, B** and **Supplementary Figure 2**). From day 7 to 41, huCD4⁺ central memory cells slowly decreased from 40% to 25% of total huCD4⁺ cells whereas effector memory T cells constantly increased from 29% to 75%. On the contrary, huCD4⁺ naïve and terminal effector cells were barely detectable from day 14 (<2.5% of huCD4⁺ T cells). Proportion of HLA-DR⁺ cells among huCD4⁺ T cells

raised from day 14 to day 41 (16% vs. 58% respectively). On the contrary, early activation marker CD25 decreased from day 14 to day 41 (63% vs 25% respectively), suggesting that it might have increased before day 14. HuCD8⁺ T cell activation increased over time, reaching a maximum at day 41. It is worth noticing that this activation seems to have occurred even before day 7, since 60% of huCD8⁺ T cells being effector memory and expressing HLA-DR marker at day 7. Central memory and CD25⁺ cells represented 15% of huCD8⁺ T cells and were stable from day 14. As for huCD4⁺ T cells, naïve and terminal effector CD8⁺ T cells were almost no detectable beyond day 14 ($\leq 1\%$ of huCD8⁺ T cells). Activation of huT cells in spleen and bone marrow followed roughly the same kinetic and amplitude. This increase in the proportion of activated T cells and in T cells with a differentiated state phenotype was consistent with the accumulation of plasma T-cell derived cytokines, i.e. huIFN- γ and huTNF- α from day 7 to day 36 (2 852 vs 176 881 pg/mL and 1.6 vs 5 194.5 pg/mL). (**Figure 2C**)

Overall, the previously observed development of GvHD was concomitant with an activation of T cell leaving only a short window of time to detect an effect of immunotherapy on T cells.

3- Human immune cell engraftment in Hu-CD34⁺ mice: immune cell reconstitution and GvHD development

An alternative approach to Hu-PBL mice allowing the reconstitution of human immune cells is the injection in immunodeficient hosts of Hu-CD34⁺ HSCs. This model requires sub-lethal irradiation of the host mice to deplete the mouse HSCs and thus facilitate human HSCs' engraftment. Human HSCs can be obtained from four main sources: umbilical cord blood, adult bone marrow, granulocyte colony-stimulating factor-(G-CSF) mobilized PBMCs or fetal liver, which give variable degrees of engraftment ⁷. In the Hu-CD34⁺ model, most human hematopoietic lineages are represented, but present a maturation default, particularly in the myeloid population. Consequently, immunodeficient mice have been genetically modified to produce human cytokines and growth factors allowing for an improved engraftment of the human HSC. Here we performed a side-by-side comparison of the four most

common commercially available HIS mouse model, namely the NSG, NSG-SGM3, NOG and NOG-EXL, xenografted with Hu-CD34⁺ HSCs. We evaluated the quality and quantity of the developing human immune cells. Each mouse strain was humanized according to the providers' recommendations by performing sub-lethal irradiation followed by i.v. injection of human Hu-CD34⁺ HSCs obtained from human umbilical cord blood (**Figure 3A**).

Eighteen weeks post-humanization, we observed high levels of human immune cell engraftment reaching around 50-70% among total hematopoietic cells (Hu-CD45⁺ plus mCD45⁺ cells) in peripheral blood (**Figure 3B**). NSG-SGM3 displayed higher percentage of human immune cells at early time points. However, 39% of mice needed to be euthanized because of major weight loss between week 10 and 17 post-humanization (data not shown), rendering this mouse strain not suitable for the evaluation of cancer immunotherapy. Overall, NSG-SGM3 mice showed quicker and higher development of T cells and in particular CD4⁺ T cells and a lower development of B cells, relative to the three other mouse strains tested (**Figure 3B**). Eighteen weeks post-humanization, no significant differences of total human immune cell proportions were observed when comparing the retained different mouse strains (NSG, NOG and NOG-EXL). This was also noticed for blood immune cell subpopulations described hereinafter and it is attributed to inter-HSC donor variability (data not shown). Myeloid, B and NK cells were detectable as soon as week 4 post-humanization whereas T cells were observable only from week 12 (**Figure 3B**). The majority of the main human immune sub-populations developed in peripheral blood of these mice at percentages comparable to human blood (T cells, NK cells, non-neutrophil-myeloid cells) with the exception of B cells that were over-represented and neutrophils that were absent (**Figure 3C** and **Supplementary Figure: dot plots**). Humanized mice contained the same ratio of CD4⁺ and CD8⁺ T cells in comparison to human blood (**Figure 3D**). However, in the tested models, we did not observe the predominance of cytotoxic NK (CD16^{hi} CD56^{dim}) cells over cytokinic NK cells (CD16⁻CD56⁺) which is characteristic of human blood but rather, similar levels of both NK sub-populations (**Supplementary Figure 3A**). When looking at monocyte subpopulations, we found similar percentages of classical and non-classical

monocytes and lower percentages of intermediate monocytes in humanized mice in comparison with human blood (**Supplementary Figure 3A**). As for the myeloid compartment reconstitution, we found no improvement in NOG-EXL and NSG-SGM3 mice at late time points. Both humanized-mouse spleen and bone marrow displayed similar levels of immune cell subpopulations across mouse strains. The reconstitution of the spleen was similar to that of the blood. Of interest, human neutrophils were observed in the bone marrow (**Figure 3** and **Supplementary Figure 3**). Finally, T cells from humanized mice did not have an activated phenotype as reflected by the comparable percentage of Naïve, Effector, Central memory and Effector Memory cells between humanized mouse spleens and human blood (**Figure 4**).

In summary, our results showed that all strains displayed high levels of human immune cell engraftment, the presence of T cells, NK cells and non-neutrophils-myeloid cells at physiological percentages found in human blood. Despite the inclusion of different transgenic mouse strains in our comparison, all mouse strains showed similar levels of each immune subpopulations at late time points, with the exception of NSG-SGM3 that showed a higher and quicker development of T cells. However, the poor and short-term survival of NSG-SGM3 mice prevents us considering this model for lengthy studies allowing for a complete human immune system reconstitution as well as tumor engraftment to evaluate immunotherapy. Given the little observed differences between the NOG and NSG mouse strains, we retained the latter strain for the following evaluations.

4- Hu-PBL model: in vivo cross talk between tumor and immune cells

Having defined the conditions allowing immune cell engraftment with delayed GvHD in the Hu-PBL model, we analyzed the optimal conditions for the timing of injection of the PBMCs and the tumor graft. Indeed, a compromise is needed between human immune engraftment, tumor development and the therapeutic window before clinical GvHD onset.

Human tumors can be mainly obtained from two sources: tumor cell lines or patient derived xenografts (PDX). Here, we used cell lines or PDXs from triple

negative breast cancer (TNBC): the cell line MDA-MB231, and the PDX BC138, generated at Institute Curie ¹⁵, and from non-small cell lung cancer (NSCLC): the cell line HCC827, and the PDX LCF29, also generated at our Institut ¹⁶. Routinely, PDXs are maintained in nude mice. Tumors grew with slightly faster kinetics in the more immunodeficient NSG mice compared to nude mice (data not shown). To analyze the impact of timing of PBMC injection on tumor graft development in the hu-PBLmice, the human immune cells (5-10 x 10⁶ CD3+ T cell-containing PBMCs) were inoculated either 15 days before tumor graft, or after tumors became palpable and as controls for tumor growth, we measured tumor growth on NSG mice engrafted with the tumors without PBMC inoculation (**Figure 5A**).

First we evaluated the impact of injecting the tumor cells after 15 days of PBMC injection, using the LCF29 PDX and the MDA-MB231 tumor cell line. As observed in **Figure 5B-C** for both models, no tumor developed, while in control mice that were grafted with the tumors but did not receive PBMCs, both the PDX and the cell line grew exponentially. Mice did not develop overt GvHD (no weight lost > 20% of initial body weight) during the first 4 weeks of the experiment (**Figure 5D**). Injected PBMCs reconstituted all mice with human immune cells as measured by the detection of Hu-CD45+ cells in the blood (**Figure 5E**). These results indicate that 15 days after PBMC-injection, the engrafted human T cells exert a potent graft-versus-tumor (GvT) effect, preventing the development of PDXs and tumor cell lines.

Second, we evaluated the effect of injecting the PBMCs after the tumor was palpable. In this setting, the four tested tumors developed. Interestingly, compared to control mice grafted with the tumors but which did not receive the PBMCs, the three tumors evaluated (LCF29, BC138, and MDA-MB231) grew more slowly, highlighting again the GvT effect exerted by the injected PBMCs. The HCC827 and MDA-MB231 tumor cell lines grew more slowly than the BC138 PDXs, mice could be monitored for longer times, and we observed that eventually the GvT effect induced the regression of the all the tumors, regression that could be complete for some mice. For the BC138 model, we observed that 4 weeks after tumor graft, HuCD45+ cells constituted up to 10 % of the tumor infiltrate, and were composed mainly by

CD4⁺ T cells, lower proportions of CD8⁺ T cells and some NK cells (**Supplementary Figure 5**).

We observed that the level of Hu-CD45⁺ cells in circulation and the kinetics and intensity of GvHD development was variable among the different tumor models (**Figure 5D, E**), and they were not predictive of tumor growth control. To have a statistical analysis of the impact of the tumor on PBMC reconstitution, we pooled the data obtained from different experiments in which NSG mice were grafted with either lung (HCC827) or breast (MDA-MB231) cell lines; or with 12 different lung or two different breast PDXs, and then injected with $5-7,5 \times 10^6$ CD3⁺ T cell-containing PBMCs. We considered that mice were reconstituted when the level of circulating Hu-CD45⁺ cells was > 2% of live blood cells at two different time points during the length of the experiment. As reference, we included a pool of NSG mice that were injected with PBMCs but received no tumor. As observed in **Figure 6A**, PBMC efficiently engrafted in the NSG mice of the reference group (percentage of reconstituted mice: 97,5%, n=79), and in mice transplanted with lung (94,1%, n=17) or breast (98,1%, n=52) cell lines. In contrast, mice grafted with PDXs showed significantly lower frequencies of Hu-PBMC reconstitution: 59,3% (n=81) for lung PDXs, and 70,9% (n=31) for breast PDXs. We also quantified the maximum level of Hu-PBMC reconstitution in the same groups of mice, which was generally observed around 30-40 days after PBMC injection (**Figure 6B**). We observed that despite high heterogeneity in the percentage of Hu-CD45⁺ cells detected in the blood of HIS mice, overall, tumor-free and mice grafted with tumor cell lines reached significantly higher levels of reconstitution compared with mice grafted with PDXs, and this was true for tumors of lung and of breast origin. These results show that compared to cell lines, PDXs negatively impact PBMC reconstitution. This novel observation let us hypothesize that compared to the tumor cell line inoculum, the different number of grafted tumor cells, the architecture of the grafted piece of tumor, and/or the presence of a tumor-educated stroma at the moment of grafting could be responsible of the lower PBMC reconstitution rate registered in PDX-transplanted mice.

Overall, these results indicate that each tumor type: i) has its own speed of growth, ii) can be readily eliminated by the engrafted human immune cells (GvT) when injected once PBMC reconstitution in the host mice is advanced, and iii) can differently impact on immune cell engraftment. Consequently, to establish a standardized protocol for the Hu-PBL-tumor models, we decided to always graft the tumor before adding the PBMCs and monitor immune reconstitution in blood and mice weight, so as to control for the above-mentioned observations.

5- Pre-clinical evaluation of anti-PD1 mAb treatment on MDA-MB231 tumor growth in the Hu-PBL and Hu-CD34+ models

We previously showed that in Hu-PBL mice grafted with tumor cell lines, GvHD becomes clinically evident between 2-5 weeks after tumor injection and that GvT reaction can lead to tumor rejection in the absence of any therapeutic intervention (figure 5). However, there is a time window in which PBMCs and tumor co-exist and during which therapeutic interventions could be evaluated by the impact on GvT effect and before GvHD onset.

Thus, we first assessed the potential of the Hu-PBL model for the evaluation of an anti-PD-1 antibody used in the clinic, Nivolumab, on the growth control of the breast cancer cell line MDA-MB231. For this, NSG mice were grafted with 5×10^6 MDA-MB231 cells, and once the tumors reached the size of 10-30 mm³ (around day 5 post-graft), mice were injected with 5.10^6 CD3+ T cell-containing-PBMCs (at least two different healthy-donor PBMCs were used per experiment). Five days later, mice were randomized to the untreated or the Nivolumab-treated (10mg/kg, twice a week) groups, and we included a reference group of mice grafted with the tumor cells, but not injected with PBMCs (**Figure 7A**). **Figure 7B-C** shows the tumor-growth curves of individual mice in one representative experiment. It can be observed that compared to the untreated group, Nivolumab administration induced a delay in tumor growth. Although responses were highly heterogeneous, similar results were obtained in an independent experiment (**supplementary Figure 7**, and **Figure 7H** showing an statistically significant, yet week effect of Nivolumab treatment in the two experiments pooled).

We monitored the effect of the treatment on immune cell reconstitution and GvHD development. At day 20 after PBMC injection, we observed a mild increase of circulating HuCD45+ cells in Nivolumab-treated mice (**Figure 7D**); in parallel with the onset of weight-loss (**Figure 7E**), although no weight-loss >20% were observed until day 24 since the beginning of the experiment, when animals were sacrificed for analysis of the immune tumor infiltrate (**Figure 7F-G**). By day 24, we observed that MDA-MB231 tumors were highly infiltrated by Hu-CD45+ cells, with the level of infiltration ranging between 32 % and 88 % (**Figure 7F**), and no significant differences were observed between the untreated and the Nivolumab-treated groups. Dual-IHC analysis of tumor from untreated animals revealed that MDA-MB231 tumors are infiltrated by mCD45+ cells and Hu-CD45+ cells indicating that molecules attracting human CD8+ T cells are secreted in such humanized model (**Figure 7G**). Interestingly, human CD8 staining performed on a consecutive slide showed that the majority of these Hu-CD45+ cells are human CD8+ T cells despite the relative low proportion of human CD8+ T cells in comparison with human CD4+ T cells that we observed in the periphery (blood and spleen). Dual human CD8 and human PD1 staining did not allow us to clearly distinguish PD1 expression on these human CD8 T cells. This figure shows that human CD8+ T cells, known to be a major contributor of anti-tumor activity, are able to infiltrate the engrafted human tumor, validating this Hu-PBL-NSG model for the evaluation of anti-tumor immunotherapies.

Second, we evaluated the potential of the Hu-CD34+ model for the evaluation of Nivolumab efficacy, using the same breast cancer cell line MDA-MB231. In a preliminary experiment, NOG mice were engrafted with cord blood huCD34+ HSC (Taconic) and 6 to 8 weeks later they were grafted with 5×10^6 MDA-MB231 tumor cells. Once the tumors reached the size of 10-30 mm³ (around day 5 post-graft), mice were treated with Nivolumab (10mg/kg, twice a week) (**supplementary Figure 7E**). We did not observe any effect of Nivolumab on tumor growth (**supplementary Figure 7F**); although mice were reconstituted with the Hu-CD45+ cells (**supplementary Figure 7G**). No observe signs of GvHD were observed (**supplementary Figure 7H**).

Our results show that the Hu-PBL and the Hu-CD34+ models grafted with the same MDA-MB231 tumor-cell line have a different sensitivity to the same immunotherapy (Nivolumab), underlying that the quality of the mounted anti-tumor immune responses and their sensitivity to reinvigoration by nivolumab is model-dependent and overrides the tumor-intrinsic sensitivity to PD1-blockade. Given this observation, and the fact that the Hu-CD34+ model is more expensive, harder to work with, and more time consuming, for the following experiments we focused in the Hu-PBL model.

6- Pre-clinical evaluation of anti-PD1 mAb treatment on NSCLC-PDXs' growth in the Hu-PBL model

The management of lung cancer is currently based on surgical resection when the tumor is limited to the lung, chemo-radiotherapy in case of locally advanced unresectable tumors, or systemic therapies for metastatic tumors ¹⁷. The latter treatment strategies include: i) chemotherapy; ii) targeted therapies directed to druggable oncogenic molecular alterations; and more recently iii) immunotherapy with PD-1 checkpoint-inhibitors -such as Nivolumab - which can lead to response in 50% of patients selected on tumoral-PD-L1 expression ¹⁸. Today, identifying biomarkers correlating with response as well as understanding the developing immune response under anti-PD-1 therapy, as single agent or in combination with other therapies in the clinic, remain a major challenge. Then, we evaluated the capacity of Hu-PBL mice to capture the anti-tumoral response to Nivolumab treatment using NSCLC-PDXs.

We designed a screening protocol, including few mice per group, to assess the pertinence of this mouse model to evaluate response to Nivolumab. We used a series of nine different NSCLC PDXs generated at our Institute from fragments of primary tumors obtained from patients and maintained by successive passages in immunodeficient nude mice. NSG mice were grafted with the PDXs and once the tumors were palpable, mice were injected with $5 \text{ to } 7,5 \cdot 10^6$ CD3+ T cell-containing PBMCs (at least two different healthy-donor PBMCs were used per experiment). Three days later, mice were randomized to the untreated or the

Nivolumab-treated (10mg/kg, twice a week) groups and tumor growth curves were recorded. For the analysis, mice showing > 2% HuCD45+ cells in circulation in at least two different time points during the experiment were included, and regularly weighted to monitor for GvHD. We observed that out of the 9 evaluable PDXs, 5 (55,6%) were resistant to Nivolumab treatment (**Figure 8A**), and 4 (44,4%) showed some delay in tumor growth (**Figure 8B**). These results indicate that, as in patients, Hu-PBL mice grafted with lung-PDXs with different molecular characteristics seem to have different sensitivities to Nivolumab treatment. In conclusion, this experimental protocol, including few mice per group, seems adapted to screen PDXs for their sensitivity to immunotherapies, as a previous step before performing larger studies.

We analyzed Nivolumab effect on human immune cell reconstitution. Figure 8C shows the proportion of reconstituted mice in untreated or Nivolumab-treated groups for each tested PDX. It can be observed that the reconstitution rate highly varied among the different PDXs. Moreover, Nivolumab administration was associated with a lower rate of PBMC-reconstituted mice in most of the models (6 out of 9), did not markedly affect the number of reconstituted mice in the ML5 and LCF13 models, and was only associated with higher numbers of reconstituted mice for the LCF17 PDX. Interestingly, when we compared Nivolumab effect on PBMC reconstitution across the different models (**supplementary Figure 8**) we observed that nivolumab treatment was associated with reduced proportions of PBMC-reconstituted mice grafted with PDXs (lung or breast), but not grafted with cell lines (lung or breast); but it did not noticeably modify the level of circulating Hu-CD45+. These data suggest PDX-tumors, different to cell line-tumors have intrinsic molecular/cellular characteristics yielding different interactions with the immune cells, which also extend into different responses to immune-modulatory therapies. We hypothesize that the different tumor-types may induce different degrees of activation of the human T cells, leading to different levels of PD-1 expression, and consequently different sensitivity to anti-PD1 treatment.

7- Pre-clinical evaluation of anti-PD1 mAb treatment combined with IL-2 complexes on NSCLC-PDXs' growth in the Hu-PBL model

In the previous screening experiment, the LCF29 PDX showed some level of sensitivity to Nivolumab (**Figure 8B**) and did not particularly hamper immune cell reconstitution (**Figure 8C**). Thus, we selected this model to perform a larger experiment evaluating the efficacy of Nivolumab alone or in a combination strategy with an IL-2 based immunotherapy. Indeed, high-dose IL-2 has been used in the clinic to stimulate T cell responses since its approval by the FDA for the treatment of metastatic melanoma and renal carcinoma, in 1992. Although high-dose IL-2 administration can induce durable cancer regression in around 5-20 % of treated patients ¹⁹, it is also toxic. Low efficacy is in part associated to the unwanted activation of Tregs. Improvements are obtained when IL-2 is administered in the form of an IL-2/anti-IL-2 antibody complex (IL-2Cx) which preferentially activates NK and CD8+ T cells -which are fundamental for mounting an effective anti-tumoral immune response- over Tregs ²⁰. Although recent studies in murine models of cancer, have shown that the IL-2Cx that stimulates NK and CD8+ T cells can boost the antitumor response ^{21,22}, encouraging the clinical development of IL-2Cx ²³, better results are expected if used in combination with immune checkpoint inhibitors.

NSG mice were grafted with the LCF29 PDX and once the tumors reached the size of 10-50 mm³, mice were injected with 5 to 7,5.10⁶ x 10⁶ CD3+ T cell-containing PBMCs (at least two different healthy-donor PBMCs were used per experiment). Nivolumab and/or IL-2Cx treatment started 3 days later, with Nivolumab injection bi-weekly and IL-2Cx injection for five consecutive days during the first week and then twice a week, and tumor growth curves were recorded (**Figure 9A**). For the analysis we only included mice in which PBMC were reconstituted (i.e., mice showing > 2% Hu-CD45+ cells in circulation in at least two different time points during the experiment), and we monitored GvHD development by recording body weight. Similar to Figure 8B, we observed a small, not significant, delay in tumor growth in mice treated with Nivolumab (**Figure 9B-C**). Administration of IL-2Cx led to a significant control of the tumor. However, the combination of both drugs had no additional effects (**Figure 9B-C**). Compared to the untreated or Nivolumab-treated mice the anti-tumoral effect of the IL-2Cx was accompanied by a faster and larger

body-weight loss (**Figure 9D**) -reflecting stronger GvHD development-. IL-2Cx administration was also associated with higher proportions of Hu-CD45+ cells in blood by day 13 after PBMCs injection (**supplementary Figure 9A**). **Supplementary Figure 9B** shows that among Hu-CD45+ cells, IL-2Cx administration induced an increase mainly in CD3+ T cells and in the proportion of CD4+ T cells compared to CD8+ T cells. IL-2Cx also induced an increase in the percentage of CD4+ T cells with the effector phenotype (CD27-), and of CD4+ T cells highly expressing CD25 (likely reflecting in vivo response to IL-2). These CD4+ CD25+ T cells did not express FoxP3 (data not shown), indicating that in this experimental setting IL-2Cx mainly activated conventional CD4+ T cells. Administration of IL-2Cx alone or in combination with Nivolumab gave similar results, most of the effect being likely attributable to IL-2Cx action.

Forty days after PDX engraftment, mice were sacrificed and tumors were analyzed by flow cytometry. We observed that the different treatments did not markedly change the level of tumor infiltration by Hu-CD45+ cells, except for a mild increase in IL-2Cx-treated mice. Hu-CD45+ cells were mainly CD3+ T cells, and IL-2Cx seemed to increase CD4+ T cells over CD8+ T cells, being the majority of the tumor-infiltrating CD4+ T cells of an effector phenotype (**Figure 5E**).

Overall, these data show that IL-2Cx immunotherapy in LCF29-NSCLC-PDX bearing Hu-PBL mice, highly delays tumor growth of an established human tumor in a human T cells reconstituted mice. IL-2Cx administration seems to increase effector CD4+ T cells, which appear as the major effectors of GvHD and GvT in this model²⁴.

Discussion

Cancer immunotherapy has become the Breakthrough of the Year for 2013²⁵, with some impressive clinical results, although benefits are observed only in few patients and for few tumor types^{1,26}. Thus, it is mandatory to understand their mechanisms of action and to identify biomarkers of response and resistance. Mouse models, and mainly syngenic mouse models have helped to progress in the field of cancer immunotherapy^{5,27}, however, this experimental model have a non-human

immune system ⁶ and show significant differences in tumorigenesis compared to human tumors ²⁸. Humanized mice, bearing human immune and tumour cells constitute an alternative and complimentary approach for the pre-clinical study of immunotherapies.

Here, we first evaluated the efficacy of reconstitution of two sources of immune cells: PBMC and Hu-CD34+ hematopoietic stem cells. We observed that engraftment of a human immune system is possible in the two cases, albeit with differences in the kinetics and quality of the immune cell reconstitution. Injection of PBMC leads to engraftment of human immune cells detected in blood and spleen one to two weeks after transfer, and is quasi exclusively constituted by CD3+ T effector lymphocytes. Immune reconstitution, after injection of Hu-CD34+ stem cells, is detectable at about four weeks, with a larger variety of hematopoietic cells including B, T, NK and myeloid cells. We observed that Hu-CD34+ mice have essentially quiescent resting T cells in circulation, whereas the Hu-PBMC mice have activated blastic T cells in circulation, which have been described to have better capacity to invade tumoral tissues ²⁹.

Here, we evaluated the potential of injected Hu-CD34+ stem cells to reconstitute a human immune cell compartment in four different strains of host mice: NSG, NOG, NSG-SGM3 and NOG-EXL. The NSG-SGM3 and NOG-EXL mice, which express human cytokines that act as growth factors for developing immune cells, are expected to increase the myeloid compartment development from the Hu-CD34+ stem cells. However, in our hands, we observed no major differences in the development of the myeloid compartment among the different strains of mice, but an increase of proportion of CD3+ T cells in the NSG-SGM3 mice.

Injection of PBMCs, in contrast to CD34+ injection, has for consequence acute xeno-GvHD with lethal outcome, which is dependent on the dose of injected PBMCs. GvHD development constitutes the major limitation of this model and restricts the therapeutic window to evaluate treatment to two to three weeks after the injection of the PBMCs.

We showed that immune and tumor cells strongly interact in humanized mice. On one side we observed a strong GvT effect of PBMCs on the two types of human

tumors tested, namely tumor cell lines and PDXs. On the other side, we observed that the PDXs can impair PBMC reconstitution, phenomenon much less observed in tumor-cell line bearing mice. The mechanisms by which PBMC are impaired to repopulate PDX-bearing NSG mice are not still identified, but NK cells presents in PDX coming from nude mice or secretome³⁰ of PDXs are interesting variables to evaluate. Our experiments studying the outcome of injecting the PBMCs before or after the tumors are developed indicated that in the Hu-PBL model, injecting the human hematopoietic cells once the tumor is palpable optimizes the reconstitution of the injected cells in the mice and allows GvHD-free period of two-three weeks to perform therapeutic interventions.

Because of the complexity of Hu-CD34+ models (price, purification of CD34+ stem cells, time for reconstitution) compared to PBMC-injected models, we focused in the study of Hu-PBMC NSG model. Moreover, the Hu-PBMC model can be adapted to a future immune-avatar approach³¹. In the avatar approach, a pharmacological experiment in which different therapies are evaluated in parallel is performed on an early PDX passage. Then, the results obtained can be used to guide the selection of the more appropriated therapy to be administrated to the PDX-originating patient³². This approach, actually used in nude mice, has the default of lacking the adaptive immune system, and is then not adapted to the study of cancer immunotherapies. Given the difficulties to obtain Hu-CD34+ cells from cancer patient, applying Hu-PBMC models in avatar approaches represent a promising tool for future experiments.

We observed that in PBMC-injected NSG models only T cells are present. Consequently, unless adoptive cell transfer strategies are used, only immunotherapies modulating anti-tumor T cell responses can be evaluated. We have tested in this model the efficacy of Nivolumab, an anti-PD1 blocking antibody approved for clinical use. We observed that Nivolumab can partially control tumor growth of a triple-negative breast tumor cell line, MDA-MB231. In the Hu-PBL mice, the developed tumors present high a level of lymphocyte infiltration, similar to “hot” or “immune-infiltrated” tumors, described in the clinic as better responder to immunotherapies, compared to poorly infiltrated “cold” tumors^{33,34}. It could be

interesting to evaluate if the efficacy of Nivolumab action in humanized models is correlated to the level of tumoral infiltration, as observed in some human tumors³⁵. Given the beneficial effect of Nivolumab in NSCLC patients, we evaluated the efficacy of Nivolumab in a series of non-small cell lung PDXs, in the form of a mouse clinical trial, similar to the one described by Gao et al³⁶. Although response to treatment was weak, we noticed a response rate ($\approx 40\%$) reminiscent of the objective response rate of 21.3% and disease control rate of 39.9% described for patients³⁷.

Combinations of cancer therapies stands today as a promising strategy to improve the response rate in patients. Here, we evaluated the efficacy of a novel therapeutic combinatory approach using one of the oldest immunotherapy, IL-2 cytokine administration, in a NSCL-PDX model (LCF29). This model presents no major impairment of PBMC reconstitution and was observed to be sensitive to Nivolumab in a preliminary screening test. Compared to plain IL-2, the IL-2Cx has been found to target more specifically CD8+ T cells and NK cells, bypassing Treg activation, and to improve pharmacodynamics of IL-2^{20,38}. Here, we evaluated the efficacy of this treatment as monotherapy or in combination with Nivolumab and we observed that IL-2Cx delayed tumor growth with no synergy when co-injected with Nivolumab. Probably the IL-2Cx dose tested was already highly effective, and consequently did not allow observing an additional effect of Nivolumab. Unexpectedly, IL-2Cx mainly boosted the effector CD4+ T cell compartment, different from the expected effect of IL-2Cx on CD8+ T cells and NK cells. It will be interesting to evaluate by depletion experiments the respective contribution of human CD4+ T or CD8+ T cells to the GvT action induced by the IL-2Cx.

In conclusion, our results show that humanized mouse models can be suitable for the evaluation of immunotherapies. However, improvements need to be done, such as minimization of GvHD- which could be achieved by using genetically modified mice knock-out for murine MHC and expressing human MHC^{39,40}, use of patient-matched tumors and PBMCs, design of more humanized mice expressing human cytokines necessary for the development of human immune populations⁷. Also, it will be interesting to do a side-by-side comparison of the architecture of the primary tumor and the PDX in the humanized mice to better understand to which degree the

murine model reproduces the human tumor microenvironment. Evaluation of combinatory therapies that increase tumor infiltration (chemotherapy, radiotherapy) as well as combination of targeted therapies (PI3 kinase inhibitor, tyrosine kinase inhibitor) could be informative to propose new clinical trials. Finally, implementation of avatar approaches with humanized mice could be of great utility for the design of personalized immunotherapies for cancer.

References

1. Hao C, Tian J, Liu H, Li F, Niu H, Zhu B. Efficacy and safety of anti-PD-1 and anti-CTLA-4 immunotherapy to advanced melanoma: A systematic review and meta-analysis of randomized controlled trials. *Medicine (Baltimore)*. 2017;96(26):e7325. doi:10.1097/MD.00000000000007325
2. Hargadon KM, Johnson CE, Williams CJ. Immune checkpoint blockade therapy for cancer: An overview of FDA-approved immune checkpoint inhibitors. *Int. Immunopharmacol.* 2018;62:29–39. doi:10.1016/j.intimp.2018.06.001
3. Seidel JA, Otsuka A, Kabashima K. Anti-PD-1 and Anti-CTLA-4 Therapies in Cancer: Mechanisms of Action, Efficacy, and Limitations. *Front. Oncol.* 2018;8. doi:10.3389/fonc.2018.00086
4. You W, Liu M, Miao J-D, Liao Y-Q, Song Y-B, Cai D-K, Gao Y, Peng H. A Network Meta-analysis Comparing the Efficacy and Safety of Anti-PD-1 with Anti-PD-L1 in Non-small Cell Lung Cancer. *J Cancer.* 2018;9(7):1200–1206. doi:10.7150/jca.22361
5. Li Q-X, Feuer G, Ouyang X, An X. Experimental animal modeling for immunoncology. *Pharmacol. Ther.* 2017;173:34–46. doi:10.1016/j.pharmthera.2017.02.002
6. Mestas J, Hughes CCW. Of Mice and Not Men: Differences between Mouse and Human Immunology. *The Journal of Immunology.* 2004;172(5):2731–2738. doi:10.4049/jimmunol.172.5.2731
7. De La Rochère P, Guil-Luna S, Decaudin D, Azar G, Sukhvinder S, Piaggio E. Humanized mice for the study of Immuno-Oncology. *Trends in Immunology.* 2018.

8. Shultz LD, Pearson T, King M, Giassi L, Carney L, Gott B, Lyons B, Rossini AA, Greiner DL. Humanized NOD/LtSz-scid IL2 receptor common gamma chain knockout mice in diabetes research. *Ann. N. Y. Acad. Sci.* 2007;1103:77–89. doi:10.1196/annals.1394.002
9. Billerbeck E, Barry WT, Mu K, Dorner M, Rice CM, Ploss A. Development of human CD4+FoxP3+ regulatory T cells in human stem cell factor-, granulocyte-macrophage colony-stimulating factor-, and interleukin-3-expressing NOD-SCID IL2R γ (null) humanized mice. *Blood.* 2011;117(11):3076–3086. doi:10.1182/blood-2010-08-301507
10. Shultz LD, Ishikawa F, Greiner DL. Humanized mice in translational biomedical research. *Nat. Rev. Immunol.* 2007;7(2):118–130. doi:10.1038/nri2017
11. Ito R, Takahashi T, Katano I, Kawai K, Kamisako T, Ogura T, Ida-Tanaka M, Suemizu H, Nunomura S, Ra C, et al. Establishment of a human allergy model using human IL-3/GM-CSF-transgenic NOG mice. *J. Immunol.* 2013;191(6):2890–2899. doi:10.4049/jimmunol.1203543
12. Pérol L, Martin GH, Maury S, Cohen JL, Piaggio E. Potential limitations of IL-2 administration for the treatment of experimental acute graft-versus-host disease. *Immunol. Lett.* 2014;162(2 Pt B):173–184. doi:10.1016/j.imlet.2014.10.027
13. Naserian S, Leclerc M, Thiolat A, Pilon C, Le Bret C, Belkacemi Y, Maury S, Charlotte F, Cohen JL. Simple, Reproducible, and Efficient Clinical Grading System for Murine Models of Acute Graft-versus-Host Disease. *Front Immunol.* 2018;9:10. doi:10.3389/fimmu.2018.00010
14. Cooke KR, Kobzik L, Martin TR, Brewer J, Delmonte J, Crawford JM, Ferrara JL. An experimental model of idiopathic pneumonia syndrome after bone marrow transplantation: I. The roles of minor H antigens and endotoxin. *Blood.* 1996;88(8):3230–3239.
15. Marangoni E, Vincent-Salomon A, Auger N, Degeorges A, Assayag F, de Cremoux P, de Plater L, Guyader C, De Pinieux G, Judde J-G, et al. A new model of patient tumor-derived breast cancer xenografts for preclinical assays. *Clin. Cancer Res.* 2007;13(13):3989–3998. doi:10.1158/1078-0432.CCR-07-0078

16. Deplater L, Ouafi L, Cremoux P de, Chouchane-Mlik O, Daniel C, Zemoura L, Nicolas A, Richardson M, Couturier J, Dahmani A, et al. Abstract A15: Establishment and characterization of a new patient-derived non-small cell lung cancer xenograft panel for pharmacological assessment. *Mol Cancer Ther.* 2011;10(11 Supplement):A15–A15. doi:10.1158/1535-7163.TARG-11-A15
17. Wakelee H, Kelly K, Edelman MJ. 50 Years of progress in the systemic therapy of non-small cell lung cancer. *Am Soc Clin Oncol Educ Book.* 2014:177–189. doi:10.14694/EdBook_AM.2014.34.177
18. Feld E, Horn L. Emerging role of nivolumab in the management of patients with non-small-cell lung cancer: current data and future perspectives. *Onco Targets Ther.* 2017;10:3697–3708. doi:10.2147/OTT.S97903
19. Atkins MB, Lotze MT, Dutcher JP, Fisher RI, Weiss G, Margolin K, Abrams J, Sznol M, Parkinson D, Hawkins M, et al. High-dose recombinant interleukin 2 therapy for patients with metastatic melanoma: analysis of 270 patients treated between 1985 and 1993. *J. Clin. Oncol.* 1999;17(7):2105–2116. doi:10.1200/JCO.1999.17.7.2105
20. Létourneau S, van Leeuwen EMM, Krieg C, Martin C, Pantaleo G, Sprent J, Surh CD, Boyman O. IL-2/anti-IL-2 antibody complexes show strong biological activity by avoiding interaction with IL-2 receptor alpha subunit CD25. *Proc. Natl. Acad. Sci. U.S.A.* 2010;107(5):2171–2176. doi:10.1073/pnas.0909384107
21. Krieg C, Létourneau S, Pantaleo G, Boyman O. Improved IL-2 immunotherapy by selective stimulation of IL-2 receptors on lymphocytes and endothelial cells. *Proc. Natl. Acad. Sci. U.S.A.* 2010;107(26):11906–11911. doi:10.1073/pnas.1002569107
22. Han K-H, Kim KW, Yan J-J, Lee J-G, Lee EM, Han M, Cho EJ, Kang SS, Lim HJ, Koo TY, et al. Effects of stimulating interleukin -2/anti- interleukin -2 antibody complexes on renal cell carcinoma. *BMC Urol.* 2016;16:2. doi:10.1186/s12894-016-0121-2
23. Arenas-Ramirez N, Zou C, Popp S, Zingg D, Brannetti B, Wirth E, Calzascia T, Kovarik J, Sommer L, Zenke G, et al. Improved cancer immunotherapy by a CD25-

mimobody conferring selectivity to human interleukin-2. *Sci Transl Med.* 2016;8(367):367ra166. doi:10.1126/scitranslmed.aag3187

24. Sanmamed MF, Rodriguez I, Schalper KA, Oñate C, Azpilikueta A, Rodriguez-Ruiz ME, Morales-Kastresana A, Labiano S, Pérez-Gracia JL, Martín-Algarra S, et al. Nivolumab and Urelumab Enhance Antitumor Activity of Human T Lymphocytes Engrafted in Rag2-/-IL2R γ null Immunodeficient Mice. *Cancer Res.* 2015;75(17):3466–3478. doi:10.1158/0008-5472.CAN-14-3510

25. Couzin-Frankel J. Breakthrough of the year 2013. Cancer immunotherapy. *Science.* 2013;342(6165):1432–1433. doi:10.1126/science.342.6165.1432

26. Zhou G-W, Xiong Y, Chen S, Xia F, Li Q, Hu J. Anti-PD-1/PD-L1 antibody therapy for pretreated advanced nonsmall-cell lung cancer: A meta-analysis of randomized clinical trials. *Medicine (Baltimore).* 2016;95(35):e4611. doi:10.1097/MD.0000000000004611

27. Talmadge JE, Singh RK, Fidler IJ, Raz A. Murine models to evaluate novel and conventional therapeutic strategies for cancer. *Am. J. Pathol.* 2007;170(3):793–804. doi:10.2353/ajpath.2007.060929

28. de Jong M, Maina T. Of mice and humans: are they the same?-- Implications in cancer translational research. *J. Nucl. Med.* 2010;51(4):501–504. doi:10.2967/jnumed.109.065706

29. Breart B, Lemaître F, Celli S, Bouso P. Two-photon imaging of intratumoral CD8+ T cell cytotoxic activity during adoptive T cell therapy in mice. *J. Clin. Invest.* 2008;118(4):1390–1397. doi:10.1172/JCI34388

30. Khwaja FW, Svoboda P, Reed M, Pohl J, Pyrzynska B, Van Meir EG. Proteomic identification of the wt-p53-regulated tumor cell secretome. *Oncogene.* 2006;25(58):7650–7661. doi:10.1038/sj.onc.1209969

31. Jespersen H, Lindberg MF, Donia M, Söderberg EMV, Andersen R, Keller U, Ny L, Svane IM, Nilsson LM, Nilsson JA. Clinical responses to adoptive T-cell transfer can be modeled in an autologous immune-humanized mouse model. *Nat Commun.* 2017;8(1):707. doi:10.1038/s41467-017-00786-z

32. Calvo E, Soria J-C, Ma WW, Wang T, Bahleda R, Tolcher AW, Gernhardt D, O'Connell J, Millham R, Giri N, et al. A Phase I Clinical Trial and Independent Patient-Derived Xenograft Study of Combined Targeted Treatment with Dacomitinib and Figitumumab in Advanced Solid Tumors. *Clin. Cancer Res.* 2017;23(5):1177–1185. doi:10.1158/1078-0432.CCR-15-2301

33. Sharma P, Allison JP. The future of immune checkpoint therapy. *Science.* 2015;348(6230):56–61. doi:10.1126/science.aaa8172

34. Teng MWL, Ngiow SF, Ribas A, Smyth MJ. Classifying Cancers Based on T-cell Infiltration and PD-L1. *Cancer Res.* 2015;75(11):2139–2145. doi:10.1158/0008-5472.CAN-15-0255

35. Pagès F, Mlecnik B, Marliot F, Bindea G, Ou F-S, Bifulco C, Lugli A, Zlobec I, Rau TT, Berger MD, et al. International validation of the consensus Immunoscore for the classification of colon cancer: a prognostic and accuracy study. *Lancet.* 2018 May 10. doi:10.1016/S0140-6736(18)30789-X

36. Gao H, Korn JM, Ferretti S, Monahan JE, Wang Y, Singh M, Zhang C, Schnell C, Yang G, Zhang Y, et al. High-throughput screening using patient-derived tumor xenografts to predict clinical trial drug response. *Nat. Med.* 2015;21(11):1318–1325. doi:10.1038/nm.3954

37. Ming B, Yue-Jiang P, Ran W, Sheng-Long L, Jie L, Jun-Ming Y, Jia L. The efficacy of nivolumab for the treatment of advanced non-small cell lung cancer: a systematic review and meta-analysis of clinical trials. *Int J Clin Exp Med.* 2017;10:153–161.

38. Boyman O, Kovar M, Rubinstein MP, Surh CD, Sprent J. Selective stimulation of T cell subsets with antibody-cytokine immune complexes. *Science.* 2006;311(5769):1924–1927. doi:10.1126/science.1122927

39. King MA, Covassin L, Brehm MA, Racki W, Pearson T, Leif J, Laning J, Fodor W, Foreman O, Burzenski L, et al. Human peripheral blood leucocyte non-obese diabetic-severe combined immunodeficiency interleukin-2 receptor gamma chain gene mouse model of xenogeneic graft-versus-host-like disease and the role of host

major histocompatibility complex. *Clin. Exp. Immunol.* 2009;157(1):104–118.
doi:10.1111/j.1365-2249.2009.03933.x

40. Zeng Y, Liu B, Rubio M-T, Wang X, Ojcius DM, Tang R, Durrbach A, Ru Z, Zhou Y, Lone Y-C. Creation of an immunodeficient HLA-transgenic mouse (HUMAMICE) and functional validation of human immunity after transfer of HLA-matched human cells. *PLoS ONE.* 2017;12(4):e0173754.
doi:10.1371/journal.pone.0173754

Materials and Methods

Mice

NOD.Cg-Prkdc^{scid} Il2rg^{tm1Wjl}/SzJ (NSG) and NOD.Cg-Prkdc^{scid} Il2rg^{tm1Wjl} Tg(CMV-IL3,CSF2,KITLG)1Eav/MloySzJ (NSG-SGM3) were purchased from The Jackson laboratory and NOD.Cg-Prkdc^{scid} Il2rg^{tm1Sug}/JicTac (NOG) and NOD.Cg-Prkdc^{scid} Il2rg^{tm1Sug} Tg(SV40/HTLV-IL3,CSF2)10-7Jic/JicTac (NOG-EXL) were purchased from TACONIC. Experimental animal procedures were approved by the ethics committee of the Institut Curie CEEA-IC #118 (APAFIS #15227) in compliance with international guidelines

Human immune cell origin

Peripheral blood mononuclear cells (PBMC) were isolated from buffy coats provided by the blood bank of Etablissement français du sang (EFS), after written informed consent. CD34⁺ cells were obtained from ABCell-bio after CD34⁺ positive selection on human cord blood, after written informed consent.

Hu-PBL-NSG mice

We used NSG mice that were grafted or not with human tumor cell line or PDX and then reconstituted with human peripheral blood mononuclear cells (PBMC) coming from two blood samples of human healthy donors in each experiment.

PBMC were isolated using Ficoll gradient (lymphoprep, Stemcell) and the quantification of CD3⁺ cells was done by flow cytometry. Total PBMC were directly injected into immunodeficient mice without irradiation or immediately stored in liquid nitrogen. Frozen PBMC cells were thawed in hot CO₂ independent medium supplemented with 0,4 g.L⁻¹ of human albumin. After centrifugation, cells were resuspended in CO₂ independent medium supplemented with 0,4 g.L⁻¹ of human albumin and 100µg/ml of DNase I during one hour. After quantification of CD3⁺ proportion, total PBMC cells are injected intravenously in mice without irradiation.

Hu-CD34⁺ HSC-NSG mice

Humanization was performed according to provider instructions depending on the mouse strain (i.e. NSG, NOG, NSG-SGM3 or NOG-EXL). Briefly, mouse received sublethal total body irradiation from a X-ray source (CP 160 Faxitron Xray) with 1.4Gy for 3 week-old NSG, with 1.1Gy for 3-4 week-old NOG mice, with 1 Gy for 5 week-old NSG-SGM3 mice and with 0.6 Gy for 4-6 week-old NOG mice. 18 to 24 hours post-irradiation, mice were injected I.V. with human CD34+ HSC cells. More precisely 130 000 cells were injected for NSG and NOG mice, 100 000 cells for NSG-SGM3 mice, and 50 000 cells for NOG-EXL mice.

Cell lines and Patient derived Xenograft

The human triple negative breast cancer-derived MDA-MB231 cell line and human NSCLC cancer-derived HCC827 cell line (ATCC) were grown in RPMI (Lifetechnologies) supplemented with 10% heat-inactivated fetal bovine serum (Biosera) and 1% penicillin-streptomycin (Life Technologies). For experiment using human tumor cell lines, 5.10⁶ tumor cells were injected subcutaneously per immunodeficient mice and tumor growth was measured using a metric caliper 2 times per week.

Patient derived xenograft from breast or lung origin was obtained following informed consent from patients undergoing surgery. Fresh tumor fragments were grafted into the interscapular fat pad of 8- to 12-week-old female Swiss nude mice (Harlan Laboratories, L'Arbresle, France) under avertin anesthesia. Mice were maintained in pathogen-free animal housing (Institut Curie, Paris, France). Xenografts appeared at the graft site 2–8 months after initial transplantation and were subsequently transplanted into secondary recipients. PDXs were considered to be established after the third in vivo passage. All experiments were performed in accordance with the UKCCCR animal ethics guidelines.

In vivo treatments

Nivolumab (OPDIVO, BMS), recombinant human IL-2 (rhIL-2, Proleukine, Novartis) and anti-human IL-2 (clone MAB602, Bio-technie) were purchased. Nivolumab was injected, biweekly, to NSG mice, 3 to 10 days after PBMCs injection, biweekly at 10mg/kg/dose. IL-2Cx was prepared mixing 50,000UI of rhIL-2 with 15µg of Ab (molar

ratio 2:1) and incubated for 30 min at 37°C. IL-2Cx was injected five consecutive days, 5 days after PBMCs injection and biweekly in the weeks after.

Preparation of cell suspension for FACS analysis

Tumors, spleen and bone marrow were collected in PBS-2% FBS. Femurs and tibias were flushed out and collected BM was dissociated through a cell strainer. When necessary (spleen, BM), red blood cells (RBC) were lysed twice with Fixative-Free Lysing Solution (Invitrogen) and used for Flow cytometry straining. Peripheral blood (PB) was collected in EDTA coated tubes and cells were stained prior RBC lysis as described under “Flow cytometry” section.

Tumor were cut into small pieces and mixed with 2ml of CO₂ independent medium (Gibco Life technologie) containing 30 µl Dnase (10mg/ml, Roche), and 60 µl liberase LT (5mg/ml, Roche) per sample. The tumor sample was processed on a Gentlemacs dissociator (Miltenyi Biotec), and then the dissociated tumor sample were filtered through a 100µm cell cell strainer (BD Biosciences), washed with PBS, and then incubated with the antibodies for FACS staining.

Flow cytometry

For phenotypic analysis of human immune cells, isolated cells or peripheral blood were first incubated with antibodies to block human and mouse Fcγ receptors (- Human TruStain FcX™ from Biolegend and Rat anti-mouse CD16/32 from BD Biosciences) and then stained for some surface markers among the followings:

huCD4-BUV395 clone SK3, huCD8-BUV496 clone RPA-T8, huCD45-BUV805 clone HI30, huCD56-BV421 clone NCAM16.2, huCD3 BV510 clone UCHT1, huCD19-BV650 clone SJ25C1, huCD16-FITC clone 3G8, huCD33-PECF594 clone WM53, mCD45-PECy7 clone 30-F11, huCD14-AF700 clone M5E2, huCD45RA-BV421 clone HI100, huCD197-PECF594 clone 150503, huCD45RO-APC clone UCHL1, huCD8-PECF594 clone RPA-T8, huCD56-PE-Cy5 clone N901, huCD45-APC Cy7 clone 2D1, huCD19-Alexa 700 clone HIB19, huTCRgd-FITC clone 11F2 purchased from BD Biosciences; and uhCD25-PE clone M-A251, huCD27-BV605 clone O323, huCD3-BV650 clone OKT3, huCD4-BV785 clone OKT4, huPD-1-BV711 clone EH12.2H7, and huCD25-BV786 clone BC96

purchased from Biolegend; huHLA-DR-FITC clone AC122 purchased from Miltenyi Biotec and huCD45RA-PECy5 clone HI100 purchased from eBiosciences.

When intracellular staining was performed, cells were fixed and permeabilized with fixation/permeabilization solution (eBiosciences) according to the manufacturer's instructions and stained with FOXP3-eFluor 450 clone 236A/E7, (eBioscience). Dead cells were stained by using either LIVE/DEAD Fixable Aqua (Life Technologies™) or Viability Dye eFluor 780 (eBiosciences).

Cells were then either kept in PBS for direct analysis on FACS or fixed/lyzed with Versalys+ I/O test 3 solution (Beckman Coulter) and washed before acquisition.

Samples were then analyzed on a Fortessa flow cytometer (BD Biosciences). FACS data were analyzed with Diva software or FlowJo Version v10.0.8 (TreeStar).

Plasma cytokine measurement

EDTA-plasma samples were analyzed using the MSD U-PLEX assay platform (U-PLEX Proinflam Combo 1 Human K15049K; Mesoscale Discovery,) according to manufacturer's instruction. In short, for this personalized version of U-plex plate, plates were prepared by incubating the capture biotinylated-antibody with a U-plex linker. Plasma samples were then thawed at room temperature just before analysis and were incubated on the MSD plates undiluted for 1 hour at room temperature while shaking. Plates were washed and incubated in additional 1 hour with detection antibodies. After washing, Read buffer T was added to each well and the plates were analyzed in a MSD Discovery Workbench.

Immunohistochemistry

Fixed tissues were dehydrated and embedded in paraffin. Automated immunostaining were performed using Ventana Discovery XT systems according manufacturer's instructions (Ventana Medical Systems, Inc, USA).

Whole sections were deparaffinized and received standard pretreatment, then covered with reaction buffer before IHC procedure.

The following primary antibodies were mouse anti huPD1 (reference ab52587, Abcam), mouse anti huCD8 (reference M7103, Dako), Rabbit anti huPD-L1 (reference 1-PR292-07, Quartett), rat anti m CD45 (reference NB100-77417, Novus Biological)

and mouse anti-huCD45 (reference MA5-13197, ThermoScientific). Primary antibodies were incubated at 25°C in discovery antibody diluent (760-108, Ventana Medical Systems, Inc, USA). For dual staining, anti-human CD45 and anti-mouse CD45 were combined with purple chromomab-kit and chromomab DAB kit respectively. For dual staining, anti-human PD1 and anti-human CD8 were combined with purple chromomab-kit and chromomab DAB kit respectively. Omission of this primary antibody step was performed in negative control assays. Detection was performed with UltraMap anti-Rabbit or anti mouse HRP then with ChromoMap DAB kit according to manufacturer's recommendations.

A counterstaining step was done with the bluing reagent. Stained slides were dehydrated and coverslipped with cyto seal XYL. Immunostaining sections were observed by microscope Eclipse E400 (Nikon) and slides were scanned and digitized using the ScanScope XT system (Aperio Technologies, Vista, CA). Digitized images were then captured using the ImageScope software (version 9.1, Aperio Technologies) at x20 magnification.

Statistical analyses

Statistical analyses were performed in GraphPad Prism v7. p values were calculated with One-way ANOVA and Kruskal-Wallis post-test or Chi-square test.

Legends

Figure 1: huPBMC reconstitution and GvHD development in Hu-PBL-NSG mice

A. Scheme of the experimental design. Non-irradiated NSG mice from 8 to 14 weeks of age were injected, intravenously, with different amount of Hu-PBMCs. Blood, spleen and bone marrow were recovered at illustrated time points to quantify human reconstitution by flow cytometry analysis. **B.** Recapitulative table of Hu-PBMCs engraftment and GvHD development upon injection of different Hu-PBMCs doses in NSG mice. **C.** NSG mice injected with $5 \cdot 10^6$ (n=12) or $10 \cdot 10^6$ (n=11) of CD3⁺ T cell-containing Hu-PBMCs were monitored for reconstitution by quantification of circulating Hu-CD45⁺ (left panel) cells and bodyweight (right panel). Results shown are percentage of initial weight. **D-E.** NSG mice were injected with $10 \cdot 10^6$ HU-PBMCs from two different donors. **D.** Changes in Hu-CD45⁺ cells engraftment in blood (n=5-15), spleen (n=5) and bone marrow (n=5) upon Hu-PBMC injection. Frequencies (%) of Hu-CD45⁺ cells relative to total CD45⁺ cells (Hu-CD45⁺ + mCD45⁺) (upper panel) and the human immune cells subpopulations (huCD3⁺ T cells, huCD3⁺ CD4⁺ T cells, huCD3⁺ CD8⁺ T cells, huCD56⁺ CD3⁺ cells, huCD19⁺ B cells) relative to Hu-CD45⁺ cells (lower panel) at different time points. Data is expressed as mean \pm SD of one representative experiment out of two.

Figure 2: Hu-T cell differentiation/activation state in Hu-PBL-NSG mice

A. Flow cytometry gating strategy used to define naïve (CD45RA⁺ CCR7⁺), central memory (CD45RA⁻ CCR7⁺), effector memory (CD45RA⁻ CCR7⁻), and effector cells (CD45RA⁺ CCR7⁻) among huCD4⁺ or huCD8⁺ gated cells in blood from Hu-PBMC-humanized mice at day 14 post-humanization. **B.** Changes in differentiation and activation state of huCD4⁺ and huCD8⁺ T cells in blood (n=5-15), spleen (n=5) and bone marrow (n=5) of reconstituted NSG mice. Frequencies (%) of naïve, memory, effector memory, and effector cells as well as activation marker-expressing cells (CD25 and HLA-DR) relative to huCD4⁺ or huCD8⁺ T cells determined by flow cytometry analysis at different timepoints. NSG mice were reconstituted with $10 \cdot 10^6$ Hu-PBMCs. Data is expressed as mean \pm SD from one representative experiment out of two. **C.** Representative experiment showing plasma concentrations (mean \pm SD) of human IFN- γ and TNF- α in Hu-PBMC-humanized NSG mice.

Figure 3: Immune cell reconstitution upon Hu-CD34⁺ HSC injection in different strains of immunodeficient mice.

A. Scheme of the experimental design. 50 000 to 130 000 $\times 10^6$ Hu-CD34⁺ HSC were injected into NSG, NOG, NOG-EXL or NSG-SGM3. Blood was recovered at weeks 4 to 6, 9, 12, 15 and 18 weeks post-injection of Hu-CD34⁺ HSC to quantify human reconstitution by flow cytometry analysis. **B.** Changes in human immune cell reconstitution. Frequencies (%) of Hu-CD45⁺ cells population relative to total CD45⁺ cells (Hu-CD45⁺ +mCD45⁺) in blood over time. **C, D.** Distribution of the Hu-CD45⁺ cell subpopulations relative to Hu-CD45⁺ cells in blood, spleen and bone marrow of different mouse strains. Mice were sacrificed at 18 weeks after Hu-CD34⁺ HSC injection and the distribution of the immune cell populations were determined by flow cytometry.

Data is expressed as mean \pm SD.

Data are from $n \geq 17$ mice per mouse strain and a minimum of 3 different Hu-CD34⁺ HSC donors were used in the experiment.

Figure 4: T cell differentiation state in HuCD34⁺-humanized mice.

Frequencies (%) of naïve, memory, effector memory, and effector cells relative to huCD4⁺ T cells (upper panel) and huCD8⁺ T cells (lower panel) determined by flow cytometry analysis. Flow cytometry gating strategy was similar to the one used for Hu-PBL-NSG mouse as illustrated in Figure 2A.

Data is expressed as mean \pm SD.

Data are from $n \geq 17$ mice per mouse strain and a minimum of 3 different Hu-CD34⁺ HSC donors were used in the experiment.

Figure 5: Impact of immune cell injection on tumor growth

A. Scheme of the experimental design. $5 \cdot 10^6$ CD3⁺ T cell-containing PBMCs were either injected two weeks before (in red) or after (in green) tumor graft was detectable (in black); 1 week for tumor cell lines, up to 8 weeks for PDXs. **B.** Individual tumor growth kinetics of LCF29 (NSCLC PDX), BC138 (TNBC PDX), HCC827 (NSCLC cell line) and MDA-MB231 (TNBC cell line). **C.** Tumor growth kinetics represented as a

mean of the individual curves shown in (B) **D.** GvHD development was followed by weight loss, represented here by percentage (%) of initial weight. **C, D.** Data are represented as mean \pm SEM of n=3-9 mice per group. **E.** Mice were bled at different time points. HuCD45⁺ cells reconstitution is observed at different time points: for LCF29, 30 days after huPBMC injection, for BC138, 22 days after huPBMC injection, for HCC827, 27 days after huPBMC injection and for MDA-MB231, 20 days after huPBMC injection.

Figure 6: Impact of PDX on human immune reconstitution

NSG mice were injected with 5.10^6 to $7.5.10^6$ CD3⁺ PBMCs. NSG mice were either not grafted with tumor (black, n=79) or grafted with; NSCLC lung tumor cell line (HCC827, red, n=17), NSCLC PDX (orange, n=81), TNBC cell line (MDA-MB231, dark green, n=52) or TNBC PDX (light green, n=31). All mice were evaluated for HuCD45 staining. **A.** Proportion of reconstituted mice. Mice were considered reconstituted when more than 2% of HuCD45⁺ were detected in blood at two different time points. Numbers indicated the reconstituted mice/total huPBMCs injected mice. **B.** Frequency (%) of Hu-CD45⁺ cells in blood of reconstituted tumor-bearing mice at the maximum percentage of Hu-CD45⁺ cells detected in A (between day 30 and day 40).

Data is from a pool of experiments. p value was calculated using Chi-square test (A). ****p<0.0001 or One-way ANOVA and Kruskal-Wallis test (B) *p<0.05; **p<0.01.

Figure 7: Effect of Nivolumab injection on MDA-MB231 tumor growth in a Hu-PBL-NSG model

A. Scheme of the experimental design. NSG mice were grafted with 5.10^6 MDA-MB231 cells. Once tumor was detectable (tumor size range= 10-30mm³), mice were injected or not with 5.10^6 CD3⁺ T cell-containing huPBMCs. Five days after huPBMCs injection, mice were treated (i.p.) with PBS (black, n=5) or Nivolumab (red, n=7) two times per week (10mg/kg/dose, red). Mice were sacrificed for flow cytometry analysis at day 24 after CD3⁺ T-cell PBMC injection. **B.** Tumor growth kinetic of one representative experiment out of two, here shown as individual curve. **C.** Tumor growth kinetic of one representative experiment out of two, here shown as individual curve merged for all conditions. **D.** Frequency (%) of Hu-CD45⁺ cells in blood at day 20

and day 24. **E.** GvHD development was followed by weight loss, represented by percentage (%) of initial weight. Data is represented as mean \pm SEM of n=4-7 mice per group. **(F)** Representative dot plot showing the frequency (%) of tumor infiltrating mCD45⁺ and Hu-CD45⁺ cells in non reconstituted mice (upper panel, left) and reconstituted mice (lower panel, left). Numbers indicate the frequency of mCD45⁺ and Hu-CD45⁺ cells. Quantification of mCD45⁺ and Hu-CD45⁺ cells in tumors (right panel). **G.** IHC characterization of TILs. **H.** Tumor growth kinetic from 2 pooled independent experiments. Data are represented as mean \pm SEM of n=17 mice per group.

p values were calculated using One-way ANOVA and Kruskal-Wallis test (F,H) *p<0.05.

Figure 8: Screening of NSCLC PDX for nivolumab action

Scheme of the experimental design. NSCLC PDX-bearing NSG mice were injected with 5 to 7,5.10⁶ CD3⁺ T cell-containing huPBMCs from two different donors, equally distributed and treated (i.p.) 3 days after huPBMC injection either with Nivolumab two times per week (10mg/kg/dose, red, n= n=2-7) or PBS (black, n=2-4). **A.** Tumor growth kinetic of Nivolumab non-responder PDX. Data is represented as mean of the tumor size. **B.** Tumor growth kinetic of Nivolumab responder PDX. Data is represented as mean of the tumor size. **C.** Proportion of reconstituted tumor-bearing mice, in 9 NSCLC PDX bearing mice models treated or not with Nivolumab. Mice were considered reconstituted when more than 2% of HuCD45⁺ were detected in blood. Numbers indicated the reconstituted mice/total huPBMCs injected mice.

Figure 9: IL-2 complexes (IL-2Cx) injection delays tumor growth of a NSCLC PDX (LCF29) without synergy with Nivolumab

A. Scheme of the experimental design. PDX (LCF29) bearing NSG mice were injected with 7,5.10⁶ CD3⁺ T cell-containing huPBMCs from two different donors, equally distributed. Mice were treated (i.p.) 3 days after huPBMC injection either with PBS (black, n=7), Nivolumab (red, n=6), IL-2Cx (green, n=7) or a combination of Nivolumab and IL-2Cx (blue, n=6). Nivolumab is injected biweekly at 10mg/kg per dose, IL-2Cx were made of 50,000 IU of IL-2 and a 2:1 molar ratio of the α -IL-2 mAb MAB602 and

injected during five consecutive days in first week, then biweekly. **B.** Tumor growth kinetics of individual mice. **C.** Tumor growth kinetic represented as mean \pm SEM of n=6-7 mice per group. **D.** GvHD development was followed by weight loss, represented by percentage (%) of initial weight. **C,D.** Data is represented as mean \pm SEM of n=6-7 mice per group. **E.** Flow cytometry analysis for tumor infiltrating cells was done at 40 days after PDX engraftment (25 days after PBMCs injection). Frequency (%) of different human immune cells populations infiltrating the tumor. p values were calculated using One-way ANOVA and Kruskal-Wallis test. NS, not significant; *p<0.05.

Supplementary Figure 1: Characterization of the human immune cell reconstitution upon Hu-CD34⁺ HSC injection

Flow cytometry gating strategy for flow cytometry analysis of human immune cell subpopulations, shown in blood of Hu-CD34⁺ HSC-humanized mouse at week 18 after humanization. Similar gating strategy was used for Hu-PBL-NSG mouse.

Supplementary Figure 2: T cell differentiation/activation state in blood from healthy donor

Frequencies (%) of naïve, memory, effector memory, and effector cells as well as activation marker-expressing cells (CD25 and HLA-DR) relative to CD4⁺ or CD8⁺ T cells of PBMC from healthy donors (n=3-4) determined by flow cytometry analysis. Data is expressed as mean \pm SD.

Supplementary Figure 3: huNK and huMyeloid cell reconstitution in Hu-CD34⁺ model.

A. Flow cytometry gating strategy used to define cytotoxic (CD16⁺), and cytokinic (CD16⁻) NK cells among huCD56⁺ CD3⁻ gated cells (see Supplementary Figure 1 for gating strategy) in blood from Hu-CD34⁺-humanized mice at week 18. **B.** Percentage of NK cell subpopulations relative to Hu-CD45⁺ cells in blood and spleen at week 18. % **C.** Flow cytometry gating strategy used to define classical (CD14⁺ CD16⁻), intermediate (CD14⁺ CD16⁺), and non-classical (CD14⁻ CD16⁺) monocytes among huNon Neutrophils (CD16⁺ SSC^{high}) CD33⁺ gated cells (see Supplementary Figure 1 for

gating strategy) in blood from Hu-PBMC-humanized mice at week 18. **D.** Percentages of monocyte subpopulations relative to Hu-CD45⁺ cells in blood, spleen, and bone marrow at week 18.

Data is expressed as mean ± SD.

Data are from n≥17 mice per mouse strain and a minimum of 3 different Hu-CD34⁺ HSC donors were used in the experiment.

Supplementary Figure 5: Human immune infiltration in TNBC PDX

TNBC PDX (BC138) was sampled 28 days after PBMC injection. Tumoral infiltration of human immune cell was assessed by flow cytometry. Frequencies (%) of tumor infiltrating CD56 (NK cells), CD3 (T cells), CD8 (T cytotoxic cells) and CD4 (T helper cells) are shown.

Supplementary Figure 7: Impact of Nivolumab injection on MDA-MB231 tumor growth in Hu-PBMC-NSG model and Hu-CD34⁺-NSG model

A. Scheme of the experimental design. NSG mice were grafted with 5.10⁶ MDA-MB231 cells. Once tumor was detectable (tumor size range= 10-30mm³), mice were injected or not with 5.10⁶ CD3⁺ T cell-containing huPBMCs . Five days after Hu-PBMCs injection, mice were treated (i.p.) with PBS (black, n=12) or Nivolumab (red, n=10) two times per week (10mg/kg/dose, red). **B.** Tumor growth kinetic of individual mice from one representative experiment out of two. **C.** Hu-CD45⁺ reconstitution was monitored in mice blood by flow cytometry staining at day 14 and 23 after tumor graft. **D.** GvHD development was followed by weight loss, represented by percentage (%) of initial weight. Data are represented as mean ± SEM of n=10-12 mice per group. **E.** Scheme of the experimental design. NOG mice already reconstituted with CD34⁺ HSC, coming from cord blood were provided by TACONIC; 6 to 8 weeks after HSC injection. NOG mice were grafted with 5.10⁶ MDA-MB231 cells. Once tumor was detectable (tumor size range= 10-30mm³), mice were treated by PBS (black, n=3) or Nivolumab (red, n=2) two times per week (10mg/kg/dose). **F.** Tumor growth kinetic. Data are represented as mean ± SEM of n=2-3 mice per group. **G.** Frequency (%) of Hu-CD45⁺ cells in blood at day 19 and 31 after tumor graft. **H.** GvHD development

was followed by weight loss, represented by percentage (%) of initial weight. Data are represented as mean \pm SEM of n=2-3 mice per group.

Supplementary Figure 8: Screening of NSCLC PDX for nivolumab action

Mice were treated as described in Figure 8. **A.** Proportion of mice reconstituted with Hu-CD45⁺ cells (more than 2% at two different time points during experiment) per total mice injected with PBMC. Numbers indicated the reconstituted mice/total huPBMCs injected mice. **B.** Percentage of Hu-CD45⁺ cells in reconstituted mice with lung or breast tumor. Mice were treated (full draws) or not (empty draws) with Nivolumab.

p value was calculated using Chi-square test (A). *p<0.05.

p values were calculated using One-way ANOVA and Kruskal-Wallis test (B). *p<0.05; **p<0.01.

Supplementary Figure 9: IL-2Cx modify blood reconstitution in Hu-PBL NSG

Mice were treated as described in Figure 9. **A.** Comparison of Hu-CD45⁺ cells reconstitution at different time points. NSG mice were bled at day 13 and day 21 after huPBMCs injection and Hu-CD45⁺ flow cytometry staining on blood cells was performed, n=6-8 mice per group. **B.** Frequencies (%) of circulating cells are shown at day 21 after PBMCs injection.

Figures

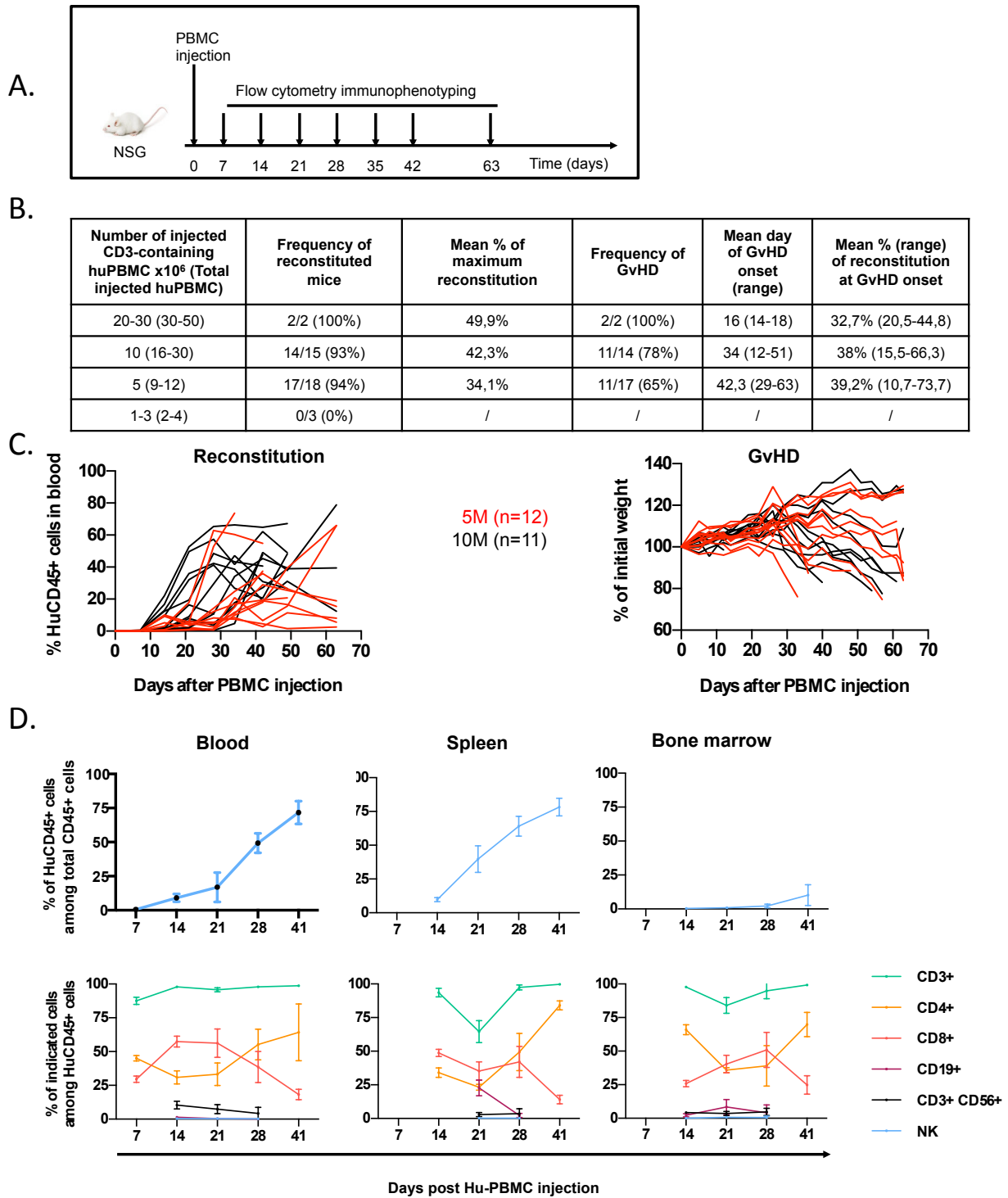


Figure 1: huPBMC reconstitution and GvHD development in Hu-PBL-NSG mice

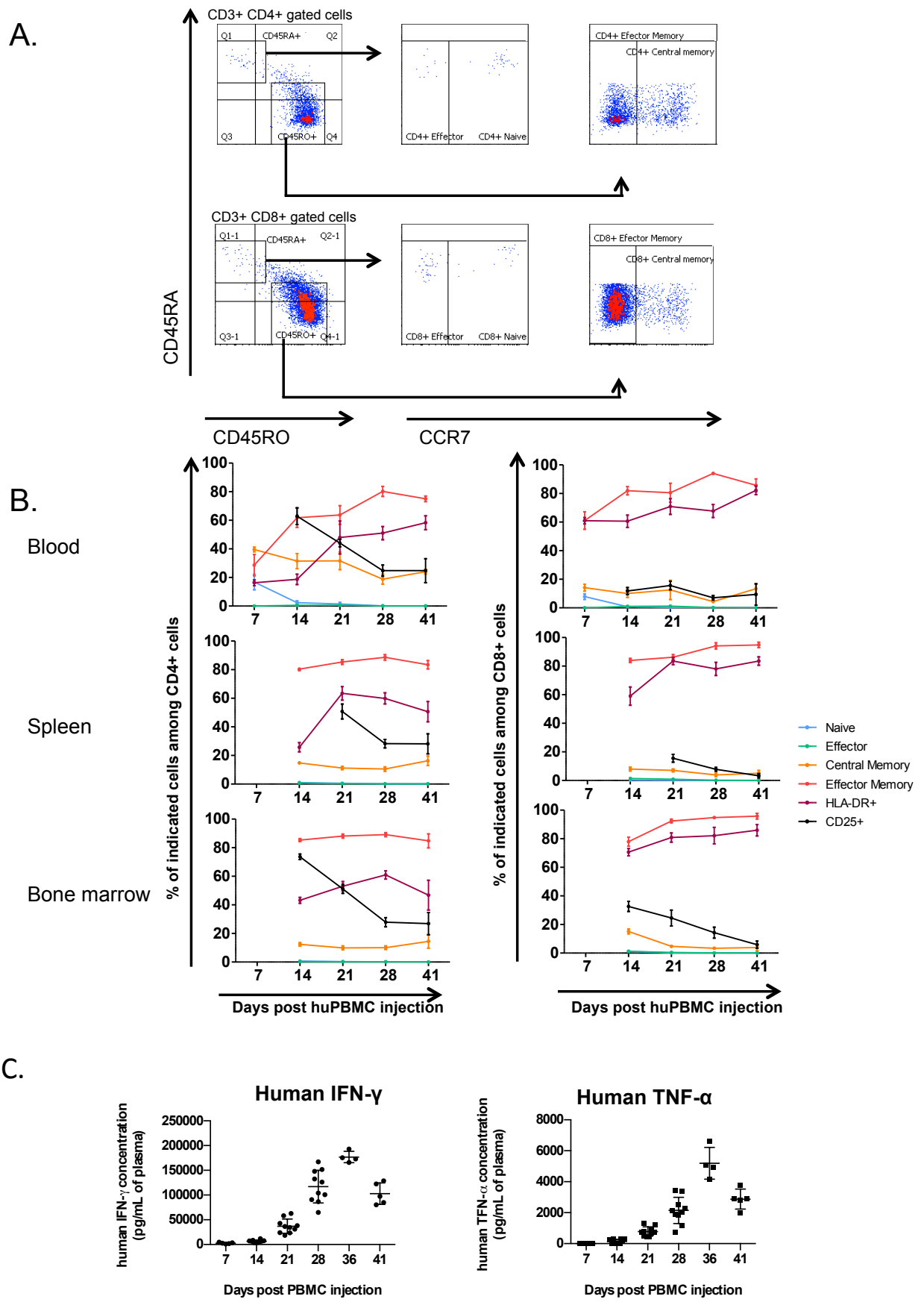


Figure 2: Hu-T cell differentiation/activation state in Hu-PBL-NSG mice

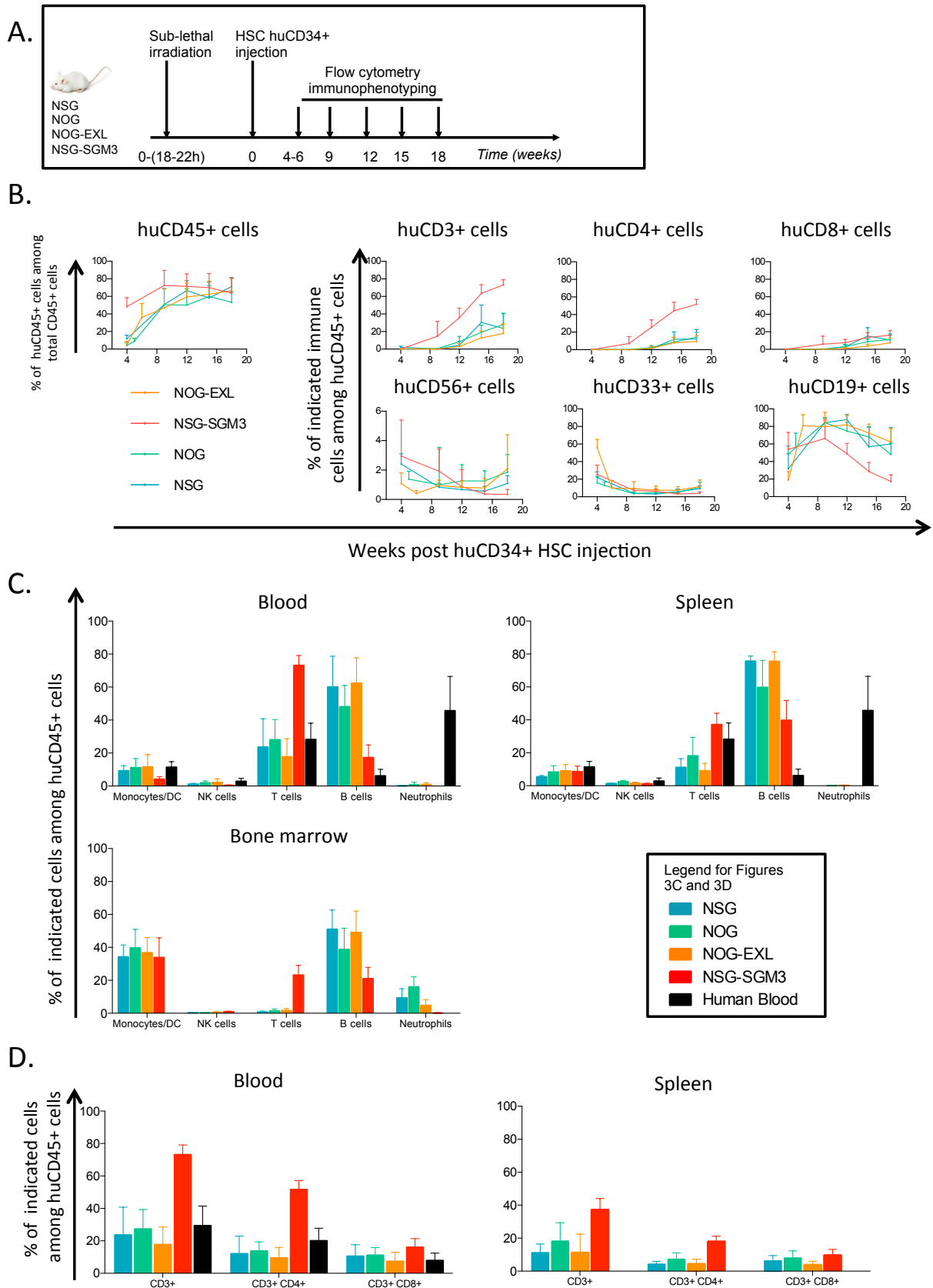


Figure 3: Immune cell reconstitution upon Hu-CD34⁺ HSC injection in different strains of immunodeficient mice.

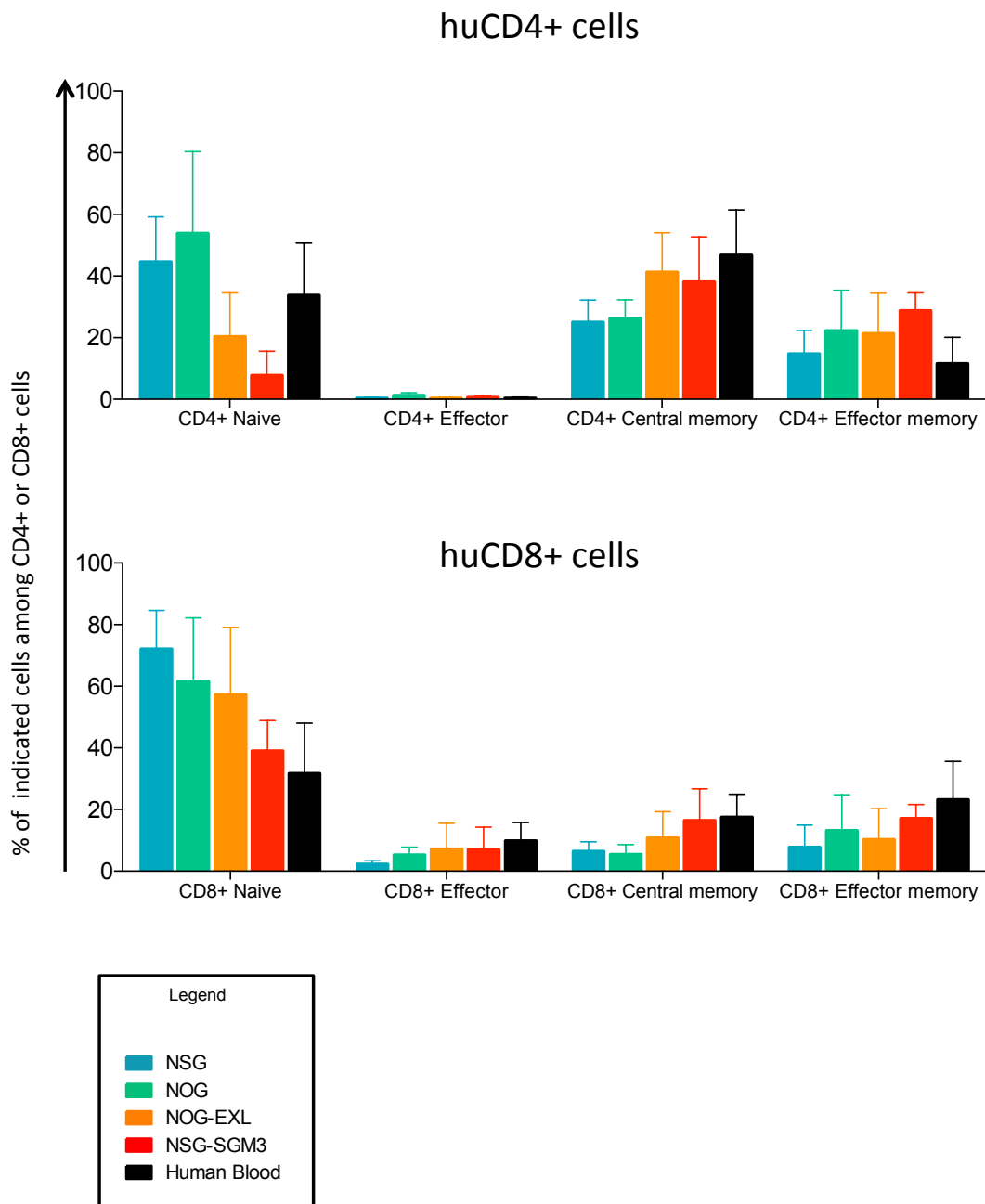


Figure 4: T cell differentiation state in HuCD34⁺-humanized mice.

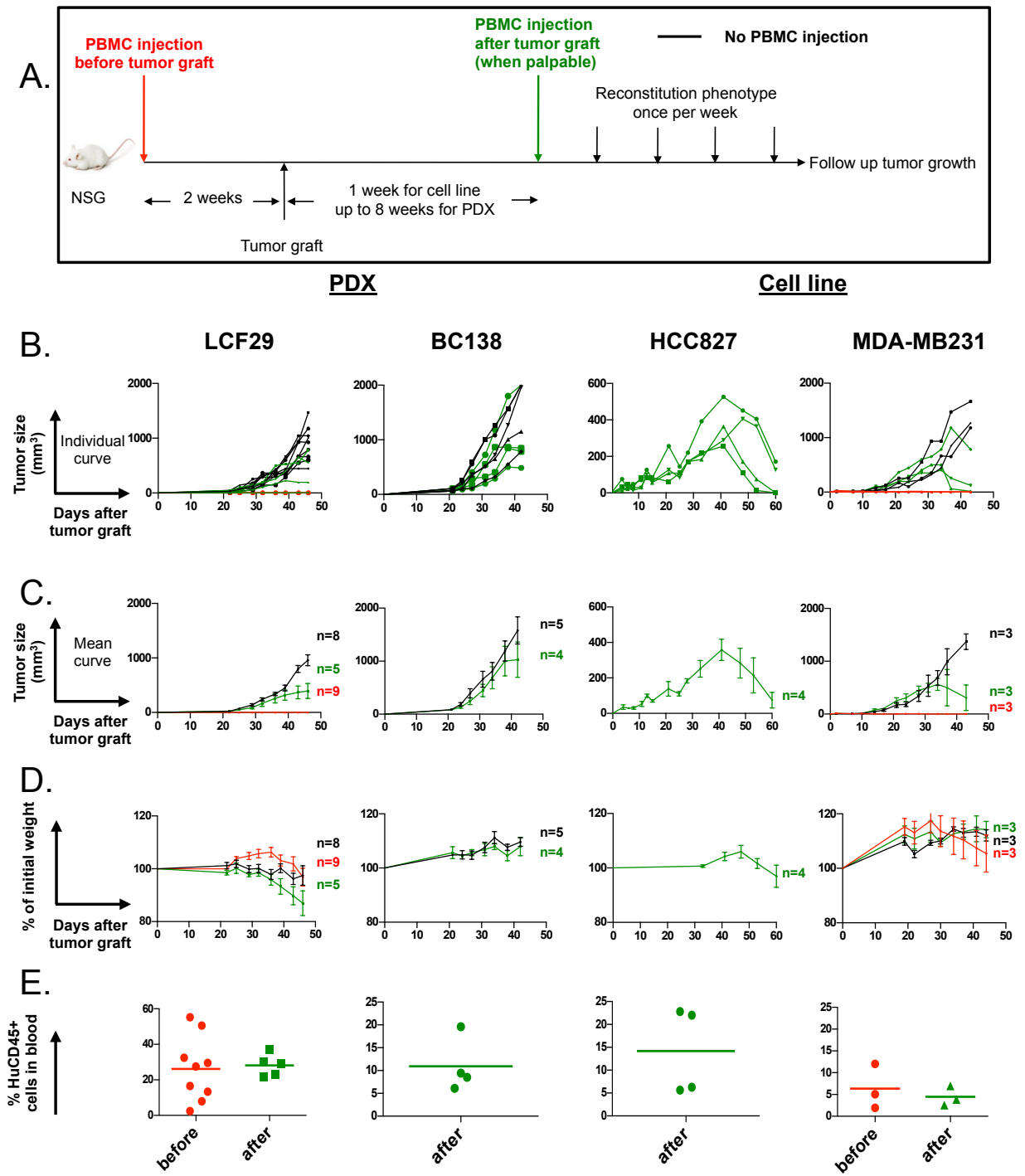


Figure 5: Impact of immune cell injection on tumor growth

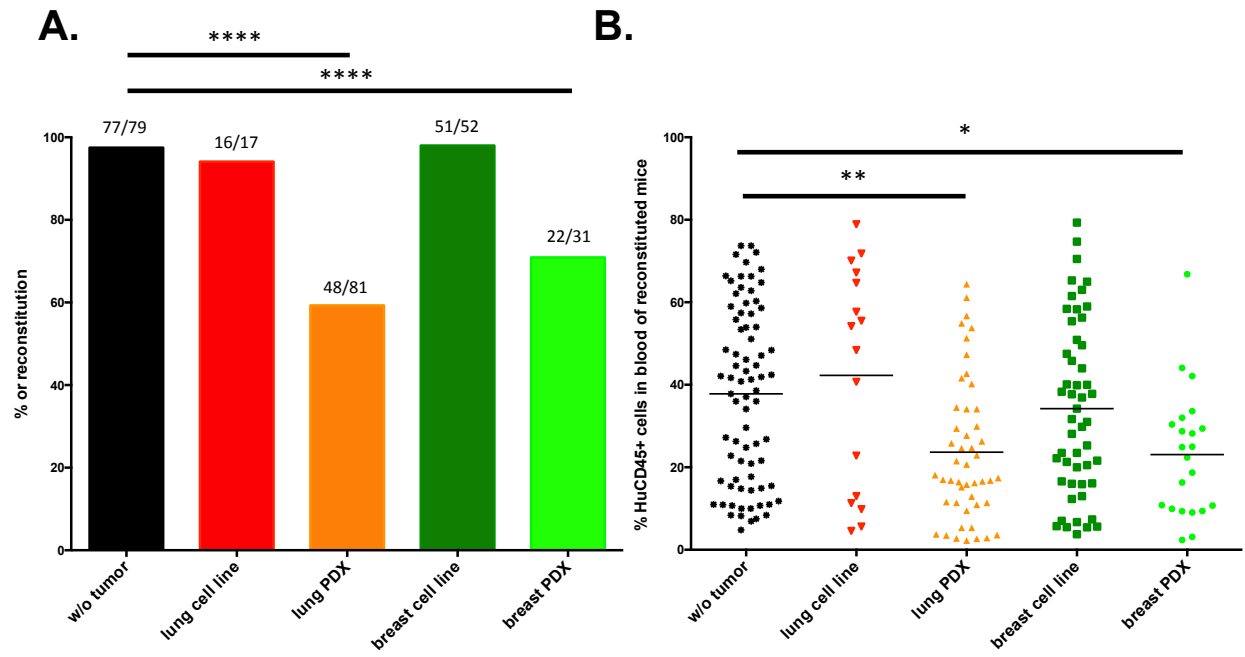


Figure 6: Impact of PDX on human immune reconstitution

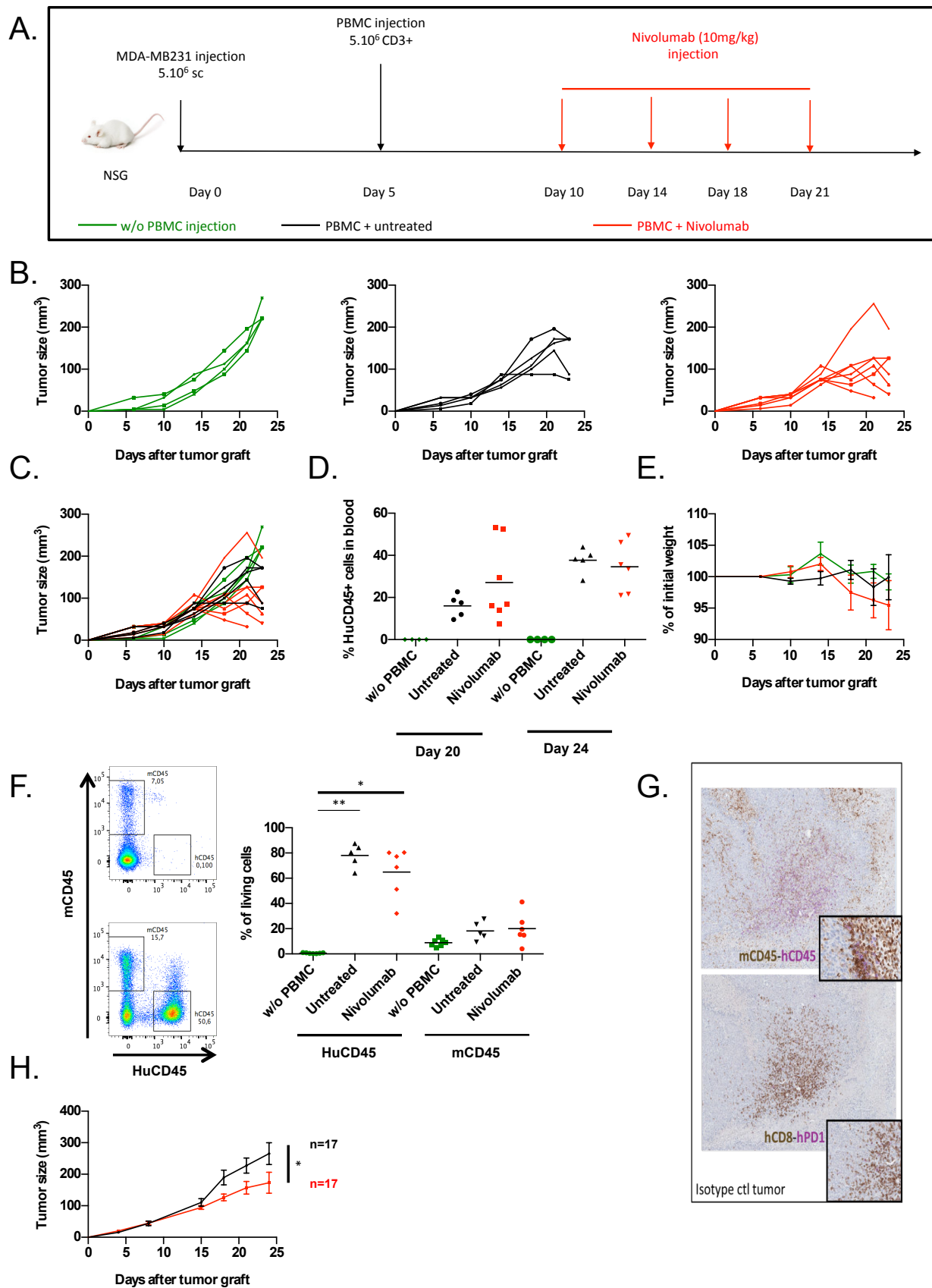


Figure 7: Effect of Nivolumab injection on MDA-MB231 tumor growth in a Hu-PBL-NSG model

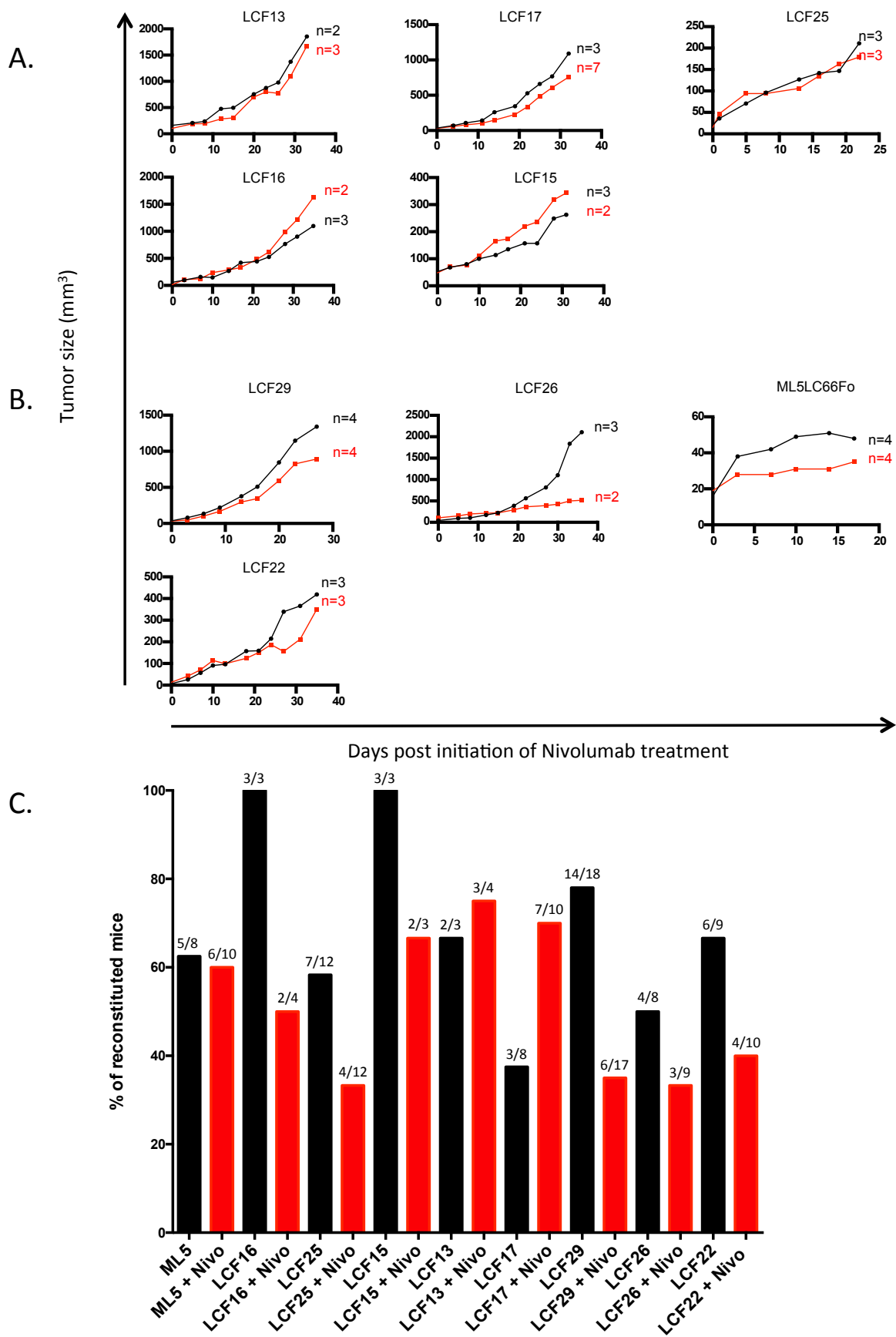


Figure 8: Screening of NSCLC PDX for nivolumab action

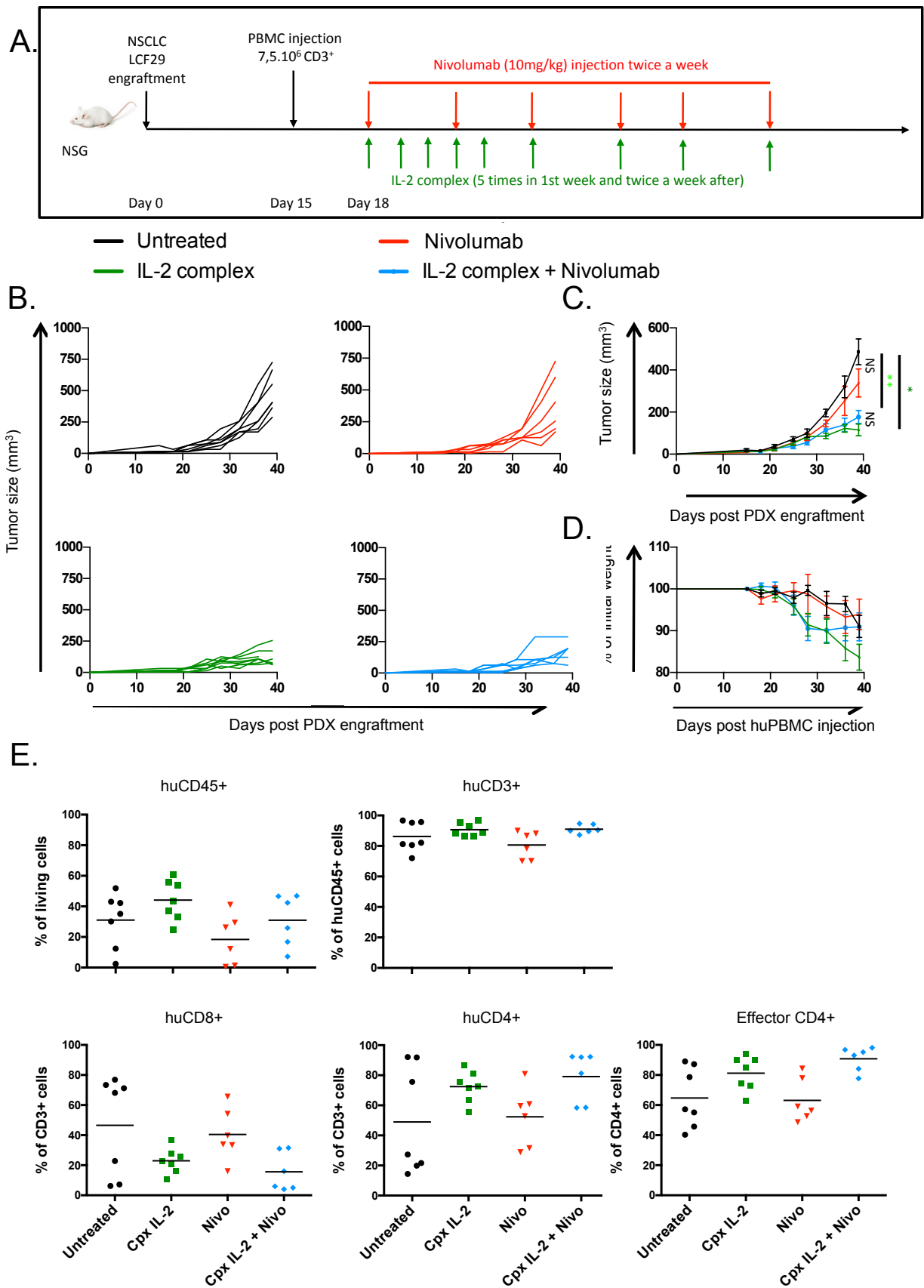
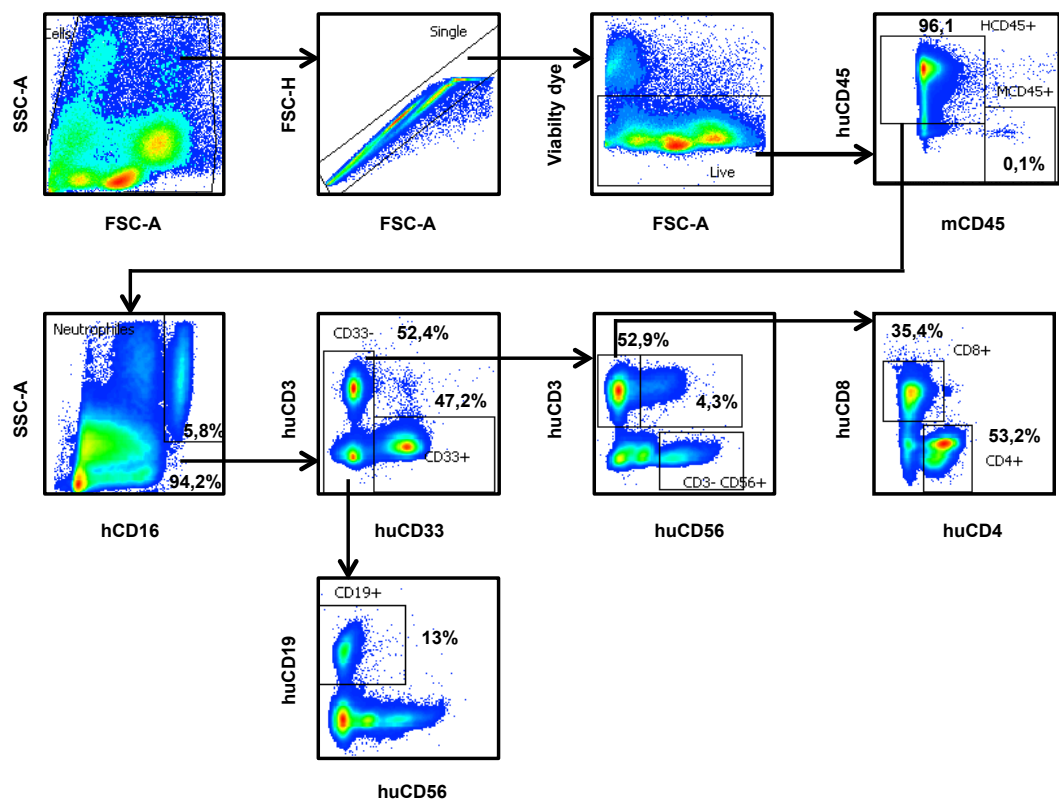
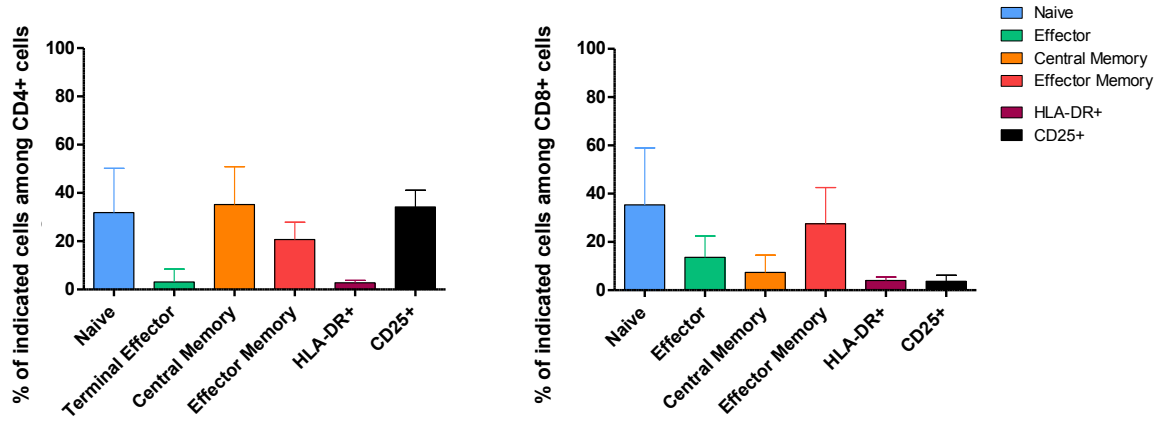


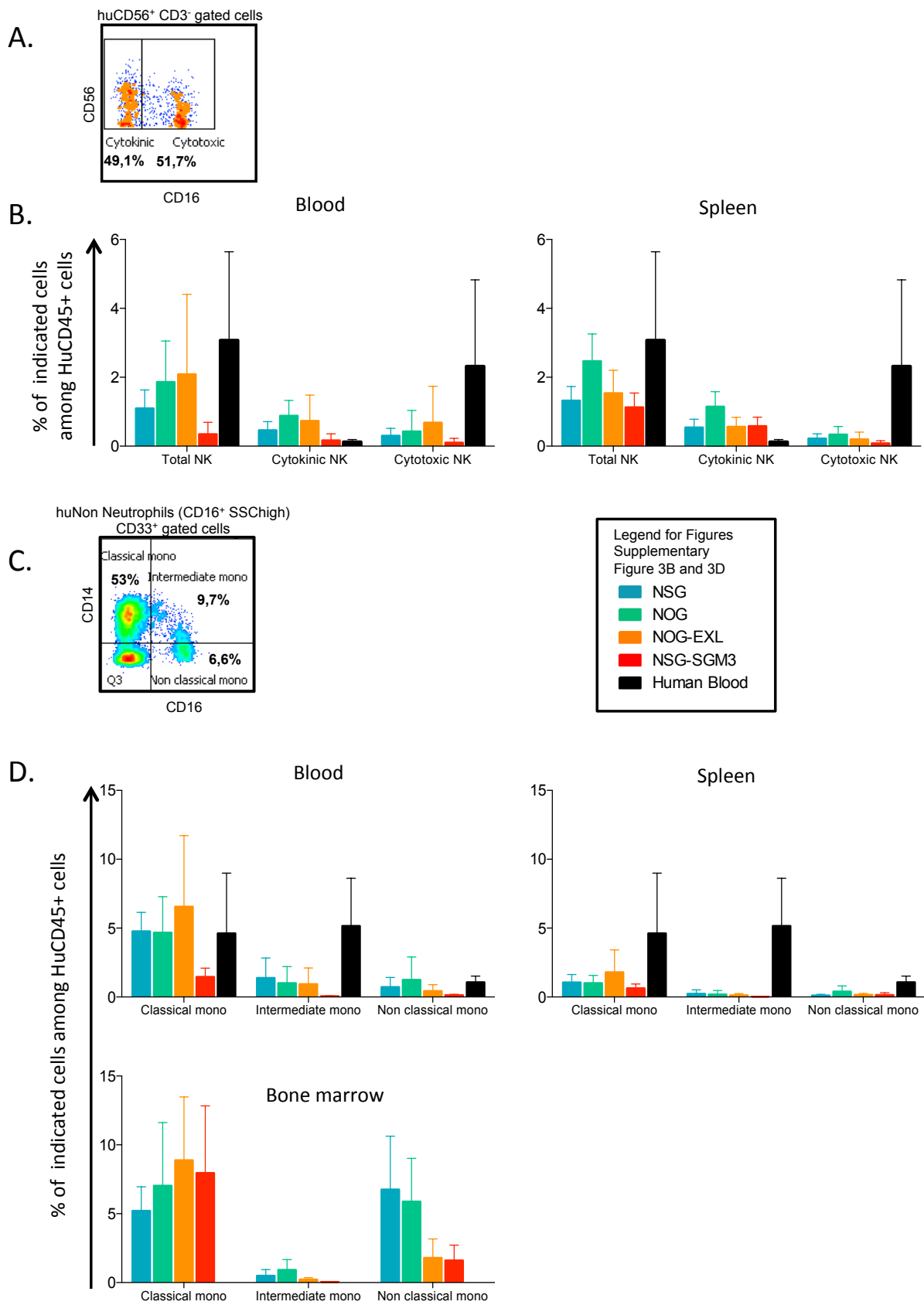
Figure 9: IL-2 complexes (IL-2Cx) injection delays tumor growth of a NSCLC PDX (LCF29) without synergy with Nivolumab



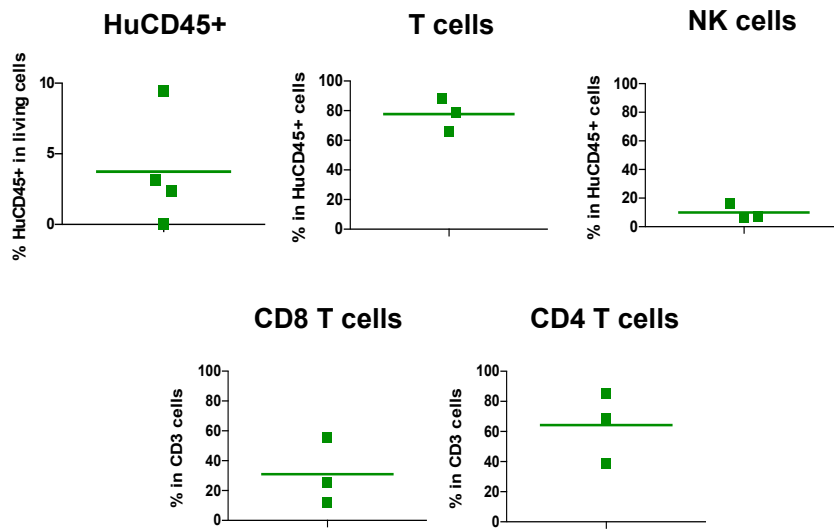
Supplementary Figure 1: Characterization of the human immune cell reconstitution upon Hu-CD34⁺ HSC injection



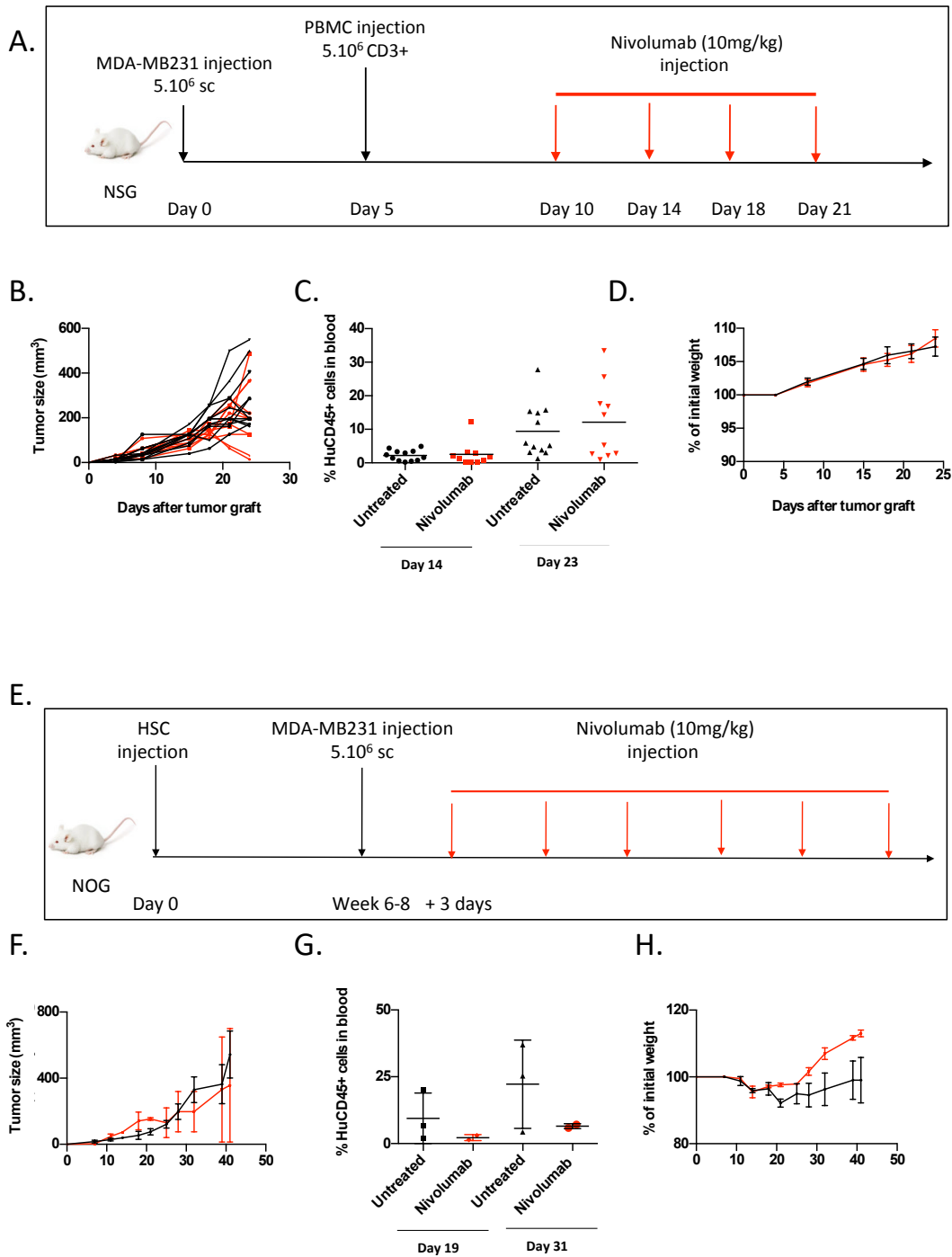
Supplementary Figure 2: T cell differentiation/activation state in blood from healthy donor



Supplementary Figure 3: huNK and huMyeloid cell reconstitution in Hu-CD34⁺ model.

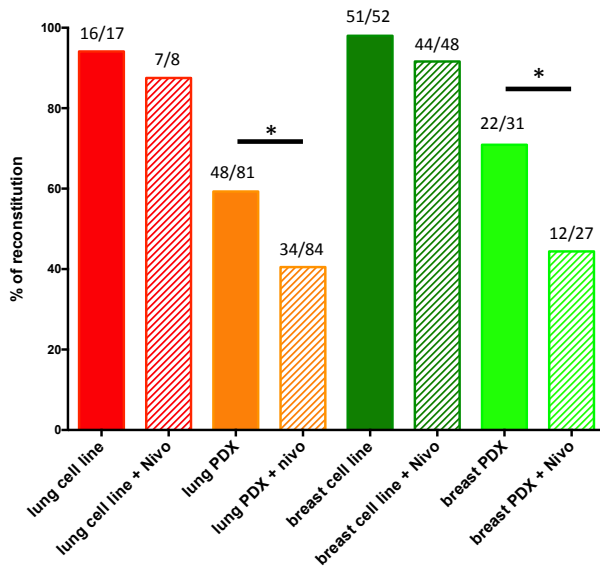


Supplementary Figure 5: Human immune infiltration in TNBC PDX

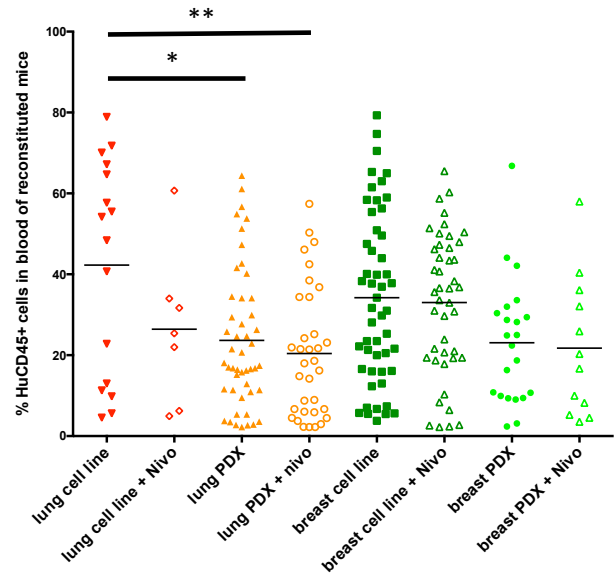


Supplementary Figure 7: Impact of Nivolumab injection on MDA-MB231 tumor growth in a Hu-PBMC-NSG model and Hu-CD34+-NSG model

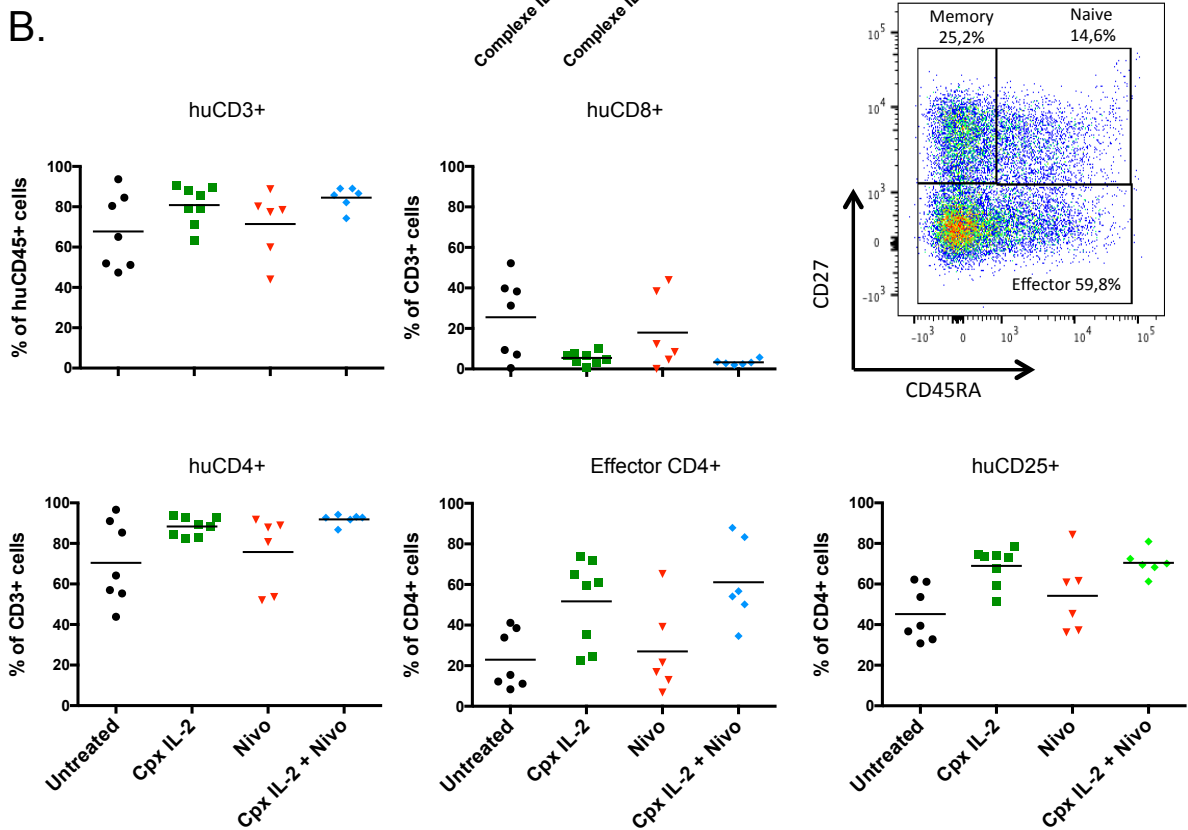
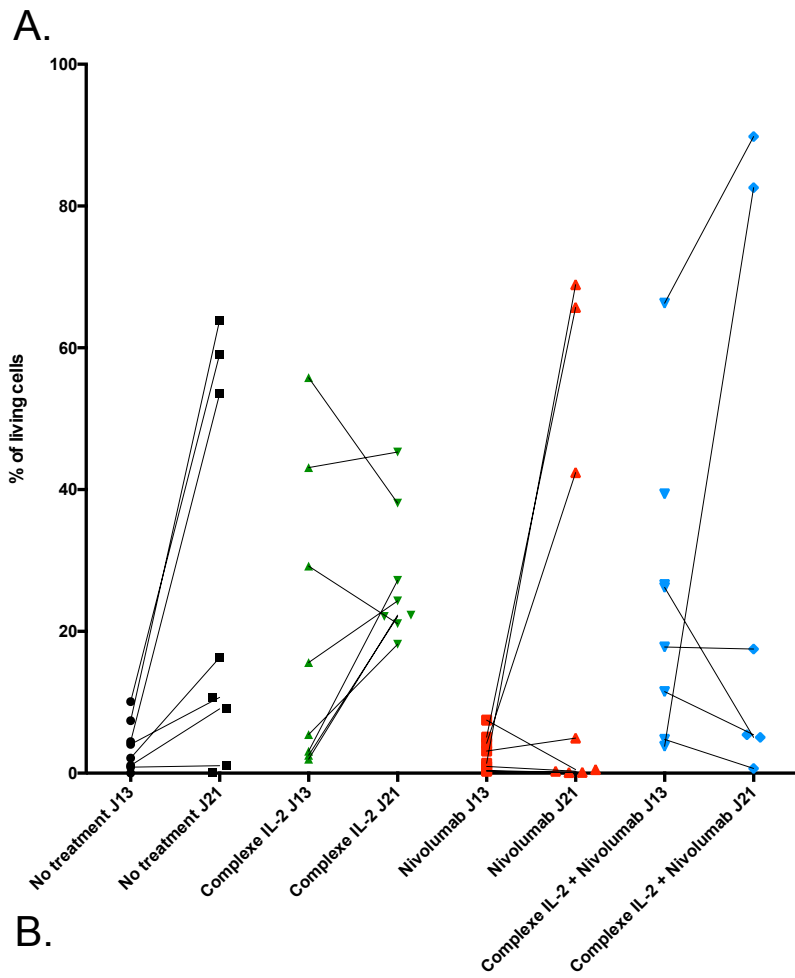
A.



B.



Supplementary Figure 8: Screening of NSCLC PDX for nivolumab action



Supplementary Figure 9: IL-2Cx modify blood reconstitution in Hu-PBL NSG

Article II

Inhibition of PI3K increases immune infiltrate in muscle invasive bladder cancer

Borcoman E^{1,2*}, De La Rochere P^{2*}, Richer W², Vacher S³, Chemlali W³, Krucker C⁴, Radvanyi F⁴, Allory Y^{5,6}, Pignot G⁷, Barry de Longchamps N⁸, Diamotte D⁹, Meseure D¹⁰, Sedlik C², Bièche I³, Piaggio E²

¹ Institut Curie, Department of Medical Oncology, 26 rue d'Ulm, Paris 75005, France.

² Institut Curie, PSL Research University, INSERM U932, 26 rue d'Ulm, Paris 75005, France.

³ Institut Curie, Unit of Pharmacogenomics, Department of Genetics, 26 rue d'Ulm, Paris 75005, France.

⁴ Institut Curie, UMR 144, 26 rue d'Ulm, Paris 75005, France.

⁵ AP-HP, Hôpitaux Universitaires Henri Mondor, Department of Pathology, 94000, Créteil, France.

⁶ INSERM, U955, 94000, Créteil, France.

⁷ Department of Urology, Institut Paoli-Calmettes, 13009, Marseille, France.

⁸ Department of Urology, Hôpital Cochin, 75014, Paris, France.

⁹ Department of Pathology, Hôpital Cochin, 75014, Paris, France.

¹⁰ Department of Pathology, Institut Curie, 75005, Paris, France.

* equal author contribution

Correspondence to:

Email: eliane.piaggio@curie.fr

Abstract

Although immune checkpoint inhibitors showed improvement in survival in comparison to chemotherapy in urothelial bladder cancer, many patients still fail to respond to those treatment and actual efforts are made to identify predictive factors of response to immunotherapy. Understanding the tumor-intrinsic molecular bases, like oncogenic pathways conditioning the presence or absence of tumor-infiltrating T cells (TILs), should provide new rationale for improved anti-tumor immune therapies. In this study, we found that urothelial bladder cancer from human samples bearing *PIK3CA* gene mutations but not *BRAF*, *RAS* or *FGFR3* mutations were significantly associated with lower expression of a defined immune gene signature, compared to unmutated ones. A reduced-10 genes immune gene signature was identified to discriminate MIBC samples according to immune infiltration and *PIK3CA* mutation, representing a low-cost and rapid technique that could be adapted in the clinic to evaluate tumor immune infiltration. Using a humanized mouse model, we observed that BKM120, a pan-PI3K inhibitor, significantly inhibited the growth of a human bladder cancer cell line bearing *PIK3CA* mutation. We observed that BKM120 treatment increased immune cell infiltration (hCD45+) in *PIK3CA* mutated tumors, in comparison to non-treated ones. By qRT-PCR, we also found an increase in immune gene expression in samples from mice bearing *PIK3CA* mutated bladder cancer treated by BKM120, reflecting an active immune infiltrate in comparison to untreated samples. Our results provide a relevant rational for combination strategies of PI3K inhibitors with immune checkpoint inhibitors to overcome resistance to immune checkpoint inhibitors.

Introduction

Bladder cancer is considered as a major source of mortality worldwide, with an estimate of 429,800 new cases and 165,100 deaths worldwide in 2012¹. About two-thirds of newly diagnosed urothelial bladder cancers are non-muscle-invasive bladder cancer (NMIBC) that can further evolve to muscle-invasive tumors in about 10% of cases; and one-third of the newly diagnosed cases are muscle-invasive bladder cancer (MIBC). Despite chemotherapy treatments, the prognostic of metastatic urothelial carcinoma remains poor after the first line of platinum-based regimen and there is an urgent need for new effective strategies in this setting^{2,3}. Immunotherapy, like immune checkpoint inhibitors, rises as a new therapeutic option in advanced urothelial carcinoma resulting in survival improvement in comparison to chemotherapy^{4,5}.

Immunotherapy has made a breakthrough in cancer treatment, in many different types of tumors, however many patients still fail to respond to immune checkpoint therapies, as around 20 to 40% of the patients will respond to those treatments⁶. Thus, there is a need to gain knowledge on the mechanism of action of these approaches and to select patients who will benefit from immune checkpoint inhibitors, identifying predictive factors.

Response to immune checkpoint inhibitors seems to be conditioned by the infiltration of tumors by activated T cells, witnessing an ongoing anti-tumor immune response⁷⁻⁹. Tumors with a T-cell-inflamed microenvironment, also referred to as “hot tumors”, are characterized by a high CD8+ T cell infiltrate, the expression of chemokines involved in T cell recruitment⁷, and a type-I interferon (IFN) signature, and are associated with improved patient survival and better responses to immunotherapies^{7,8,10}. Otherwise, tumors that lack infiltration of activated T cells in the tumor microenvironment, defined as “cold” tumors, have been described as presenting low or no clinical response to immunotherapies¹¹.

Actual efforts are made to better understand the mechanisms leading to T cell exclusion or T cell inactivation in the tumor microenvironment. Hence, understanding

the tumor-intrinsic molecular bases, like oncogenic pathways, dictating the presence or absence of tumor infiltrating T cells (TILs), should provide new rationale for improved anti-tumor immune therapies.

The PI3K/AKT/mTOR pathway is involved in different cellular functions and regulates cell cycle, cell growth, metabolism, proliferation and survival that are all hallmarks of cancer cells implicated in initial growth and extension of cancer¹¹. Phosphoinositide 3-kinases (PI3Ks) phosphorylate the 3'-hydroxyl group of phosphoinositides, generating phosphatidylinositol-3,4,5-trisphosphate (PIP3), a critical second messenger that recruits Protein Kinase B (AKT) for activation of growth, proliferation and survival¹². PIP3 is negatively regulated by phosphatase and tensin homolog (PTEN), a tumor suppressor, leads to the dephosphorylation of PIP3, acting as a negative feedback loop in the PI3K/AKT/mTOR pathway.

Genetic alterations, leading to overactivation of the PI3K/AKT/mTOR pathway are frequent events in many types of cancers¹². The PIK3CA gene is an oncogene frequently implicated in the overactivation of the PI3K/AKT/mTOR pathway, somatic PIK3CA mutations leading to an increase of kinase activity of PI3Ks. It has been found that recurrent somatic mutations of PIK3CA, known as hotspot mutations, are frequently involved in overactivation of the PI3K/AKT/mTOR pathway in tumors. These hotspot mutations were found either on the exon 9 (encoding for the helical domain of the protein, E542K and E545K) or on exon 20 (encoding for the kinase domain of the protein, H1047R and H1047L) (COSMIC database). Other frequent genetic alterations leading to PTEN loss can also result in the overactivation of the PI3K/AKT/mTOR pathway.

Interestingly, Parsa and colleagues described in human glioma that the expression of PD-L1 is increased post transcriptionally after the deletion of PTEN and the activation of the PI3K/AKT/mTOR pathway¹³. It has already been shown in a melanoma model that loss of PTEN and consequent activation of the PI3K/AKT/mTOR pathway promotes resistance to T cell-mediated immunotherapy¹⁴.

These molecular events do not explain all the cases of non-T cell-infiltrated melanomas, and the particular cases of other types of tumors remain to be studied so as to better understand resistance mechanisms to anti-immune checkpoint

inhibitors. Along these lines, Sweis and colleagues showed that β -Catenin, PPAR- γ , and FGFR3 pathways were activated in non-T-cell-inflamed bladder tumors, correlating those tumor-intrinsic oncogenic pathways with T-cell exclusion, and thus identifying those pathways as potential targetable pathways of tumor-intrinsic immunotherapy resistance¹⁵.

Therefore in our study, we assessed the correlation between genetic alterations of selected druggable tumor-intrinsic oncogenic pathways and immune cell infiltration in bladder cancer, more specifically in MIBC, so as to provide new rationale for improved anti-tumor immune therapies in this setting.

We first selected, according to the literature, an immune gene signature that could discriminate T-cell infiltrated bladder tumors from non-T-cell infiltrated tumors. We first found that NMIBC showed a significantly lower expression of the selected immune gene signature than MIBC. We then found that mutations activating PI3K pathway correlated with non-T-cell infiltrated bladder tumors among MIBC, but no other correlation where found with oncogenic alterations of RAS/BRAF pathway or FGFR3 pathway and immune infiltration in MIBC. We then tested the hypothesis that targeted therapies inhibiting PI3K pathway could increase the immune infiltration of bladder tumors *in vivo*, using a humanized mouse model. We observed that BKM120 treatment, a pan-PI3K inhibitor, effectively increased tumor immune infiltration in a PI3K-mutated bladder tumor cell line, thus transforming a “cold” into a “hot” tumor. These results bring a new rational for combining this therapeutic strategy with immune checkpoint blockade, which should likely be more efficient in face of more T-cell infiltrated tumors.

Results

Mutation of PIK3CA correlates with non-T-cell-inflamed MIBC.

We first aimed to determine whether T-cell-inflamed and non-T-cell-inflamed bladder tumors could be identified by evaluating the immune gene expression profile using qRT-PCR analysis. For that, we first defined an immune gene signature, according to the literature, and selected a panel of 57 immune genes that comprised either genes identifying immune cell populations, immunomodulatory genes, major histocompatibility complex (MHC) genes or IFN genes. The detailed list of genes selected with gene symbol and corresponding annotation are listed in **Table 1**.

We applied the 57-immune gene signature to a first cohort of 98 human bladder cancer samples for which we also analyzed the mutational status of PIK3CA, BRAF, RAS and FGFR3 genes, which are implicated in the activation of the respective oncogenic pathways. Using unsupervised hierarchical clustering bladder cancers were segregated tumors into “hot” or “cold”, based on the degree of expression of the immune gene signature¹⁵.

We observed that urothelial bladder cancers showed different levels of immune infiltration depending on the histological group type, independently of the mutational status of the PI3K, RAS/RAF or FGFR3 oncogenic pathways. Indeed, NMIBC showed a significantly lower expression of the immune gene signature than MIBC (Fisher’s exact test, $p < 0.001$) (**Supplementary data Figure 1**).

Given that NMIBC showed very low levels of expression of the immune gene signature, we then focused on the MIBC. Among the 56 MIBC subtype samples, we observed that tumors bearing a PIK3CA mutation showed a significantly lower expression of the immune gene signature compared to non-PIK3CA mutated ones (Fisher’s exact test, $p = 0.04$, **Figure 1A**).

There was no significant correlation between the expression of the immune gene signature and BRAF mutational status (Fisher’s exact test, $p = 1$), RAS mutational status (Fisher’s exact test, $p = 1$), or FGFR3 mutational status (Fisher’s exact test, $p = 0.38$, **Figure 1A**).

We then defined a minimal immune gene signature that could discriminate high-versus low-immune infiltrated tumors, among the MIBC subgroup (**Figure 1B**). The selected genes for the minimal signature were the most differentially expressed genes between wild type and PIK3CA mutated samples. The expression of a minimal

signature of 10 immune genes could discriminate high- versus low-immune infiltrated MIBC tumors. The low-infiltrated tumors were associated with the presence of a *PIK3CA* mutation, in comparison to the wild type ones, that showed a higher expression of the minimal 10-immune gene signature (Fisher's exact test, $p=0.02$, **Figure 1B**), but showed no correlation with *BRAF*, *RAS* or *FGFR3* mutations. The minimal 10-immune genes (*TIGIT*, *CTLA4*, *CD8*, *GZMA*, *PVRIG*, *PDCD1*, *HAVCR2*, *ENTPD1*, *HLA-DRA*, *HLA-DRB*) reflect an activated effector CD8+ T cell infiltrate in the tumor.

Overall, our results suggest that mutations of the *PIK3CA* gene, leading to the activation of the PI3K pathway impair T-cell infiltration of the tumor stroma of MIBC.

Targeted therapy inhibition of PI3K pathway increases tumor-immune infiltration *in vivo*.

In order to confirm the correlation between the tumoral T-cell-infiltrate in MIBC and mutations of the *PIK3CA* gene, we set up a humanized mouse model allowing to directly assess the effect of a clinical-grade PI3K inhibitor on human tumor cells and human immune cells *in vivo*.

We used as recipient mice NOD scid gamma (NSG) mice, which are highly immunodeficient mice that have no B, T and NK cells, and consequently allow the transplantation of tumor and immune cells of human origin¹⁶. Mice were subcutaneously injected with cells of either the VMCUB1 cell line, a *PIK3CA* mutated (*PIK3CA_m*) human bladder cancer cell line, or as a control, the HT1376 cell line, a *PIK3CA* wild type (*PIK3CA* WT), human bladder cancer cell line. When the tumors were palpable, mice were grafted with human PBMCs, isolated from blood samples of human healthy donors. Three days later, mice were assigned to no treatment, or treatment with a pan-PI3K inhibitor, BKM120 (**Figure 2A**). Individual and mean tumor growth curves of each cell line are shown in **Figure 2B and C**, respectively. In the *PIK3CA_m* VMCUB1 group, tumors in mice treated with BKM120 grew at a significantly slower rate, in comparison to the non-treated mice (Mann-Whitney test, $p<0.01$ at day 17, 20 and 24, **Figure 2B and C**). In the *PIK3CA* WT HT1376 group, there was a

little effect of BKM120 on tumor growth that became statistically significantly different only by day 25 (Man-Whitney test, $p < 0.01$, **Figure 2B and C**).

The main caveat of this model is that the injected human PBMCs react against mice xeno-antigens, invariably leading to xeno-graft-versus-host-disease (GvHD), which induces body-weight loss and death of the mice^{17,18}. Consequently, the therapeutic observational window in this model is of around 3-6 weeks after PBMCs injection, before evident signs of GvHD^{19,20}. To evaluate GvHD development, we recorded mice body weight along the length of the experiment. As shown in **Figure 2D**, mice in the *PIK3CA*^m VMCUB1 group started to lose weight at around 3 weeks after tumor graft, and following ethical guidance, were sacrificed upon a loss of 20% of body weight. Mice in the *PIK3CA* WT HT1376 group did not show significant loss of body weight during this period.

The clinical onset of GvHD is directly correlated with the level of human T cell engraftment, thus we assessed the human immune cell reconstitution in mice's blood by performing a human CD45 staining by FACS assessed human CD45+ (HuCD45+) cell reconstitution in blood of mice (**Figure 2E**). We observed that the majority of mice presented more than 2% of HuCD45+ in blood, indicating that reconstitution was effective.

Overall, our data showed that the pan-PI3K inhibitor BKM120 significantly inhibited the growth of the *PIK3CA* mutated VMCUB1 human bladder cancer cell line in a humanized mouse model.

We then examined changes operated in the intra-tumoral immune infiltrate upon inhibition of the PI3K pathway by BKM120. Total immune infiltration (hCD45+ cells) was quantified by FACS in tumor samples harvested at sacrifice of mice (**Figure 3A**). We observed that in the *PIK3CA*^m VMCUB1 group, BKM120 treatment significantly increased the proportion of HuCD45+ cells in the tumor ($p < 0.001$), as well as of CD3+ T cells ($p < 0.05$), in comparison to untreated mice. In tumors harvested from mice of the *PIK3CA* WT HT1376 group, there were no significant changes in the percentage of total immune cells or CD3+ T cells.

We then evaluated the composition of the immune infiltrate. In the *PIK3CA* VMCUB1 group and in the *PIK3CA* WT HT1376 group, there were no significant differences between the non-treated and treated groups regarding the composition of immune T cells (including CD8+ cytotoxic T cells, CD4+ FOXP3- conventional T cells and CD4+ FOXP3+ Tregs), B cells and NK cells (**Figure 3B**). These data indicate that chemical inhibition of mutated *PIK3CA* enhances tumor infiltration by hematopoietic cells, without significantly modifying the proportions of the different immune subpopulations.

We further assessed the impact of the treatment with BKM120 on the immune gene expression profile using qRT-PCR analysis of tumor samples from the humanized mouse model (**Figure 4**). For the *PIK3CA* VMCUB1 cell line, we used frozen samples obtained from 13 untreated and 15 BKM120-treated humanized mice. For the *PIK3CA* WT HT1376 cell line, we used frozen samples from 12 untreated and 13 BKM120-treated humanized mice. Interestingly, we did not observe any major effect of the BKM120 treatment on the immune gene expression profile of the *PIK3CA* WT HT1376 samples, but we did observe that BKM120 treatment significantly increased the immune signature in the *PIK3CA* VMCUB1 tumors, in comparison to the untreated humanized mice. Indeed, we observed an increase of *HLA-DRA* ($p < 0.05$), *PTPRC* (hCD45) ($p < 0.005$), *CD3E* (CD3) ($p < 0.005$), *CD8A* (CD8) ($p < 0.05$) *GZMA* (granzyme A) ($p < 0.005$) immune gene expression and a decrease of *MERTK* (macrophages) ($p < 0.005$) gene expression with BKM120 treatment in the *PIK3CA* VMCUB1 tumors. We also observed an increase of immune checkpoint gene expression: *TIGIT* ($p < 0.005$), *CTLA-4* ($p < 0.05$), *PDCD1* (PD-1) ($p < 0.005$), *HAVCR2* (TIM-3) ($p < 0.0005$) and *ENTPD1* (CD39) ($p < 0.0005$) after BKM120 treatment of the *PIK3CA* VMCUB1 humanized mice. We also assessed the expression profile of proliferation genes such as *ETVA*, *ETV5*, *DUSP1*, *CA9*, which were significantly less expressed in the *PIK3CA* VMCUB1 humanized mice after BKM120 treatment, in comparison to untreated ones, indicating an anti-proliferative effect, likely on the tumor cell – although with this technique we cannot dissociate whether the anti-proliferative effect is occurring on the tumor cells alone, or also in the other stromal cells which are present in the

analyzed samples (**Supplementary data Figure 2**). These results confirm the data obtained by FACS analysis indicating that BKM120 treatment promotes tumor immune infiltration and further suggest that the drug inhibits tumor cell proliferation.

Discussion

Sensitivity of tumors to therapies targeting immune-checkpoints seems to be conditioned by the quality and quantity of the tumor immune infiltrate.

We defined a RT-qPCR-based immune gene signature that allows to weight in a semi-quantitative way the immune infiltrate of solid tumors. This signature, which can be reduced to less than 10 genes, represent a low-cost and rapid technique that could be adapted in the clinic to evaluate tumor immune infiltration, so as help for the clinical management of cancer patients.

Moreover, combination of this signature to the mutational status of oncogenic genes represent a simple way to identify tumoral oncogenic pathways responsible for the exclusion of the immune infiltrate out of the tumor microenvironment. The identified druggable mutations could become a potential target for combination with anti-checkpoint antibodies, allowing that T cells re-invigorated by the immunotherapy effectively access the tumor bed.

We found that urothelial bladder cancers from patients bearing *PIK3CA* gene mutations but not *BRAF*, *RAS* or *FGFR3* mutations were significantly associated with lower expression of the immune gene signature, compared to unmutated ones, that could reflect the presence of a less active tumor immune infiltrate. These results indicate that the identified molecular events do not explain all the cases of infiltrated or non-infiltrated tumors. On the contrary, our work indicates that the influence of each oncogenic pathway on the immune infiltrate is tumor-type dependent and even tumor-sub-type dependent as was the case for the muscle invasive and non invasive bladder tumors in our studied series. We then validated "*in vivo*" this first correlation observed in bladder cancer between *PIK3CA* gene mutation and lower expression of our immune gene signature.

Using a humanized mouse model, we observed that BKM120, a pan-PI3K inhibitor, significantly inhibited the growth of a human bladder cancer cell line bearing *PIK3CA*

mutation. We observed that BKM120 treatment increased the total quantity of immune cells infiltration (hCD45+) and CD3+ T cells in *PIK3CA* mutated tumors, in comparison to non-treated ones. No significant differences in term of distribution of the different immune subpopulations of the infiltrate were observed under BKM120 treatment.

Inhibition of P3IK pathway could also have an inhibitory effect on myeloid-derived suppressor cells (MSDC), that could restore the activity of T-cells, without increasing the quantity of T-cells into the tumor micro-environment, but leading to an increase of activated T-cells. This has been showed with anti-angiogenic treatments for example, that could potentially reduce number of MSDC in tumor immune infiltrate, promoting the activation of T-cells²¹. This hypothesis has been investigated recently in a head and neck squamous cell carcinoma model, authors could demonstrate that inhibition of PI3K pathway could inhibit MDSCs into the tumor microenvironment, which could enhance responses to PD-L1 blockade, and that combination therapy induced CD8+ T cell dependent primary tumor growth delay, only in T-cell inflamed tumor models of head and neck cancers²². Interestingly in our results using immune gene expression on samples from the humanized mouse model we did observed a decrease of MERTK expression that could reflect a decrease in macrophage infiltration in the tumor microenvironment and could lead to a more active immune infiltrate in tumors under BKM120 treatment.

Our results suggest a relevant rational for combination strategies of PI3K inhibitors with immune checkpoint inhibitors. Further studies will be needed to better decipher the mechanisms on immune resistance, and also to define the more efficient combination strategies, with the more efficient timing, dosage between immunotherapies and targeted therapies.

Materials and Methods

Classification of urothelial bladder cancer subtypes by immune gene expression profile and presence of mutations in oncogenic pathways.

Patients and samples.

Patients included 17 women (17.3%) and 81 men (82.7%). Pathotological staging included 42 NMIBC, 18 low-grade (42.9%) and 24 high-grade (57.1%) NMIBC, and 56 high-grade MIBC. Clinical and histological characteristics of patients along with survival are resumed in **Table 2 and 3**.

Patients included in this study had undergone transurethral bladder resection or radical cystectomy in our hospital between January 2002 and January 2006. Specimen from normal bladder tissue from 15 patients undergoing surgery unrelated to bladder tumors were used as normal bladder tissue. Data were obtained from patient's medical records. All patients signed an informed consent. This study received approval from an institutional review board and was conducted according to the principles outlined in the Declaration of Helsinki.

Immediately after surgery, tumors samples were frozen in liquid nitrogen and stored at -80°C (for RNA extraction) and fixed in formaldehyde.

qRT-PCR analysis of the immune gene signature in human bladder tumor samples.

The theoretical basis, primers and PCR consumables, RNA extraction, cDNA synthesis, and PCR reaction conditions have been previously described in detail²³. Briefly, quantitative values were obtained from the threshold cycle (Ct) number at which the increase in the signal associated with the exponential growth of PCR products began to be detected. One endogenous RNA control gene involved in two cellular metabolic pathways was chosen, namely TBP (Gen-Bank Accession No.NM_003194), which encodes TATA boxbinding protein. Each sample was normalized based on its TBP content. Results, expressed as N-fold differences in target gene expression relative to the TBP gene and termed *Ntarget*, were determined as $N_{target} = 2^{Ct_{sample}}$, where the

Ct value of the sample was determined by subtracting the average Ct value of the target gene from the average Ct value of the TBP gene. A Ct value above 35 was considered as not quantifiable and expression equal to 0. Positive controls for all genes were obtained by performing an RNA pool control, which was prepared by mixing identical amounts of RNA from various human normal and tumor tissues. Hierarchical clustering was performed on log₂ expression values using Ward's method on euclidean distances. Fisher's exact test was applied to verify if identified clusterings permit to discriminate wild type and mutated samples for each oncogenic pathway according to the immune gene signature.

Mann-Whitney-Wilcoxon test was applied between wild type and mutated gene sample populations on each gene to identify the genes that were statistically differentially expressed between both populations.

Evaluation of the effect of targeted therapy inhibition of PI3K pathway on tumor-immune infiltration *in vivo*

Humanized mouse model.

We used NOD-scid-IL2 γ ^{-/-} (NSG) mice were grafted with human tumor cell line and then reconstituted with human peripheral blood mononuclear cells (PBMC) from blood samples of human healthy donors.

PBMC were isolated using Ficoll and the quantification of CD3⁺ cells was done by Fluorescence-activated cell sorting (FACS) with CD3⁺ staining and then total PBMC were immediately stored in liquid nitrogen.

Human bladder cancer cell lines, either VMCUB1, a PI3K mutated human bladder cell line, or HT1376, a wild type human bladder cancer cell line, were injected ectopically in the right flank of each NSG mouse subcutaneously with 10 or 20 x 10⁶ of cancer cells/mouse.

When the tumors were palpable (above 3x3mm), we injected intra-venously (IV), by retro orbital injection, the amount of PBMC that corresponds to 7.5 x 10⁶ human CD3⁺ T cells/mouse.

Tumor growth was measured twice a week using a caliper to determine the tumor size, calculated as $((\text{length} \times \text{width}^2)/2)$. Mice were sacrificed before the tumor reached 2 cm³. Mice were weighted at the same time points, to follow graft versus host disease (GvHD).

Starting seven days after PBMC injection and then once a week, we assessed the human immune cells reconstitution in mice by performing an hCD45+ cells staining by FACS on 50µl blood sample collected by at the retro-orbital site.

Starting 3 days after PBMC injection, BKM120, a pan-PI3K inhibitor, was administered at a dose of 30 mg/kg per day, via oral gavage.

At the experimental endpoint, mice were sacrificed; the tumors were collected and processed individually. Half of each tumor sample was used for FACS staining and the other half was divided in two, one part for the histochemistry analysis, and the other kept in liquid nitrogen directly after dissection for future qPCR analysis to assess our immune gene signature on tumor samples from the humanized mouse model.

Flow cytometry.

Tumor was removed, and half of the tumor was processed for FACS analysis. Tumor was cut into small pieces and mixed with 2ml of CO₂ independent medium (Gibco® Life technologies) containing 30 µl Dnase (10mg/ml, Roche®), and 60 µl liberase LT (5mg/ml, Roche®) per sample. The tumor sample was processed on a Gentlemacs dissociator (Miltenyi Biotec, San Diego, CA), then the dissociated tumor sample was filtered through a cell strainer (BD Biosciences), washed with PBS, then incubated with the antibodies (Abs) for FACS staining.

For the phenotypic analysis of human immune cell populations, tumor cells were stained for surface markers with LIVE/DEAD Fixable Aqua (Life Technologies™), hCD27-BV605 clone O323 (Biolegend), hCD3-BV650 clone OKT3 (Biolegend), hCD4-BV785 clone OKT4 (Biolegend), hPD-1-BV711 clone EH12.2H7 (Biolegend), hCD8-PECF594 clone RPA-T8 (BD Biosciences), hCD56-PE-Cy5 clone N901 (BD Biosciences), hCD45-APC Cy7 clone 2D1 (BD Biosciences), hCD19-Alexa 700 clone HIB19 (BD Biosciences), hCD45RA-PECy5 clone HI100 (eBiosciences), hCD25-PE (BD Biosciences), hTCRgd-FITC clone 11F2 (BD Biosciences). Then for intracellular staining, cells were

fixed and permeabilized with fixation/permeabilization solution (eBiosciences) according to the manufacturer's instructions and stained with FOXP3-efluor 450 clone 236A/E7, (eBioscience).

Samples were then analyzed on a Fortessa flow cytometer (BD Biosciences). FACS data were analyzed with FlowJo Version v10.0.8 (TreeStar).

Authors' Contributions:

B.E., DLR. P. B. I. and. P. E. designed the research. B.E., DLR. P., V.S., D. M., C. S. and C.W. performed experiments and analyzed data. R.A. R.W. performed bioinformatic analysis. K.C., R.F.AND Y.A. provided reagents and contributed to experimental design. P.G., B.L. and D.D contributed with patient data and sample, B. I., A. Y; R.F and P. E. critically revised the manuscript. B.E., DLR. P. and. P. E. wrote the manuscript. P. E. conceived and designed the project and wrote the manuscript.

Acknowledgements:

We thank Virginie Dangles-Marie, Celine Daviaud, Isabelle Grandjean, Mikael Garcial and Cedrik Purchase, the mouse facility technicians and flow cytometry core at Institut Curie. This work was supported by the institute Curie, Institut National de la Santé et de la Recherche Médicale, Association pour la Recherche sur le Cancer (ARC PJA 20131200444); Labex DCBIOL (ANR-10-IDEX-0001-02 PSL and ANR-11-LABX0043), SIRIC INCa-DGOS-Inserm_12554. B.E. was supported by a master 2 fellowship from Institut Curie.

Conflicts of interest:

The authors declare no competing financial interests.

References

1. Torre LA, Bray F, Siegel RL, Ferlay J, Lortet-Tieulent J, Jemal A. Global cancer statistics, 2012. *CA Cancer J Clin.* 2015;65(2):87–108. doi:10.3322/caac.21262
2. von der Maase H, Hansen SW, Roberts JT, Dogliotti L, Oliver T, Moore MJ, Bodrogi I, Albers P, Knuth A, Lippert CM, et al. Gemcitabine and cisplatin versus methotrexate, vinblastine, doxorubicin, and cisplatin in advanced or metastatic bladder cancer: results of a large, randomized, multinational, multicenter, phase III study. *J. Clin. Oncol.* 2000;18(17):3068–3077. doi:10.1200/JCO.2000.18.17.3068
3. Bellmunt J, Fougeray R, Rosenberg JE, von der Maase H, Schutz FA, Salhi Y, Culine S, Choueiri TK. Long-term survival results of a randomized phase III trial of vinflunine plus best supportive care versus best supportive care alone in advanced urothelial carcinoma patients after failure of platinum-based chemotherapy. *Ann. Oncol.* 2013;24(6):1466–1472. doi:10.1093/annonc/mdt007
4. Rosenberg JE, Hoffman-Censits J, Powles T, van der Heijden MS, Balar AV, Necchi A, Dawson N, O'Donnell PH, Balmanoukian A, Loriot Y, et al. Atezolizumab in patients with locally advanced and metastatic urothelial carcinoma who have progressed following treatment with platinum-based chemotherapy: a single-arm, multicentre, phase 2 trial. *Lancet.* 2016;387(10031):1909–1920. doi:10.1016/S0140-6736(16)00561-4
5. Bellmunt J, de Wit R, Vaughn DJ, Fradet Y, Lee J-L, Fong L, Vogelzang NJ, Climent MA, Petrylak DP, Choueiri TK, et al. Pembrolizumab as Second-Line Therapy for Advanced Urothelial Carcinoma. *N. Engl. J. Med.* 2017;376(11):1015–1026. doi:10.1056/NEJMoa1613683
6. Topalian SL, Hodi FS, Brahmer JR, Gettinger SN, Smith DC, McDermott DF, Powderly JD, Carvajal RD, Sosman JA, Atkins MB, et al. Safety, activity, and immune correlates of anti-PD-1 antibody in cancer. *N. Engl. J. Med.* 2012;366(26):2443–2454. doi:10.1056/NEJMoa1200690
7. Harlin H, Meng Y, Peterson AC, Zha Y, Tretiakova M, Slingluff C, McKee M, Gajewski TF. Chemokine expression in melanoma metastases associated with CD8+ T-cell recruitment. *Cancer Res.* 2009;69(7):3077–3085. doi:10.1158/0008-5472.CAN-08-2281

8. Ji R-R, Chasalow SD, Wang L, Hamid O, Schmidt H, Cogswell J, Alaparthi S, Berman D, Jure-Kunkel M, Siemers NO, et al. An immune-active tumor microenvironment favors clinical response to ipilimumab. *Cancer Immunol. Immunother.* 2012;61(7):1019–1031. doi:10.1007/s00262-011-1172-6
9. Kirilovsky A, Marliot F, El Sissy C, Haicheur N, Galon J, Pagès F. Rational bases for the use of the Immunoscore in routine clinical settings as a prognostic and predictive biomarker in cancer patients. *Int. Immunol.* 2016;28(8):373–382. doi:10.1093/intimm/dxw021
10. Pagès F, Berger A, Camus M, Sanchez-Cabo F, Costes A, Molidor R, Mlecnik B, Kirilovsky A, Nilsson M, Damotte D, et al. Effector memory T cells, early metastasis, and survival in colorectal cancer. *N. Engl. J. Med.* 2005;353(25):2654–2666. doi:10.1056/NEJMoa051424
11. Ramos RN, Piaggio E, Romano E. Mechanisms of Resistance to Immune Checkpoint Antibodies. *Handb Exp Pharmacol.* 2017 Mar 18. doi:10.1007/164_2017_11
12. Yuan TL, Cantley LC. PI3K pathway alterations in cancer: variations on a theme. *Oncogene.* 2008;27(41):5497–5510. doi:10.1038/onc.2008.245
13. Parsa AT, Waldron JS, Panner A, Crane CA, Parney IF, Barry JJ, Cachola KE, Murray JC, Tihan T, Jensen MC, et al. Loss of tumor suppressor PTEN function increases B7-H1 expression and immunoresistance in glioma. *Nat. Med.* 2007;13(1):84–88. doi:10.1038/nm1517
14. Peng W, Chen JQ, Liu C, Malu S, Creasy C, Tetzlaff MT, Xu C, McKenzie JA, Zhang C, Liang X, et al. Loss of PTEN Promotes Resistance to T Cell-Mediated Immunotherapy. *Cancer Discov.* 2016;6(2):202–216. doi:10.1158/2159-8290.CD-15-0283
15. Sweis RF, Spranger S, Bao R, Paner GP, Stadler WM, Steinberg G, Gajewski TF. Molecular Drivers of the Non-T-cell-Inflamed Tumor Microenvironment in Urothelial Bladder Cancer. *Cancer Immunol Res.* 2016;4(7):563–568. doi:10.1158/2326-6066.CIR-15-0274
16. Shultz LD, Ishikawa F, Greiner DL. Humanized mice in translational biomedical research. *Nat. Rev. Immunol.* 2007;7(2):118–130. doi:10.1038/nri2017

17. Pérol L, Martin GH, Maury S, Cohen JL, Piaggio E. Potential limitations of IL-2 administration for the treatment of experimental acute graft-versus-host disease. *Immunol. Lett.* 2014;162(2 Pt B):173–184. doi:10.1016/j.imlet.2014.10.027
18. Naserian S, Leclerc M, Thiolat A, Pilon C, Le Bret C, Belkacemi Y, Maury S, Charlotte F, Cohen JL. Simple, Reproducible, and Efficient Clinical Grading System for Murine Models of Acute Graft-versus-Host Disease. *Front Immunol.* 2018;9:10. doi:10.3389/fimmu.2018.00010
19. Ito M, Hiramatsu H, Kobayashi K, Suzue K, Kawahata M, Hioki K, Ueyama Y, Koyanagi Y, Sugamura K, Tsuji K, et al. NOD/SCID/gamma(c)(null) mouse: an excellent recipient mouse model for engraftment of human cells. *Blood.* 2002;100(9):3175–3182. doi:10.1182/blood-2001-12-0207
20. King MA, Covassin L, Brehm MA, Racki W, Pearson T, Leif J, Laning J, Fodor W, Foreman O, Burzenski L, et al. Human peripheral blood leucocyte non-obese diabetic-severe combined immunodeficiency interleukin-2 receptor gamma chain gene mouse model of xenogeneic graft-versus-host-like disease and the role of host major histocompatibility complex. *Clin. Exp. Immunol.* 2009;157(1):104–118. doi:10.1111/j.1365-2249.2009.03933.x
21. Du Four S, Maenhout SK, Niclou SP, Thielemans K, Neyns B, Aerts JL. Combined VEGFR and CTLA-4 blockade increases the antigen-presenting function of intratumoral DCs and reduces the suppressive capacity of intratumoral MDSCs. *Am J Cancer Res.* 2016;6(11):2514–2531.
22. Davis RJ, Moore EC, Clavijo PE, Friedman J, Cash H, Chen Z, Silvin C, Van Waes C, Allen C. Anti-PD-L1 Efficacy Can Be Enhanced by Inhibition of Myeloid-Derived Suppressor Cells with a Selective Inhibitor of PI3K δ / γ . *Cancer Res.* 2017;77(10):2607–2619. doi:10.1158/0008-5472.CAN-16-2534
23. Bièche I, Onody P, Tozlu S, Driouch K, Vidaud M, Lidereau R. Prognostic value of ERBB family mRNA expression in breast carcinomas. *Int. J. Cancer.* 2003;106(5):758–765. doi:10.1002/ijc.11273

Figure legends

Figure 1: Heatmap clustering of T-cell-inflamed and non-T-cell-inflamed MIBC distinguished by immune gene expression correlate with mutation of *PIK3CA*.

A. Heatmap clustering of 56 MIBC according to the expression level of 57 immune genes and the presence or absence of activating mutations of several oncogenic pathways (*PIK3CA*, *BRAF*, *RAS*, *FGFR3*). MIBC bearing a *PIK3CA* mutation showed a significantly lower expression of the immune gene signature than wild type tumors, Fisher's exact test, $p=0.04$. The dot-line illustrates the defined cluster of "hot" and "cold" tumors, taking into consideration the level of expression of immune genes, and the presence or absence of *PIK3CA* mutation.

B. Heatmap clustering of 56 MIBC according to the 10 most significant genes obtained by qPCR level expression to define high- versus low-infiltrated tumors according to *PIK3CA*, *BRAF*, *RAS* and *FGFR3* mutational status. The expression of a minimal signature of 10 immune genes could discriminate high- versus low-infiltrated MIBC. Fisher's exact test, $p=0.02$. The dot-line illustrates the defined cluster of "hot" and "cold" tumors, taking into consideration the level of expression of immune genes, and the presence or absence of *PIK3CA* mutation.

Figure 2: Impact of BKM120 treatment on growth of VMCUB1, *PIK3CA* mutated and HT1376, *PIK3CA* wild type human bladder cancer cell lines.

A. Experimental protocol. All mice were s. c. grafted with tumor cells in the right flank, and when tumors were palpable, they were i.v. injected with PBMC. **B.** Tumor growth kinetics (individual) for each group; untreated (black line) and treated with BKM120 (blue line), for each cell line, VMCUB1 and HT1376. Tumors were measured twice per week. **C.** Tumor growth kinetics (mean) for each group. **D.** GvHD was followed by lost of body weight plotted as a percentage of initial weight (mean). **E.** HuCD45⁺ cells reconstitution was immunomonitored at different time points, one time per week. Statistical significance was calculated using the Mann-Whitney test. NS, not significant; *, $P < 0.05$; **, $P < 0.01$.

Figure 3: Impact of BKM120 treatment on tumor immune infiltrate of VMCUB1, PIK3CA mutated and HT1376, PIK3CA wild-type human bladder cancer cell lines.

A. Relative proportion of total HuCD45+ and CD3+ immune cells infiltrating the tumor, gated among live cells. For the *PIK3CA* mutated VMCUB1 cell line, N=8 in each group and for the *PIK3CA* WT HT1376 cell line, N=6 in the untreated group and N=7 in the BKM120 group.

B. Relative proportion of T-cell subsets within hCD45+ tumor immune infiltrate. Statistical significance was calculated using the Mann-Whitney test. NS, not significant; *, $P < 0.05$; **, $P < 0.01$.

Figure 4: Heatmap of tumor immune infiltration changes induced by BKM120 treatment on PIK3CA mutated VMCUB1 and PIK3CA wild type HT1376 human bladder cancer cell lines, in a humanized mouse model.

Data correspond to 2 replicates. Mice were injected with either 10×10^6 or 20×10^6 tumor cells SC.

Supplementary data Figure 1: Heatmap clustering of T-cell-inflamed and non-T-cell-inflamed bladder tumors distinguished by immune gene expression.

A. Heatmap clustering of 98 human bladder cancer samples according to the expression level of 57 immune genes and the mutational status of *PIK3CA*, *BRAF*, *RAS*, and *FGFR3* genes. T-cell-inflamed and non-T-cell-inflamed bladder tumors can be distinguished by immune gene expression profiling. The dot-line illustrates the defined cluster of “hot” and “cold” tumors, taking into consideration the level of expression of immune genes. Urothelial bladder cancers showed different levels of immune infiltration depending on the histological group type: NMIBC showed a significantly lower expression of the immune gene signature than MIBC (Fisher’s exact test, $p < 0.001$).

Supplementary data Figure 2: BKM120 treatment effect on the expression of proliferation genes in PIK3CA mutated VMCUB1 human bladder cancer cell line in a humanized mouse model.

Data correspond to 2 replicates. Mice were injected with either 10×10^6 or 20×10^6 tumor cells SC. Statistical significance was calculated using the Mann-Whitney test; *** $p < 0,0005$, **** $p < 0,0001$.

Tables

Table 1: List of 57 genes selected for the immune gene signature

ID	GeneID	GeneSymbol	GeneName
CD2	914	CD2	CD2 molecule
CD3E	916	CD3E	CD3e molecule
CD4	920	CD4	CD4 molecule
CD8A	925	CD8A	CD8a molecule
CTLA4	1493	CTLA4	cytotoxic T-lymphocyte associated protein 4
FOXP3	50943	FOXP3	forkhead box P3
XCR1	2829	XCR1	chemokine (C motif) receptor 1
MERTK	10461	MERTK	MER proto-oncogene, tyrosine kinase
PTPRC	5788	PTPRC CD45	protein tyrosine phosphatase, receptor type C
MS4A1	931	MS4A1 CD20	membrane spanning 4-domains A1
NCAM1	4684	NCAM1 CD56	neural cell adhesion molecule 1
PDGFRB	5159	PDGFRB	platelet derived growth factor receptor beta
PECAM1	5175	PECAM1	platelet/endothelial cell adhesion molecule 1
PRF1	5551	PRF1	perforin 1
GZMA	3001	GZMA	granzyme A
GZMB	3002	GZMB	granzyme B
CD28	940	CD28	CD28 molecule
ENTPD1	953	ENTPD1 cd39	Ectonucleoside triphosphate diphosphohydrolase 1
NT5E	4907	NT5E cd73	5'-nucleotidase ecto

CD96	10225	CD96	CD96 molecule, TIGIT family
TIGIT	201633	TIGIT	T-cell immunoreceptor with Ig and ITIM domains
CD226	10666	CD226	CD226 molecule, TIGIT family
TNFRSF14	8764	TNFRSF14	tumor necrosis factor receptor superfamily member 14
TNFRSF18	8784	GITR	tumor necrosis factor receptor superfamily member 18
TNFRSF4	7293	OX-40, CD134	tumor necrosis factor receptor superfamily member 4
TNFRSF7	939	CD27	CD27 molecule
TNFRSF9	3604	CD137, 4-1BB	tumor necrosis factor receptor superfamily member 9
HAVCR2	84868	HAVCR2, Tim-3	hepatitis A virus cellular receptor 2
ICOS	29851	ICOS	inducible T-cell co-stimulator
LAG3	3902	LAG3	lymphocyte activating 3
PDCD1	5133	PDCD1	programmed cell death 1
IDO1	3620	IDO1	indoleamine 2,3-dioxygenase 1
CD80	941	CD80, B7-1	CD80 molecule
CD86	942	CD86, B7-2	CD86 molecule
CD276	80381	CD276, B7H3, inhibitory	CD276 molecule
LGALS9	3965	LGALS9	lectin, galactoside-binding, soluble, 9
CD274	29126	CD274, PDL1	CD274 molecule

PDCD1LG2	80380	PDCD1LG2	programmed cell death 1 ligand 2
ICOSLG	23308	ICOSLG	inducible T-cell co-stimulator ligand
PVR	5817	PVR, CD155 (Tigit ligand)	poliovirus receptor
PVRIG	79037	PVRIG, CD112R	poliovirus receptor related immunoglobulin domain containing
TNFSF4	7292	OX40L	tumor necrosis factor superfamily member 4
CXCL10	3627	CXCL10	C-X-C motif chemokine ligand 10
IFI27	3429	IFI27	interferon, alpha-inducible protein 27
IFI44L	10964	IFI44L	interferon induced protein 44 like
IFI6	2537	IFI6	interferon, alpha-inducible protein 6
IFIT1	3434	IFIT1	interferon induced protein with tetratricopeptide repeats 1
IRF8	3394	IRF8	interferon regulatory factor 8
MX1	4599	MX1	MX dynamin like GTPase 1
OAS1	4938	OAS1	2'-5'-oligoadenylate synthetase 1
RSAD2	91543	RSAD2	radical S-adenosyl methionine domain containing 2
G1P2	9636	ISG15	ISG15 ubiquitin-like modifier
HLA-A	3105	HLA-A	major histocompatibility complex, class I, A
HLA-B			
U3/L3	3106	HLA-B	major histocompatibility complex, class I, B
HLA-C	3107	HLA-C	major histocompatibility complex, class I, C

U2/L2			
HLA-DRA	3122	HLA-DRA	major histocompatibility complex, class II, DR alpha
HLA-DRB	3123	HLA-DRB1	major histocompatibility complex, class II, DR beta 1

Table 2: Clinico-pathological characteristics and survival of 42 patients with NMIBC

	Whole population	No recurrence	Recurrence		Muscle-invasive progression	
	Number of patients (%)	Number (%)	Number (%)	p-value*	Number (%)	p-value**
Total population	42 (100)	13 (31.0)	21 (50.0)		8 (19.0)	
Age (years)						
≥60	33 (78.6)	9 (69.2)	16 (76.2)	0.96 (NS)	8 (100.0)	0.17 (NS)
<60	9 (21.4)	4 (30.8)	5 (23.8)		0 (0.0)	
Sex						
Male	39 (92.9)	12 (92.3)	19 (90.5)	>0.99 (NS)	8 (100.0)	>0.99 (NS)
Female	3 (7.1)	1 (7.7)	2 (9.5)		0 (0.0)	
Smoking status						
Non-smoker	17 (40.5)	3 (23.1)	11 (52.4)	0.092 (NS)	3 (37.5)	0.83 (NS)
Smoker	25 (59.5)	10 (76.9)	10 (47.6)		5 (62.5)	
History of NMIBC						
No	22 (52.4)	10 (76.9)	9 (42.9)	0.052 (NS)	3 (37.5)	0.59 (NS)
Yes	20 (47.6)	3 (23.1)	12 (57.1)		5 (62.5)	
Associated pTis						
No	40 (95.2)	13 (100.0)	21 (100.0)	>0.99 (NS)	6 (75.0)	0.033
Yes	2 (4.8)	0 (0.0)	0 (0.0)		2 (25.0)	
Grade						
Low grade	18 (42.9)	8 (61.5)	9 (42.9)	0.29 (NS)	1 (12.5)	0.13 (NS)
High grade	24 (57.1)	5 (38.5)	12 (57.1)		7 (87.5)	
Tumor stage ^a						
Ta	28 (68.3)	9 (69.2)	17 (81.0)	0.71 (NS)	2 (28.6)	0.024
T1-2	13 (31.7)	4 (30.8)	4 (19.0)		5 (71.4)	

* Chi² test, Chi² test with Yates' correction or Fisher test if appropriate (recurrence versus no recurrence)

** Chi² test, Chi² test with Yates' correction or Fisher test if appropriate (muscle-invasive progression versus others)

NS: not significant

^a data available for 41 patients

Table 3: Clinico-pathological characteristics and survival of 56 patients with MIBC

	Whole population	Disease-free survival		Overall survival	
	Number of patients (%)	Number of events (%) ^a	p-value*	Number of events (%) ^b	p-value*
Total population	56 (100.0)	36 (64.3)		34 (60.7)	
Age (years)					
≥60	40 (71.4)	30 (83.3)	0.0082	30 (88.2)	0.0005
<60	16 (28.6)	6 (16.7)		4 (11.8)	
Sex					
Male	42 (75.0)	24 (66.7)	0.053 (NS)	26 (76.5)	0.75 (NS)
Female	14 (25.0)	12 (33.3)		8 (23.5)	
Smoking status^c					
Non-smoker	9 (18.0)	7 (23.3)	0.41 (NS)	7 (24.1)	0.34 (NS)
Smoker	41 (82.0)	23 (76.7)		22 (75.9)	
History of NMIBC					
No	35 (62.5)	21 (58.3)	0.39 (NS)	20 (58.8)	0.48 (NS)
Yes	21 (37.5)	15 (41.7)		14 (41.2)	
Associated pTis					
No	50 (89.3)	34 (94.4)	0.17 (NS)	32 (94.1)	0.20 (NS)
Yes	6 (10.7)	2 (5.6)		2 (5.9)	
Tumor stage					
T1-2	19 (33.9)	11 (30.6)	0.47 (NS)	8 (23.5)	0.041
≥T3	37 (66.1)	25 (69.4)		26 (76.5)	
Lymph node status^d					
N-	35 (63.6)	18 (51.4)	0.013	17 (50.0)	0.0075
N+	20 (36.4)	17 (48.6)		17 (50.0)	
FGFR3 status					
Mutated	6 (10.7)	4 (11.1)	>0.99 (NS)	4 (11.8)	>0.99 (NS)
Not mutated	50 (89.3)	32 (88.9)		30 (88.2)	
PIK3CA status					
Mutated	6 (10.7)	2 (5.6)	0.17 (NS)	2 (5.9)	0.20 (NS)
Not mutated	50 (89.3)	34 (94.4)		32 (94.1)	

* Chi² test, Chi² test with Yates' correction or Fisher test if appropriate

NS: not significant

^a first recurrence (local or metastatic)

^b death

^c data available for 50 patients

^d data available for 55 patients

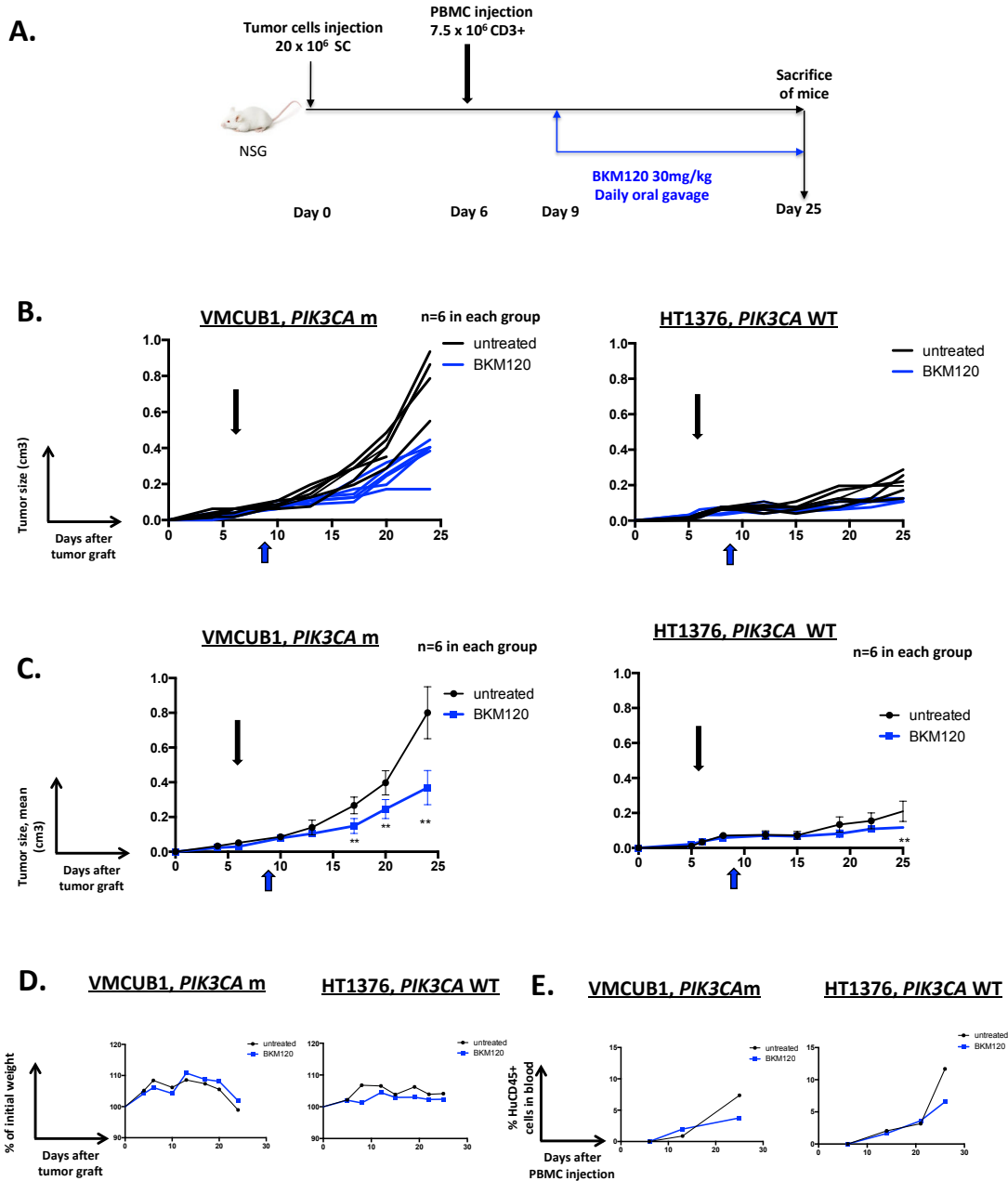


Figure 2: Impact of BKM120 treatment on growth of VMCUB1, *PIK3CA* mutated and HT1376, *PIK3CA* wild type human bladder cancer cell lines.

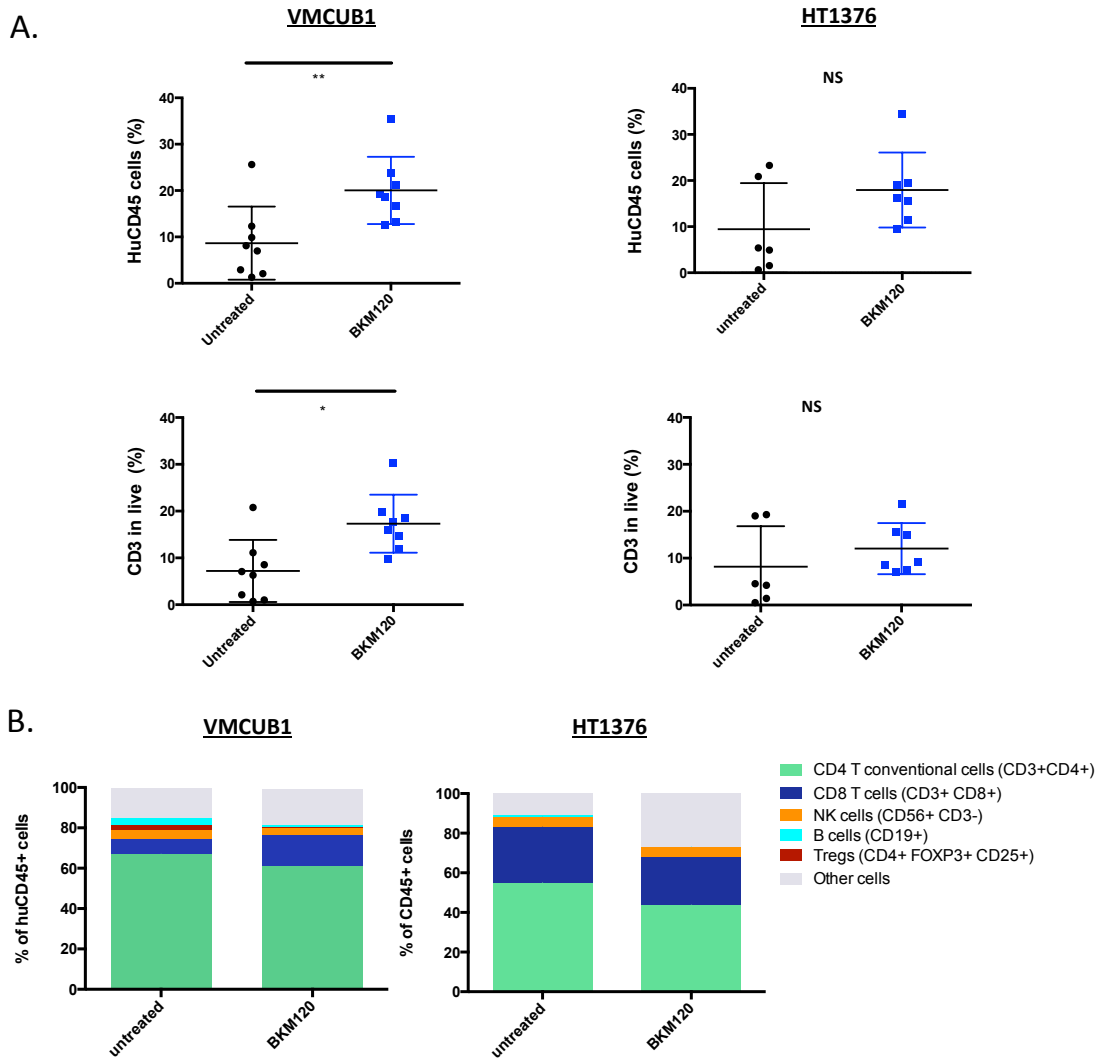


Figure 3: Impact of BKM120 treatment on tumor immune infiltrate of VMCUB1, *PIK3CA* mutated and HT1376, *PIK3CA* wild-type human bladder cancer cell lines.

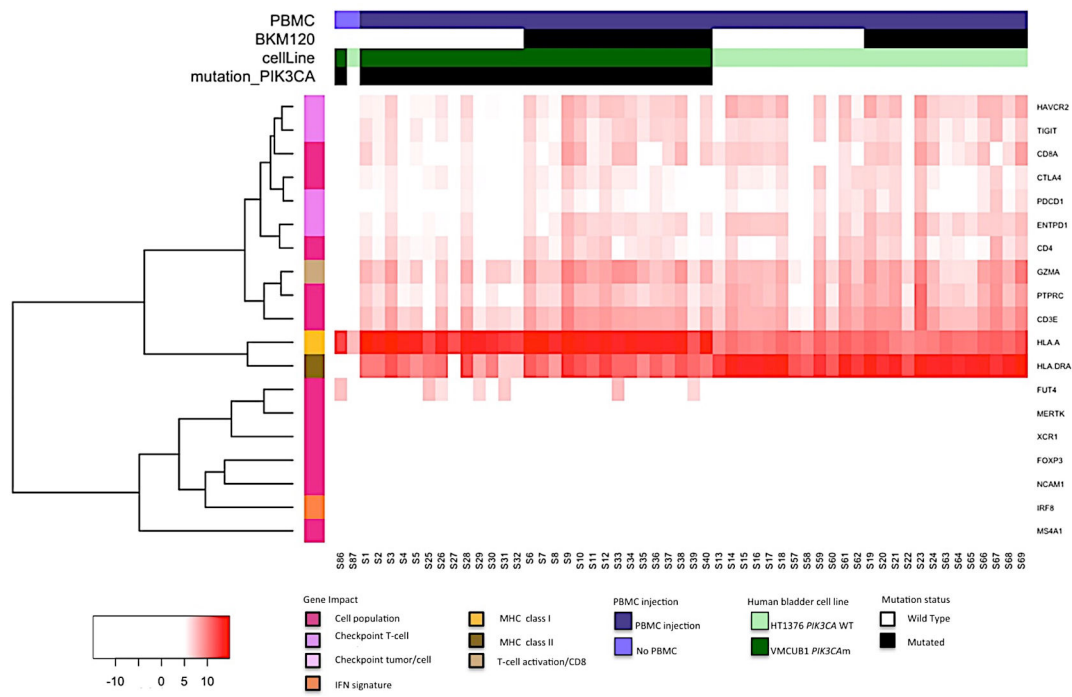
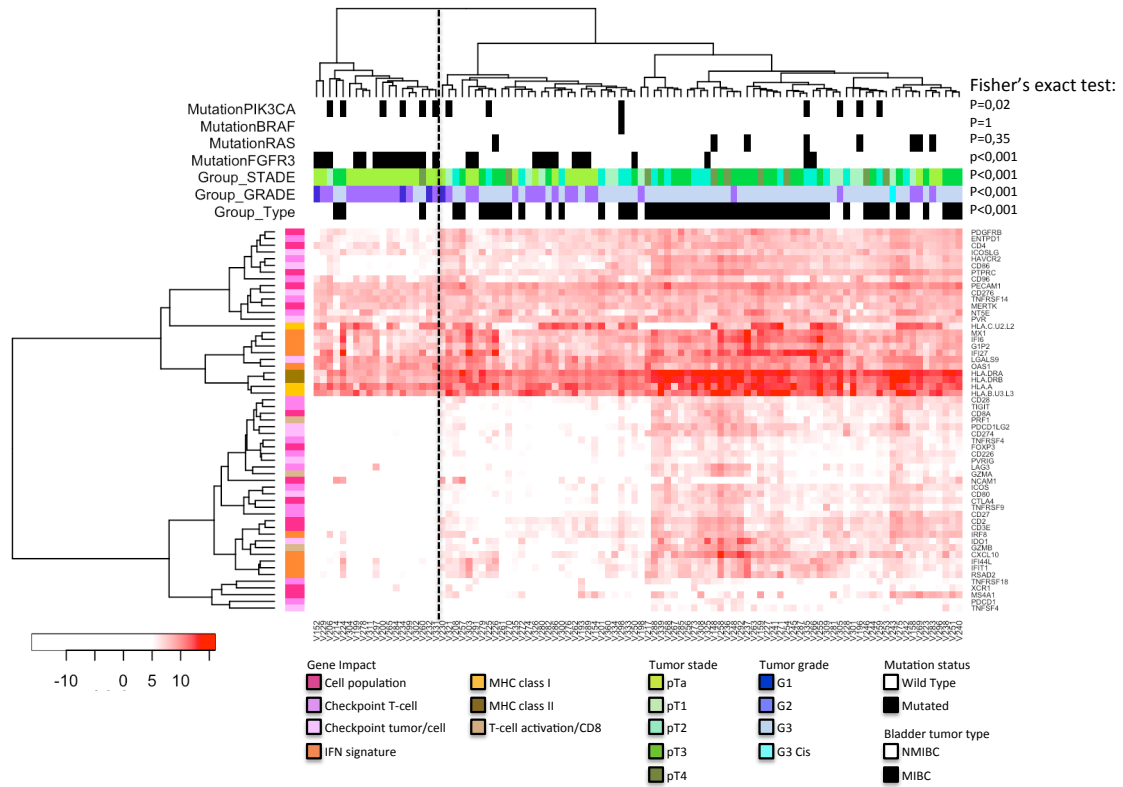
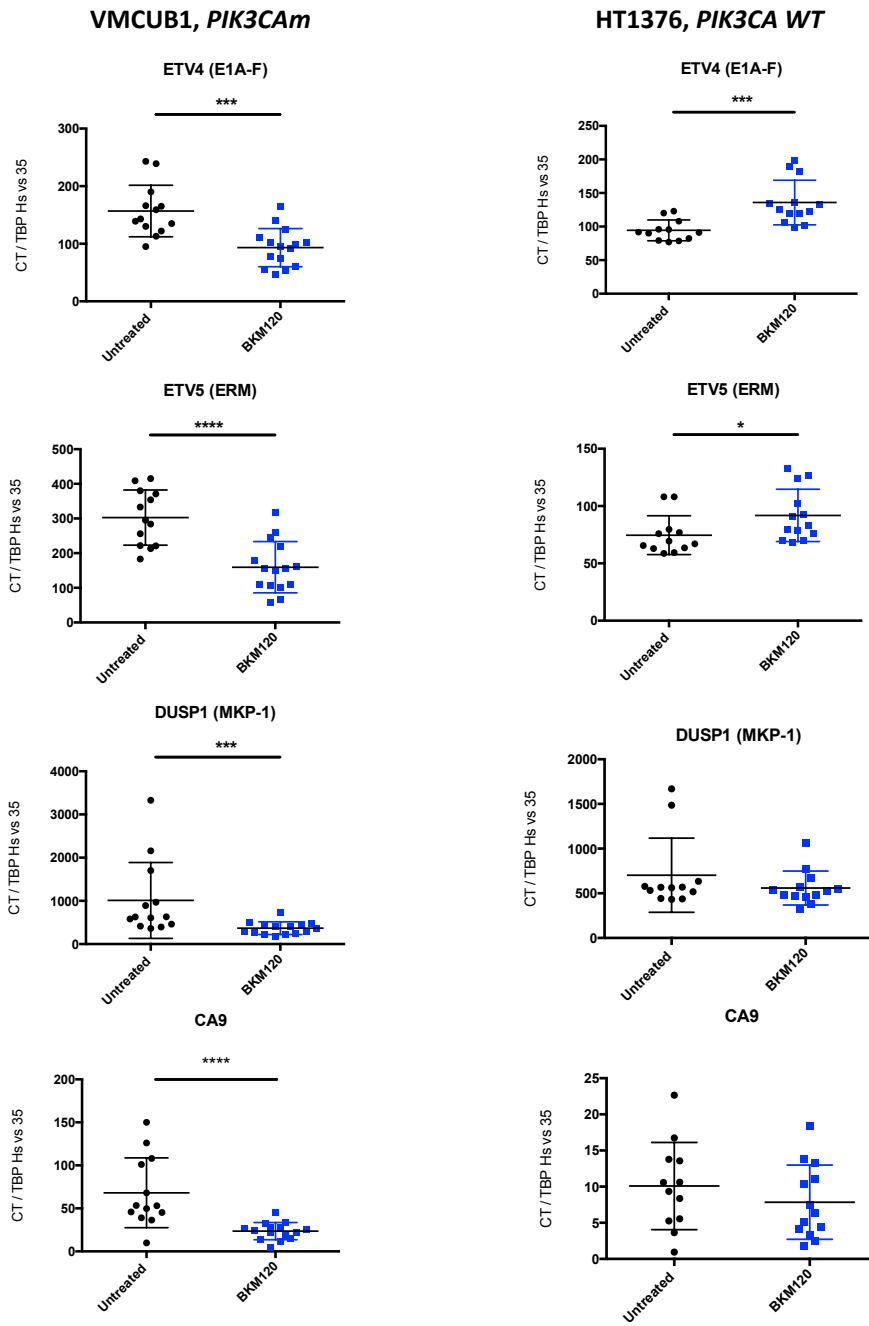


Figure 4: Heatmap of tumor immune infiltration changes induced by BKM120 treatment on *PIK3CA* mutated VMCUB1 and *PIK3CA* wild type HT1376 human bladder cancer cell lines, in a humanized mouse model.



Supplementary data Figure 1: Heatmap clustering of T-cell-inflamed and non-T-cell-inflamed bladder tumors distinguished by immune gene expression.



Supplementary data Figure 2: BKM120 treatment effect on the expression of proliferation genes in *PIK3CA* mutated VMCUB1 human bladder cancer cell line in a humanized mouse model.

Discussion

L'utilisation des modèles de souris a permis des avancées majeures dans la compréhension des relations entre le système immunitaire et le cancer. En particulier, les modèles syngéniques permettent d'élucider les mécanismes d'action des nouvelles immunothérapies et d'établir des preuves de concept de l'utilité de ces thérapies innovantes. Cependant, les modèles syngéniques présentent deux inconvénients majeurs : (1) les tumeurs murines ne représentent pas l'ensemble des caractéristiques des tumeurs humaines avec notamment l'expression d'antigènes non-humains [363], (2) les systèmes immunitaires humains et murins présentent des différences [364].

A travers mon travail de thèse, j'ai mis en place, un savoir faire manquant au sein du laboratoire et de l'Institut Curie : un modèle de souris humanisées pour les études immuno-oncologiques. L'humanisation des souris est un domaine complexe qui comprend trois composantes : la souris immunodéficente, la tumeur humaine et le système immunitaire humain.

Nous avons, en premier lieu, évalué l'efficacité et la qualité de la reconstitution immunitaire humaine suivant l'injection de PBMC dans des souris immunodéficientes NSG (modèles Hu-PBL). J'ai pu détecter la reconstitution hématopoïétique humaine dans le sang, la rate et la moelle osseuse des souris environ dix jours après l'injection des PBMC ; la quantité de cellules hématopoïétiques humaines augmentant au fil des jours. Elle est accompagnée d'une GvHD aiguë dont la rapidité d'apparition est liée à un fort niveau de reconstitution. La rapidité à laquelle la GvHD apparaît est corrélée positivement à l'efficacité de la reconstitution initiale. La majorité des cellules humaines retrouvées dans la souris est constituée de lymphocytes T CD4⁺ et CD8⁺ en proportion équivalente. Ces lymphocytes ont, pour leur majorité, un phénotype effecteur CD45RA⁻CD45RO⁺CCR7⁻, et expriment des marqueurs de cellules activées, HLA-DR⁺ et CD25⁺. Afin d'obtenir une « fenêtre thérapeutique » suffisamment longue pour pouvoir évaluer l'efficacité thérapeutique des traitements, dans le modèle Hu-PBL, nous avons choisi d'injecter une quantité de cellules humaines suffisamment importante pour permettre une reconstitution hématopoïétique efficace sans induire

une GvHD trop précoce. Au vu de nos résultats, qui indiquaient une reconstitution quasi exclusivement composée de lymphocytes T, nous avons décidé d'injecter une quantité de PBMC contenant entre $5 \cdot 10^6$ et $10 \cdot 10^6$ de lymphocytes T CD3⁺.

Il est aussi possible de reconstituer des souris, avec un système immunitaire humain, à partir de l'injection de cellules souches hématopoïétiques CD34⁺ (modèle Hu-SRC). L'avantage d'un tel modèle est, notamment, l'absence de GvHD aiguë. Nous avons évalué l'efficacité et la qualité de la reconstitution dans plusieurs lignées de souris. En effet, la reconstitution myéloïde dans les souris immunodéficientes est incomplète [261] alors qu'il est connu que les TAM, les MDSC et les neutrophiles jouent un rôle important dans le contrôle de la progression du cancer [285,286]. L'utilisation de souris NSG-SGM3 et NOG-EXL, exprimant des cytokines et facteurs de croissance myéloïdes humains (IL-3, GM-SCF, SCF), n'a pas montré une augmentation de la génération de cellules myéloïdes en comparaison des lignées parentales NSG et NOG. Pour ces quatre lignées, la reconstitution immunitaire est plus diversifiée après injection de CD34⁺ qu'après injection de PBMC. La majorité des cellules, reconstituant ces souris, sont des lymphocytes B ($\approx 60\%$) mais on note la présence de lymphocytes T ($\approx 20\%$), de cellules NK ($\approx 5\%$), de monocytes et de neutrophiles ($\approx 10\%$). La seule lignée de souris présentant une différence avec les autres est la lignée NSG-SGM3 qui a une capacité de reconstitution en lymphocyte T plus importante. Les lymphocytes T, dans le modèle Hu-SRC, contrairement à ce que nous avons observé dans le modèle Hu-PBL, n'ont pas de phénotype effecteur mais un phénotype plus mémoire CD45RO⁺ ou naïf CD45RA⁺CD45RO⁻CCR7⁺. Ces souris ne présentent pas de signe de GvHD, ce qui est cohérent avec l'absence de lymphocytes T effecteurs.

La mise en place des modèles Hu-PBL et Hu-SRC nous a permis de passer à l'étape suivante de l'établissement de modèles de souris humanisées optimisées pour l'étude de l'immuno-oncologie. Nous avons testé la greffe de cellules tumorales de différentes origines dans ces modèles. Alors que la greffe de tumeur dans le modèle Hu-SRC est toujours suivi d'un développement tumoral, et n'a pas d'impact macroscopique sur la reconstitution immunitaire humaine, cela n'est pas le cas dans le modèle Hu-PBL. En effet, avant tout traitement thérapeutique, il existe un ensemble de preuves montrant l'existence d'interactions fortes entre les cellules

immunitaires humaines injectées dans les souris et la greffe de cellules tumorales et ça dans les deux sens. En premier lieu, nous avons observé l'absence de développement tumoral dans le cas de l'injection de cellules de lignées tumorales ou de greffe de PDX, dans des souris déjà reconstituées après injection de PBMC. Nous avons aussi observé que l'injection de PBMC dans des souris ayant déjà une tumeur développée entraîne, après reconstitution, une régression des tumeurs pouvant entraîner la disparition totale de la tumeur dans les cas des souris ayant reçu une injection de cellules de lignée tumorale. Dans les deux cas, il semble que les lymphocytes T humains, repeuplant les souris, peuvent rejeter la tumeur comme décrit dans le phénomène de rejet de « greffe contre la tumeur » (GvT) [365].

D'autre part, nous observons que la reconstitution hématopoïétique des souris immunodéficientes est compromise dans les modèles de souris porteuses de PDX. En effet, l'injection de PBMC n'est pas toujours suivie d'une reconstitution observable dans le sang des souris greffées avec une PDX. Plusieurs hypothèses peuvent expliquer ce phénomène propre aux PDX. En premier lieu, les PDX sont entretenues sur des souris immunodéficientes de la lignée nude. Ces souris ne possèdent pas de lymphocytes T et B murins mais conservent cependant des cellules NK qui peuvent potentiellement infiltrer les PDX. Ces cellules NK peuvent donc être co-transférées dans les souris NSG lors de la greffe de PDX et, ainsi transférées, pourraient reconnaître les PBMC humains portant des molécules d'histocompatibilité différentes et les tuer. La déplétion des NK chez la souris nude donneuse de la PDX avant la greffe de celle-ci sur la NSG permettrait de valider cette hypothèse. Une autre stratégie pour évaluer l'impact des NK provenant de la PDX de la souris nude sur la reconstitution des PBMC serait d'effectuer un passage intermédiaire de la PDX sur une souris NSG, sans injection de PBMC, puis de se servir de cette PDX, dépourvue de cellules NK, comme réservoir de greffe tumorale. Une autre hypothèse pouvant expliquer l'absence de reconstitution des PBMC dans ces souris porteuses de PDX est que la tumeur pourrait sécréter des facteurs immunosuppresseurs. L'étude du sécrétome de ces tumeurs, comme décrit par Khwaja et al. [366] pourrait être une piste pour comprendre l'origine de ce mécanisme. L'ensemble de ces observations faites sur l'interaction entre le système immunitaire humain et les tumeurs humaines dans les souris Hu-PBL, nous a permis de statuer sur la cinétique d'injection des

PBMC par rapport à la greffe des cellules tumorales. Au vu du fort effet de GvT observé lorsque les cellules tumorales sont injectées dans des souris déjà reconstituées, nous avons décidé d'injecter les PBMC uniquement quand la tumeur est palpable.

Suivant ce protocole, nous avons décidé de tester la pertinence de ces modèles dans l'évaluation préclinique des immunothérapies dans le modèle HU-PBL. En effet, la reconstitution avec les PBMC présente plusieurs avantages comparativement à l'injection de progéniteurs. L'injection des progéniteurs nécessite au préalable la purification des cellules CD34⁺ et l'irradiation sublétales des souris, contrairement à l'injection de PBMC. Par ailleurs, le temps nécessaire à la reconstitution des souris après injection de progéniteurs est plus long qu'après injection de PBMC. De plus, un des objectifs du développement, de ces modèles de souris humanisées, est d'améliorer le modèle Avatar, en lui supplémentant l'injection de cellules immunes autologues du patient dont la tumeur a été greffée dans la souris. La disponibilité de cellules souches hématopoïétiques, de patients atteints de cancer étant une étape limitante, nous nous sommes focalisés sur l'évaluation de l'efficacité des immunothérapies dans les modèles de souris Hu-PBL.

En premier lieu, nous avons étudié l'effet du Nivolumab, un anticorps bloquant dirigé contre la molécule PD1, utilisé en clinique. Nous avons montré un ralentissement de la croissance tumorale dans une lignée du cancer du sein triple négatif, MDA-M231. Le fort niveau d'infiltration, autour de 70% de cellules HuCD45⁺ dans la tumeur, peut expliquer l'effet du traitement par Nivolumab. Il a été, en effet, montré, chez l'homme, que le niveau de réponse à l'injection des anticorps anti-PD1 et anti-PD-L1 était lié au niveau d'infiltration des tumeurs [115,116]. Afin d'être au plus proche de la pathologie humaine, nous nous sommes ensuite intéressés à l'évaluation de l'efficacité du Nivolumab dans des souris Hu-PBL porteuses de PDX de NSCLC. Nous avons évalué l'efficacité du Nivolumab dans une dizaine de modèles de PDX et nous avons observé un ralentissement de la croissance tumorale dans près de 40% des cas. Ce chiffre est à rapprocher de ceux observés chez les patients avec un taux de réponse objective de 21,3% et un taux de contrôle de la maladie de 39,9% [367]. Comprendre les mécanismes impliqués dans la différence de réponse aux traitements

est un challenge que les souris HIS peuvent aider à résoudre. Après l'analyse de la réponse au Nivolumab et de l'expression de PD-L1 dans différents modèles de PDX nous nous sommes intéressés à un modèle de PDX particulier, LCF29 qui est infiltrée par des cellules humaines après injection de PBMC (~30%). Par ailleurs, la mise en place dans le laboratoire des souris humanisées avait pour objectif de pouvoir tester des immunothérapies innovantes ainsi que les combinaisons thérapeutiques possibles chez l'homme. Au sein du laboratoire, un autre projet de recherche est axé sur l'utilisation de complexe IL-2/anticorps anti-IL-2 (Cpx IL-2) en thérapie immunologique en synergie avec l'injection d'anticorps anti-PD1 et anti-PD-L1. Nous avons montré que la combinaison des traitements par le Cpx IL-2 et anticorps anti-PD1/anti-PD-L1 présentait une synergie pour contrôler la croissance tumorale d'une tumeur murine (publication soumise). Nous avons décidé de tester dans ce modèle de PDX de NSCLC l'efficacité de ce traitement en combinaison ou non avec le Nivolumab. Nous montrons, que le Nivolumab a un faible effet anti-tumoral dans cette expérience mais que le traitement par le Cpx IL-2, permet un ralentissement de la croissance tumorale qui n'est, cependant, pas augmenté par l'injection de Nivolumab. Le Cpx IL-2 semble agir sur le compartiment immunitaire en augmentant la reconstitution et l'infiltration tumorale de HuCD45⁺ et plus particulièrement les lymphocytes T CD4⁺ effecteurs. Il serait intéressant de comprendre pourquoi le Nivolumab n'a pas d'action synergique dans ce modèle tumoral alors même que le traitement par le Cpx IL-2 entraîne une augmentation de l'infiltration tumorale de lymphocytes T. Par ailleurs, nous avons observé que le Nivolumab pouvait avoir un effet déplétant sur la reconstitution des cellules humaines observée dans le sang des souris injectées avec des PBMC. Une hypothèse pour expliquer cette observation serait une action de type ADCC des cellules humaines par les macrophages de souris, même si le Nivolumab ne présente pas de capacité d'ADCC *in vitro* [368]. En effet, le Nivolumab est une IgG4 qui peut se fixer sur les récepteurs Fc et sur les molécules CD64 présentes à la surface des macrophages en absence d'immunoglobuline. Afin d'évaluer le rôle des cellules myéloïdes de souris dans l'effet déplétant du Nivolumab, l'administration de chlodronate pour tuer les cellules douées de capacité de phagocytose est une alternative à évaluer. L'injection d'immunoglobulines

humaines avant l'injection de Nivolumab pourrait permettre d'empêcher la fixation non spécifique du Nivolumab sur les macrophages murins.

En effet, le rôle des cellules myéloïdes de souris dans nos modèles reste à évaluer. Ces cellules peuvent exprimer un ligand de PD1 : PD-L1. Il serait intéressant de savoir si le PD1 humain peut lier le PD-L1 de souris et si le Nivolumab peut interagir à ce niveau. Une des limites de ces modèles est en effet l'absence des TAM et MDSC humains dans les tumeurs qui peuvent jouer un rôle majeur dans la progression tumorale liée à l'échappement au système immunitaire.

En parallèle, les souris Hu-PBL nous ont permis d'évaluer l'efficacité d'une thérapie ciblée dans des tumeurs de vessie mutées ou non pour la PI3 kinase. Cette mutation entraîne une surexpression de cette voie d'activation cellulaire et les tumeurs de vessie présentant cette mutation ont une signature immunitaire plus faible que les tumeurs non mutées. Le BKM120 est un pan-inhibiteur de la PI3 kinase, dont l'injection a permis de réduire la croissance tumorale dans la tumeur mutée. De plus, l'injection du BKM120 entraîne une augmentation de l'infiltration de cellules HuCD45⁺ dans la tumeur, par rapport à la tumeur non traitée. Il semble intéressant, dans un futur proche, de poursuivre l'évaluation des combinaisons thérapeutiques par l'injection du Nivolumab ou du Cpx IL-2 avec le BKM120 dans des souris Hu-PBL porteuses de tumeurs de vessie mutées pour la PI3 kinase. Par ailleurs, nous avons utilisé, dans cette étude, des tumeurs mutées ou non pour la PI3 kinase qui ne sont, cependant, pas différentes uniquement par l'expression de cette mutation. Afin de pouvoir affirmer avec certitude que les effets du BKM120 sur la croissance tumorale et sur l'augmentation de l'infiltration tumorale sont reliés à cette mutation, il serait intéressant de tester plusieurs lignées mutées ou non. Une autre possibilité serait de modifier par transgénèse (CRISPR-Cas9) une lignée mutée afin de déleter la mutation de la PI3 kinase et d'obtenir une lignée non mutée.

Perspectives

La mise en place, dans notre laboratoire, des modèles de souris humanisées pour étudier l'immuno-oncologie est un challenge en passe d'être réussi. Cependant, il reste des travaux majeurs à effectuer pour améliorer ces modèles.

En effet, un des écueils principaux de l'utilisation de ces souris est l'apparition de la GvHD. Cependant, plusieurs stratégies peuvent être utilisées pour limiter l'apparition de la GvHD dont la modification de l'inoculum de cellules immunitaires humaines ou la modification des souris receveuses de cellules immunitaires humaines (modulation des molécules de CMH).

Sanmamed et al. ont montré que des souris injectées avec des PBMC déplétées de leurs lymphocytes T CD4⁺ ne développaient pas de GvHD pendant 80 jours. De plus, la déplétion des autres cellules immunitaires, lymphocytes T CD8⁺ ou cellules NK notamment, n'entraînaient pas un report dans l'apparition de la GvHD [245]. L'utilisation de PBMC déplétées en lymphocyte T CD4⁺ pourrait être une solution pour étudier l'efficacité d'immunothérapie ciblant les lymphocytes T CD8⁺. L'immunoscore montrant que l'infiltration tumorale T CD8⁺ semble être un bon marqueur de réponse à ce type d'immunothérapie [369,370]; cette stratégie pourrait être une piste à poursuivre pour évaluer les tumeurs répondeuses dans un système d'Avatar immunologique. Cependant, le modèle Hu-PBL présente des limitations dans la qualité de la reconstitution immunitaire avec notamment une absence de reconstitution myéloïde. En déplaçant encore une partie du système immunitaire humain, la compréhension des mécanismes entrant en jeu dans l'immunothérapie des cancers sera plus ardue. La déplétion des lymphocytes T CD4⁺ entraînera, en conséquence, celle des Treg. Le rôle important joué par les Treg dans le développement des cancers est à prendre en compte [371]. En effet, l'évaluation des immunothérapies dans un modèle dépourvu de Treg peut être problématique, surtout si les Treg interviennent dans leur mécanisme d'action. Il est notamment connu que l'efficacité d'anticorps anti-CTLA-4, en phase clinique, passe par une déplétion des Treg chez les patients (cf chapitre 2.4.2). Dans le cas de l'évaluation des

thérapies impliquant des Cpx IL-2, l'absence de Treg dans ces modèles pourrait aussi entraîner une mauvaise interprétation des résultats.

La deuxième stratégie pour limiter l'apparition de la GvHD est la modulation des molécules de CMH dans la souris. La xéno-GvHD est, en effet, la conséquence de la reconnaissance par les lymphocytes T, contenus dans les PBMC injectées, des molécules de CMH de la souris hôte. Supprimer ce système de reconnaissance pour retarder l'apparition de la GvHD est une piste que nous avons suivie. L'injection de PBMC dans trois lignées de souris NSG, différentes par leur expression de la molécule $\beta 2m$, montre des résultats préliminaires intéressants, même si statistiquement pas encore concluants. La molécule $\beta 2m$ est une composante des molécules de CMH de classe I, présentes sur l'ensemble des cellules nucléées de souris [372]. Les souris $\beta 2m$ wt/ko et ko/ko sont déficientes en molécule de CMH de classe I (données non montrées) et ont une capacité de reconstitution plus faible que les souris $\beta 2m$ wt/wt **Figure 13A**. Par ailleurs, l'apparition de la GvHD est retardée après l'injection de PBMC en comparaison à des souris $\beta 2m$ wt/wt (**Figure 13B, C**). On constate, également, que la cinétique et la qualité de la reconstitution dans les souris $\beta 2m$ ko/ko semblent différentes en comparaison aux souris contrôles $\beta 2m$ wt/wt. Les cellules CD3⁺ et plus particulièrement les lymphocytes T CD4⁺ semblent reconstituer plus lentement dans les souris $\beta 2m$ ko/ko (**Figure 13D**). Ces données suggèrent que des souris, déficientes en molécule de classe I, pourraient être utiles pour obtenir des modèles de souris Hu-PBL avec une fenêtre thérapeutique élargie afin d'étudier l'efficacité des immunothérapies. Il existe d'autres modèles, décrits dans l'introduction (chapitre 4.2.4.3), qui pourraient, également, faire l'objet d'une investigation plus approfondie de notre part et notamment l'utilisation des souris HUMAMICE (C57BL/6 HLA-2^{+/+}/DR1^{+/+}/H-2- $\beta 2m$ ^{-/-}/Ia β ^{-/-}/Rag2^{-/-}/IL2Ryc^{-/-}/perf^{-/-}) [308]. Nous sommes actuellement en train d'étudier les capacités de reconstitution de ces souris après injection de cellules de donneurs HLA-2^{+/+}/DR1^{+/+}. Nous évaluons si cette reconstitution s'effectue sans déclencher de GvHD, notamment grâce à l'absence de molécule de CMH de classe II, ligand des lymphocytes T CD4⁺ qui paraissent être les médiateurs principaux de la GvHD [245].

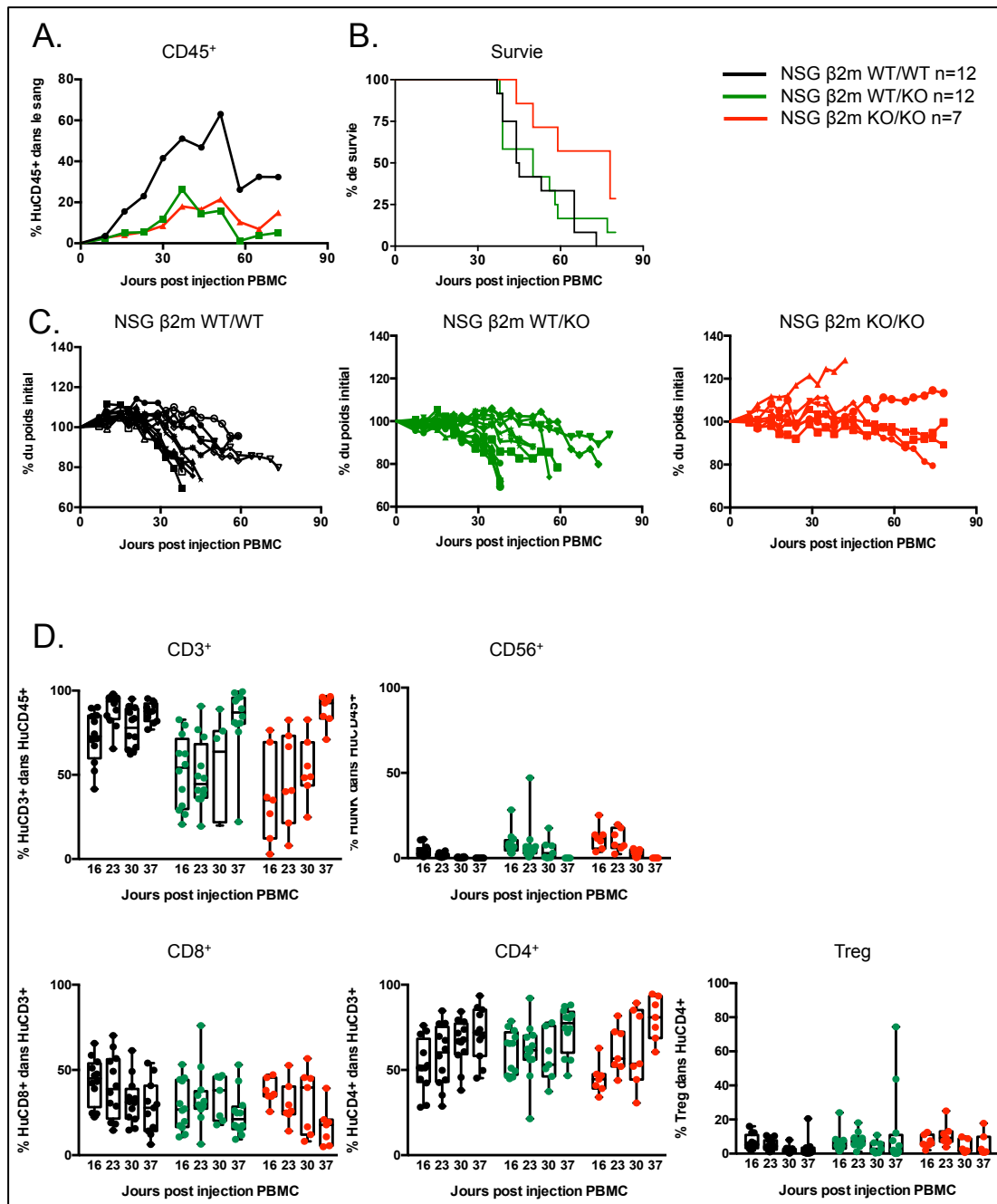


Figure 13 : La suppression de l'expression de la molécule β2m dans les souris NSG retarde l'apparition de la GvHD après injection de PBMC.

A. Cinétique de la reconstitution, HuCD45⁺, détectée par FACS dans le sang des souris injectées avec des PBMC de deux donneurs différents, contenant $5 \cdot 10^6$ cellules CD3⁺. NSG βm wt/wt n=12, NSG βm wt/ko n=12, NSG βm ko/ko n=7. **B.** Courbe de survie après injection des PBMC. **C.** L'apparition de la GvHD est suivie par l'évolution de la perte de poids, exprimée en pourcentage du poids initial (moyenne). **D.** Evolution de

la reconstitution des sous-populations contenues dans les cellules HuCD45⁺ aux jours 16, 23, 30 et 37.

L'utilisation des souris porteuses de PDX injectées avec des cellules immunitaires du même patient est un des buts de l'évolution de ce projet. En effet, le développement des thérapies anti-cancer nous incite à trouver un rationnel dans la prescription aux patients. L'évaluation des thérapies dans des modèles « Avatar immunologique » peut être une étape supplémentaire dans le processus. Par exemple, la tumeur LCF29 a acquis, par mutation, une surexpression de l'activité tyrosine kinase liée à l'EGFR. Cette tumeur avait déjà montré être répondeuse à une thérapie ciblée ; l'Erlotinib, inhibiteur sélectif de la tyrosine kinase de l'EGFR. Nous avons voulu évaluer l'efficacité de la combinaison du Nivolumab et de l'Erlotinib sur cette PDX dans des souris Hu-PBL. L'Erlotinib montre son efficacité en monothérapie mais ne présente pas de synergie avec le Nivolumab (**Figure 14**). Contrairement à l'action des Cpx IL-2, sur cette PDX, l'Erlotinib ne semble pas montrer d'effet sur le compartiment immunitaire humain (données non montrées). La combinaison entre cette thérapie ciblant les cellules tumorales et une thérapie ciblant les cellules immunitaires, comme le Cpx IL-2, est une piste intéressante à exploiter.

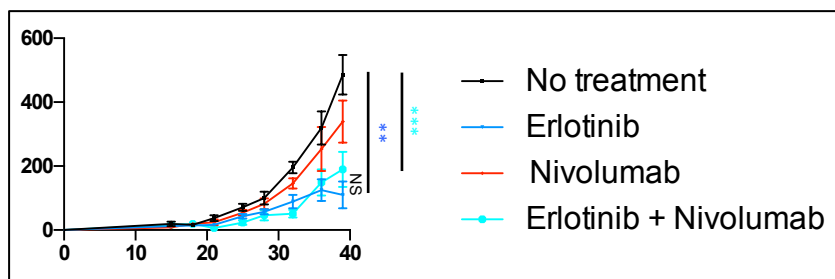


Figure 14 : L'erlotinib retarde la croissance tumorale d'une PDX (LCF29), mutée pour l'EGFR récepteur, sans synergie avec le Nivolumab.

Les souris greffées avec la PDX sont injectées avec des PBMC contenant $7,5 \cdot 10^6$ cellules CD3⁺. Quatre jours après injection de PBMC, les souris sont soit non traitées n=7, soit traitées par le Nivolumab n=6 (10mg/kg), deux fois par semaine, soit par l'Erlotinib n=7 (30mg/kg), cinq fois par semaine ou soit par la combinaison des deux n=6. Les tumeurs sont mesurées deux fois par semaine et les données sont

représentées en moyenne \pm SEM. La valeur de p est calculée par test One-way ANOVA et Kruskal-Wallis. NS : non significatif, **p<0.01, ***p<0.01

Une des limitations importantes des modèles de souris HIS est que chaque modèle de souris promeut préférentiellement la différenciation de lignées cellulaires particulières ; les cellules NK pour les souris SRG-15, les cellules myéloïdes pour les souris NOG-EXL et NSG-SGM3, les érythrocytes et les plaquettes pour les souris NSGW41. Ainsi il est difficile de choisir entre les lignées de souris au moment d'étudier les relations que peuvent entretenir le système immunitaire et les cellules cancéreuses. C'est d'autant plus ardu si on souhaite rajouter un troisième acteur au scénario, tel que le microbiome. Le microbiome représente l'ensemble des microorganismes vivants chez un hôte. Il comprend les bactéries, les archées, les virus et les microchampignons. Il est impliqué dans le développement des cancers [373]. En effet, il a, notamment, été montré que le traitement par des antibiotiques spécifiques entraîne une réduction de l'activité anti-tumorale d'anticorps anti-CTLA-4 et anti-PD1 [374,375]. Par ailleurs, l'irradiation, précédant l'injection de thérapies cellulaires, a aussi montré un effet bénéfique en endommageant les muqueuses intestinales et en activant les cellules dendritiques via l'activation de TLR4 [376]. L'impact du microbiote intestinal sur les thérapies oncologiques est résumé **Figure 15**. Les souris de laboratoire présentent la particularité d'être élevées sous des conditions exemptes de pathogènes et ont donc une flore microbienne ne reflétant pas celle d'individus « normaux ». Le transfert de microbiome de souris sauvage, dans des souris de laboratoire, a montré l'induction d'effets immunomodulateurs sur le long terme (notamment à travers les générations) qui améliorent notamment les réponses aux infections virales et la protection contre la tumorigenèse [377]. L'étude des interactions, dans un modèle entièrement humanisé, entre le système immunitaire, le microbiome et les tumeurs serait l'étape suivante dans la compréhension des mécanismes impliqués dans les immunothérapies.

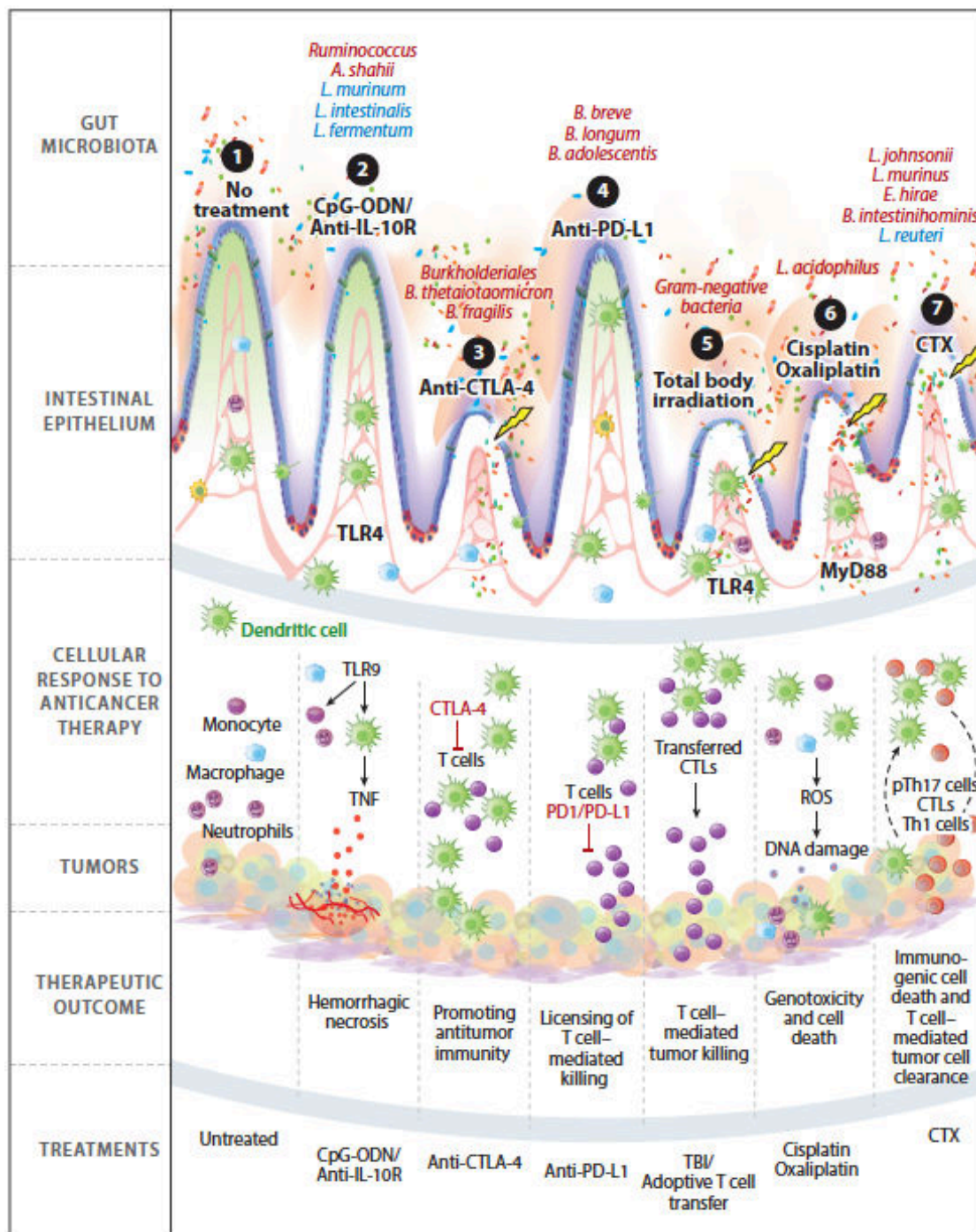


Figure 15 : Interaction entre le système immunitaire, le microbiome digestif et la tumeur. Les facteurs activant (rouge) et inhibant (bleu) l'efficacité des traitements sont indiqués. Adapté de Dzutsev at al. *Annual review of Immunology*, 2017. [373].

Bibliographie

- 1 Ferlay, J. *et al.* (2015) Cancer incidence and mortality worldwide: sources, methods and major patterns in GLOBOCAN 2012. *Int. J. Cancer* 136, E359-386
- 2 Stehelin, D. *et al.* (1976) Purification of DNA complementary to nucleotide sequences required for neoplastic transformation of fibroblasts by avian sarcoma viruses. *J. Mol. Biol.* 101, 349–365
- 3 Stehelin, D. *et al.* (1976) DNA related to the transforming gene(s) of avian sarcoma viruses is present in normal avian DNA. *Nature* 260, 170–173
- 4 Vogelstein, B. and Kinzler, K.W. (2004) Cancer genes and the pathways they control. *Nat. Med.* 10, 789–799
- 5 Nigro, J.M. *et al.* (1989) Mutations in the p53 gene occur in diverse human tumour types. *Nature* 342, 705–708
- 6 Baretta, M. and Le, D.T. (2018) DNA mismatch repair in cancer. *Pharmacol. Ther.* DOI: 10.1016/j.pharmthera.2018.04.004
- 7 Hanahan, D. and Weinberg, R.A. (2000) The hallmarks of cancer. *Cell* 100, 57–70
- 8 Hanahan, D. and Weinberg, R.A. (2011) Hallmarks of cancer: the next generation. *Cell* 144, 646–674
- 9 Sanford, K.K. *et al.* (1948) The growth in vitro of single isolated tissue cells. *J. Natl. Cancer Inst.* 9, 229–246
- 10 Scherer, W.F. *et al.* (1953) Studies on the propagation in vitro of poliomyelitis viruses. IV. Viral multiplication in a stable strain of human malignant epithelial cells (strain HeLa) derived from an epidermoid carcinoma of the cervix. *J. Exp. Med.* 97, 695–710
- 11 Hayflick, L. (1965) THE LIMITED IN VITRO LIFETIME OF HUMAN DIPLOID CELL STRAINS. *Exp. Cell Res.* 37, 614–636
- 12 Blasco, M.A. (2005) Telomeres and human disease: ageing, cancer and beyond. *Nat. Rev. Genet.* 6, 611–622
- 13 Kim, N.W. *et al.* (1994) Specific association of human telomerase activity with immortal cells and cancer. *Science* 266, 2011–2015
- 14 Coppé, J.-P. *et al.* (2010) The senescence-associated secretory phenotype: the dark side of tumor suppression. *Annu. Rev. Pathol.* 5, 99–118
- 15 Coppé, J.-P. *et al.* (2008) Senescence-associated secretory phenotypes reveal cell-nonautonomous functions of oncogenic RAS and the p53 tumor suppressor. *PLoS Biol.* 6, 2853–2868
- 16 Sun, P. *et al.* (2007) PRAK is essential for ras-induced senescence and tumor suppression. *Cell* 128, 295–308
- 17 Ohuchida, K. *et al.* (2004) Radiation to stromal fibroblasts increases invasiveness of pancreatic cancer cells through tumor-stromal interactions. *Cancer Res.* 64, 3215–3222
- 18 Coppe, J.-P. *et al.* (2008) A role for fibroblasts in mediating the effects of tobacco-induced epithelial cell growth and invasion. *Mol. Cancer Res. MCR* 6, 1085–1098
- 19 Folkman, J. (1971) Tumor angiogenesis: therapeutic implications. *N. Engl. J.*

Med. 285, 1182–1186

- 20 Folkman, J. *et al.* (1989) Induction of angiogenesis during the transition from hyperplasia to neoplasia. *Nature* 339, 58–61
- 21 Folkman, J. and Hanahan, D. (1991) Switch to the angiogenic phenotype during tumorigenesis. *Princess Takamatsu Symp.* 22, 339–347
- 22 Wang, G.L. and Semenza, G.L. (1993) General involvement of hypoxia-inducible factor 1 in transcriptional response to hypoxia. *Proc. Natl. Acad. Sci. U. S. A.* 90, 4304–4308
- 23 Zhong, H. *et al.* (1999) Overexpression of Hypoxia-inducible Factor 1 α in Common Human Cancers and Their Metastases. *Cancer Res.* 59, 5830–5835
- 24 Talks, K.L. *et al.* (2000) The Expression and Distribution of the Hypoxia-Inducible Factors HIF-1 α and HIF-2 α in Normal Human Tissues, Cancers, and Tumor-Associated Macrophages. *Am. J. Pathol.* 157, 411–421
- 25 Ikeda, E. *et al.* (1995) Hypoxia-induced transcriptional activation and increased mRNA stability of vascular endothelial growth factor in C6 glioma cells. *J. Biol. Chem.* 270, 19761–19766
- 26 Kaelin, W.G. (2004) The Von Hippel-Lindau Tumor Suppressor Gene and Kidney Cancer. *Clin. Cancer Res.* 10, 6290S–6295S
- 27 Pepper, M.S. *et al.* (1992) Potent synergism between vascular endothelial growth factor and basic fibroblast growth factor in the induction of angiogenesis in vitro. *Biochem. Biophys. Res. Commun.* 189, 824–831
- 28 Berger, D.P. *et al.* (1995) Vascular endothelial growth factor (VEGF) mRNA expression in human tumor models of different histologies. *Ann. Oncol. Off. J. Eur. Soc. Med. Oncol.* 6, 817–825
- 29 Donnem, T. *et al.* (2013) Vessel co-option in primary human tumors and metastases: an obstacle to effective anti-angiogenic treatment? *Cancer Med.* 2, 427–436
- 30 Leenders, W.P.J. *et al.* (2004) Antiangiogenic Therapy of Cerebral Melanoma Metastases Results in Sustained Tumor Progression via Vessel Co-Option. *Clin. Cancer Res.* 10, 6222–6230
- 31 Patan, S. *et al.* (1996) Intussusceptive microvascular growth in a human colon adenocarcinoma xenograft: a novel mechanism of tumor angiogenesis. *Microvasc. Res.* 51, 260–272
- 32 Burri, P.H. and Djonov, V. (2002) Intussusceptive angiogenesis—the alternative to capillary sprouting. *Mol. Aspects Med.* 23, 1–27
- 33 Maniotis, A.J. *et al.* (1999) Vascular Channel Formation by Human Melanoma Cells in Vivo and in Vitro: Vasculogenic Mimicry. *Am. J. Pathol.* 155, 739–752
- 34 Yang, J.P. *et al.* (2016) Tumor vasculogenic mimicry predicts poor prognosis in cancer patients: a meta-analysis. *Angiogenesis* 19, 191–200
- 35 Valastyan, S. and Weinberg, R.A. (2011) Tumor Metastasis: Molecular Insights and Evolving Paradigms. *Cell* 147, 275–292
- 36 Guo, W. *et al.* (2012) Slug and Sox9 Cooperatively Determine the Mammary Stem Cell State. *Cell* 148, 1015–1028
- 37 Zhang, K. *et al.* (2013) The Collagen Receptor Discoidin Domain Receptor 2 Stabilizes Snail1 Protein to Facilitate Breast Cancer Metastasis. *Nat. Cell Biol.* 15, 677–687
- 38 Tran, H.D. *et al.* (2014) Transient SNAIL1 Expression is Necessary for

- Metastatic Competence in Breast Cancer. *Cancer Res.* 74, 6330–6340
- 39 Cano, A. *et al.* (2000) The transcription factor snail controls epithelial-mesenchymal transitions by repressing E-cadherin expression. *Nat. Cell Biol.* 2, 76–83
- 40 van de Wetering, M. *et al.* (2001) Mutant E-cadherin breast cancer cells do not display constitutive Wnt signaling. *Cancer Res.* 61, 278–284
- 41 Nieman, M.T. *et al.* (1999) N-Cadherin Promotes Motility in Human Breast Cancer Cells Regardless of Their E-Cadherin Expression. *J. Cell Biol.* 147, 631–644
- 42 Qian, X. *et al.* (2014) N-cadherin/FGFR promotes metastasis through epithelial-to-mesenchymal transition and stem/progenitor cell-like properties. *Oncogene* 33, 3411–3421
- 43 Karnoub, A.E. *et al.* (2007) Mesenchymal stem cells within tumour stroma promote breast cancer metastasis. *Nature* 449, 557–563
- 44 Kessenbrock, K. *et al.* (2010) Matrix metalloproteinases: regulators of the tumor microenvironment. *Cell* 141, 52–67
- 45 Shuman Moss, L.A. *et al.* (2012) Matrix metalloproteinases: changing roles in tumor progression and metastasis. *Am. J. Pathol.* 181, 1895–1899
- 46 Gocheva, V. *et al.* (2010) IL-4 induces cathepsin protease activity in tumor-associated macrophages to promote cancer growth and invasion. *Genes Dev.* 24, 241–255
- 47 Wyckoff, J.B. *et al.* (2007) Direct Visualization of Macrophage-Assisted Tumor Cell Intravasation in Mammary Tumors. *Cancer Res.* 67, 2649–2656
- 48 Ségaliny, A.I. *et al.* (2015) Interleukin-34 promotes tumor progression and metastatic process in osteosarcoma through induction of angiogenesis and macrophage recruitment. *Int. J. Cancer* 137, 73–85
- 49 Guba, M. *et al.* (2001) A primary tumor promotes dormancy of solitary tumor cells before inhibiting angiogenesis. *Cancer Res.* 61, 5575–5579
- 50 Volpert, O.V. *et al.* (1998) A human fibrosarcoma inhibits systemic angiogenesis and the growth of experimental metastases via thrombospondin-1. *Proc. Natl. Acad. Sci. U. S. A.* 95, 6343–6348
- 51 Naumov, G.N. *et al.* (2009) Tumor dormancy due to failure of angiogenesis: role of the microenvironment. *Clin. Exp. Metastasis* 26, 51–60
- 52 Lu, Z. *et al.* (2008) The tumor suppressor gene ARHI regulates autophagy and tumor dormancy in human ovarian cancer cells. *J. Clin. Invest.* 118, 3917–3929
- 53 Teng, M.W.L. *et al.* (2008) Immune-mediated dormancy: an equilibrium with cancer. *J. Leukoc. Biol.* 84, 988–993
- 54 Katsuno, Y. *et al.* (2013) TGF- β signaling and epithelial-mesenchymal transition in cancer progression. *Curr. Opin. Oncol.* 25, 76–84
- 55 Pickup, M. *et al.* (2013) The roles of TGF β in the tumour microenvironment. *Nat. Rev. Cancer* 13, 788–799
- 56 Jiang, B.-H. and Liu, L.-Z. (2009) PI3K/PTEN signaling in angiogenesis and tumorigenesis. *Adv. Cancer Res.* 102, 19–65
- 57 O’Reilly, K.E. *et al.* (2006) mTOR inhibition induces upstream receptor tyrosine kinase signaling and activates Akt. *Cancer Res.* 66, 1500–1508
- 58 Engel, B.E. *et al.* (2015) THE RETINOBLASTOMA PROTEIN: A MASTER TUMOR SUPPRESSOR ACTS AS A LINK BETWEEN CELL CYCLE AND CELL ADHESION. *Cell Health Cytoskelet.* 7, 1–10
- 59 Stracquadanio, G. *et al.* (2016) The importance of p53 pathway genetics in

- inherited and somatic cancer genomes. *Nat. Rev. Cancer* 16, 251–265
- 60 Abercrombie, M. (1979) Contact inhibition and malignancy. *Nature* 281, 259–262
- 61 Adams, J.M. and Cory, S. (2007) The Bcl-2 apoptotic switch in cancer development and therapy. *Oncogene* 26, 1324–1337
- 62 Brahmkhatri, V.P. *et al.* (2015) Insulin-Like Growth Factor System in Cancer: Novel Targeted Therapies. *BioMed Res. Int.* 2015,
- 63 Degenhardt, K. *et al.* (2002) BAX and BAK mediate p53-independent suppression of tumorigenesis. *Cancer Cell* 2, 193–203
- 64 Schreiber, R.D. *et al.* (2011) Cancer immunoediting: integrating immunity's roles in cancer suppression and promotion. *Science* 331, 1565–1570
- 65 Blankenstein, T. *et al.* (2012) The determinants of tumour immunogenicity. *Nat. Rev. Cancer* 12, 307–313
- 66 Ochsenbein, A.F. *et al.* (1999) Immune surveillance against a solid tumor fails because of immunological ignorance. *Proc. Natl. Acad. Sci. U. S. A.* 96, 2233–2238
- 67 Willimsky, G. *et al.* (2008) Immunogenicity of premalignant lesions is the primary cause of general cytotoxic T lymphocyte unresponsiveness. *J. Exp. Med.* 205, 1687–1700
- 68 Aoto, K. *et al.* (2018) Immunogenic tumor cell death induced by chemotherapy in patients with breast cancer and esophageal squamous cell carcinoma. *Oncol. Rep.* 39, 151–159
- 69 Lamm, D.L. *et al.* (1991) A randomized trial of intravesical doxorubicin and immunotherapy with bacille Calmette-Guérin for transitional-cell carcinoma of the bladder. *N. Engl. J. Med.* 325, 1205–1209
- 70 Shankaran, V. *et al.* (2001) IFN γ and lymphocytes prevent primary tumour development and shape tumour immunogenicity. *Nature* 410, 1107–1111
- 71 van den Broek, M.E. *et al.* (1996) Decreased tumor surveillance in perforin-deficient mice. *J. Exp. Med.* 184, 1781–1790
- 72 Kaplan, D.H. *et al.* (1998) Demonstration of an interferon gamma-dependent tumor surveillance system in immunocompetent mice. *Proc. Natl. Acad. Sci. U. S. A.* 95, 7556–7561
- 73 Grulich, A.E. *et al.* (2007) Incidence of cancers in people with HIV/AIDS compared with immunosuppressed transplant recipients: a meta-analysis. *Lancet Lond. Engl.* 370, 59–67
- 74 Gasser, S. *et al.* (2005) The DNA damage pathway regulates innate immune system ligands of the NKG2D receptor. *Nature* 436, 1186–1190
- 75 Ladoire, S. *et al.* (2014) Cell-death-associated molecular patterns as determinants of cancer immunogenicity. *Antioxid. Redox Signal.* 20, 1098–1116
- 76 Lanier, L.L. (2015) NKG2D Receptor and Its Ligands in Host Defense. *Cancer Immunol. Res.* 3, 575–582
- 77 MacKie, R.M. *et al.* (2003) Fatal melanoma transferred in a donated kidney 16 years after melanoma surgery. *N. Engl. J. Med.* 348, 567–568
- 78 Koebel, C.M. *et al.* (2007) Adaptive immunity maintains occult cancer in an equilibrium state. *Nature* 450, 903–907
- 79 Chen, D.S. and Mellman, I. (2013) Oncology meets immunology: the cancer-immunity cycle. *Immunity* 39, 1–10
- 80 Schumacher, T.N. and Schreiber, R.D. (2015) Neoantigens in cancer

immunotherapy. *Science* 348, 69–74

- 81 Lawrence, M.S. *et al.* (2013) Mutational heterogeneity in cancer and the search for new cancer-associated genes. *Nature* 499, 214–218
- 82 Burg, S.H. van der *et al.* (2016) Vaccines for established cancer: overcoming the challenges posed by immune evasion. *Nat. Rev. Cancer* 16, 219–233
- 83 Sahin, U. *et al.* (2017) Personalized RNA mutanome vaccines mobilize poly-specific therapeutic immunity against cancer. *Nature* 547, 222–226
- 84 Li, T. and Chen, Z.J. (2018) The cGAS-cGAMP-STING pathway connects DNA damage to inflammation, senescence, and cancer. *J. Exp. Med.* 215, 1287–1299
- 85 Casares, N. *et al.* (2005) Caspase-dependent immunogenicity of doxorubicin-induced tumor cell death. *J. Exp. Med.* 202, 1691–1701
- 86 Dudek, A.M. *et al.* (2013) Inducers of immunogenic cancer cell death. *Cytokine Growth Factor Rev.* 24, 319–333
- 87 Fucikova, J. *et al.* (2011) Human Tumor Cells Killed by Anthracyclines Induce a Tumor-Specific Immune Response. *Cancer Res.* 71, 4821–4833
- 88 Galluzzi, L. *et al.* (2017) Immunogenic cell death in cancer and infectious disease. *Nat. Rev. Immunol.* 17, 97–111
- 89 Golden, E.B. and Apetoh, L. (2015) Radiotherapy and immunogenic cell death. *Semin. Radiat. Oncol.* 25, 11–17
- 90 Adkins, I. *et al.* (2018) High hydrostatic pressure in cancer immunotherapy and biomedicine. *Biotechnol. Adv.* 36, 577–582
- 91 Dolmans, D.E.J.G.J. *et al.* (2003) Photodynamic therapy for cancer. *Nat. Rev. Cancer* 3, 380–387
- 92 Rosenberg, S.A. *et al.* (1994) Treatment of 283 consecutive patients with metastatic melanoma or renal cell cancer using high-dose bolus interleukin 2. *JAMA* 271, 907–913
- 93 Fyfe, G. *et al.* (1995) Results of treatment of 255 patients with metastatic renal cell carcinoma who received high-dose recombinant interleukin-2 therapy. *J. Clin. Oncol. Off. J. Am. Soc. Clin. Oncol.* 13, 688–696
- 94 Malek, T.R. (2008) The biology of interleukin-2. *Annu. Rev. Immunol.* 26, 453–479
- 95 Assier, E. *et al.* (2004) NK Cells and Polymorphonuclear Neutrophils Are Both Critical for IL-2-Induced Pulmonary Vascular Leak Syndrome. *J. Immunol.* 172, 7661–7668
- 96 Vignali, D.A.A. *et al.* (2008) How regulatory T cells work. *Nat. Rev. Immunol.* 8, 523–532
- 97 Shang, B. *et al.* (2015) Prognostic value of tumor-infiltrating FoxP3⁺ regulatory T cells in cancers: a systematic review and meta-analysis. *Sci. Rep.* 5, 15179
- 98 Curiel, T.J. *et al.* (2004) Specific recruitment of regulatory T cells in ovarian carcinoma fosters immune privilege and predicts reduced survival. *Nat. Med.* 10, 942–949
- 99 Ghiringhelli, F. *et al.* (2005) CD4⁺CD25⁺ regulatory T cells inhibit natural killer cell functions in a transforming growth factor-beta-dependent manner. *J. Exp. Med.* 202, 1075–1085
- 100 Ghiringhelli, F. *et al.* (2005) Tumor cells convert immature myeloid dendritic cells into TGF-beta-secreting cells inducing CD4⁺CD25⁺ regulatory T cell proliferation. *J. Exp. Med.* 202, 919–929

- 101 Valzasina, B. *et al.* (2006) Tumor-induced expansion of regulatory T cells by conversion of CD4+CD25- lymphocytes is thymus and proliferation independent. *Cancer Res.* 66, 4488–4495
- 102 Liu, V.C. *et al.* (2007) Tumor evasion of the immune system by converting CD4+CD25- T cells into CD4+CD25+ T regulatory cells: role of tumor-derived TGF-beta. *J. Immunol. Baltim. Md 1950* 178, 2883–2892
- 103 Wing, K. *et al.* (2008) CTLA-4 Control over Foxp3+ Regulatory T Cell Function. *Science* 322, 271–275
- 104 Walunas, T.L. *et al.* (1994) CTLA-4 can function as a negative regulator of T cell activation. *Immunity* 1, 405–413
- 105 Leach, D.R. *et al.* (1996) Enhancement of antitumor immunity by CTLA-4 blockade. *Science* 271, 1734–1736
- 106 Saoulli, K. *et al.* (1998) CD28-independent, TRAF2-dependent costimulation of resting T cells by 4-1BB ligand. *J. Exp. Med.* 187, 1849–1862
- 107 Valzasina, B. *et al.* (2005) Triggering of OX40 (CD134) on CD4(+)CD25+ T cells blocks their inhibitory activity: a novel regulatory role for OX40 and its comparison with GITR. *Blood* 105, 2845–2851
- 108 Melero, I. *et al.* (1997) Monoclonal antibodies against the 4-1BB T-cell activation molecule eradicate established tumors. *Nat. Med.* 3, 682–685
- 109 Weinberg, A.D. *et al.* (2000) Engagement of the OX-40 receptor in vivo enhances antitumor immunity. *J. Immunol. Baltim. Md 1950* 164, 2160–2169
- 110 Schoenberger, S.P. *et al.* (1998) T-cell help for cytotoxic T lymphocytes is mediated by CD40-CD40L interactions. *Nature* 393, 480–483
- 111 French, R.R. *et al.* (1999) CD40 antibody evokes a cytotoxic T-cell response that eradicates lymphoma and bypasses T-cell help. *Nat. Med.* 5, 548–553
- 112 Melero, I. *et al.* (2007) Immunostimulatory monoclonal antibodies for cancer therapy. *Nat. Rev. Cancer* 7, 95–106
- 113 Fridman, W.H. *et al.* (2012) The immune contexture in human tumours: impact on clinical outcome. *Nat. Rev. Cancer* 12, 298–306
- 114 Igarashi, T. *et al.* (2002) Effect of tumor-infiltrating lymphocyte subsets on prognosis and susceptibility to interferon therapy in patients with renal cell carcinoma. *Urol. Int.* 69, 51–56
- 115 Sharma, P. and Allison, J.P. (2015) The future of immune checkpoint therapy. *Science* 348, 56–61
- 116 Teng, M.W.L. *et al.* (2015) Classifying Cancers Based on T-cell Infiltration and PD-L1. *Cancer Res.* 75, 2139–2145
- 117 Galon, J. *et al.* (2014) Towards the introduction of the “Immunoscore” in the classification of malignant tumours. *J. Pathol.* 232, 199–209
- 118 Nagtegaal, I.D. *et al.* (2011) Has the new TNM classification for colorectal cancer improved care? *Nat. Rev. Clin. Oncol.* 9, 119–123
- 119 Pagès, F. *et al.* (2018) International validation of the consensus Immunoscore for the classification of colon cancer: a prognostic and accuracy study. *Lancet Lond. Engl.* DOI: 10.1016/S0140-6736(18)30789-X
- 120 Galon, J. *et al.* (2016) Immunoscore and Immunoprofiling in cancer: an update from the melanoma and immunotherapy bridge 2015. *J. Transl. Med.* 14,
- 121 Kershaw, M.H. *et al.* (2002) Redirecting migration of T cells to chemokine secreted from tumors by genetic modification with CXCR2. *Hum. Gene Ther.* 13,

1971–1980

- 122 Di Stasi, A. *et al.* (2009) T lymphocytes coexpressing CCR4 and a chimeric antigen receptor targeting CD30 have improved homing and antitumor activity in a Hodgkin tumor model. *Blood* 113, 6392–6402
- 123 Bellone, M. and Calcinotto, A. (2013) Ways to Enhance Lymphocyte Trafficking into Tumors and Fitness of Tumor Infiltrating Lymphocytes. *Front. Oncol.* 3,
- 124 Shrimali, R.K. *et al.* (2010) Antiangiogenic Agents Can Increase Lymphocyte Infiltration into Tumor and Enhance the Effectiveness of Adoptive Immunotherapy of Cancer. *Cancer Res.* 70, 6171–6180
- 125 Freeman, G.J. *et al.* (2000) Engagement of the PD-1 immunoinhibitory receptor by a novel B7 family member leads to negative regulation of lymphocyte activation. *J. Exp. Med.* 192, 1027–1034
- 126 Francisco, L.M. *et al.* (2009) PD-L1 regulates the development, maintenance, and function of induced regulatory T cells. *J. Exp. Med.* 206, 3015–3029
- 127 Gordon, S.R. *et al.* (2017) PD-1 expression by tumour-associated macrophages inhibits phagocytosis and tumour immunity. *Nature* 545, 495–499
- 128 Zhao, T. *et al.* (2017) Prognostic value of PD-L1 expression in tumor infiltrating immune cells in cancers: A meta-analysis. *PLoS ONE* 12,
- 129 Hirano, F. *et al.* (2005) Blockade of B7-H1 and PD-1 by monoclonal antibodies potentiates cancer therapeutic immunity. *Cancer Res.* 65, 1089–1096
- 130 Mosely, S.I.S. *et al.* (2017) Rational Selection of Syngeneic Preclinical Tumor Models for Immunotherapeutic Drug Discovery. *Cancer Immunol. Res.* 5, 29–41
- 131 Woo, S.-R. *et al.* (2012) Immune inhibitory molecules LAG-3 and PD-1 synergistically regulate T-cell function to promote tumoral immune escape. *Cancer Res.* 72, 917–927
- 132 Ngiow, S.F. *et al.* (2011) Anti-TIM3 antibody promotes T cell IFN- γ -mediated antitumor immunity and suppresses established tumors. *Cancer Res.* 71, 3540–3551
- 133 Johnston, R.J. *et al.* (2014) The immunoreceptor TIGIT regulates antitumor and antiviral CD8(+) T cell effector function. *Cancer Cell* 26, 923–937
- 134 Barber, D.L. *et al.* (2006) Restoring function in exhausted CD8 T cells during chronic viral infection. *Nature* 439, 682–687
- 135 Wherry, E.J. *et al.* (2003) Viral persistence alters CD8 T-cell immunodominance and tissue distribution and results in distinct stages of functional impairment. *J. Virol.* 77, 4911–4927
- 136 Redpath, S.A. *et al.* (2013) ICOS controls Foxp3(+) regulatory T-cell expansion, maintenance and IL-10 production during helminth infection. *Eur. J. Immunol.* 43, 705–715
- 137 Fu, T. *et al.* (2011) The ICOS/ICOSL pathway is required for optimal antitumor responses mediated by anti-CTLA-4 therapy. *Cancer Res.* 71, 5445–5454
- 138 Knee, D.A. *et al.* (2016) Rationale for anti-GITR cancer immunotherapy. *Eur. J. Cancer Oxf. Engl.* 1990 67, 1–10
- 139 Maleki Vareki, S. *et al.* (2015) IDO Downregulation Induces Sensitivity to Pemetrexed, Gemcitabine, FK866, and Methoxyamine in Human Cancer Cells. *PLoS One* 10, e0143435
- 140 Munn, D.H. and Mellor, A.L. (2007) Indoleamine 2,3-dioxygenase and tumor-induced tolerance. *J. Clin. Invest.* 117, 1147–1154
- 141 Spranger, S. *et al.* (2014) Mechanism of tumor rejection with doublets of

- CTLA-4, PD-1/PD-L1, or IDO blockade involves restored IL-2 production and proliferation of CD8(+) T cells directly within the tumor microenvironment. *J. Immunother. Cancer* 2, 3
- 142 Berrong, Z. *et al.* (2018) Antigen-Specific Antitumor Responses Induced by OX40 Agonist Are Enhanced by the IDO Inhibitor Indoximod. *Cancer Immunol. Res.* 6, 201–208
- 143 Gutterman, J.U. *et al.* (1980) Leukocyte interferon-induced tumor regression in human metastatic breast cancer, multiple myeloma, and malignant lymphoma. *Ann. Intern. Med.* 93, 399–406
- 144 Lane, H.C. *et al.* (1988) Anti-retroviral effects of interferon-alpha in AIDS-associated Kaposi's sarcoma. *Lancet Lond. Engl.* 2, 1218–1222
- 145 (1997) Interferon alfa versus chemotherapy for chronic myeloid leukemia: a meta-analysis of seven randomized trials: Chronic Myeloid Leukemia Trialists' Collaborative Group. *J. Natl. Cancer Inst.* 89, 1616–1620
- 146 Ferrantini, M. *et al.* (2007) Interferon- α and cancer: Mechanisms of action and new perspectives of clinical use. *Biochimie* 89, 884–893
- 147 Quesada, J.R. *et al.* (1986) Clinical toxicity of interferons in cancer patients: a review. *J. Clin. Oncol. Off. J. Am. Soc. Clin. Oncol.* 4, 234–243
- 148 Rosenberg, S.A. *et al.* (1988) Use of tumor-infiltrating lymphocytes and interleukin-2 in the immunotherapy of patients with metastatic melanoma. A preliminary report. *N. Engl. J. Med.* 319, 1676–1680
- 149 Atkins, M.B. *et al.* (1999) High-dose recombinant interleukin 2 therapy for patients with metastatic melanoma: analysis of 270 patients treated between 1985 and 1993. *J. Clin. Oncol. Off. J. Am. Soc. Clin. Oncol.* 17, 2105–2116
- 150 Ma, C. and Armstrong, A.W. (2014) Severe adverse events from the treatment of advanced melanoma: a systematic review of severe side effects associated with ipilimumab, vemurafenib, interferon alfa-2b, dacarbazine and interleukin-2. *J. Dermatol. Treat.* 25, 401–408
- 151 Boyman, O. *et al.* (2006) Selective stimulation of T cell subsets with antibody-cytokine immune complexes. *Science* 311, 1924–1927
- 152 Kamimura, D. *et al.* (2006) IL-2 in vivo activities and antitumor efficacy enhanced by an anti-IL-2 mAb. *J. Immunol. Baltim. Md* 1950 177, 306–314
- 153 Létourneau, S. *et al.* (2010) IL-2/anti-IL-2 antibody complexes show strong biological activity by avoiding interaction with IL-2 receptor alpha subunit CD25. *Proc. Natl. Acad. Sci. U. S. A.* 107, 2171–2176
- 154 Krieg, C. *et al.* (2010) Improved IL-2 immunotherapy by selective stimulation of IL-2 receptors on lymphocytes and endothelial cells. *Proc. Natl. Acad. Sci. U. S. A.* 107, 11906–11911
- 155 Arenas-Ramirez, N. *et al.* (2016) Improved cancer immunotherapy by a CD25-mimobody conferring selectivity to human interleukin-2. *Sci. Transl. Med.* 8, 367ra166
- 156 Lasek, W. *et al.* (2014) Interleukin 12: still a promising candidate for tumor immunotherapy? *Cancer Immunol. Immunother. CII* 63, 419–435
- 157 Lowy, D.R. and Schiller, J.T. (2006) Prophylactic human papillomavirus vaccines. *J. Clin. Invest.* 116, 1167–1173
- 158 Rosalia, R.A. *et al.* (2013) Dendritic cells process synthetic long peptides better than whole protein, improving antigen presentation and T-cell activation. *Eur. J.*

Immunol. 43, 2554–2565

- 159 Soiffer, R. *et al.* (1998) Vaccination with irradiated autologous melanoma cells engineered to secrete human granulocyte-macrophage colony-stimulating factor generates potent antitumor immunity in patients with metastatic melanoma. *Proc. Natl. Acad. Sci. U. S. A.* 95, 13141–13146
- 160 Sedlik, C. *et al.* (2014) Different immunogenicity but similar antitumor efficacy of two DNA vaccines coding for an antigen secreted in different membrane vesicle-associated forms. *J. Extracell. Vesicles* 3,
- 161 Butterfield, L.H. (2015) Cancer vaccines. *The BMJ* 350,
- 162 Garcia, J.A. (2011) Sipuleucel-T in patients with metastatic castration-resistant prostate cancer: an insight for oncologists. *Ther. Adv. Med. Oncol.* 3, 101–108
- 163 Wahler, J. and Suh, N. (2015) Targeting HER2 Positive Breast Cancer with Chemopreventive Agents. *Curr. Pharmacol. Rep.* 1, 324–335
- 164 Pohlmann, P.R. *et al.* (2009) Resistance to Trastuzumab in Breast Cancer. *Clin. Cancer Res. Off. J. Am. Assoc. Cancer Res.* 15, 7479–7491
- 165 Harbeck, N. *et al.* (2013) HER2 Dimerization Inhibitor Pertuzumab - Mode of Action and Clinical Data in Breast Cancer. *Breast Care Basel Switz.* 8, 49–55
- 166 Welslau, M. *et al.* Patient-reported outcomes from EMILIA, a randomized phase 3 study of trastuzumab emtansine (T-DM1) versus capecitabine and lapatinib in human epidermal growth factor receptor 2–positive locally advanced or metastatic breast cancer. *Cancer* 120, 642–651
- 167 Rosell, R. *et al.* (2012) Erlotinib versus standard chemotherapy as first-line treatment for European patients with advanced EGFR mutation-positive non-small-cell lung cancer (EURTAC): a multicentre, open-label, randomised phase 3 trial. *Lancet Oncol.* 13, 239–246
- 168 Dhillon, S. (2015) Gefitinib: a review of its use in adults with advanced non-small cell lung cancer. *Target. Oncol.* 10, 153–170
- 169 Ramos, R.N. *et al.* (2017) Mechanisms of Resistance to Immune Checkpoint Antibodies. *Handb. Exp. Pharmacol.* DOI: 10.1007/164_2017_11
- 170 Samuels, Y. *et al.* (2004) High frequency of mutations of the PIK3CA gene in human cancers. *Science* 304, 554
- 171 Muul, L.M. *et al.* (1987) Identification of specific cytolytic immune responses against autologous tumor in humans bearing malignant melanoma. *J. Immunol. Baltim. Md 1950* 138, 989–995
- 172 Dudley, M.E. *et al.* (2002) Cancer regression and autoimmunity in patients after clonal repopulation with antitumor lymphocytes. *Science* 298, 850–854
- 173 Morgan, R.A. *et al.* (2006) Cancer regression in patients after transfer of genetically engineered lymphocytes. *Science* 314, 126–129
- 174 Johnson, L.A. *et al.* (2009) Gene therapy with human and mouse T-cell receptors mediates cancer regression and targets normal tissues expressing cognate antigen. *Blood* 114, 535–546
- 175 Cameron, B.J. *et al.* (2013) Identification of a Titin-derived HLA-A1-presented peptide as a cross-reactive target for engineered MAGE A3-directed T cells. *Sci. Transl. Med.* 5, 197ra103
- 176 Rapoport, A.P. *et al.* (2015) NY-ESO-1-specific TCR-engineered T cells mediate sustained antigen-specific antitumor effects in myeloma. *Nat. Med.* 21, 914–921
- 177 Tran, E. *et al.* (2014) Cancer immunotherapy based on mutation-specific CD4+

- T cells in a patient with epithelial cancer. *Science* 344, 641–645
- 178 Garrido, F. *et al.* (2016) The urgent need to recover MHC class I in cancers for effective immunotherapy. *Curr. Opin. Immunol.* 39, 44–51
- 179 Kuwana, Y. *et al.* (1987) Expression of chimeric receptor composed of immunoglobulin-derived V regions and T-cell receptor-derived C regions. *Biochem. Biophys. Res. Commun.* 149, 960–968
- 180 Gross, G. *et al.* (1989) Expression of immunoglobulin-T-cell receptor chimeric molecules as functional receptors with antibody-type specificity. *Proc. Natl. Acad. Sci. U. S. A.* 86, 10024–10028
- 181 Sadelain, M. *et al.* (2013) The basic principles of chimeric antigen receptor design. *Cancer Discov.* 3, 388–398
- 182 Elahi, R. *et al.* (2018) Immune Cell Hacking: Challenges and Clinical Approaches to Create Smarter Generations of Chimeric Antigen Receptor T Cells. *Front. Immunol.* 9, 1717
- 183 June, C.H. *et al.* (2018) CAR T cell immunotherapy for human cancer. *Science* 359, 1361–1365
- 184 Kelly, E. and Russell, S.J. (2007) History of oncolytic viruses: genesis to genetic engineering. *Mol. Ther. J. Am. Soc. Gene Ther.* 15, 651–659
- 185 Kaufman, H.L. *et al.* (2015) Oncolytic viruses: a new class of immunotherapy drugs. *Nat. Rev. Drug Discov.* 14, 642–662
- 186 Im, S.J. *et al.* (2016) Defining CD8+ T cells that provide the proliferative burst after PD-1 therapy. *Nature* 537, 417–421
- 187 Kamphorst, A.O. *et al.* (2017) Rescue of exhausted CD8 T cells by PD-1-targeted therapies is CD28-dependent. *Science* 355, 1423–1427
- 188 Koyama, S. *et al.* (2016) Adaptive resistance to therapeutic PD-1 blockade is associated with upregulation of alternative immune checkpoints. *Nat. Commun.* 7, 10501
- 189 Shayan, G. *et al.* (2017) Adaptive resistance to anti-PD1 therapy by Tim-3 upregulation is mediated by the PI3K-Akt pathway in head and neck cancer. *Oncoimmunology* 6, e1261779
- 190 Chang, C.-H. *et al.* (2015) Metabolic Competition in the Tumor Microenvironment Is a Driver of Cancer Progression. *Cell* 162, 1229–1241
- 191 Dempke, W.C.M. *et al.* (2017) Second- and third-generation drugs for immuno-oncology treatment-The more the better? *Eur. J. Cancer Oxf. Engl.* 1990 74, 55–72
- 192 Michot, J.M. *et al.* (2016) Immune-related adverse events with immune checkpoint blockade: a comprehensive review. *Eur. J. Cancer Oxf. Engl.* 1990 54, 139–148
- 193 Stucci, S. *et al.* (2017) Immune-related adverse events during anticancer immunotherapy: Pathogenesis and management. *Oncol. Lett.* 14, 5671–5680
- 194 Hao, C. *et al.* (2017) Efficacy and safety of anti-PD-1 and anti-PD-1 combined with anti-CTLA-4 immunotherapy to advanced melanoma: A systematic review and meta-analysis of randomized controlled trials. *Medicine (Baltimore)* 96, e7325
- 195 Jin, C. *et al.* (2016) The efficacy and safety of nivolumab in the treatment of advanced melanoma: a meta-analysis of clinical trials. *OncoTargets Ther.* 9, 1571–1578
- 196 Zhou, G.-W. *et al.* (2016) Anti-PD-1/PD-L1 antibody therapy for pretreated

advanced nonsmall-cell lung cancer: A meta-analysis of randomized clinical trials. *Medicine (Baltimore)* 95, e4611

197 Kershaw, M.H. *et al.* (2013) Enhancing immunotherapy using chemotherapy and radiation to modify the tumor microenvironment. *Oncoimmunology* 2,

198 Koller, K.M. *et al.* (2017) Improved survival and complete response rates in patients with advanced melanoma treated with concurrent ipilimumab and radiotherapy versus ipilimumab alone. *Cancer Biol. Ther.* 18, 36–42

199 Talmadge, J.E. *et al.* (2007) Murine models to evaluate novel and conventional therapeutic strategies for cancer. *Am. J. Pathol.* 170, 793–804

200 Li, Q.-X. *et al.* (2017) Experimental animal modeling for immuno-oncology. *Pharmacol. Ther.* 173, 34–46

201 Livshits, G. and Lowe, S.W. (2013) Accelerating cancer modeling with RNAi and nongerm-line genetically engineered mouse models. *Cold Spring Harb. Protoc.* 2013,

202 DuPage, M. *et al.* (2009) Conditional mouse lung cancer models using adenoviral or lentiviral delivery of Cre recombinase. *Nat. Protoc.* 4, 1064–1072

203 Alonso, R. *et al.* (2018) Induction of anergic or regulatory tumor-specific CD4+ T cells in the tumor-draining lymph node. *Nat. Commun.* 9, 2113

204 Flament, H. *et al.* (2015) Modeling the Specific CD4+ T Cell Response against a Tumor Neoantigen. *J. Immunol.* 194, 3501–3512

205 Bosma, G.C. *et al.* (1983) A severe combined immunodeficiency mutation in the mouse. *Nature* 301, 527–530

206 Mosier, D.E. *et al.* (1988) Transfer of a functional human immune system to mice with severe combined immunodeficiency. *Nature* 335, 256–259

207 McCune, J.M. *et al.* (1988) The SCID-hu mouse: murine model for the analysis of human hematolymphoid differentiation and function. *Science* 241, 1632–1639

208 Lapidot, T. *et al.* (1992) Cytokine stimulation of multilineage hematopoiesis from immature human cells engrafted in SCID mice. *Science* 255, 1137–1141

209 Namikawa, R. *et al.* (1988) Infection of the SCID-hu mouse by HIV-1. *Science* 242, 1684–1686

210 Washburn, M.L. *et al.* (2011) A humanized mouse model to study hepatitis C virus infection, immune response, and liver disease. *Gastroenterology* 140, 1334–1344

211 Gurer, C. *et al.* (2008) Targeting the nuclear antigen 1 of Epstein-Barr virus to the human endocytic receptor DEC-205 stimulates protective T-cell responses. *Blood* 112, 1231–1239

212 Libby, S.J. *et al.* (2010) Humanized nonobese diabetic-scid IL2rgammanull mice are susceptible to lethal *Salmonella Typhi* infection. *Proc. Natl. Acad. Sci. U. S. A.* 107, 15589–15594

213 Ellmerich, S. *et al.* (2005) High incidence of spontaneous disease in an HLA-DR15 and TCR transgenic multiple sclerosis model. *J. Immunol. Baltim. Md* 1950 174, 1938–1946

214 Brehm, M.A. *et al.* (2010) Human immune system development and rejection of human islet allografts in spontaneously diabetic NOD-Rag1null IL2rgammanull Ins2Akita mice. *Diabetes* 59, 2265–2270

215 Pérol, L. *et al.* (2014) Potential limitations of IL-2 administration for the treatment of experimental acute graft-versus-host disease. *Immunol. Lett.* 162, 173–184

- 216 Fogh, J. *et al.* (1977) One hundred and twenty-seven cultured human tumor cell lines producing tumors in nude mice. *J. Natl. Cancer Inst.* 59, 221–226
- 217 Hudson, W.A. *et al.* (1998) Xenotransplantation of human lymphoid malignancies is optimized in mice with multiple immunologic defects. *Leukemia* 12, 2029–2033
- 218 Oettinger, M.A. *et al.* (1990) RAG-1 and RAG-2, adjacent genes that synergistically activate V(D)J recombination. *Science* 248, 1517–1523
- 219 Mombaerts, P. *et al.* (1992) RAG-1-deficient mice have no mature B and T lymphocytes. *Cell* 68, 869–877
- 220 Shinkai, Y. *et al.* (1992) RAG-2-deficient mice lack mature lymphocytes owing to inability to initiate V(D)J rearrangement. *Cell* 68, 855–867
- 221 Strowig, T. *et al.* (2011) Transgenic expression of human signal regulatory protein alpha in Rag2^{-/-}-gamma(c)^{-/-} mice improves engraftment of human hematopoietic cells in humanized mice. *Proc. Natl. Acad. Sci. U. S. A.* 108, 13218–13223
- 222 Shultz, L.D. *et al.* (1995) Multiple defects in innate and adaptive immunologic function in NOD/LtSz-scid mice. *J. Immunol. Baltim. Md 1950* 154, 180–191
- 223 Shultz, L.D. *et al.* (2000) NOD/LtSz-Rag1null mice: an immunodeficient and radioresistant model for engraftment of human hematolymphoid cells, HIV infection, and adoptive transfer of NOD mouse diabetogenic T cells. *J. Immunol. Baltim. Md 1950* 164, 2496–2507
- 224 Shultz, L.D. *et al.* (2007) Humanized mice in translational biomedical research. *Nat. Rev. Immunol.* 7, 118–130
- 225 Ishikawa, F. *et al.* (2005) Development of functional human blood and immune systems in NOD/SCID/IL2 receptor {gamma} chain(null) mice. *Blood* 106, 1565–1573
- 226 Ito, M. *et al.* (2002) NOD/SCID/gamma(c)(null) mouse: an excellent recipient mouse model for engraftment of human cells. *Blood* 100, 3175–3182
- 227 Traggiai, E. *et al.* (2004) Development of a human adaptive immune system in cord blood cell-transplanted mice. *Science* 304, 104–107
- 228 Rochman, Y. *et al.* (2009) New insights into the regulation of T cells by gamma(c) family cytokines. *Nat. Rev. Immunol.* 9, 480–490
- 229 Gimeno, R. *et al.* (2004) Monitoring the effect of gene silencing by RNA interference in human CD34⁺ cells injected into newborn RAG2^{-/-} gammac^{-/-} mice: functional inactivation of p53 in developing T cells. *Blood* 104, 3886–3893
- 230 Takenaka, K. *et al.* (2007) Polymorphism in Sirpa modulates engraftment of human hematopoietic stem cells. *Nat. Immunol.* 8, 1313–1323
- 231 Takizawa, H. and Manz, M.G. (2007) Macrophage tolerance: CD47-SIRP-alpha-mediated signals matter. *Nat. Immunol.* 8, 1287–1289
- 232 van den Berg, T.K. and van der Schoot, C.E. (2008) Innate immune “self” recognition: a role for CD47-SIRPalpha interactions in hematopoietic stem cell transplantation. *Trends Immunol.* 29, 203–206
- 233 Legrand, N. *et al.* (2011) Functional CD47/signal regulatory protein alpha (SIRP(alpha)) interaction is required for optimal human T- and natural killer- (NK) cell homeostasis in vivo. *Proc. Natl. Acad. Sci. U. S. A.* 108, 13224–13229
- 234 Kwong, L.S. *et al.* (2014) Signal-regulatory protein α from the NOD mouse binds human CD47 with an exceptionally high affinity-- implications for engraftment

- of human cells. *Immunology* 143, 61–67
- 235 Veillette, A. *et al.* (1998) High expression of inhibitory receptor SHPS-1 and its association with protein-tyrosine phosphatase SHP-1 in macrophages. *J. Biol. Chem.* 273, 22719–22728
- 236 Pearson, T. *et al.* (2008) Humanized SCID mouse models for biomedical research. *Curr. Top. Microbiol. Immunol.* 324, 25–51
- 237 Brehm, M.A. *et al.* (2013) Overcoming current limitations in humanized mouse research. *J. Infect. Dis.* 208 Suppl 2, S125-130
- 238 King, M. *et al.* (2008) A new Hu-PBL model for the study of human islet alloreactivity based on NOD-scid mice bearing a targeted mutation in the IL-2 receptor gamma chain gene. *Clin. Immunol. Orlando Fla* 126, 303–314
- 239 Kim, K.C. *et al.* (2016) A Simple Mouse Model for the Study of Human Immunodeficiency Virus. *AIDS Res. Hum. Retroviruses* 32, 194–202
- 240 Ali, N. *et al.* (2012) Xenogeneic graft-versus-host-disease in NOD-scid IL-2R γ null mice display a T-effector memory phenotype. *PloS One* 7, e44219
- 241 Shultz, L.D. *et al.* (2007) Humanized NOD/LtSz-scid IL2 receptor common gamma chain knockout mice in diabetes research. *Ann. N. Y. Acad. Sci.* 1103, 77–89
- 242 King, M.A. *et al.* (2009) Human peripheral blood leucocyte non-obese diabetic-severe combined immunodeficiency interleukin-2 receptor gamma chain gene mouse model of xenogeneic graft-versus-host-like disease and the role of host major histocompatibility complex. *Clin. Exp. Immunol.* 157, 104–118
- 243 Moser, J. *et al.* (2016) Distinct Differences on Neointima Formation in Immunodeficient and Humanized Mice after Carotid or Femoral Arterial Injury. *Sci. Rep.* 6, 35387
- 244 Cooke, K.R. *et al.* (1996) An experimental model of idiopathic pneumonia syndrome after bone marrow transplantation: I. The roles of minor H antigens and endotoxin. *Blood* 88, 3230–3239
- 245 Sanmamed, M.F. *et al.* (2015) Nivolumab and Urelumab Enhance Antitumor Activity of Human T Lymphocytes Engrafted in Rag2 $^{-/-}$ IL2R γ null Immunodeficient Mice. *Cancer Res.* 75, 3466–3478
- 246 Hayakawa, J. *et al.* (2009) Busulfan produces efficient human cell engraftment in NOD/LtSz-Scid IL2R γ (null) mice. *Stem Cells Dayt. Ohio* 27, 175–182
- 247 Kang, Y.K. *et al.* (2016) Humanizing NOD/SCID/IL-2R γ null (NSG) mice using busulfan and retro-orbital injection of umbilical cord blood-derived CD34+ cells. *Blood Res.* 51, 31–36
- 248 Czechowicz, A. *et al.* (2007) Efficient transplantation via antibody-based clearance of hematopoietic stem cell niches. *Science* 318, 1296–1299
- 249 Holyoake, T.L. *et al.* (1999) Functional differences between transplantable human hematopoietic stem cells from fetal liver, cord blood, and adult marrow. *Exp. Hematol.* 27, 1418–1427
- 250 Shultz, L.D. *et al.* (2005) Human lymphoid and myeloid cell development in NOD/LtSz-scid IL2R gamma null mice engrafted with mobilized human hemopoietic stem cells. *J. Immunol. Baltim. Md* 1950 174, 6477–6489
- 251 Lepus, C.M. *et al.* (2009) Comparison of human fetal liver, umbilical cord blood, and adult blood hematopoietic stem cell engraftment in NOD-scid/ γ null, Balb/c-Rag1 $^{-/-}$ / γ null, and C.B-17-scid/bg immunodeficient mice. *Hum. Immunol.* 70, 790–802

- 252 Matsumura, T. *et al.* (2003) Functional CD5+ B cells develop predominantly in the spleen of NOD/SCID/gammac(null) (NOG) mice transplanted either with human umbilical cord blood, bone marrow, or mobilized peripheral blood CD34+ cells. *Exp. Hematol.* 31, 789–797
- 253 Lan, P. *et al.* (2006) Reconstitution of a functional human immune system in immunodeficient mice through combined human fetal thymus/liver and CD34+ cell transplantation. *Blood* 108, 487–492
- 254 Werner-Klein, M. *et al.* (2014) Immune humanization of immunodeficient mice using diagnostic bone marrow aspirates from carcinoma patients. *PLoS One* 9, e97860
- 255 McDermott, S.P. *et al.* (2010) Comparison of human cord blood engraftment between immunocompromised mouse strains. *Blood* 116, 193–200
- 256 Notta, F. *et al.* (2010) Engraftment of human hematopoietic stem cells is more efficient in female NOD/SCID/IL-2R γ -null recipients. *Blood* 115, 3704–3707
- 257 Volk, V. *et al.* (2016) The gender gap: discrepant human T-cell reconstitution after cord blood stem cell transplantation in humanized female and male mice. *Bone Marrow Transplant.* 51, 596–597
- 258 André, M.C. *et al.* (2010) Long-term human CD34+ stem cell-engrafted nonobese diabetic/SCID/IL-2R γ null mice show impaired CD8+ T cell maintenance and a functional arrest of immature NK cells. *J. Immunol. Baltim. Md 1950* 185, 2710–2720
- 259 Watanabe, Y. *et al.* (2009) The analysis of the functions of human B and T cells in humanized NOD/shi-scid/gammac(null) (NOG) mice (hu-HSC NOG mice). *Int. Immunol.* 21, 843–858
- 260 Yajima, M. *et al.* (2009) T cell-mediated control of Epstein-Barr virus infection in humanized mice. *J. Infect. Dis.* 200, 1611–1615
- 261 Gille, C. *et al.* (2012) Monocytes derived from humanized neonatal NOD/SCID/IL2R γ (null) mice are phenotypically immature and exhibit functional impairments. *Hum. Immunol.* 73, 346–354
- 262 Lang, J. *et al.* (2013) Studies of lymphocyte reconstitution in a humanized mouse model reveal a requirement of T cells for human B cell maturation. *J. Immunol. Baltim. Md 1950* 190, 2090–2101
- 263 Halkias, J. *et al.* (2015) Conserved and divergent aspects of human T-cell development and migration in humanized mice. *Immunol. Cell Biol.* 93, 716–726
- 264 Denton, P.W. *et al.* (2010) Systemic administration of antiretrovirals prior to exposure prevents rectal and intravenous HIV-1 transmission in humanized BLT mice. *PLoS One* 5, e8829
- 265 Daniel, V.C. *et al.* (2009) A primary xenograft model of small-cell lung cancer reveals irreversible changes in gene expression imposed by culture in vitro. *Cancer Res.* 69, 3364–3373
- 266 Vrignaud Patricia (2016) Les tumeurs dérivées de patients : un ancien concept redevenu populaire dans la recherche translationnelle en oncologie. *Innov. Thérapeutiques En Oncol.* 2,
- 267 Némati, F. *et al.* (2010) Establishment and characterization of a panel of human uveal melanoma xenografts derived from primary and/or metastatic tumors. *Clin. Cancer Res. Off. J. Am. Assoc. Cancer Res.* 16, 2352–2362
- 268 Surdez, D. and Daudigeos-Dubus, E. (2016) PDX ou xénogreffe dérivée de la

tumeur du patient, la renaissance d'un modèle oublié : son implication dans la recherche et la clinique de demain. *Rev. Oncol. Hématologie Pédiatrique* 4, 237–245

269 Beroukhim, R. *et al.* (2010) The landscape of somatic copy-number alteration across human cancers. *Nature* 463, 899–905

270 Byrne, A.T. *et al.* (2017) Interrogating open issues in cancer precision medicine with patient-derived xenografts. *Nat. Rev. Cancer* 17, 254–268

271 Reyat, F. *et al.* (2012) Molecular profiling of patient-derived breast cancer xenografts. *Breast Cancer Res. BCR* 14, R11

272 Ben-David, U. *et al.* (2017) Patient-derived xenografts undergo mouse-specific tumor evolution. *Nat. Genet.* 49, 1567–1575

273 Gao, H. *et al.* (2015) High-throughput screening using patient-derived tumor xenografts to predict clinical trial drug response. *Nat. Med.* 21, 1318–1325

274 Izumchenko, E. *et al.* (2017) Patient-derived xenografts effectively capture responses to oncology therapy in a heterogeneous cohort of patients with solid tumors. *Ann. Oncol. Off. J. Eur. Soc. Med. Oncol.* 28, 2595–2605

275 Calvo, E. *et al.* (2017) A Phase I Clinical Trial and Independent Patient-Derived Xenograft Study of Combined Targeted Treatment with Dacomitinib and Figitumumab in Advanced Solid Tumors. *Clin. Cancer Res. Off. J. Am. Assoc. Cancer Res.* 23, 1177–1185

276 Zayed, A.A. *et al.* (2015) Molecular and clinical implementations of ovarian cancer mouse avatar models. *Chin. Clin. Oncol.* 4, 30

277 Pearson, T. *et al.* (2008) Non-obese diabetic-recombination activating gene-1 (NOD-Rag1 null) interleukin (IL)-2 receptor common gamma chain (IL2r gamma null) null mice: a radioresistant model for human lymphohaematopoietic engraftment. *Clin. Exp. Immunol.* 154, 270–284

278 Cosgun, K.N. *et al.* (2014) Kit regulates HSC engraftment across the human-mouse species barrier. *Cell Stem Cell* 15, 227–238

279 Rahmig, S. *et al.* (2016) Improved Human Erythropoiesis and Platelet Formation in Humanized NSGW41 Mice. *Stem Cell Rep.* 7, 591–601

280 McIntosh, B.E. *et al.* (2015) Nonirradiated NOD,B6.SCID Il2ry^{-/-} Kit(W41/W41) (NBSGW) mice support multilineage engraftment of human hematopoietic cells. *Stem Cell Rep.* 4, 171–180

281 Gasic, G.J. *et al.* (1968) Antimetastatic effects associated with platelet reduction. *Proc. Natl. Acad. Sci. U. S. A.* 61, 46–52

282 Mahalingam, M. *et al.* (1988) Functional role of platelets in experimental metastasis studied with cloned murine fibrosarcoma cell variants. *Cancer Res.* 48, 1460–1464

283 Li, Y. *et al.* (2016) A novel Flt3-deficient HIS mouse model with selective enhancement of human DC development. *Eur. J. Immunol.* 46, 1291–1299

284 Lopez-Lastra, S. *et al.* (2017) A functional DC cross talk promotes human ILC homeostasis in humanized mice. *Blood Adv.* 1, 601–614

285 Gabrilovich, D.I. (2017) Myeloid-Derived Suppressor Cells. *Cancer Immunol. Res.* 5, 3–8

286 Elliott, L.A. *et al.* (2017) Human Tumor-Infiltrating Myeloid Cells: Phenotypic and Functional Diversity. *Front. Immunol.* 8, 86

287 Tanaka, S. *et al.* (2012) Development of mature and functional human myeloid subsets in hematopoietic stem cell-engrafted NOD/SCID/IL2ryKO mice. *J. Immunol.*

Baltim. Md 1950 188, 6145–6155

- 288 Chen, Q. *et al.* (2009) Expression of human cytokines dramatically improves reconstitution of specific human-blood lineage cells in humanized mice. *Proc. Natl. Acad. Sci. U. S. A.* 106, 21783–21788
- 289 Wunderlich, M. *et al.* (2010) AML xenograft efficiency is significantly improved in NOD/SCID-IL2RG mice constitutively expressing human SCF, GM-CSF and IL-3. *Leukemia* 24, 1785–1788
- 290 Billerbeck, E. *et al.* (2011) Development of human CD4+FoxP3+ regulatory T cells in human stem cell factor-, granulocyte-macrophage colony-stimulating factor-, and interleukin-3-expressing NOD-SCID IL2Rγ(null) humanized mice. *Blood* 117, 3076–3086
- 291 Ito, R. *et al.* (2013) Establishment of a human allergy model using human IL-3/GM-CSF-transgenic NOG mice. *J. Immunol. Baltim. Md 1950* 191, 2890–2899
- 292 Willinger, T. *et al.* (2011) Human IL-3/GM-CSF knock-in mice support human alveolar macrophage development and human immune responses in the lung. *Proc. Natl. Acad. Sci. U. S. A.* 108, 2390–2395
- 293 Rongvaux, A. *et al.* (2011) Human thrombopoietin knockin mice efficiently support human hematopoiesis in vivo. *Proc. Natl. Acad. Sci. U. S. A.* 108, 2378–2383
- 294 Rongvaux, A. *et al.* (2014) Development and function of human innate immune cells in a humanized mouse model. *Nat. Biotechnol.* 32, 364–372
- 295 Vivier, E. *et al.* (2012) Targeting natural killer cells and natural killer T cells in cancer. *Nat. Rev. Immunol.* 12, 239–252
- 296 Pilipow, K. *et al.* (2015) IL15 and T-cell Stemness in T-cell-Based Cancer Immunotherapy. *Cancer Res.* 75, 5187–5193
- 297 Katano, I. *et al.* (2015) Predominant development of mature and functional human NK cells in a novel human IL-2-producing transgenic NOG mouse. *J. Immunol. Baltim. Md 1950* 194, 3513–3525
- 298 Guimond, M. *et al.* (2010) In vivo role of Flt3 ligand and dendritic cells in NK cell homeostasis. *J. Immunol. Baltim. Md 1950* 184, 2769–2775
- 299 Herndler-Brandstetter, D. *et al.* (2017) Humanized mouse model supports development, function, and tissue residency of human natural killer cells. *Proc. Natl. Acad. Sci. U. S. A.* DOI: 10.1073/pnas.1705301114
- 300 Katano, I. *et al.* (2017) Long-term maintenance of peripheral blood derived human NK cells in a novel human IL-15- transgenic NOG mouse. *Sci. Rep.* 7, 17230
- 301 Shiokawa, M. *et al.* (2010) In vivo assay of human NK-dependent ADCC using NOD/SCID/gammac(null) (NOG) mice. *Biochem. Biophys. Res. Commun.* 399, 733–737
- 302 Vahedi, F. *et al.* (2017) Ex Vivo Expanded Human NK Cells Survive and Proliferate in Humanized Mice with Autologous Human Immune Cells. *Sci. Rep.* 7, 12083
- 303 Sonntag, K. *et al.* (2015) Chronic graft-versus-host-disease in CD34(+)-humanized NSG mice is associated with human susceptibility HLA haplotypes for autoimmune disease. *J. Autoimmun.* 62, 55–66
- 304 Yaguchi, T. *et al.* (2017) Human PBMC-transferred murine MHC class I/II-deficient NOG mice enable long-term evaluation of human immune responses. *Cell. Mol. Immunol.* DOI: 10.1038/cmi.2017.106
- 305 Shultz, L.D. *et al.* (2010) Generation of functional human T-cell subsets with HLA-restricted immune responses in HLA class I expressing NOD/SCID/IL2r

- gamma(null) humanized mice. *Proc. Natl. Acad. Sci. U. S. A.* 107, 13022–13027
- 306 Danner, R. *et al.* (2011) Expression of HLA class II molecules in humanized NOD.Rag1KO.IL2RgckO mice is critical for development and function of human T and B cells. *PloS One* 6, e19826
- 307 Suzuki, M. *et al.* (2012) Induction of human humoral immune responses in a novel HLA-DR-expressing transgenic NOD/Shi-scid/ γ cnul mouse. *Int. Immunol.* 24, 243–252
- 308 Zeng, Y. *et al.* (2017) Creation of an immunodeficient HLA-transgenic mouse (HUMAMICE) and functional validation of human immunity after transfer of HLA-matched human cells. *PloS One* 12, e0173754
- 309 Lute, K.D. *et al.* (2005) Human CTLA4 knock-in mice unravel the quantitative link between tumor immunity and autoimmunity induced by anti-CTLA-4 antibodies. *Blood* 106, 3127–3133
- 310 Burova, E. *et al.* (2017) Characterization of the Anti-PD-1 Antibody REGN2810 and Its Antitumor Activity in Human PD-1 Knock-In Mice. *Mol. Cancer Ther.* 16, 861–870
- 311 Wen, X. *et al.* (2013) Human CD1d knock-in mouse model demonstrates potent antitumor potential of human CD1d-restricted invariant natural killer T cells. *Proc. Natl. Acad. Sci. U. S. A.* 110, 2963–2968
- 312 Van Duyne, R. *et al.* (2009) The utilization of humanized mouse models for the study of human retroviral infections. *Retrovirology* 6, 76
- 313 Zhang, L. *et al.* (2010) Current humanized mouse models for studying human immunology and HIV-1 immuno-pathogenesis. *Sci. China Life Sci.* 53, 195–203
- 314 Mosier, D.E. *et al.* (1991) Human immunodeficiency virus infection of human-PBL-SCID mice. *Science* 251, 791–794
- 315 Torbett, B.E. *et al.* (1991) hu-PBL-SCID mice: a model for human immune function, AIDS, and lymphomagenesis. *Immunol. Rev.* 124, 139–164
- 316 Ruxrungtham, K. *et al.* (1996) Potent activity of 2'-beta-fluoro-2',3'-dideoxyadenosine against human immunodeficiency virus type 1 infection in hu-PBL-SCID mice. *Antimicrob. Agents Chemother.* 40, 2369–2374
- 317 Shultz, L.D. *et al.* (2012) Humanized mice for immune system investigation: progress, promise and challenges. *Nat. Rev. Immunol.* 12, 786–798
- 318 Walsh, N.C. *et al.* (2017) Humanized Mouse Models of Clinical Disease. *Annu. Rev. Pathol.* 12, 187–215
- 319 Kenney, L.L. *et al.* (2016) Humanized Mouse Models for Transplant Immunology. *Am. J. Transplant. Off. J. Am. Soc. Transplant. Am. Soc. Transpl. Surg.* 16, 389–397
- 320 Zheng, J. *et al.* (2013) Human CD8+ regulatory T cells inhibit GVHD and preserve general immunity in humanized mice. *Sci. Transl. Med.* 5, 168ra9
- 321 May, K.F. *et al.* (2005) Anti-human CTLA-4 monoclonal antibody promotes T-cell expansion and immunity in a hu-PBL-SCID model: a new method for preclinical screening of costimulatory monoclonal antibodies. *Blood* 105, 1114–1120
- 322 Jangalwe, S. *et al.* (2016) Improved B cell development in humanized NOD-scid IL2R γ (null) mice transgenically expressing human stem cell factor, granulocyte-macrophage colony-stimulating factor and interleukin-3. *Immun. Inflamm. Dis.* 4, 427–440
- 323 Zhao, Y. *et al.* (2010) Multiple injections of electroporated autologous T cells

expressing a chimeric antigen receptor mediate regression of human disseminated tumor. *Cancer Res.* 70, 9053–9061

324 Abate-Daga, D. *et al.* (2014) A novel chimeric antigen receptor against prostate stem cell antigen mediates tumor destruction in a humanized mouse model of pancreatic cancer. *Hum. Gene Ther.* 25, 1003–1012

325 Guedan, S. *et al.* (2014) ICOS-based chimeric antigen receptors program bipolar TH17/TH1 cells. *Blood* 124, 1070–1080

326 Hudecek, M. *et al.* (2013) Receptor affinity and extracellular domain modifications affect tumor recognition by ROR1-specific chimeric antigen receptor T cells. *Clin. Cancer Res. Off. J. Am. Assoc. Cancer Res.* 19, 3153–3164

327 Gill, S. *et al.* (2014) Preclinical targeting of human acute myeloid leukemia and myeloablation using chimeric antigen receptor-modified T cells. *Blood* 123, 2343–2354

328 Pizzitola, I. *et al.* (2014) Chimeric antigen receptors against CD33/CD123 antigens efficiently target primary acute myeloid leukemia cells in vivo. *Leukemia* 28, 1596–1605

329 Casucci, M. *et al.* (2013) CD44v6-targeted T cells mediate potent antitumor effects against acute myeloid leukemia and multiple myeloma. *Blood* 122, 3461–3472

330 Song, D.-G. *et al.* (2012) CD27 costimulation augments the survival and antitumor activity of redirected human T cells in vivo. *Blood* 119, 696–706

331 Diaconu, I. *et al.* (2017) Inducible Caspase-9 Selectively Modulates the Toxicities of CD19-Specific Chimeric Antigen Receptor-Modified T Cells. *Mol. Ther. J. Am. Soc. Gene Ther.* 25, 580–592

332 Hombach, A.A. *et al.* (2016) Superior Therapeutic Index in Lymphoma Therapy: CD30(+) CD34(+) Hematopoietic Stem Cells Resist a Chimeric Antigen Receptor T-cell Attack. *Mol. Ther. J. Am. Soc. Gene Ther.* 24, 1423–1434

333 Brown, C.E. *et al.* (2012) Stem-like tumor-initiating cells isolated from IL13R α 2 expressing gliomas are targeted and killed by IL13-zetakine-redirected T Cells. *Clin. Cancer Res. Off. J. Am. Assoc. Cancer Res.* 18, 2199–2209

334 Lopez-Lastra, S. and Di Santo, J.P. (2017) Modeling Natural Killer Cell Targeted Immunotherapies. *Front. Immunol.* 8, 370

335 Lee, S.J. *et al.* (2015) Natural killer (NK) cells inhibit systemic metastasis of glioblastoma cells and have therapeutic effects against glioblastomas in the brain. *BMC Cancer* 15, 1011

336 Hoogstad-van Evert, J.S. *et al.* (2017) Umbilical cord blood CD34+ progenitor-derived NK cells efficiently kill ovarian cancer spheroids and intraperitoneal tumors in NOD/SCID/IL2R γ null mice. *Oncoimmunology* 6, e1320630

337 Veluchamy, J.P. *et al.* (2017) In Vivo Efficacy of Umbilical Cord Blood Stem Cell-Derived NK Cells in the Treatment of Metastatic Colorectal Cancer. *Front. Immunol.* 8, 87

338 Geller, M.A. *et al.* (2013) Intraperitoneal delivery of human natural killer cells for treatment of ovarian cancer in a mouse xenograft model. *Cytotherapy* 15, 1297–1306

339 Ames, E. *et al.* (2015) NK Cells Preferentially Target Tumor Cells with a Cancer Stem Cell Phenotype. *J. Immunol. Baltim. Md 1950* 195, 4010–4019

340 Laffont, S. *et al.* (2014) X-Chromosome complement and estrogen receptor signaling independently contribute to the enhanced TLR7-mediated IFN- α production

of plasmacytoid dendritic cells from women. *J. Immunol. Baltim. Md 1950* 193, 5444–5452

341 Fisher, T.S. *et al.* (2012) Targeting of 4-1BB by monoclonal antibody PF-05082566 enhances T-cell function and promotes anti-tumor activity. *Cancer Immunol. Immunother. CII* 61, 1721–1733

342 Ashizawa, T. *et al.* (2017) Antitumor Effect of Programmed Death-1 (PD-1) Blockade in Humanized the NOG-MHC Double Knockout Mouse. *Clin. Cancer Res. Off. J. Am. Assoc. Cancer Res.* 23, 149–158

343 Ma, S.-D. *et al.* (2016) PD-1/CTLA-4 Blockade Inhibits Epstein-Barr Virus-Induced Lymphoma Growth in a Cord Blood Humanized-Mouse Model. *PLoS Pathog.* 12, e1005642

344 Cherkassky, L. *et al.* (2016) Human CAR T cells with cell-intrinsic PD-1 checkpoint blockade resist tumor-mediated inhibition. *J. Clin. Invest.* 126, 3130–3144

345 Ito, A. *et al.* (2009) Defucosylated anti-CCR4 monoclonal antibody exercises potent ADCC-mediated antitumor effect in the novel tumor-bearing humanized NOD/Shi-scid, IL-2Rgamma(null) mouse model. *Cancer Immunol. Immunother. CII* 58, 1195–1206

346 Chang, D.-K. *et al.* (2015) Human anti-CAIX antibodies mediate immune cell inhibition of renal cell carcinoma in vitro and in a humanized mouse model in vivo. *Mol. Cancer* 14, 119

347 Wege, A.K. *et al.* (2017) IL-15 enhances the anti-tumor activity of trastuzumab against breast cancer cells but causes fatal side effects in humanized tumor mice (HTM). *Oncotarget* 8, 2731–2744

348 Leskov, I. *et al.* (2013) Rapid generation of human B-cell lymphomas via combined expression of Myc and Bcl2 and their use as a preclinical model for biological therapies. *Oncogene* 32, 1066–1072

349 Pallasch, C.P. *et al.* (2014) Sensitizing protective tumor microenvironments to antibody-mediated therapy. *Cell* 156, 590–602

350 Mahne, A.E. *et al.* (2017) Dual Roles for Regulatory T-cell Depletion and Costimulatory Signaling in Agonistic GITR Targeting for Tumor Immunotherapy. *Cancer Res.* 77, 1108–1118

351 Wulf-Goldenberg, A. *et al.* (2011) Intrahepatically transplanted human cord blood cells reduce SW480 tumor growth in the presence of bispecific EpCAM/CD3 antibody. *Cytotherapy* 13, 108–113

352 Smith, E.J. *et al.* (2015) A novel, native-format bispecific antibody triggering T-cell killing of B-cells is robustly active in mouse tumor models and cynomolgus monkeys. *Sci. Rep.* 5, 17943

353 Stadler, C.R. *et al.* (2016) Characterization of the first-in-class T-cell-engaging bispecific single-chain antibody for targeted immunotherapy of solid tumors expressing the oncofetal protein claudin 6. *Oncoimmunology* 5, e1091555

354 Bacac, M. *et al.* (2016) CEA TCB: A novel head-to-tail 2:1 T cell bispecific antibody for treatment of CEA-positive solid tumors. *Oncoimmunology* 5, e1203498

355 Münch, R.C. *et al.* (2015) Off-target-free gene delivery by affinity-purified receptor-targeted viral vectors. *Nat. Commun.* 6, 6246

356 Cany, J. *et al.* (2013) Natural killer cells generated from cord blood hematopoietic progenitor cells efficiently target bone marrow-residing human leukemia cells in NOD/SCID/IL2Rg(null) mice. *PLoS One* 8, e64384

- 357 Vallera, D.A. *et al.* (2016) IL15 Trispecific Killer Engagers (TriKE) Make Natural Killer Cells Specific to CD33+ Targets While Also Inducing Persistence, In Vivo Expansion, and Enhanced Function. *Clin. Cancer Res. Off. J. Am. Assoc. Cancer Res.* 22, 3440–3450
- 358 Li, Y. *et al.* (2017) Regulatory T cells control toxicity in a humanized model of IL-2 therapy. *Nat. Commun.* 8, 1762
- 359 Schilbach, K. *et al.* (2015) Cancer-targeted IL-12 controls human rhabdomyosarcoma by senescence induction and myogenic differentiation. *Oncoimmunology* 4, e1014760
- 360 Ueda, O. *et al.* (2013) Novel genetically-humanized mouse model established to evaluate efficacy of therapeutic agents to human interleukin-6 receptor. *Sci. Rep.* 3, 1196
- 361 Alcantar-Orozco, E.M. *et al.* (2013) Potential Limitations of the NSG Humanized Mouse as a Model System to Optimize Engineered Human T cell Therapy for Cancer. *Hum. Gene Ther. Methods* 24, 310–320
- 362 Durost, P.A. *et al.* (2018) Gene Therapy with an Adeno-Associated Viral Vector Expressing Human Interleukin-2 Alters Immune System Homeostasis in Humanized Mice. *Hum. Gene Ther.* 29, 352–365
- 363 de Jong, M. and Maina, T. (2010) Of mice and humans: are they the same?-- Implications in cancer translational research. *J. Nucl. Med. Off. Publ. Soc. Nucl. Med.* 51, 501–504
- 364 Mestas, J. and Hughes, C.C.W. (2004) Of Mice and Not Men: Differences between Mouse and Human Immunology. *J. Immunol.* 172, 2731–2738
- 365 Fowler, D.H. (2006) Shared biology of GVHD and GVT effects: potential methods of separation. *Crit. Rev. Oncol. Hematol.* 57, 225–244
- 366 Khwaja, F.W. *et al.* (2006) Proteomic identification of the wt-p53-regulated tumor cell secretome. *Oncogene* 25, 7650–7661
- 367 Ming, B. *et al.* (2017) The efficacy of nivolumab for the treatment of advanced non-small cell lung cancer: a systematic review and meta-analysis of clinical trials. *Int J Clin Exp Med* 10, 153–161
- 368 Wang, C. *et al.* (2014) In vitro characterization of the anti-PD-1 antibody nivolumab, BMS-936558, and in vivo toxicology in non-human primates. *Cancer Immunol. Res.* 2, 846–856
- 369 Ji, R.-R. *et al.* (2012) An immune-active tumor microenvironment favors clinical response to ipilimumab. *Cancer Immunol. Immunother. CII* 61, 1019–1031
- 370 Kirilovsky, A. *et al.* (2016) Rational bases for the use of the Immunoscore in routine clinical settings as a prognostic and predictive biomarker in cancer patients. *Int. Immunol.* 28, 373–382
- 371 Frydrychowicz, M. *et al.* The Dual Role of Treg in Cancer. *Scand. J. Immunol.* 86, 436–443
- 372 Pedersen, L.O. *et al.* (1995) The interaction of beta 2-microglobulin (beta 2m) with mouse class I major histocompatibility antigens and its ability to support peptide binding. A comparison of human and mouse beta 2m. *Eur. J. Immunol.* 25, 1609–1616
- 373 Dzutsev, A. *et al.* (2017) Microbes and Cancer. *Annu. Rev. Immunol.* 35, 199–228
- 374 Vétizou, M. *et al.* (2015) Anticancer immunotherapy by CTLA-4 blockade relies on the gut microbiota. *Science* 350, 1079–1084

- 375 Routy, B. *et al.* (2018) Gut microbiome influences efficacy of PD-1-based immunotherapy against epithelial tumors. *Science* 359, 91–97
- 376 Paulos, C.M. *et al.* (2007) Microbial translocation augments the function of adoptively transferred self/tumor-specific CD8+ T cells via TLR4 signaling. *J. Clin. Invest.* 117, 2197–2204
- 377 Rosshart, S.P. *et al.* (2017) Wild Mouse Gut Microbiota Promotes Host Fitness and Improves Disease Resistance. *Cell* 171, 1015-1028.e13

Annexes

Je joins à mon travail de thèse les publications auxquelles j'ai participé au cours de mon travail d'ingénieur d'étude au sein de l'U932, avant de débiter mon doctorat. Ces travaux permettent d'illustrer mon parcours scientifique, au cours de ces 10 dernières années, qui, n'étant pas dans la norme estudiantine, suit tout de même une constance, accès sur l'immunothérapie anti-cancer.

Je joins, par ailleurs, mon Curriculum vitæ, afin de rendre visible mon parcours scientifique particulier.

ORIGINAL RESEARCH ARTICLE

Different immunogenicity but similar antitumor efficacy of two DNA vaccines coding for an antigen secreted in different membrane vesicle-associated forms

Christine Sedlik^{1,2}, James Vigneron^{1,3,4,5}, Lea Torrieri-Dramard^{3,4,5}, Fabien Pitoiset^{3,4,5}, Jordan Denizeau², Caroline Chesneau¹, Philippe de la Rochere¹, Olivier Lantz^{1,2}, Clotilde Thery^{1,2*} and Bertrand Bellier^{3,4,5,6*}

¹INSERM U932, Paris, France; ²Clinical Investigation Center-IGR-Curie 1428 and Institut Curie, Paris, France; ³Sorbonne University, Université Pierre et Marie Curie, Paris, UMR5_959, I³, Paris, France; ⁴INSERM, UMR5_959, Paris, France; ⁵CNRS, FRE3632, Paris, France; ⁶Department of Biotherapies, Clinical Investigation Center in Biotherapy, AP-HP, Groupe Hospitalier Pitié-Salpêtrière, Paris, France

The induction of an active immune response to control or eliminate tumours is still an unfulfilled challenge. We focused on plasmid DNA vaccines using an innovative approach whereby the antigen is expressed in association with extracellular vesicles (EVs) to facilitate antigen cross-presentation and improve induced immunity. Our two groups had independently shown previously that DNA vaccines encoding EV-associated antigens are more efficient at inducing cytotoxic T-cell responses than vaccines encoding the non-EV-associated antigen. Here, we compared our two approaches to associate the ovalbumin (OVA) antigen to EVs: (a) by fusion to the lipid-binding domain C1C2 of MFG8 (=lactadherin), which is exposed on the surface of secreted membrane vesicles; and (b) by fusion to retroviral Gag capsid protein, which is incorporated inside membrane-enclosed virus-like particles. Plasmids encoding either form of modified OVA were used as DNA-based vaccines (i.e. injected into mice to allow *in vivo* expression of the antigen associated to EVs). We show that both DNA vaccines induced, with similar efficiency, OVA-specific CD8⁺ T cells and total IgG antibodies. By contrast, each vaccine preferentially stimulated different isotypes of immunoglobulins, and the OVA-C1C2-encoding vaccine favoured antigen-specific CD4⁺ T lymphocyte induction as compared to the Gag-OVA vaccine. Nevertheless, both OVA-C1C2 and Gag-OVA vaccines efficiently prevented *in vivo* outgrowth of OVA-expressing tumours and reduced tumour progression when administered to tumour-bearing mice, although with variable efficacies depending on the tumour models. DNA vaccines encoding EV-associated antigens are thus promising immunotherapy tools in cancer but also potentially other diseases.

Keywords: *extracellular vesicles; microvesicles; exosomes; virus-like particles; tumour immunity; vaccination*

Responsible Editor: Aled Clayton, Cardiff University, United Kingdom.

*Correspondence to: Clotilde Thery, INSERM U932, Institut Curie, 26 rue d'Ulm, 75005 Paris, France, Email: clotilde.thery@curie.fr; Bertrand Bellier, I³: Immunologie-Immunopathologie-Immunothérapie, UPMC INSERM UMR5959; CNRS FRE3632, Bat CERVI, Hôpital Pitié-Salpêtrière, 83 Bd Hôpital, 75013 Paris, France, Email: bertrand.bellier@upmc.fr

To access the supplementary material to this article, please see Supplementary files under Article Tools online.

Received: 14 April 2014; Revised: 2 July 2014; Accepted: 17 July 2014; Published: 27 August 2014

Antitumour vaccination is a promising means to induce systemic immunity against malignant cells during both early and metastatic cancer (1). Several sources of tumour-specific antigens can be used,

such as tumour cell extracts, purified proteins, or synthetic peptides known to bind to MHC class I and/or MHC class II molecules and thus activate CD8⁺ and/or CD4⁺ T cells, respectively. However, to induce strong enough immune

[†]These authors contributed equally to the work.

Journal of Extracellular Vesicles 2014. © 2014 Christine Sedlik et al. This is an Open Access article distributed under the terms of the Creative Commons Attribution-NonCommercial 3.0 Unported License (<http://creativecommons.org/licenses/by-nc/3.0/>), permitting all non-commercial use, distribution, and reproduction in any medium, provided the original work is properly cited.

Citation: Journal of Extracellular Vesicles 2014, **3**: 24646 - <http://dx.doi.org/10.3402/jev.v3.24646>

(page number not for citation purpose)

responses, notably cytotoxic T lymphocyte (CTL) responses, these vaccine antigens must be injected together with adjuvants.

Alternatively, genetic immunization using naked plasmid DNA encoding tumour antigens is attracting increasing interest in tumour immunology due to many potential advantages, especially because no adjuvants are required to induce both T-cell and humoral immune responses (2). Injection of DNA in a tissue leads to local transfection of cells, which thus express the desired antigen in a sustained manner. Local dendritic cells (DCs) either can directly express the antigen after DNA transfection and present it to CD8⁺ T cells, or can capture the antigen from surrounding transfected muscle or skin cells, for presentation on major histocompatibility complex (MHC) class II to CD4⁺ T lymphocytes, and cross-presentation on MHC class I to CD8⁺ T lymphocytes (2,3). The specific mechanisms of antigen uptake and presentation by DCs have been the subject of numerous studies, which are reviewed in Refs (4,5). Soluble antigens were shown more than a decade ago to be less efficiently presented *in vivo* to CD4⁺ and, more strikingly, to CD8⁺ T cells than their cell-associated counterparts (6). Consistently, it was shown recently that a soluble antigen fed to DCs was only presented on MHC class II molecules, whereas a liposome-encapsulated form directed to early endosomes was presented on both MHC class I and class II (7) and that specific signalling pathways in DCs controlled cross-presentation of particulate but not soluble antigens (8). Thus, to promote both cross-presentation on MHC class I and presentation on MHC class II molecules, especially for tumour vaccination, particulate antigens might be preferentially used.

Membrane-enclosed vesicles, such as exosomes or any type of extracellular vesicles (EVs), represent an interesting source of particulate antigens. Exosomes secreted by tumours have been shown to contain endogenous tumour antigens and to transfer them to DCs for induction of antitumour immune responses (9). Immunization of mice with exosomes purified from antigen-pulsed DCs induced much more efficiently antibody and CD4⁺ T-cell responses than immunization with the native antigen itself (10). We have shown that tumour cells secreting a model antigen as an EV-associated form induced antitumour immune responses and were controlled by the adaptive immune system, as opposed to the same tumour cells secreting the antigen as a soluble form (11). Thus, inducing secretion of an antigen as an EV-associated form upon DNA vaccination represents a promising strategy for immunotherapy.

We previously validated two strategies that allow antigen secretion in association with EVs. In one approach (11), antigen was fused to the lipid-binding C1C2 domain of milk fat globule – EGF Factor VIII (MFGE8), also called lactadherin, a secreted protein that is highly enriched on mouse DC-derived exosomes (12). This C1C2 domain is homologous to the C-terminal domain of blood coagulation

factor V and factor VIII, and binds to phosphatidylserine exposed at the surface of apoptotic cells (13) or DC-derived exosomes (14). As a result, antigens fused to C1C2 and coupled to a signal peptide are secreted on small EVs, including exosomes (11). Consequently, we showed that a DNA vaccine encoding EV-associated ovalbumin (OVA) antigen was more efficient to induce antigen-specific CD8⁺ T cells *in vivo* and to protect mice against growth of an OVA-expressing tumour than a DNA vaccine encoding the soluble secreted OVA (11). The C1C2 fusion approach has also been recently used by two other groups, in the context of prostate (15) or breast (16) tumour antigens.

In the second approach, the antigen is carried by recombinant virus-like particles (VLPs). VLPs, composed of one or more structural viral proteins but no genome of native viruses, mimic the organization and conformation of authentic virions but have no capability to replicate in cells, potentially yielding safe vaccine candidates. VLPs have been recently used as a platform for inducing immune responses against heterologous antigens. We have developed recombinant retrovirus-derived VLPs made of Gag from the Moloney murine leukaemia virus (MLV), which induces budding of pseudo-viruses from the plasma membrane (17). Antigens can be inserted onto or into the retroviral VLPs by fusion with the transmembrane domain of vesicular stomatitis virus glycoprotein or with MLV Gag, respectively (18,19). These recombinant VLPs can be produced either *ex vivo* after cell transfection with plasmid DNA encoding wild-type or chimeric Gag proteins and envelope glycoproteins, or *in vivo* after injection of the same plasmid DNA. We previously demonstrated that retroVLP-encoding DNA induces higher cellular and humoral immune responses against viral antigens than a control DNA vaccine encoding viral antigens but unable to form VLPs due to a mutation in Gag (18–20). This strategy was initially developed and validated as an antiviral vaccine (e.g. against hepatitis C), but we recently pointed out its usefulness in oncology (21).

Because we had already demonstrated the superiority of these two types of EV-targeted antigens over their corresponding non-EV-targeted version in a DNA vaccination approach (11,18), here we compared side-by-side our two EV-targeting approaches in terms of induction of immune responses and antitumour efficacy, using OVA as a model tumour antigen. Two DNA vaccines encoding either Gag-OVA or OVA-C1C2 fusion proteins were *in vivo* administered, and we analysed CD4⁺ T, CD8⁺ T, and B lymphocyte-induced immune responses, and growth of OVA-expressing tumours, in prophylactic and therapeutic settings using several tumour cell lines. Our results show that the two DNA vaccines encoding an antigen secreted in association with vesicles induce efficient immune responses and antitumour activities, but with differences in the quality of these immune responses, especially in terms of resulting immunoglobulins.

Materials and methods

Plasmids and DNA vaccination

Empty pcDNA3.1/hygro (mock) and pcDNA3-OVA-C1C2 (OVA-C1C2) plasmids have been described previously (11). pGag-OVA (pBL196 Gag-OVA) encodes, under cytomegalovirus promoter, a full-length OVA protein fused with MLV Gag p55 protein in the C-terminal position. The OVA-encoding cDNA (*OVAL* gene) was amplified by PCR from the chicken OVA cDNA (pcDNA3-OVA) with primers containing Mlu-I and Xba-I restriction sites, digested with Mlu-I and Xba-I, and then inserted by ligation into pBL36 as previously described (21). All DNA plasmids were purified using the Nucleobond PC endotoxin-free kit (Macherey-Nagel) according to the manufacturer's instructions and resuspended in H₂O. DNA concentration was measured using a nanodrop (LabTech France).

Cells

HEK293T (CRL-1573; ATCC), MCA-OVA [MCA101 fibrosarcoma secreting soluble OVA (11)], B16F10-OVA (melanoma expressing OVA, kindly provided by K. Rock), and EL4-OVA (EG7 thymoma, ATCC, CRL-2113) cells were grown in Dulbecco's Modified Eagle Medium (DMEM) supplemented with β -mercaptoethanol, 2 mM L-glutamine, 100 U/mL penicillin, 100 μ g/mL streptomycin (all from LifeTechnologies, Cergy Pontoise, France), and 10% heat-inactivated foetal calf serum. Hygromycin or Geneticin[®] was included in the culture medium of MCA-OVA or B16F10-OVA/EL4-OVA, respectively.

OVA-containing EV purification

HEK-293T cells were transfected using a calcium phosphate transfection protocol, as previously described (21) with plasmids encoding Gag-OVA or OVA-C1C2 or with pcDNA3.1, as control. Supernatants were collected, filtered through 0.45- μ m pore-sized membranes, and concentrated with Centricon (Millipore, Molsheim, France). For total EV isolation, supernatants were layered on top of a sucrose step gradient (2.5 mL, 35%; 2.5 mL, 50%) and centrifuged at 100,000g for 2 hours at 4°C. Interface was collected and washed with phosphate-buffered saline (PBS) (21). For separation of different types of EVs (22), supernatants were centrifuged in a SW32.1 rotor (Beckman) at 300g for 5 minutes to eliminate floating cells, at 2,000g for 20 minutes to remove cell debris, and at 10,000g for 40 minutes to separate large vesicles. An ultracentrifugation step at 100,000g for 75 minutes was performed to pellet small EVs, including exosomes and VLPs, and an extra centrifugation at 200,000g for 90 minutes was performed to isolate vesicles smaller than 100 nm and protein aggregates. Each pellet was washed in PBS and centrifuged at the same speed to eliminate contaminant proteins.

Western blot

Ten percent of each pellet was diluted in LDS sample buffer containing sample-reducing agent (LifeTechnologies), boiled for 5 minutes at 95°C, and separated by SDS-PAGE (LifeTechnologies) for 75 minutes at 150 V. Proteins were transferred from gels to a nitrocellulose membrane using the iBlot[®] Dry Blot System (LifeTechnologies). Membranes were incubated in Western dot blocking buffer (Molecular probes) for 30 minutes. Primary anti-OVA antibody (#ABIN400491; Antibodies-Online) was incubated in wash buffer (Molecular Probes) overnight at 4°C in a rotating shaker. Secondary anti-rabbit antibodies labelled with biotin (Molecular Probes) were incubated for 60 minutes in wash buffer. Streptavidin coupled to Qdot 655 were incubated for 60 minutes in wash buffer. Membranes were analysed under ultraviolet light camera.

Nanoparticle tracking analysis (NTA)

Suspensions containing purified Gag-OVA or OVA-C1C2 EVs were analysed using a LM10 instrument (NanoSight, UK). Each sample was diluted 1:1,000, and 5 measurements (video of 60 seconds) were done with a frame rate of 30 frames/s; the camera gain and shutter were set at 250 and 11.23 ms, respectively. Particle movement was analysed by NTA software (NanoSight) with a single detection threshold for all samples; minimal track length and minimal expected particle size were set at automatic level and 30 nm, respectively.

OVA quantification in the EVs

Anti-OVA polyclonal rabbit antibody (#ABIN400491; Antibodiesonline) was diluted in carbonate–bicarbonate buffer at 1:2,000, coated overnight at 4°C on MediSorp 96-well plates (ThermoFischer), and washed with PBS-0.05% Tween 20. Plates were incubated during 1 hour with PBS-5% bovine serum albumin, and samples were added for 2 hours at room temperature after washing. Samples were either supernatants collected from 0.5×10^6 plated cells 2 days after transfection with Gag-OVA, OVA-C1C2, or mock plasmids and treated with Triton-X100 detergent; or the pellets obtained after EV purification, treated or not with Triton-X100. Bound OVA was revealed by polyclonal mouse anti-OVA (#ABIN316446, at 1:2,000), followed by HRP-conjugated anti-mouse antibodies (Jackson Immunoresearch, 115-035-166) revealed by TMB-substrate solution (BD OptEIA). Reaction was stopped with 1 N HCl, and absorbance was read at 450 nm.

Mice and vaccination

Five or six-week-old female C57BL/6J mice were purchased from Charles River France, and C57BL/6 *Rag2*^{-/-} mice were bred at the Institut Curie animal facility. The care and use of animals used here strictly apply the European and National Regulation for the Protection of Vertebrate

Animals Used for Experimental and Other Scientific Purposes in force (facility licence #C75-05-18). It complies also with internationally established principles of replacement, reduction, and refinement in accordance with Guide for the Care and Use of Laboratory Animals (NRC 2011). Mice were anesthetized with ketamine (100 mg/kg) and xylazine (7.25 mg/kg), and plasmid DNA (5 or 30 µg) was administered intramuscularly (i.m.) in one hind leg or intradermally (i.d.) at 2 sites on the lower back in 50 µl of saline buffer using a 500 µl insulin needle (Terumo). DNA injection was followed by electroporation applied with a generator (BTX, ECM30) with 20 ms/pulse, 8 pulses at 200 V/cm using specific electrodes: CUY647 or CUY650 (Sonidel Limited, Ireland) for i.m. or i.d. immunization, respectively. Conductive gel was used to ensure electrical contact between the electrodes and the skin.

Quantification of CD4⁺ and CD8⁺ T-cell responses

Ten to twelve days after immunization, blood samples were collected by retro-orbital puncture. Total peripheral blood mononuclear cells (PBMC) were stained with PE-conjugated H-2Kb-SIINFEKL tetramer (Beckman Coulter), anti-CD8 and anti-T cell receptor (TCR) antibodies (BD Biosciences), followed by red blood cell lysis to quantify OVA-specific CD8⁺ T cells. Cells were analysed using a standard LSR-II flow cytometer (BD Biosciences), and the fluorescence-activated cell scanner (FACS) data were analysed using FlowJo software. The tetramer⁺ cells were gated on TCR⁺ CD8⁺ cells. Interferon (IFN) γ -producing OVA-specific CD4⁺ or CD8⁺ T cells were measured by ELISPOT on PBMC after red blood cell lysis. Briefly, microplates (Multiscreen HTS IP, Millipore) were coated with anti-murine IFN γ antibody (Diaclone). PBMC (0.2 \times 10⁶/well) were cultured overnight in the presence of either control medium or the 257–264 (SIINFEKL) class I-restricted OVA peptide (10 µM) or the 265–280 (TEWTSSNVMEERKIKV) class II-restricted OVA peptide (40 µM) (Polypeptide Group, Strasbourg, France) in complete medium (RPMI-Glutamax, 10% foetal calf serum, antibiotics, and β -mercaptoethanol). The detection was performed with biotinylated anti-IFN γ (matched pairs, Diaclone) followed by streptavidin-alkaline phosphatase (Mabtech) and revealed using the appropriate substrate (Biorad). Spots were counted using an ELISPOT Reader System ELR02 (AID, Germany), and results were expressed as the number of cytokine-producing cells per 1 \times 10⁶ PBMC.

In vivo cytotoxicity assay

CD45.1⁺ carboxyfluorescein succinimidyl ester (CFSE) high (CFSE^{hi}) peptide-pulsed (5 µg/mL SIINFEKL peptide for 60 minutes at 37°C) C57BL/6 splenocytes (target cells) and CFSE low (CFSE^{lo}) unpulsed splenocytes (control cells), previously labelled with respectively 5 or 0.5 µM CFSE (LifeTechnologies) for 15 minutes at 37°C,

were mixed at a 1:1 ratio, and 1 \times 10⁷ total cells were injected intravenously (i.v.) into CD45.2⁺ mice immunized 10 days before with 10 µg of DNA (i.m. or i.d.). Five hours later, splenocytes from each mouse were analysed by FACS to detect the presence of CD45.1⁺ cells. Antigen-specific CTL lytic activity was measured by the disappearance of peptide-pulsed targets, and expressed as clearance efficiency calculated as follows: $\{1 - [\% \text{ antigen-pulsed (CFSE}^{\text{hi}}) \text{ cells} / \% \text{ antigen-unpulsed (CFSE}^{\text{lo}}) \text{ cells}]\} \times 100\%$.

Quantification of OVA-specific antibody responses

Twelve days after immunization, sera were collected by retro-orbital puncture and OVA-specific immunoglobulins were measured by standard ELISA. Briefly, Maxisorp 96-well plates were coated at 4°C with OVA (10 µg/mL) in carbonate-bicarbonate buffer. After blocking with PBS–5% milk for 2 hours, serially diluted sera were added for 2 hours at room temperature. After extensive washing, alkaline phosphatase-conjugated anti-mouse IgG, IgG1, or IgG2b (Jackson ImmunoResearch) was added to each well, and plates were incubated 1 hour at room temperature. After extensive washing, alkaline phosphatase activity was measured adding the CDP-star[®] Ready-to-Use substrate (Applied Biosystems). The microplates were read using a Centro LB 960 luminometer (Berthold), and sample sera were compared to a positive standard curve to express the results in arbitrary units (AU).

In vivo tumour assays

0.5 \times 10⁶ MCA-OVA or B16F10-OVA cells, or 1 \times 10⁶ EL4-OVA cells, were administered subcutaneously (s.c.) into the shaved flank of the mice. Tumour growth was measured twice a week using a caliper to determine the tumour size, calculated as $\text{length} \times \text{width} \times [(\text{length} + \text{width})/2]$. Mice were sacrificed when the tumour reached 2 to 2.5 cm³, and the sacrifice day was recorded to plot survival of the mice. For the lung tumour model, 0.5 \times 10⁶ MCA-OVA or 0.2 \times 10⁶ B16F10-OVA cells were injected i.v. Mice were sacrificed 20 days later, and tumour burden was assessed by counting lung foci. The MCA-OVA lung nodules were counted after ink injection. For tumour prevention experiments, mice were immunized with DNA vaccines as indicated in the figures, and tumour cells were injected s.c. 10 days later. For tumour therapeutic settings, tumour cells were injected s.c. or i.v., and mice received DNA vaccines 3 or 6 days later.

Statistical analyses

For all experiments, normality of distribution of the samples and similarity of dispersions of the groups were tested. In most cases, these criteria were not reached, hence non-parametric statistical tests were used as follows: for experiments comparing a single measure of more than 2 experimental groups, Kruskal–Wallis followed by Dunn post-hoc test; for tumour growth measurement over time,

one-way ANOVA with repeated measures followed by Tukey's post-hoc test; and, for survival, a log-rank test was performed.

Results

Characterization of OVA-associated EVs generated from the two DNA vaccines

We developed two different vaccine strategies whereby the antigen is expressed in association with EVs. First, OVA was fused in-frame in the C-terminal part of the MLV Gag polypeptide precursor (p55) and thus incorporated into the pseudo-particles produced after self-assembly and budding of Gag-OVA from the plasma membrane (Fig. 1A). Second, OVA was inserted between the mouse MFG8-derived signal sequence and lipid-binding C1C2 domain, resulting in an antigen exposed on the surface of secreted membrane vesicles (OVA-C1C2; Fig. 1A). Therefore, fusion of OVA antigen to either Gag or MFG8 domains allows the secretion of the antigen associated in a topologically different manner to EVs, predicted inside the vesicles secreted by Gag-OVA-expressing cells, but at the surface of vesicles from OVA-C1C2-expressing cells. To confirm this predicted topology, we quantified OVA by ELISA in the conditioned medium of transfected HEK293T cells, and in EVs recovered by differential ultracentrifugation from this conditioned medium, after or not, disruption of membranes by detergent. From the two plasmids, OVA was as efficiently expressed as shown by a similar overall level of OVA detected in the conditioned medium treated with detergent (Fig. 1B, supernatant). Similar levels of OVA were also quantified in vesicles recovered by 100,000g ultracentrifugation in the presence of Triton-X100 (Fig. 1B, Pellet+Det). By contrast, OVA was efficiently detected by OVA-specific antibodies in intact vesicles secreted by OVA-C1C2-transfected cells, whereas it was hardly detectable when Gag-OVA-derived vesicles were kept intact (Fig. 1B, Pellet), thus confirming that antigen is inside these Gag-OVA EVs, whereas antigen is outside the OVA-C1C2 EVs.

To characterize more precisely the type of EVs produced after expression of Gag-OVA or OVA-C1C2 DNA vaccines, we performed Western blot analysis of transfected cell supernatants purified by different methods. When concentrated conditioned medium was ultracentrifuged into a gradient of sucrose solutions with different concentrations, both Gag-OVA and OVA-C1C2 were detected at the interface between 35 and 50% sucrose (Fig. 1C, left panel), that is, in vesicles of 1.15–1.20g/mL density, classically described for EVs (23). Interestingly, OVA was associated with a large range of EVs produced from Gag-OVA-expressing cells, as shown by the presence of OVA in all the pellets collected upon differential ultracentrifugation (2,000g, 10,000g, 100,000g, and 200,000g; Fig. 1C, right panel). Both full-length and cleaved Gag-

OVA-containing fragments were observed (bands 1 and 3 in Fig. 1C). By contrast, in OVA-C1C2-transfected cell supernatants, OVA was recovered mainly in the 100,000g pellet (Fig. 1C, right panel). Again, both OVA-C1C2 and OVA-containing fragments (respectively, bands 2 and 4 in Fig. 1C) were detected. Interestingly, we observed that Gag-OVA and OVA-C1C2 vesicles of the 100,000g pellets were of similar and homogeneous diameters of 180–220 nm, as measured by nanoparticle tracking analysis (Fig. 1D), thus slightly bigger than the expected diameters of 80–100 nm and 80–120 nm, respectively. This observation is probably due to analysis of EVs and VLPs in their native conformation by NTA, rather than after fixation and dehydration as classically done by electron microscopy. Thus, both OVA fusion proteins are secreted in association with EVs, but they display different topologies, and Gag-OVA appears to be associated with more subtypes of vesicles.

CD8⁺ and CD4⁺ T-cell responses induced by the two DNA vaccines

The two plasmids were used as vaccines in mice resulting in *in vivo* secretion of OVA in an EV-associated form. Electroporation (i.e. a mild local electric shock administered immediately after DNA injection) was used to improve efficacy of *in vivo* transfection (24). The presence of OVA-specific T lymphocytes was quantified in the blood, 10 days after a single vaccination with 5 µg (Fig. 2A) or 30 µg (Fig. 2B) of DNA, by flow cytometry. The percentage of CD8⁺ T cells binding H-2Kb-SIINFEKL tetramers (Fig. 2, left panels) and the number of IFN γ spot-forming cells after restimulation with MHC-I or MHC-II binding peptides (Fig. 2, middle and right panels, respectively) were measured. We observed that Gag-OVA and OVA-C1C2 DNA vaccines induced OVA-specific CD8⁺ T lymphocyte expansion with identical efficacy whatever the dose used for vaccination (Fig. 2A and B, left panels). Interestingly, CD8⁺ T-cell responses were also induced at similar levels when mice were vaccinated with Gag-OVA or OVA-C1C2 by i.d. DNA injection (Supplementary Fig. 1A). These OVA-specific CD8⁺ T cells were similarly functional because they produced IFN γ with the same frequency in response to the specific antigenic peptide after i.m. vaccination (Fig. 2A–B, centre panels) or lysed *in vivo* with the same efficacy peptide-loaded target cells after i.d. or i.m. vaccination (Supplementary Fig. 1B). Induction of OVA-specific CD4⁺ T lymphocytes was also equally efficient upon vaccination with 30 µg of Gag-OVA or OVA-C1C2 (Fig. 2B, right panel). However, when a lower dose (5 µg) of DNA vaccine was injected, OVA-C1C2 induced significantly higher numbers of OVA-specific CD4⁺ T cells as compared to both mock or Gag-OVA vaccination (Fig. 2A, right panel).

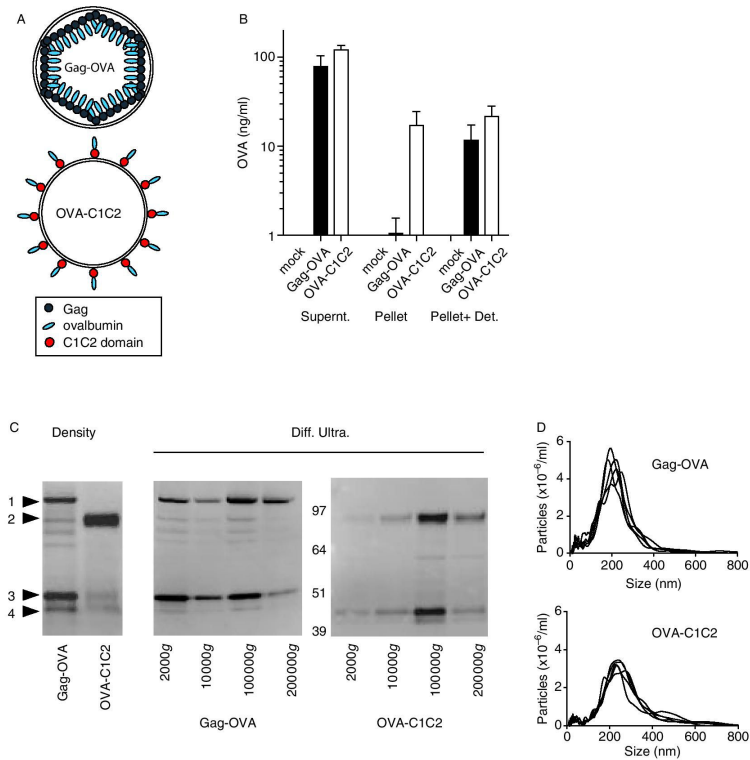


Fig. 1. Characterization of the vesicles with associated antigen generated from the two constructs. (A) Schematic representation of the expected topology of Gag-OVA- and OVA-C1C2-containing vesicles. Recombinant retroviral VLPs (top) are formed by MLV Gag capsid proteins fused with OVA antigen. Secreted vesicles (bottom) carry on their surface OVA antigens fused to the lipid-binding domains (C1C2) of MFGE8. (B) Quantification by ELISA of OVA secretion by HEK cells upon transfection with mock (non-OVA-encoding), Gag-OVA, and OVA-C1C2 plasmids. Total conditioned medium in the presence of detergent (supernatant), the pellet obtained after 100,000g ultracentrifugation, and the same pellet in the presence of detergent (Pellet+Det.) were compared. Mean \pm SD of 4 independent experiments are shown. (C) Western blot analysis of OVA in Gag-OVA- or OVA-C1C2-expressing cells and their supernatant after pelleting into a sucrose gradient (density, left blot) or after differential centrifugation (Diff. Ultra.: pellets obtained at 2,000g, 10,000g, 100,000g, and 200,000g). Arrows indicate the four main forms of OVA detected in the different samples. (D) Particle size distribution profiles of Gag-OVA and OVA-C1C2 vesicles measured by nanoparticle tracking analysis. Supernatant of HEK cells transfected with plasmids encoding Gag-OVA or OVA-C1C2 was submitted to ultracentrifugation at 100,000g, and pellets were analysed by nanoparticle tracking (distribution of 5 videos per sample is shown).

Antibody responses induced by the two DNA vaccines

Because a difference in helper CD4⁺ T cell responses was observed after vaccination with the two plasmids, we then asked if antibody responses, most of which are dependent on helper T cells, were also different. When quantifying total OVA-specific IgG in blood at day 12, we observed efficient and comparable responses induced by both i.m. vaccines, whatever the amount of DNA used (Fig. 3A

and B, left panels). However, isotypes of IgGs induced by the two vaccines were different. OVA-C1C2 induced significantly higher levels of specific IgG1 antibody as compared to Gag-OVA (at 5 μ g/mouse), whereas levels of OVA-specific IgG2b antibodies were slightly higher in the Gag-OVA group at the low and high doses of vaccines, even if the difference was not statistically significant (Fig. 3A and B, two middle panels). The ratio of OVA-specific

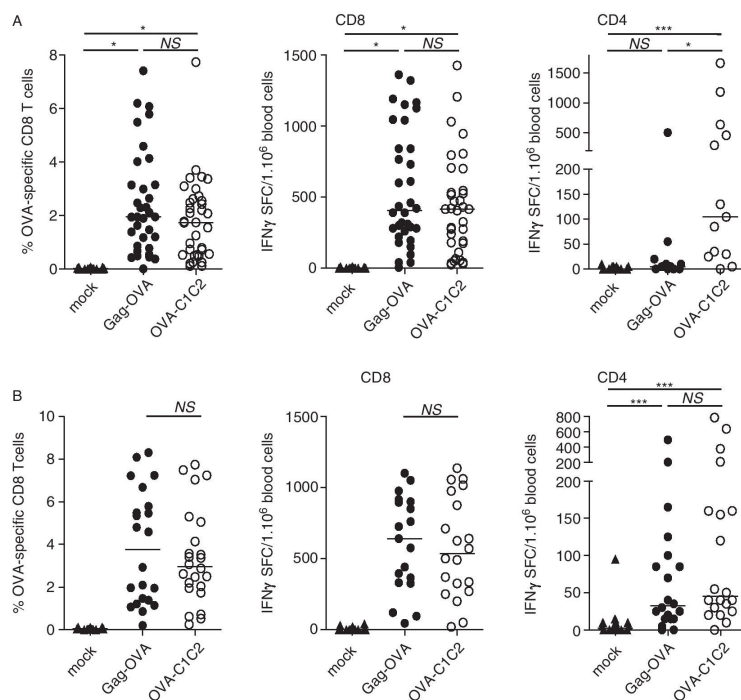


Fig. 2. CD8⁺ and CD4⁺ T cell responses induced by the two DNA vaccines. Mice were immunized once with either 5 µg (A) or 30 µg (B) of DNA coding for mock, Gag-OVA, or OVA-C1C2 plasmids. Immune responses were *ex vivo* analysed on blood cells at day 10–12 after immunization. Frequency of OVA-specific CD8⁺ T cells was measured using the H-2Kb-SIINFEKL tetramer (left panels), and the number of OVA-specific IFN γ -producing CD8⁺ or CD4⁺ T cells was determined by ELISPOT after 18 hours of stimulation with the appropriate peptide (middle and right panels). Each dot represents an individual mouse, and lines indicate the median. Pooled data from 3 or 4 independent experiments are shown. * $p < 0.05$; *** $p < 0.001$; NS = not significantly different (Kruskal–Wallis with Dunn post-hoc test).

IgG2b to IgG1 antibodies, commonly used as an indicator of CD4⁺ helper T-cell bias toward either Th1 or Th2, was significantly higher after low-dose Gag-OVA than OVA-C1C2 vaccination (Fig. 3A, right panel), suggesting that Gag-OVA may bias more strongly immune responses toward Th1. In contrast, OVA-C1C2, which induced higher levels of IgG1 than Gag-OVA when a low dose of DNA was used (Fig. 3A), may induce a mixture of Th1- and Th2-type helper cells. However, these differences are not significant when high doses of DNA are used (Fig. 3B). Altogether, these results thus show dose-dependent specific immune properties of the two vaccines. Interestingly, the same differences in the ratio of IgG2b to IgG1 isotypes induced after Gag-OVA or OVA-C1C2 were obtained after vaccination by *i.d.* route (Supplementary Fig. 1C).

Prevention of tumour outgrowth by the two DNA vaccines

We then asked if adaptive immune responses induced by the two vaccines could affect the tumour growth. The C57BL/6-derived MCA101 fibrosarcoma secreting OVA (MCA-OVA) was used, as it is known to be poorly immunogenic (11,25). Mice were *i.m.* vaccinated with either mock or EV-associated OVA antigen encoding plasmids, 10 days before *s.c.* graft of the MCA-OVA tumour cells. In preventive settings, we observed that a low dose (5 µg) of either Gag-OVA or OVA-C1C2 was sufficient to strongly reduce subsequent growth of the tumour and extended the survival of tumour-bearing mice (Fig. 4A), whereas a high dose of DNA fully abolished tumour growth and fully protected mice (Fig. 4B). Importantly, this antitumour effect was not observed after vaccination

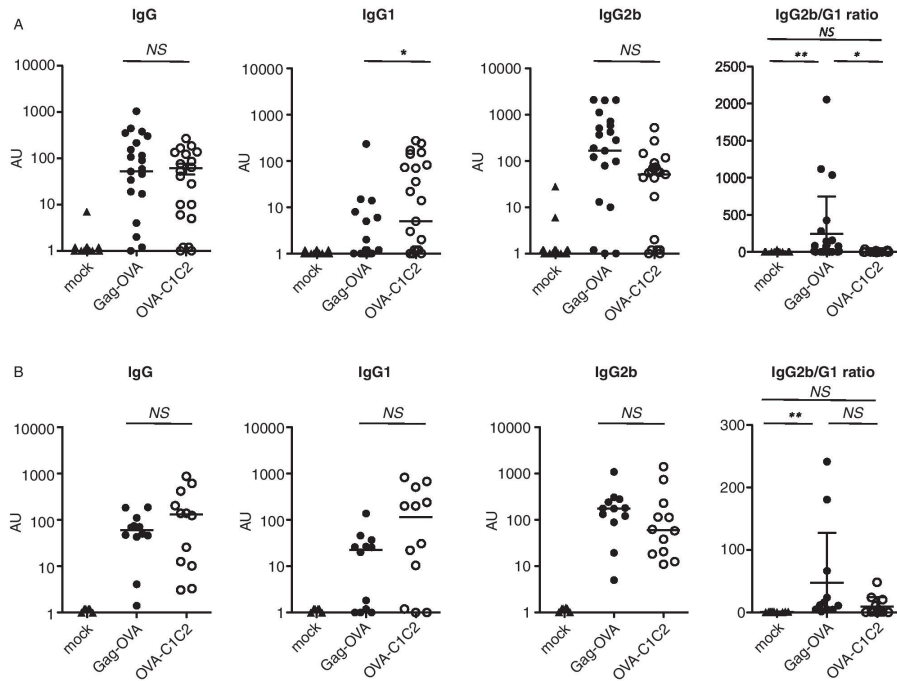


Fig. 3. Different types of antibody isotypes are produced in response to the two DNA vaccines. Mice were immunized once with either 5 µg (A) or 30 µg (B) of plasmids coding for mock, Gag-OVA, or OVA-C1C2. OVA-specific total IgG, IgG1, and IgG2b were measured by ELISA in sera at day 12 after immunization. Arbitrary units for individual mice and median are represented. The ratio between IgG2b and IgG1 isotypes was calculated and shown on the right panels. Pooled data from 3 (A) or 2 (B) independent experiments are shown. * $p < 0.05$; NS = non-significant (Kruskal–Wallis with Dunn post-hoc test).

in *Rag2*^{-/-} mice, which are devoid of functional T and B cells (Fig. 4C), demonstrating that the antitumour activity observed in Fig. 4A and B is due to specific adaptive immune responses generated by the vaccines.

Antitumour efficacy of the two DNA vaccines administered in therapeutic settings

Next, we sought to examine the vaccines' potency in more relevant therapeutic models, through the treatment of mice that have already been inoculated with tumours. C57BL/6 mice grafted s.c. with OVA-expressing tumours were i.m. vaccinated with Gag-OVA, OVA-C1C2, or control plasmids. Different tumour cell lines displaying different levels of MHC class I molecules and different levels of aggressiveness were tested. Although both vaccines efficiently prevented MCA-OVA growth in a prophylactic setting (Fig. 4B), they did not impair progression of the already growing tumour implanted s.c. (Fig. 5A, left panel).

Similar results were observed with B16F10-OVA tumours (Fig. 5A, right panel). By contrast, when a more immunogenic tumour was used (the OVA-expressing EL4 thymoma), both vaccines efficiently delayed tumour growth and even prevented the tumour growth in about 60% of surviving animals (Fig. 5B). For the two tumours that were not controlled by vaccination when growing s.c., we next investigated whether the EV-associated OVA-encoding vaccines affected their ability to form pseudo-metastases. Mice were injected i.v. with OVA-expressing MCA or B16F10 tumour cells, vaccinated or not 3 days later, and tumour nodules were monitored in lungs at day 20 (Fig. 5C and Supplementary Fig. 2). In these conditions, vaccination with the Gag-OVA plasmid efficiently reduced development of metastases in the MCA-OVA tumour model as compared to the mock vaccine, and vaccination with OVA-C1C2 significantly reduced metastases in both tumour models (Fig. 5C).

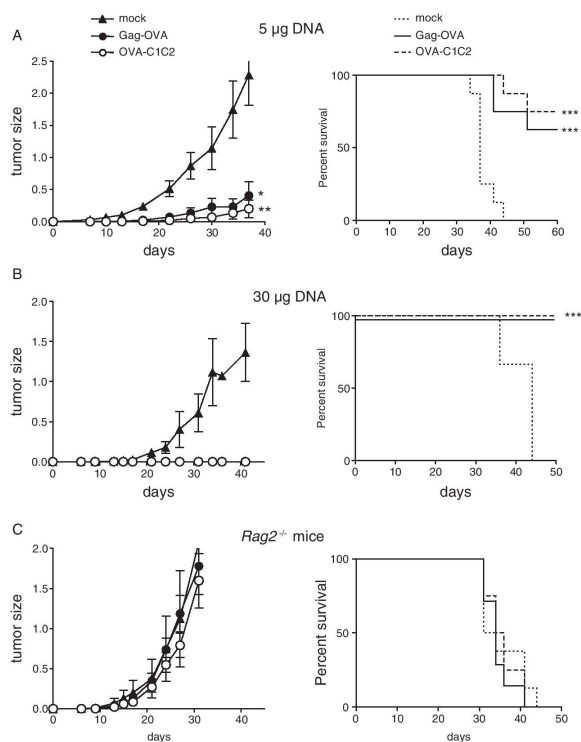


Fig. 4. Prevention of tumour outgrowth by the two DNA vaccines. WT C57BL/6 (A, B) or immunodeficient *Rag2*^{-/-} C57BL/6 mice (C) were vaccinated once with Gag-OVA or OVA-C1C2 plasmid DNA at the dose of 5 µg (A) or 30 µg (B, C); and 10 days later, MCA-OVA tumour cells were grafted. Control mice were injected with the mock DNA. Results from the same experiment are shown as tumour size (left panel, mean ± SD of 8 mice) and survival percentage (right panel). (A, B) are representative of 3 experiments, and (C) of 2 experiments. **p* < 0.05; ***p* < 0.01 for tumour size (one-way ANOVA with repeated measures and Tukey post-hoc test); ****p* = 0.0005 for Gag-OVA; ****p* = 0.0002 for OVA-C1C2 for mice survival (log rank test).

Discussion

Among the variety of vaccine formulations, immunization with plasmid DNA has several advantages compared with other approaches: DNA plasmids are easy to produce in large amounts and in clinical-grade conditions, safe, stable upon storage at various temperatures, ready to deliver, and molecularly defined. However, translation of DNA vaccines into the clinical setting has been hampered by their limited immunogenic potency in humans, especially due to the difficulty to scale up from mice to humans the injected volume for the i.m. route. In recent years, however, the development of electroporation devices designed to increase the efficacy of *in vivo* transfection of tissues by injected DNA (26,27) and authorization of these devices for clinical use in humans

(28,29) have renewed the clinical interest in this approach, and led to several on-going clinical trials for both cancer and infectious diseases (24,30).

Immunogenicity of DNA vaccines can also be improved by controlling the nature of the expressed antigens. Our two groups had previously independently shown that an EV- (11) or VLP-associated antigen (18) induced more efficient CD8⁺ T-cell immune responses than the non-EV-associated counterpart, in the context of DNA vaccination. We thus compared side-by-side here these two strategies associating the same model antigen to different types of vesicles. Our results show that both induce, with similar efficacy, antigen-specific CD8⁺ CTLs and antibodies, as well as antitumour activity. Interestingly, however, the CD4⁺ helper T-cell immune responses induced by our

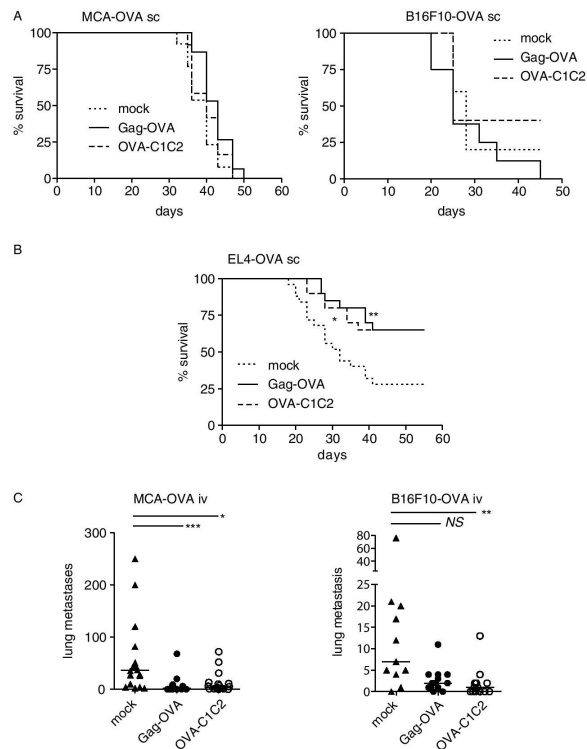


Fig. 5. Antitumour efficacy of the two DNA vaccines administered in therapeutic settings. Mice were subcutaneously grafted with (A) MCA-OVA (left panel) or B16F10-OVA (right panel) or (B) EL4-OVA tumour cells and immunized 3 days (MCA-OVA and EL4-OVA) or 6 days (B16F10-OVA) later with 30 μ g of mock, Gag-OVA, or OVA-C1C2 plasmids. Results are shown as survival percentage. * $p < 0.05$; ** $p = 0.01$ (log rank test). Pooled data from 2 (MCA-OVA), 1 (B16F10-OVA), or 3 (EL4-OVA) independent experiments are shown ($n = 20$ –25 per group). (C) MCA-OVA or B16F10-OVA tumour cell lines were injected intravenously, and mice were immunized 3 days later with 30 μ g of mock, Gag-OVA, or OVA-C1C2 plasmids. After 20 days, tumour nodules in lungs were counted. Quantification of the lung nodules in individual mice is represented. Pooled data from 2 (B16F10-OVA) or 3 (MCA-OVA) independent experiments are shown, and horizontal bars are the medians. * $p < 0.05$; ** $p < 0.01$; *** $p < 0.001$; NS = not significant (Kruskal–Wallis followed by Dunn post-hoc test).

two vaccines are different: the EV-associated antigen (OVA-C1C2) promotes efficiently $CD4^+$ T-cell activation and induces a balanced mix of IgG1 and IgG2b, whereas the VLP-associated antigen (Gag-OVA) induces lower amounts of $CD4^+$ T cells, and more IgG2b than IgG1 antibodies. This antibody pattern suggests that the Gag-OVA vaccine induces $CD4^+$ Th1-polarized responses (known to promote class switching to IgG2b in B cells), whereas OVA-C1C2 induces Th1 but also Th2 immune responses (which direct the B-cell class switch to IgG1). We could not, however, directly demonstrate a specific $CD4^+$ Th cell orientation

induced by the two vaccines, because $IFN\gamma$ was the only cytokine we could detect by cytokine-secretion assay (data not shown) and by ELISPOT (Fig. 2); all other tested cytokines (IL-4, IL-5, IL-13, IL-10, IL-2, and $TNF-\alpha$) secreted by T cells were below the detection limit, as measured by cytokine secretion assay in *in vitro* antigen-restimulated PBMC (data not shown). Our results are consistent with previously published results of Qazi et al. (10) showing induction of both IgG1 and IgG2a upon vaccination of mice with exosomes secreted by OVA-fed dendritic cells, whereas non-exosome-associated OVA

induced mostly IgG1 (i.e. Th2 responses). The OVA-C1C2 plasmid used here induces similar mixed Th1 and Th2 helper responses as OVA-loaded exosomes (10), whereas the Gag-OVA plasmid biases these responses more strongly toward Th1.

Our results thus highlight a difference in presentation of the OVA antigen to CD4⁺ T cells and B lymphocytes, but no difference in MHC class I-restricted presentation to CD8⁺ T cells, upon vaccination with our two different forms of OVA. The reasons for these differences are beyond the purpose of the present study. We can, however, propose some hypotheses worth exploring in future work, based on previously reported or here observed structural differences of the EVs generated by the two DNA vaccines.

First, as shown in Fig. 1, OVA antigen fused with the C1C2 domain of MFGE8 is exposed onto secreted EVs, whereas when fused with the retroviral Gag capsid protein, it is incorporated inside VLPs. Therefore, secreted EVs with exposed OVA-C1C2 can bind directly to the B-cell receptor of OVA-specific B cells, thus allowing formation of MHC class II-OVA peptide complexes in the B cells and proper stimulation by helper CD4⁺ T cells. In contrast, the intra-VLP Gag-OVA must be released from its envelope to be recognized by B lymphocytes, and efficiently allow activation by helper CD4⁺ T cells and consequent IgG production. Such release could take place upon necrosis of the Gag-OVA-expressing cells in the vaccinated tissue.

Endogenous EVs and Gag-induced VLPs also differ by other characteristics. In particular, we observed (Fig. 1C) that, upon transient *in vitro* transfection, Gag-OVA is secreted in a wide range of vesicles, including large EVs pelleting at low speed, which may contain apoptotic cell-derived materials (31), whereas OVA-C1C2 is not detected in this low-speed pellet. The different types of EVs and VLPs released upon Gag-OVA transfection may have opposite effects on the immune responses, and the final outcome would thus depend on the relative level of each type of EV available *in vivo*, which is difficult to quantify. These different EVs, however, were observed *in vitro* and, due to technical reasons, could not be confirmed for *in vivo*-produced vesicles induced by the DNA vaccines. We cannot exclude that EVs produced after *in vivo* Gag-OVA or OVA-C1C2 plasmid injection in muscle are not identical to those obtained *in vitro*, especially because the producing cells (i.e. myoblasts *in vivo* versus kidney-derived HEK293T cells *in vitro*) are different and may use different EV secretion pathways. But we can still speculate on the possible outcomes in terms of immune responses of secretion of an antigen associated with different EVs.

Presentation to CD4⁺ T cells of the plasmid-encoded antigen on MHC class II molecules requires capture of the antigen by antigen presenting cells (APCs), especially

dendritic cells and macrophages. The way that large membrane vesicles or apoptotic cells and smaller EVs interact with these phagocytes is different, in part because of size differences: large particles are captured by phagocytosis, whereas small particles are endocytosed. Additionally, particle size determines the mechanism of trafficking to the draining lymph node, and only small particles can specifically target LN-resident cells (32). In contrast, larger EVs will be more efficiently captured locally by highly phagocytic macrophages and/or neutrophils than by DCs. Thus, the large OVA-containing VLPs induced after vaccination with Gag-OVA could be captured by macrophages and/or neutrophils, in parallel with capture of small EVs and VLPs by DCs in the draining lymph node, possibly leading to different outcomes in terms of antigen presentation and induction of innate immune signalling.

In addition, Gag-OVA- and OVA-C1C2-generated EVs may display differences in surface ligands, and thus be differently targeted to DCs and macrophages. It is possible, for instance, that OVA-C1C2 competes with endogenous MFGE8 at the surface of EVs. MFGE8 is a known opsonin allowing phagocytosis of apoptotic cells by $\alpha\text{v}\beta\text{3}$ - and $\alpha\text{v}\beta\text{5}$ -expressing cells such as macrophages, to which it binds by its RGD-containing EGF domain (13). Even though mouse DC exosomes are coated with MFGE8, we showed that it is not required for their capture by DCs *in vitro* (14). Thus, if the EVs bearing OVA-C1C2 do not bear MFGE8, their capture by macrophages could be impaired, leaving intact their capture by DCs, whereas the Gag-OVA VLPs should be captured by both APCs. Therefore, careful examination of the kinetics and nature of cells capturing OVA-containing EVs or VLPs after vaccination will be required to fully understand the reasons for differential MHC class II-restricted presentation. Fluorescent EVs or VLPs (21) have been developed and could be used to characterize the specific priming mechanisms.

Interestingly, while the types of EVs generated by the two vaccines are different in terms of structure and antigen position, both strategies induced similar levels of OVA-specific CD8⁺ T-cell immune responses. For presentation of an exogenous antigen on MHC class I to CD8⁺ T cells, and initiation of immune responses, the antigen must be internalized by DCs, the only APCs able to efficiently perform cross-presentation and cross-priming to naïve T cells (5). Acquisition of antigen by DCs *in vivo* after DNA injection can occur via phagocytosis of dead cells or fragments of locally transfected fibroblasts or muscle cells. This pathway will also take place for DNA vaccines encoding soluble or non-secreted antigens, and will thus allow induction of the CD8⁺ responses observed with such vaccines (11,18,21). In addition, secretion of VLP- or EV-associated antigens by our modified vaccines further enhances these responses (11,18,21). Both VLPs and EVs

have been shown to be internalized in endocytic compartments by DCs and induced efficient CD8⁺ T-cell responses. We previously demonstrated that tumour cells secrete exosomes carrying tumour antigens, which, after transfer to DCs, mediate CD8⁺ T cell-dependent anti-tumour effects (9). Similarly, we observed in two different models that recombinant retroviral VLPs can be easily captured by DCs that cross-present the antigen fused to Gag to prime CD8⁺ T cells (19,21). Here, we observed comparable levels of CD8⁺ T-cell immune responses induced after Gag-OVA or OVA-C1C2 vaccination (Fig. 2), demonstrating that antigen localization inside or at the surface of EVs has no impact on the CTL response induction. Moreover, because the amount of antigens carried by the two types of EVs produced from transfected cells is quite similar (Fig. 1B), we can conclude that the two types of vesicles provide a source of antigen that can be cross-presented by DCs with the same efficacy. Our results are in line with those of others demonstrating that HIV Nef viral antigens incorporated in exosomes were cross-presented at similar levels to what was observed when the antigens were delivered by engineered lentiviral VLPs (33). Simultaneously, direct presentation of OVA on their MHC class I molecules by DCs locally transfected by the plasmid *in vivo* could also take place. In this case, secretion of the OVA-containing EVs or VLPs would not be involved, mimicking the conditions of DNA vaccines that encode non-particulate antigens, and also accounting for the CD8⁺ T-cell responses observed with such vaccines (11,18,23).

Finally, we observed that both VLP- and secreted vesicle-bound antigen encoding DNA vaccines efficiently control *in vivo* outgrowth of tumours in preventive setting, and could reduce tumour progression or metastasis in therapeutic situations, with similar efficacy. Considering their specific immune properties and their equal capacity to induce antigen-specific CD8⁺ T-cell immune responses, our results highlight the major role of CD8⁺ T cells in antitumour immunity, although complementary experiments should be performed to demonstrate it formally. Antitumoral efficacy of these vaccines was evaluated here in classical models based on transplantable tumour cell lines expressing model antigen; alternative mouse models, using spontaneous or carcinogen-induced tumours, should be also developed to appreciate more precisely the efficacy of our vaccines. Nonetheless, our work highlights the interest of DNA vaccines coding for a vesicle-associated antigen in oncology and suggests that, for other applications where a specific type of CD4⁺ helper T-cell response must be favoured (e.g. Th2 in parasitic infection and Th1 in viral infection), one or the other of the two strategies described here should be preferentially selected.

Acknowledgements

This work was supported by Institut Curie, INSERM, CNRS, Université Pierre et Marie Curie, and a grant from Institut National du Cancer (2008-PL-BIO, DNAVaccVesic) to CT, BB, and OL. OL's team is "équipe labellisée de la Ligue contre le Cancer". We thank Claude Leclerc for useful scientific discussions. We acknowledge the staff of the Animal Facility from Institut Curie for animal husbandry and care.

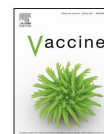
Conflict of interest and funding

The authors have not received any funding or benefits from industry or any for-profit organism to conduct this study.

References

1. Finn OJ. Cancer vaccines: between the idea and the reality. *Nat Rev Immunol.* 2003;3:630–41.
2. Rice J, Ottensmeier CH, Stevenson FK. DNA vaccines: precision tools for activating effective immunity against cancer. *Nat Rev Cancer.* 2008;8:108–20.
3. Liu MA. DNA vaccines: an historical perspective and view to the future. *Immunol Rev.* 2011;239:62–84.
4. Guermonprez P, Valladeau J, Zitvogel L, Thery C, Amigorena S. Antigen presentation and T cell stimulation by dendritic cells. *Annu Rev Immunol.* 2002;20:621–67.
5. Joffre OP, Segura E, Savina A, Amigorena S. Cross-presentation by dendritic cells. *Nat Rev Immunol.* 2012;12:557–69.
6. Li M, Davey GM, Sutherland RM, Kurts C, Lew AM, Hirst C, et al. Cell-associated ovalbumin is cross-presented much more efficiently than soluble ovalbumin *in vivo*. *J Immunol.* 2001;166:6099–103.
7. Belizaire R, Unanue ER. Targeting proteins to distinct subcellular compartments reveals unique requirements for MHC class I and II presentation. *Proc Natl Acad Sci U S A.* 2009;106:17463–8.
8. Graham DB, Stephenson LM, Lam SK, Brim K, Lee HM, Bautista J, et al. An ITAM-signaling pathway controls cross-presentation of particulate but not soluble antigens in dendritic cells. *J Exp Med.* 2007;204:2889–97.
9. Wolfers J, Lozier A, Raposo G, Regnault A, Thery C, Masurier C, et al. Tumor-derived exosomes are a source of shared tumor rejection antigens for CTL cross-priming. *Nat Med.* 2001;7:297–303.
10. Qazi KR, Gehrman U, Domange Jordo E, Karlsson MC, Gabrielson S. Antigen-loaded exosomes alone induce Th1-type memory through a B-cell-dependent mechanism. *Blood.* 2009;113:2673–83.
11. Zeelenberg IS, Ostrowski M, Krumeich S, Bobrie A, Jancic C, Boissonnas A, et al. Targeting tumor antigens to secreted membrane vesicles *in vivo* induces efficient antitumor immune responses. *Cancer Res.* 2008;68:1228–35.
12. Thery C, Regnault A, Garin J, Wolfers J, Zitvogel L, Ricciardi-Castagnoli P, et al. Molecular characterization of dendritic cell-derived exosomes. Selective accumulation of the heat shock protein hsc73. *J Cell Biol.* 1999;147:599–610.
13. Hanayama R, Tanaka M, Miwa K, Shinohara A, Iwamatsu A, Nagata S. Identification of a factor that links apoptotic cells to phagocytes. *Nature.* 2002;417:182–7.
14. Veron P, Segura E, Sugano G, Amigorena S, Thery C. Accumulation of MFG-E8/lactadherin on exosomes from immature dendritic cells. *Blood Cells Mol Dis.* 2005;35:81–8.
15. Rountree RB, Mandl SJ, Nachtwey JM, Dalpozzo K, Do L, Lombardo JR, et al. Exosome targeting of tumor antigens

- expressed by cancer vaccines can improve antigen immunogenicity and therapeutic efficacy. *Cancer Res.* 2011;71:5235–44.
16. Hartman ZC, Wei J, Glass OK, Guo H, Lei G, Yang XY, et al. Increasing vaccine potency through exosome antigen targeting. *Vaccine.* 2011;29:9361–7.
 17. Bellier B, Klatzmann D. Virus-like particle-based vaccines against hepatitis C virus infection. *Expert Rev Vaccines.* 2013; 12:143–54.
 18. Bellier B, Dalba C, Clerc B, Desjardins D, Drury R, Cosset FL, et al. DNA vaccines encoding retrovirus-based virus-like particles induce efficient immune responses without adjuvant. *Vaccine.* 2006;24:2643–55.
 19. Huret C, Desjardins D, Miyalou M, Levacher B, Amadoudji Zin M, Bonduelle O, et al. Recombinant retrovirus-derived virus-like particle-based vaccines induce hepatitis C virus-specific cellular and neutralizing immune responses in mice. *Vaccine.* 2013;31:1540–7.
 20. Bellier B, Huret C, Miyalou M, Desjardins D, Frenkiel MP, Despres P, et al. DNA vaccines expressing retrovirus-like particles are efficient immunogens to induce neutralizing antibodies. *Vaccine.* 2009;27:5772–80.
 21. Lescaille G, Pitoiset F, Macedo R, Baillou C, Huret C, Klatzmann D, et al. Efficacy of DNA vaccines forming e7 recombinant retroviral virus-like particles for the treatment of human papillomavirus-induced cancers. *Hum Gene Ther.* 2013;24:533–44.
 22. Thery C, Amigorena S, Raposo G, Clayton A. Isolation and characterization of exosomes from cell culture supernatants and biological fluids. *Curr Protoc Cell Biol.* 2006;Chapter 3:Unit 3 22.
 23. Thery C, Ostrowski M, Segura E. Membrane vesicles as conveyors of immune responses. *Nat Rev Immunol.* 2009;9: 581–93.
 24. Chiarella P, Fazio VM, Signori E. Electroporation in DNA vaccination protocols against cancer. *Curr Drug Metab.* 2013; 14:291–9.
 25. Zeelenberg IS, van Maren WW, Boissonnas A, Van Hout-Kuijer MA, Den Brok MH, Wagenaars JA, et al. Antigen localization controls T cell-mediated tumor immunity. *J Immunol.* 2011;187:1281–8.
 26. Ahlén G, Söderholm J, Tjelle T, Kjekken R, Frelin L, Höglund U, et al. *In vivo* electroporation enhances the immunogenicity of hepatitis C virus nonstructural 3/4A DNA by increased local DNA uptake, protein expression, inflammation, and infiltration of CD3+ T cells. *J Immunol.* 2007;179:4741–53.
 27. Widera G, Austin M, Rabussay D, Goldbeck C, Barnett SW, Chen M, et al. Increased DNA vaccine delivery and immunogenicity by electroporation *in vivo*. *J Immunol.* 2000;164: 4635–40.
 28. Daud AI, DeConti RC, Andrews S, Urbas P, Riker AI, Sondak VK, et al. Phase I trial of interleukin-12 plasmid electroporation in patients with metastatic melanoma. *J Clin Oncol.* 2008;26:5896–903.
 29. Tjelle T, Rabussay D, Ottensmeier C, Mathiesen I, Kjekken R. Taking electroporation-based delivery of DNA vaccination into humans: a generic clinical protocol. *Methods Mol. Biol.* 2008;423:497–507.
 30. Senovilla L, Vacchelli E, Garcia P, Eggermont A, Fridman WH, Galon J, et al. Trial watch: DNA vaccines for cancer therapy. *Oncoimmunology.* 2013;2:e23803.
 31. Crescitelli R, Lasser C, Szabo TG, Kittel A, Eldh M, Dianzani I, et al. Distinct RNA profiles in subpopulations of extracellular vesicles: apoptotic bodies, microvesicles and exosomes. *J Extracell Vesicles.* 2013;2:20677. doi: 10.3402/jev.v2i0.20677.
 32. Manolova V, Flace A, Bauer M, Schwarz K, Saudan P, Bachmann MF. Nanoparticles target distinct dendritic cell populations according to their size. *Eur J Immunol.* 2008;38: 1404–13.
 33. Lattanzi L, Federico M. A strategy of antigen incorporation into exosomes: comparing cross-presentation levels of antigens delivered by engineered exosomes and by lentiviral virus-like particles. *Vaccine.* 2012;30:7229–37.



Heparan sulfates targeting increases MHC class I- and MHC class II-restricted antigen presentation and CD8⁺ T-cell response



Delphine Knittel^a, Adeline Gadzinski^a, Stéphane Hua^a, Jordan Denizeau^{b,c,d}, Alexandra Savatier^a, Philippe de la Rochère^{b,c,d}, Jean-Claude Boulain^a, Sebastian Amigorena^{b,c,d}, Eliane Piaggio^{b,c,d}, Christine Sedlik^{b,c,d}, Michel Léonetti^{a,*}

^a Commissariat à l'Énergie Atomique et aux Energies Alternatives, Institut de Biologie et Technologies de Saclay, Service de Pharmacologie et d'Immunoanalyse, Laboratoire d'Études et de Recherches en Immunoanalyse, Gif-Sur-Yvette F-91191, France

^b Institut Curie, Centre de Recherche, Paris 75005, France

^c INSERM, U932, Paris F-75005, France

^d Centre d'Investigation Clinique Biothérapie CICBT 507, Institut Curie, Paris F-75005, France

ARTICLE INFO

Article history:

Received 8 October 2015

Received in revised form 31 March 2016

Accepted 25 April 2016

Available online 4 May 2016

Keywords:

Heparan sulfate
Antigen targeting
Cross presentation
Tumour control

ABSTRACT

Heparan sulfates (HS) are carbohydrate moieties of HS proteoglycans (HSPGs). They often represent alternative attachment points for proteins or microorganisms targeting receptors. HSPGs, which are ubiquitously expressed, thereby participate in numerous biological processes. We previously showed that MHC class II-restricted antigen presentation is increased when antigens are coupled to HS ligands, suggesting that HSPGs might contribute to adaptive immune responses. Here, we examined if HSPG targeting influences other aspects of immune responses. We found that coupling of an HS ligand to the antigen increases antigen presentation to CD4⁺ and CD8⁺ T-cells after antigen targeting to membrane immunoglobulins or to MHC-II molecules. Moreover, this increased stimulating capacity correlates with an enhanced CD8⁺ immune response in mice. Last, animals control more effectively the growth of Ova-expressing tumour cells when they are immunized with an Ova construct targeting HSPGs and MHC-II molecules. Our results indicate that ubiquitous molecules can influence both MHC class I- and MHC class II-restricted antigen presentation and behave as co-receptors during T-cell stimulation. Moreover, they suggest that tumour-antigens endowed with the ability to target both HSPGs and MHC-II molecules could be of value to increase CD8⁺ immune response and control tumour-growth, opening new perspectives for the design of highly immunogenic protein-based vaccines.

© 2016 Elsevier Ltd. All rights reserved.

1. Introduction

Extracellular proteins have to be captured by Ag-presenting cells (APCs) to stimulate CD4⁺ and CD8⁺ T-lymphocytes. This uptake is particularly efficient when mediated by receptors increasing internalization in endocytic compartments [1–3]. Thus, the amount of Ag required to stimulate CD8⁺ and CD4⁺ T-lymphocytes can be respectively up to 10⁴-fold and 10⁵-fold lower than that required during nonspecific endocytosis [4,5]. As ubiquitously expressed

receptors may cause Ag dissemination to non-immune cells, it is generally anticipated that they do not play a major role in Ag presentation and that the crucial receptors are selectively expressed on the APC surface. However, this scenario should be re-examined considering our findings that heparan sulfate proteoglycans (HSPGs), which are ubiquitously distributed on cells and on the extracellular matrix [6,7], can contribute to T-helper cell stimulation [8]. Thus, Ags with the ability to bind the heparan sulfate (HS) moiety of HSPGs undergo an increased APC uptake. Furthermore, HSPGs boost T-cell responses and act as co-receptors during FcγRII-mediated presentation of immune complexes (ICs). These *in vitro* findings raise the question of their contribution to other aspects of the adaptive immune response, *in vitro* and *in vivo*.

Here, we examined whether an Ag targeting both HSPGs and an APC-specific receptor is more efficiently supported by the immune system and if it impacts the control of tumour-growth.

Abbreviations: Tat, transcriptional transactivator; DT, diphtheria toxin; DC, dendritic cell; HSPG, heparan sulfate proteoglycan.

* Corresponding author at: Service de Pharmacologie et d'Immunoanalyse, Bâtiment 136, CEA Saclay, 91191 Gif-Sur-Yvette Cedex, France. Tel.: +33 169086456; fax: +33 169085907.

E-mail address: michel.leonetti@cea.fr (M. Léonetti).

<http://dx.doi.org/10.1016/j.vaccine.2016.04.073>

0264-410X/© 2016 Elsevier Ltd. All rights reserved.

2. Materials and methods

2.1. Antigens

Ova, ZZOva, ZZOvaTat22-57S and ZZOvaDTR-BD were produced by inserting the genetic fragments into a pCP vector using SacI/KpnI/BamHI restriction sites. *Escherichia coli* BL21 (DE3pLysS) cells were transformed with plasmids encoding ZZOva, ZZOvaTat22-57S, or ZZOvaDTR-BD. *E. coli* tuner-cells were transformed with Ova-encoding plasmid.

The ZZ-fusions were incubated at 4 °C in NaCl (2 M) and protamine sulfate (2 mg/mL) to remove nucleic acids. Samples were dialyzed in PBS-Tween 20 (0.1%) and loaded on an IgG-Sepharose column (Amersham). The IgG-bound fraction was purified using a MonoQ5/50GL anion-exchange column (GE-Healthcare) and a 0.01–0.15 M gradient of Na-phosphate buffer (10 mM) pH6. Ova was purified as described previously [9]. Purity was assessed by gel electrophoresis.

Complexes between ZZAg proteins and antibodies (AF6-120.1, isotype control or Y3P) were prepared by incubating ZZAg with an equimolar amount of Ab overnight at 4 °C.

2.2. Cells

The JAWSII cell-line is a GM-CSF-dependent dendritic-cell (DC) line derived from C57BL/6 mice (ATCC).

Splenocytes were isolated from C57BL/6, OT-I or OT-II mice (kindly provided by Dr Olivier Lantz, Institut Curie, Paris). OT-I mice have a transgenic T-cell receptor specific to p257–264 MHC-I Ova peptide, while OT-II mice have a transgenic T-cell receptor specific to p323–339 MHC-II Ova peptide.

2.3. Heparin binding assays

Microtiter plates (Nunc) were coated overnight at 4 °C with a 0.05 M phosphate buffer pH 7.2 containing 0.1 µg/mL heparin-albumin (Sigma-Aldrich) and saturated with 0.1 M phosphate buffer pH 7.2 containing 0.3% BSA. Proteins were serially diluted with 0.1 M phosphate buffer pH 7.2 containing 0.1% BSA in wells coated with heparin-albumin or BSA. After 30-min RT, plates were incubated for 30-min with a rabbit IgG. Binding was assessed using a peroxidase-labelled goat anti-rabbit Ab (Jackson ImmunoResearch) and 2,2'-azinobis(3-ethylbenzothiazoline-6-sulphonic acid) (Sigma) as substrate. Specific binding was determined by subtracting BSA binding from heparin-albumin binding.

For competition assay, ZZDTR-BD (30 nM) was incubated with serial dilutions of ZZ or HS (kindly provided by Dr. Lortat-Jacob) in heparin-albumin coated plates. ZZDTR-BD binding was assessed as above.

2.4. Cell binding assays

Serial dilutions of Ag were incubated with 10⁵ JAWSII cells for 30-min at 4 °C in PBS-0.5% BSA. Then, cells were incubated with a rabbit anti-Ova Ab (1 µg) for Ova, ZZOva, ZZOvaTat22-57S and ZZOvaDTR-BD. After 30-min, cells incubated with a fluorescein-labelled donkey anti-rabbit F(ab')₂ (FITC-DAR) (Jackson ImmunoResearch). 30-min later, binding was assessed by flow cytometry.

To examine binding of Ova, ZZOva, ZZOvaTat22-57S and ZZOvaDTR-BD complexed or not with AF6-120.1 Ab on splenocytes (2 × 10⁵ cells), the Ags were incubated with splenocytes for 30-min at 4 °C. Binding was assessed as above using an anti-Ova Ab and FITC-DAR.

To examine binding on different sub-populations, splenocytes were incubated with Ags as above. Interaction was examined after incubation with an anti-Ova Ab, phycoerythrin-labelled donkey anti-rabbit F(ab')₂ (PE-DAR) and FITC-labelled anti-CD markers. Data were analyzed using a student t-test.

2.5. Uptake experiments

A fixed amount (300 nM) of Ag was incubated overnight at 4 °C with or without an anti-MHC-II Ab (AF6-120.1, BD). The mixtures were added to JAWSII cells (10⁵/well). After 1-h, a rabbit anti-Ova Ab (1 µg) was added. After 1-h, a FITC-DAR was added and incubated for 1-h. Then, cells were incubated for 4-h at 37 °C. Cells were fixed, nuclei were stained using DRAQ5 and analyzed by confocal microscopy.

2.6. In vitro T-cell-stimulating assays

T-cell stimulation experiments using splenocytes from OT-I and OT-II mice.

Serial dilutions of Ags were incubated overnight in polypropylene microplates (Greiner Bio-One) with different Abs in complete medium (RPMI supplemented with 10% FCS, 2 mM L-glutamine, 100 U/mL penicillin, 100 µg/mL streptomycin and 50 µM mercaptoethanol). Splenocytes from OT-I mice and OT-II mice were added (9 × 10⁴ cells/well) and incubated for 3-days at 37 °C. Then, 1 µCi/well of [³H]-methyl thymidine (5 Ci/mmol, Perkin Elmer) was added for 16-h to assess proliferation. Error bars correspond to standard deviation.

T-cell stimulation experiments using BMDC and T-cells from OT-I and OT-II mice.

BMDCs were prepared as previously described [10]. Serial dilutions of ZZOva and ZZOvaTat22-57S were incubated overnight with or without equimolar amounts of anti-I-A[b] MHC-II Ab (AF6-120.1) and added to BMDC (3 × 10⁴ cells/well). After 5-h at 37 °C, BMDCs were fixed. OT-I or OT-II splenocytes (1 × 10⁵ cells/well) were added and proliferation assessed as above.

2.7. Mice and immunizations

C57BL/6j mice were obtained from Charles River. Care and use of animals followed European and national regulations for Protection of Animals used for Experimental and Scientific Purposes (facility licence #C75-05-18) complying with principles of replacement, reduction and refinement (Guide for Care and Use of Laboratory Animals, NRC 2011). Mice were immunized subcutaneously in the footpads with 115 pmoles of Ags (equivalent to 5 µg of Ova protein) mixed with aluminium hydroxide (Serva) and CpG (40 µg/mouse) (CpG1018, Trilink) adjuvants.

2.8. Ab and T-cell responses

Mice were bled 2-weeks after immunization. Ova-specific IFN-γ-producing cells were detected by ELISPOT as previously described [11] using anti-IFN-γ Abs (Diaclone) and anti-IL-4 Abs (11B11 and BVD6-24G2, Pharmingen) for coating and detection. CD4⁺ T-cell response was assessed by re-stimulating cells with the Ova CD4 epitope Ova265-280 and CD8⁺ T-cell response was assessed by re-stimulating cells with the Ova CD8 epitope p257-264. Data were analyzed using a Mann-Whitney test. Anti-Ova specific antibodies secretion was measured in the sera by ELISA as previously described [11] using alkaline phosphatase-conjugated anti-mouse IgG, IgG1, or IgG2b (Jackson ImmunoResearch).

2.9. In vivo tumour assay

Eleven days after vaccination, blood samples were collected to investigate CD8⁺ T-cell response to p257-264 Ova-peptide. Then, mice were injected i.v. with 0.2×10^6 B16F10-OVA melanoma cells. Mice were sacrificed 20 days later and tumour burden was assessed by counting lung foci. Data were analyzed using a Mann–Whitney test.

3. Results

3.1. Fusion proteins with HS-binding ability interact more efficiently with DCs

To examine whether an HS-ligand influences presentation mechanisms when an Ag is targeted towards receptors expressed by APC, we took advantage of a fusion protein containing a ZZ dimer derived from protein A of *Staphylococcus aureus* [15]. It (i) allows expression of various Ags in fusion [16], (ii) targets to Igs located on the APC via its ZZ moiety [16,17], (iii) can be used to form complexes with Abs specific to proteins expressed on APCs [17]. In the first fusion protein, named ZZOva, we fused ZZ to full-length Ova, which contains well characterized CD4 and CD8 T-cell epitopes [13,18] (Table 1A). In the second, named ZZOvaTat22-57S, we fused ZZOva to a fragment derived from region 22–57 of Tat, named Tat22-57S, which is an HS-ligand with 7 cysteines mutated to serine [19] to avoid cysteine-mediated oligomerization [20]. In the third fusion protein, named ZZOvaDTR-BD, we fused ZZOva to fragment 385–535 of diphtheria toxin (DT), named DTR-BD. We selected DTR-BD, as we found it binds HS. Thus, a fusion protein containing DTR-BD, called ZZ-DTR [21] or ZZ-DTR-BD, interacts with albumin/heparin-coated plates (Fig. 1A) and binding is inhibited by HS, but not by ZZ, demonstrating the role of

DTR-BD in the interaction (Fig. 1B). To assess whether Tat22-57S and DTR-BD allow ZZOva to bind HS, we assessed heparin-binding. We observed that ZZOvaTat22-57S and ZZOvaDTR-BD interact with albumin/heparin-coated plates (Fig. 1C), whereas ZZOva do not interact demonstrating that Tat22-57S or DTR-BD makes ZZOva able to bind HS.

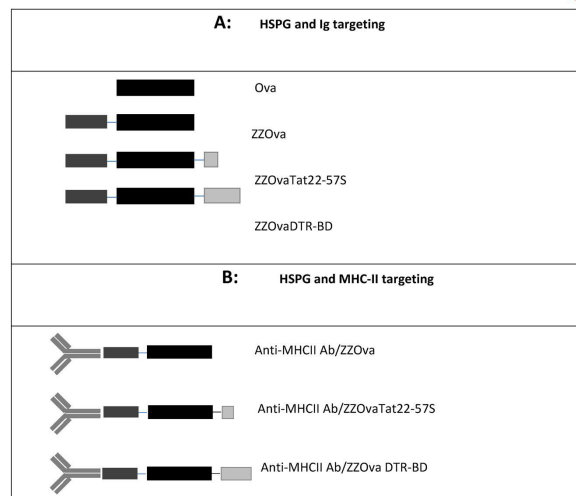
Next, we assessed whether Tat22-57S and DTR-BD increase ZZOva binding to DCs. At 333 nM, ZZOva interacts with JAWSII DC cell-line. Binding increases with ZZOvaTat22-57S and ZZOvaDTR-BD (Fig. 1D). However, it decreases in the presence of HS (Fig. 1E). Furthermore, competition experiments made with ZZOvaTat22-57S and serial dilutions of HS clearly show that binding vanishes in a dose-dependent manner (see supplemental data). Therefore, the HS-ligands increase Ag interaction with DCs. Next, as ubiquitous distribution of HSPGs can lead to HS-ligand dissemination, we investigated whether Tat22-57S increases ZZOva binding to primary DCs contained in splenocytes. With CD11c⁺ gated-cells, we observed an absence of binding for Ova, and a significant interaction for ZZOva, indicating that ZZ targets Ova to DCs (Fig. 1F), in agreement with reports showing that ZZ mediates Ag-targeting to APCs [16,17]. We found an increased interaction with ZZOvaTat22-57S indicating that Tat22-57S makes ZZOva able to bind more efficiently primary DCs. Then, we focused on B-lymphocytes, CD4⁺ and CD8⁺ T-lymphocytes. We observed that ZZOva binds these cell types only when it is coupled to Tat22-57S (Fig. 1G). Therefore, coupling of an HS-binding domain makes ZZOva able to bind to a large variety of cells, including primary DCs, in agreement with ubiquitous expression of HSPGs [6,7].

3.2. CD8⁺ T-cell immune response is increased when Ova is fused to ZZ and to an HS-ligand

To study T-cell stimulation ability of those fusion proteins, we investigated the Ova-specific CD8⁺ and CD4⁺ T-cell responses

Table 1

Diagram of targeting constructs. (A) Ova was expressed in a free form or fused to ZZ (ZZOva) to target surface Igs. ZZOva was fused either to Tat22-57S (ZZOvaTat22-57S) or to DTR-BD (ZZOvaDTR-BD) to target both HSPGs and Igs. (B) ZZOva, ZZOvaTat22-57S and ZZOvaDTR-BD were incubated with an anti-MHCII Ab to make complexes able to bind either the MHCII molecule or the MHCII molecule and HSPGs.



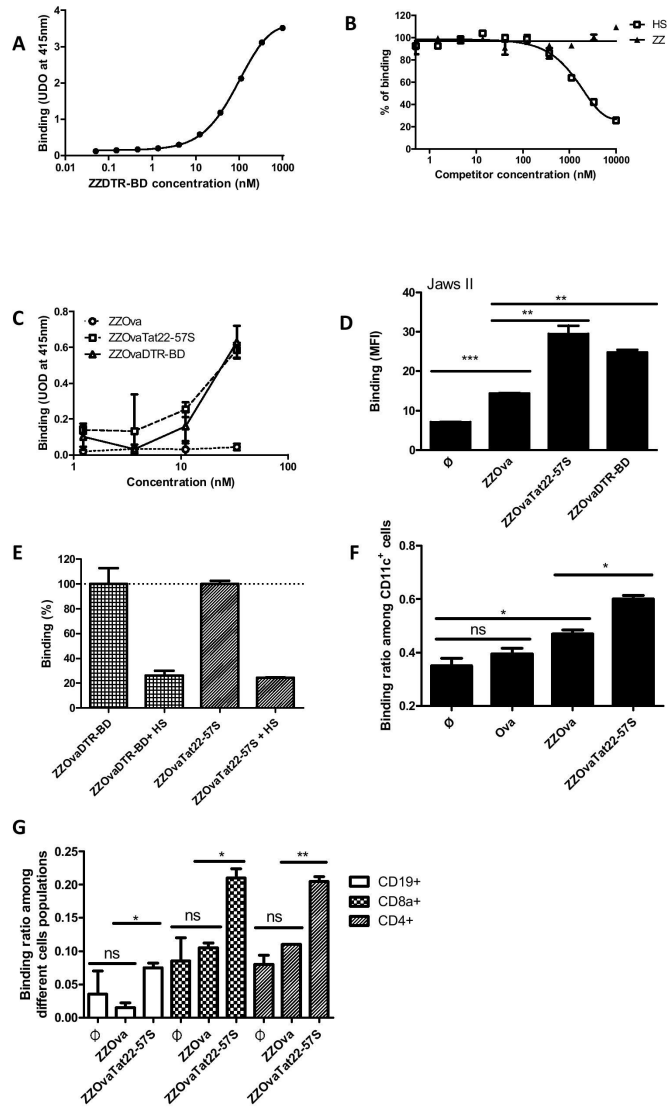


Fig. 1. DTR-BD and Tat22-57S are HS-ligands enabling ZZOva binding to heparin, JAWSII DCs and primary CD11c⁺ DCs. (A) To examine heparin-binding, ZZDTR-BD was incubated in albumin/heparin-coated plates. Binding was assessed using a non-specific rabbit IgG, a peroxidase-labelled goat anti-rabbit Ab and ABTS. Units of optical density (UOD) ± SD are shown. (B) Specific HS-binding was determined by incubating serial dilutions of HS or ZZ with ZZDTR-BD (30 nM) in albumin/heparin-coated plates. Percentage of binding is shown. (C) Heparin-binding of ZZOva, ZZOvaTat22-57S and ZZOvaDTR-BD was determined as in (A). UOD ± SD are shown. (D) JAWSII DCs were incubated in the absence (φ) or presence of a fixed amount (333 nM) of ZZOva, ZZOvaDTR-BD and ZZOvaTat22-57S, respectively, to compare binding. A rabbit anti-Ova Ab and a FITC-Donkey anti-rabbit F(ab)₂ were added. Interaction was measured by flow cytometry using a Guava cytometer (Millipore, France) and the data were analyzed using Guava Express Pro software. The mean of fluorescence intensity (MFI) is shown. (E) To evaluate the role of the HS moieties, ZZOvaTat22-57S and ZZOvaDTR-BD were respectively incubated with JAWSII cells with or without HS (3 μM). Binding was assessed as in (D). (F) Binding to CD11c⁺ DCs was assessed after incubation of Ova, ZZOva

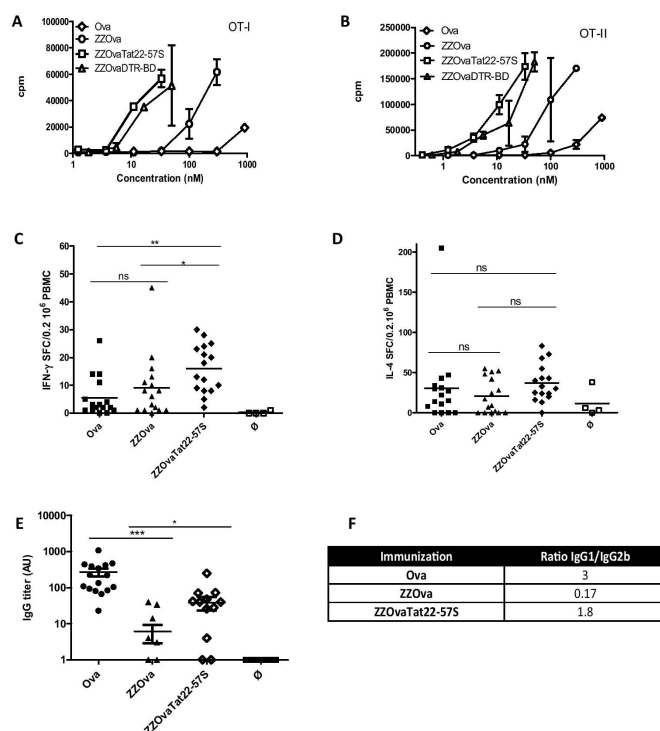


Fig. 2. CD4⁺ and CD8⁺ *in vitro* T-cell stimulations as well as CD8⁺ immune response *in vivo* are increased when Ova is fused both to ZZ and a HS-ligand. (A) CD8⁺ T-cell stimulation was assessed using Ova, ZZOva, ZZOvaTat22-57S and ZZOvaDTR-BD incubated with splenocytes from OT-I mice. After 3-days of incubation, proliferation was assessed using [³H]-methyl-thymidine. Data are expressed as cpm ± S.D. (B); CD4⁺ T-cell stimulation was assessed using splenocytes from OT-II mice and the Ags in (A). (C)–(E) *In vivo* immune response in C57BL/6 mice injected with Ova, ZZOva, and ZZOvaTat22-57S, respectively. Presence of IFN- γ -secreting CD8⁺ T-cells specific of p257-264 Ova-peptide (C) and of IL-4 secreting CD4⁺ T-cells specific of p265-280 Ova-peptide (D) was assessed by ELISPOT. Anti-Ova Ab response was assessed by ELISA with individual sera (E). Data pooled from two separate experiments are shown. t-test was used for statistical analysis. (F) The content in specific IgG1 and IgG2b was measured by ELISA and the IgG1/IgG2a ratio was calculated.

in vitro, using OT-I and OT-II mice. As splenocyte-binding experiments indicated that ZZOvaTat22-57S can spread on non-APC cell types (T-lymphocytes), we used whole splenocytes to assess whether stimulation of Ova-specific T-cells is increased in conditions that we assumed to be less favourable for Ag presentation as compared with experiments with purified DCs. We found that the amount of free Ova required to trigger OT-I cell proliferation is about 10 times higher than that of ZZOva (Fig. 2A) suggesting that ZZ-mediated targeting to CD11c⁺ DCs (see Fig. 1F) increases CD8⁺ T-cell stimulation by Ova. Furthermore, ZZOvaTat22-57S and ZZOvaDTR-BD required quantities 125 and 100 times lower than Ova. Similar behaviour was noted when OT-II cells were used for CD4⁺ T-cell activation (Fig. 2B). Therefore, Ova fusion to ZZ

increases Ova-specific CD4⁺ and CD8⁺ T-cell stimulations and coupling of a HS-ligand, although promoting Ova dissemination to various cell types (see Fig. 1G), increases the phenomenon.

Next, we examined the immune response in mice injected with Ova, ZZOva, ZZOvaTat22-57S, respectively. We found a low number of Ova-specific IFN- γ -secreting CD8⁺ T-cells in Ova-immunized mice, which is not significantly increased in animals injected with ZZOva (Fig. 2C). However, we measured a higher number of Ova-specific CD8⁺ T-cells in ZZOvaTat22-57S-vaccinated animals ($p = 0.012$). In contrast, we found a number of IL-4-producing CD4⁺ T-cells that did not differ significantly between the groups (Fig. 2D), indicating that the anti-Ova CD4⁺ response is not increased, whatever the construct used.

and ZZOvaTat22-57S with splenocytes. A rabbit anti-Ova Ab, a PE-DAR F(ab)₂, and FITC-labelled anti-CD11c⁺ Ab were added. Interaction was measured by flow cytometry. Gating was done on CD11c⁺ live cells. Ratio between double positive cells and whole CD11c⁺ cells was calculated and reported on the graph. (G) Binding to B-lymphocytes, CD4⁺ and CD8⁺ T-lymphocytes was assessed after incubation of Ova, ZZOva and ZZOvaTat22-57S with splenocytes. A polyclonal rabbit anti-Ova Ab, a FITC-DAR F(ab)₂, and PE-labelled anti-CDs Ab were added. Interaction was measured by flow cytometry, double-labelled cells in each subpopulation of lymphocytes is shown. S.D. are shown. Similar results were observed in at least two independent experiments. \emptyset stand for no stimulus, *i.e.* buffer only.

We assessed the IgG anti-Ova immune response by ELISA (Fig. 2E). In sera from Ova-immunized mice, we found 45 times more Ab than in sera from ZZOva-immunized mice. Furthermore, we measured six times more anti-Ova Ab in sera from ZZOvaTat22-57S-immunized mice than in sera from ZZOva-immunized mice, indicating that Tat22-57S increases Ab response. To investigate whether these differences are related to a modification of the Th1/Th2 balance, we measured the amounts of anti-Ova IgG1 and IgG2b. We found an IgG1/IgG2b ratio of 3 for sera from Ova-immunized mice, 0.17 for sera from ZZOva-immunized mice, and 1.8 for sera from ZZOvaTat22-57S-immunized mice. Therefore, Ab

response raised by free Ova tends to exhibit a Th2 pattern that might be biased towards a Th1 profile when Ova is coupled to ZZ and redirected towards a Th2 pattern when ZZOva is coupled to Tat22-57S.

3.3. Ability to bind both MHC class II molecules and HS affects ZZOva binding and uptake by DCs

As the ZZ moiety of ZZ-fusions can bind to the Fc region of IgG [17], we incubated ZZOva and ZZOvaTat22-57S with or without an anti-MHC-II Ab (Table 1B) in order to make

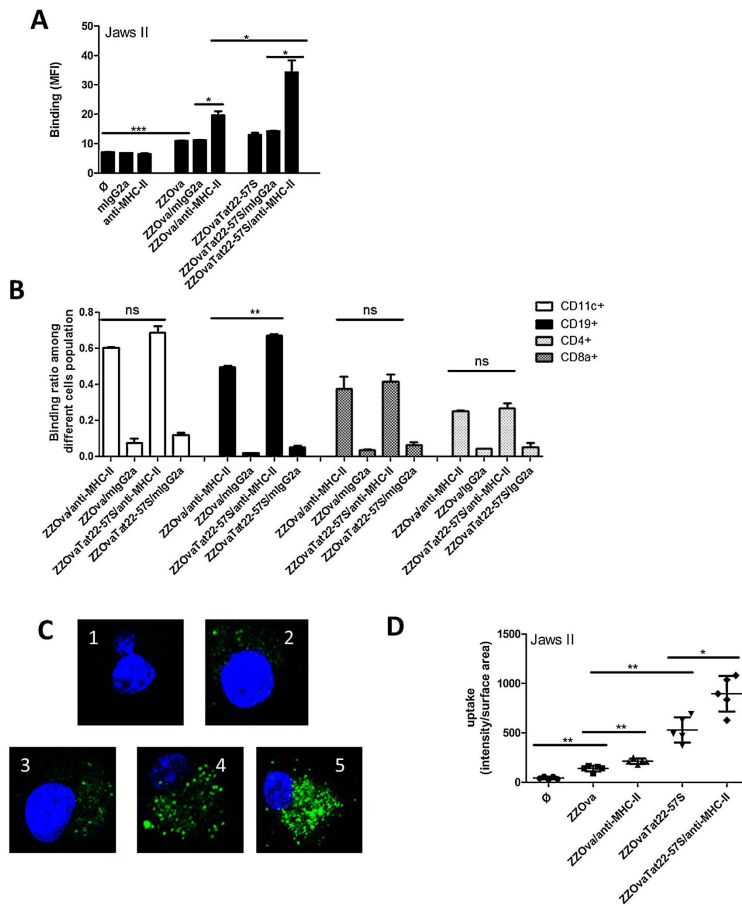


Fig. 3. Ab-mediated targeting and uptake are increased when ZZOva is coupled to an HS-ligand. (A) Binding to JawsII DCs was assessed using a fixed amount (37 nM) of ZZOva and ZZOvaTat22-57S with or without either an anti-MHC-II Ab or an unrelated IgG2a. The mixtures were added to DCs and binding was assessed as in 2D. MFI \pm SD are shown. (B) Binding to primary CD11c⁺ DCs was assessed using splenocytes and Ags described in (A). Percentage of labelled DCs in CD11c⁺, CD19⁺, CD4⁺ and CD8⁺ gated cells are shown. (C) DC uptake was assessed using ZZOva and ZZOvaTat22-57S (300 nM) incubated with or without an anti-MHC-II Ab. The mixtures were added to JawsII DCs. Fluorescence by confocal microscopy was visualized after a 4-hour incubation at 37 °C using a rabbit anti-Ova Ab and a FITC-DAR F(ab)₂; (1: no Ag; 2: ZZOva; 3: ZZOva/anti-MHC-II; 4: ZZOvaTat22-57S; 5: ZZOvaTat22-57S/anti-MHC-II). (D): Quantification of uptake in several cells. Results are expressed as fluorescence intensity/area \pm S.D. ∅ stand for no stimulus, i.e. buffer only.

non-covalent complexes. Then, we examined binding to JAWSII cells. At the concentration used (9-fold lower than that used for the experiments shown in Fig. 1D), we observed poor but significant binding of ZZOva to DCs and a slight higher interaction of ZZOvaTat22-57S (Fig. 3A). We did not find any increase when ZZOva and ZZOvaTat22-57S were respectively complexed with an IgG2a isotype control, indicating an absence of involvement of the Fc moiety and FcγR. In contrast, we found an enhanced interaction when complexed with the anti-MHC-II Ab indicating targeting to MHC-II molecules. Moreover, we observed that binding of ZZOvaTat22-57S/anti-MHC-II is approximately 2 times higher than that of ZZOva/anti-MHC-II indicating that the HS-ligand affects Ab-targeting.

Then we examined whether an HS-ligand affects Ab-mediated interaction in splenocytes. For this we used a concentration of anti-MHC-II Ab-containing complexes allowing Ova detection in over 50% of B-cells contained within splenocytes. At this low concentration (1 nM) the control IgG2a-containing complexes only bound a small proportion of DCs, CD19⁺, CD4⁺, and CD8⁺ (3–10%), while ZZOvaTat22-57S/anti-MHC-II bound 70% of DCs, 60% of B-lymphocytes, 27% of CD4⁺ T-lymphocytes and 42% of CD8⁺ T-lymphocytes indicating that the anti-MHC-II Ab mainly increases interaction with MHC-II-expressing cells (Fig. 3B). When we compared ZZOvaTat22-57S/anti-MHC-II with ZZOva/anti-MHC-II, we did not find a significant ($p = 0.0694$) difference in the number of bound DCs, CD4⁺ T-cells ($p = 0.43$), CD8⁺ T-cells ($p = 0.55$) while we measured significant differences for binding to B-cells ($p < 0.005$). Therefore, the anti-MHC-II Ab increases interaction with B-cells and DCs and the HS-ligand enhances MHC-mediated binding to B-lymphocytes.

Next, we investigated the effect on ZZOva uptake by JAWSII DCs. We found a low intracellular fluorescence when cells were incubated with ZZOva (panel 2, Fig. 3C). The intensity was slightly higher with ZZOva/anti-MHC-II (panel 3). We observed a more dramatic effect with ZZOvaTat22-57S (panel 4). However, we found the highest intensity with ZZOvaTat22-57S/anti-MHC-II (panel 5). Uptake quantification in several cells indicated that it varied depending on the construct used (Fig. 3D). Therefore, combining a HS-ligand – and an anti-MHC-II Ab affects ZZOva uptake.

3.4. Ability to bind both MHC class II molecules and HS affects T-stimulating capacity of ZZOva

As T-cell stimulating ability of an Ag can be increased when it is coupled to Abs that target molecules expressed on APCs [17,22–25], we assessed whether an HS-ligand may influence the increased T-cell stimulation provided by MHC-II-targeting. Using whole splenocytes as APC source, we observed that CD8⁺ T-cell stimulating capacity of ZZOva is lower than ZZOvaTat22-57S and ZZOvaDTR-BD and is enhanced when ZZOva is complexed to an anti-MHC-II Ab (Fig. 4A). However, stimulation is further increased when ZZOva is coupled to either Tat22-57S or DTR-BD and complexed with the anti-MHC-II Ab, indicating that these HS-ligands heightened the effect provided by the Ab. Moreover, FcγRs are not involved in the phenomenon since T-stimulating capacity is not increased when the fusions are complexed to the control IgG2a (data not shown). We found similar behaviours with splenocytes from OT-II mice (Fig. 4B) indicating that the HS-ligands also increase MHC-II-restricted Ag presentation.

Next, we assessed whether MHC class I- and MHC class II-restricted presentation is increased when BMDCs are used as APCs. We found that ZZOvaTat22-57S is more efficient than ZZOva at stimulating CD8⁺ T-lymphocytes from OT-I mice and the anti-MHC-II Ab increases ability of ZZOva and ZZOvaTat22-57S to stimulate CD8⁺ T-cells (Fig. 4C). Therefore, HS-binding ability and anti-MHC-II

Ab-mediated targeting cumulatively affect CD8⁺ T-cell stimulation. When we examined MHC class II-restricted presentation by BMDCs to OT-II cells, we found a less pronounced behaviour with weak differences of stimulation between ZZOva and ZZOvaTat22-57S as well as between ZZOva/anti-MHC-II and ZZOvaTat22-57S/anti-MHC-II (Fig. 4D) indicating that Tat22-57S targeting impacts less efficiently MHC-II-restricted presentation by BMDCs.

3.5. ZZOvaTat22-57S and ZZOvaTat22-57S/anti-MHC-II immunizations trigger Ova-specific T-cell responses and make mice able to control tumour-growth

We assessed whether ZZOvaTat22-57S, and ZZOvaTat22-57S/anti-MHC-II immunization induce an OVA-specific CD8⁺ response and an anti-tumour activity against B16F10-OVA melanoma cells. We observed an increased CD8⁺ T-cell response after immunization with ZZOvaTat22-57S/anti-MHC-II as compared to ZZOvaTat22-57S (Fig. 4E). We counted a high number of metastases in lungs of unvaccinated mice while this number remain low (<20) in ten out of twelve animals previously injected with ZZOvaTat22-57S indicating that mice injected with this fusion protein control tumour-growth (Fig. 4F). In addition, we found that metastases remain barely detectable (<2) in all animals vaccinated with ZZOvaTat22-57S/anti-MHC-II indicating that MHCII targeting increases the protective effect.

4. Discussion

We assessed whether different aspects of the adaptive immune response vary when a protein Ag is endowed with the ability to bind HS. We examined this issue with Ova and two unrelated HS-ligands respectively derived from Tat or from DT. Comparison of ZZOvaDTR-BD and ZZOvaTat22-57S shows that DTR-BD and Tat22-57S similarly enhance Ova interaction with JAWSII DCs and that soluble HS abolish the effect, indicating that it depends on HS-binding ability. In addition, to stimulate CD8⁺ and CD4⁺ T-cells, approximately 100 times lower amounts of ZZOvaDTR-BD and ZZOvaTat22-57S are required as compared to what is required with free Ova. Therefore, two HS-ligands from different origins affect Ova ability to bind cells and to stimulate T-lymphocytes, suggesting that these behaviours are representative of most HS-ligands.

Our binding studies performed with splenocytes show that ZZOva does not bind to T-CD4⁺, T-CD8⁺ and B-lymphocytes, but interacts with CD11c⁺ DCs. When ZZOva is coupled to Tat22-57S, it remains capable of DC-targeting, but also spreads to the three populations of lymphocytes with a variable efficiency that might be due to differences in HSPG expression [26]. However, spreading does not cause a major impairment of T-cell activation and the HS-ligand has beneficial effects since the amounts of ZZOvaTat22-57S and ZZOvaDTR-BD required to stimulate CD8⁺ and CD4⁺ T-cells are approximately 10 times lower than those required for ZZOva. As HSPGs are ubiquitously expressed [6,7], we assumed that ZZOvaDTR-BD and ZZOvaTat22-57S might also spread *in vivo*. However, this spreading does not cause a major alteration of the cellular immune response since ZZOvaTat22-57S raises more IFN-γ-secreting Ova-specific CD8⁺ T-cells than ZZOva and Ova.

To assess the effect on Ab-targeting, we made complexes involving the ZZOva fusion proteins and an anti-MHC-II Ab. We selected the MHC-II molecule as target because it can increase APC internalization, T-cell stimulation, and immunogenicity [23,25]. We showed that subnanomolar concentrations of either anti-MHC-II/ZZOvaDTR-BD or anti-MHC-II/ZZOvaTat22-57S suffice to induce proliferation of OT-I and OT-II cells. These amounts are respectively around 15 to 50 times lower than those required when

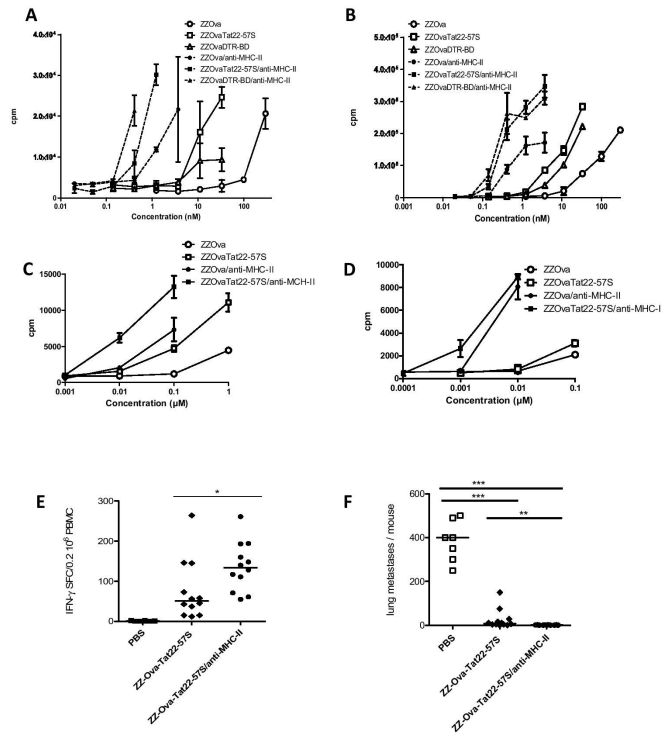


Fig. 4. Ability to bind both MHC class II molecules and HS affect T-stimulating capacity of ZZOva *in vitro* and allows control of tumour-growth. (A) CD8⁺ T-cell stimulation in splenocytes from OTI mice was assessed using ZZOva, ZZOvaTat22-57S and ZZOvaDTR-BD either free or complexed with an anti-I-A[b] MHC-II Ab. Data are expressed as cpm ± S.D. CD4⁺ T-cell stimulation in splenocytes from OT-II mice was assessed similarly to (A) (B and C) BMDC-mediated stimulation was assessed by incubating for 5-h at 37 °C these cells with the Ags described in (A). Splenocytes from OT-I mice were added to assess CD8⁺ T-cell stimulation. Splenocytes from OT-II mice were added to assess CD4⁺ T-cell stimulation (D). cpm ± SD are shown. (E and F) Mice were immunized with PBS (7 mice) or with ZZOvaTat22-57S (12 mice per group) either free or complexed to anti-MHC-II Ab. Presence of IFN-γ-secreting p257-264-specific CD8⁺ T-cells was assessed by ELISPOT (E). Mice injected with PBS or the Ags were challenged with B16F10-OVA melanoma cells to assess ability to control growth. Lung foci were counted to assess tumour burden (F). Data pooled from two independent experiments are shown.

ZZOvaTat22-57S is complexed to an IgG2a isotype control (not shown) and 300–500 times lower than those required for ZZOva. We found a similar behaviour with BMDCs as APCs indicating that dual-targeting affects dendritic-mediated cross-presentation. Altogether, these results indicate that HS-ligands can act synergistically with ligands targeting receptors selectively expressed on APCs.

We assessed whether increased T-cell stimulations are found *in vivo*, and we did not observed significant differences in the number of Ova-specific CD4⁺ and CD8⁺ T-cells between animals injected with Ova and ZZOva. Moreover, in sera from Ova-immunized mice we found 45 times more Ab than in sera from ZZOva-immunized mice. Lastly, we calculated an IgG1/IgG2b ratio of 0.17 for ZZOva-immunized mice and 3 for Ova-immunized animals. Thus, while the ZZ moiety targets APCs and increases T-cell stimulation *in vitro*, it has no effect on T-cell response and impairs Ab response *in vivo*, presumably due to a switch towards a Th1 pattern of immune response. In contrast, when Tat22-57S was fused to ZZOva we observed an increase in CD8⁺ T-cell responses. Thus, we measured

more IFN-γ-secreting CD8⁺ T-cells than in mice immunized with either Ova or ZZOva, while IL-4-secreting CD4⁺ T-cells were not affected by HS-ligand coupling. Furthermore, we calculated an IgG1/IgG2b ratio of 1.8 for sera from ZZOvaTat22-57S-immunized mice and found that these sera contained 6 times more anti-Ova Abs than sera from ZZOva-immunized mice, indicating that coupling of Tat22-57S to ZZOva causes a Th1/Th2 shift and an increase in Ab response. Altogether, these results indicate that the HS-ligand increases anti-Ova CD8⁺ response and directs Ab response to a mixed Th1/Th2 profile. In addition, comparison of the immune response raised by ZZOvaTat22-57S/anti-MHC-II and ZZOvaTat22-57S shows that the CD8⁺ and CD4⁺ T-cell response is further increased when the fusion is targeted to MHC-II molecules, which is consistent with studies showing that MHC-II targeting impacts the immune response [17,22,23].

When we made adjuvant-free immunizations, we did not find any IFN-γ and IL-4 response in mice injected with Ova, ZZOva and ZZOvaTat22-57S indicating that the HS-ligand cannot boost the

anti-Ova immune response in the absence of adjuvant (data not shown). In contrast, we found IFN- γ -secreting CD8⁺ T-cells in the eight mice immunized with ZZOvaTat22-57S/anti-MHC-II indicating that the adjuvant is not required when the fusion protein is targeted to the MHC-II molecule.

ZZOvaTat22-57S-vaccinated mice control the growth of B16F10-OVA melanoma cells. Furthermore they have Ova-specific CD8⁺ T-lymphocytes while control animals are devoid of such cells suggesting that the immune response elicited by the vaccine enables tumour-control. In support of this assumption, when we compared ZZOvaTat22-57S and ZZOvaTat22-57S/anti-MHC-II-vaccinated mice we found a significantly higher number of Ova-specific CD8⁺ T-lymphocytes in the later group and a higher tumour-control. Therefore, these data indicate that the immune response raised by the dual-targeting approach can make animals able to control tumour-growth.

Altogether, our data indicate that an Ag targeting both HSPGs and an APC-specific receptor is more efficiently supported by the immune system. Furthermore, they showed that a vaccine based on this dual-targeting approach can confer on mice the ability to control growth of a tumour cell-line opening new perspectives for the design of highly immunogenic protein vaccines.

Conflict of interest: Adeline Gadzinski, Alexandra Savatier, Jean-Claude Boulain, and Michel Léonetti have filed a patent application for the dual-targeting approach in vaccination.

Appendix A. Supplementary data

Supplementary data associated with this article can be found, in the online version, at <http://dx.doi.org/10.1016/j.vaccine.2016.04.073>.

References

- [1] Burgdorf S, Kautz A, Böhnert V, Knolle PA, Kurts C. Distinct pathways of antigen uptake and intracellular routing in CD4 and CD8 T-cell activation. *Science* 2007;316:612–6.
- [2] Guermontprez P, Valladeau J, Zitvogel L, Théry C, Amigorena S. Antigen presentation and T-cell stimulation by dendritic cells. *Annu Rev Immunol* 2002;20:621–67.
- [3] Lanzavecchia A. Mechanisms of antigen uptake for presentation. *Curr Opin Immunol* 1996;8:348–54.
- [4] Regnault A, Lankar D, Lacabanne V, Rodriguez A, Théry C, Rescigno M, et al. Fc γ receptor-mediated induction of dendritic cell maturation and major histocompatibility complex class I-restricted antigen presentation after immune complex internalization. *J Exp Med* 1999;189:371–80.
- [5] Sallusto F, Lanzavecchia A. Efficient presentation of soluble antigen by cultured human dendritic cells is maintained by granulocyte/macrophage colony-stimulating factor plus interleukin 4 and downregulated by tumor necrosis factor alpha. *J Exp Med* 1994;179:1109–18.
- [6] Lindahl U. Heparan sulfate-protein interactions – a concept for drug design? *Thromb Haemost* 2007. <http://dx.doi.org/10.1160/TH07-04-0310>.
- [7] Park PW, Reizes O, Bernfield M. Cell surface heparan sulfate proteoglycans: selective regulators of ligand-receptor encounters. *J Biol Chem* 2000;275:29923–6.
- [8] Léonetti M, Gadzinski A, Moine G. Cell surface heparan sulfate proteoglycans influence MHC class II-restricted antigen presentation. *J Immunol* 2010;185:3847–56.
- [9] Arai Y, Takahashi N, Tatsumi E, Hirose M. Structural properties of recombinant ovalbumin and its transformation into a thermostabilized form by alkaline treatment. *Biosci Biotechnol Biochem* 1999;63:1392–9.
- [10] Sedlik C, Orbach D, Veron P, Schweighoffer E, Colucci F, Gamberale R, et al. A critical role for Syk protein tyrosine kinase in Fc receptor-mediated antigen presentation and induction of dendritic cell maturation. *J Immunol* 2003;170(2):846–52.
- [11] Sedlik C, Vigneron J, Torrieri-Dramard L, Pitoiset F, Denizeau J, Chesneau C, et al. Different immunogenicity but similar antitumor efficacy of two DNA vaccines coding for an antigen secreted in different membrane vesicle-associated forms. *J Extracell Vesicles* 2014;3. <http://dx.doi.org/10.3402/jev.v3.24646.24646>.
- [13] Röttschke O, Falk K, Stevanović S, Jung G, Walden P, Rammensee HG. Exact prediction of a natural T-cell epitope. *Eur J Immunol* 1991;21:2891–4.
- [15] Nilsson B, Moks T, Jansson B, Abrahamson L, Elmblad A, Holmgren E, et al. A synthetic IgG-binding domain based on staphylococcal protein A. *Protein Eng* 1987;1:107–13.
- [16] Löwenadler B, Lycke N. Fusion proteins with heterologous T helper epitopes. Recombinant *E. coli* heat-stable enterotoxin proteins. *Int Rev Immunol* 1994;11:103–11.
- [17] Léonetti M, Thai R, Cotton J, Leroy S, Drevet P, Ducancel F, et al. Increasing immunogenicity of antigens fused to Ig-binding proteins by cell surface targeting. *J Immunol* 1998;160:3820–7.
- [18] Shimonkevitz R, Colon S, Kappeler JW, Marrack P, Grey HM. Antigen recognition by H-2-restricted T-cells. II. A tryptic ovalbumin peptide that substitutes for processed antigen. *J Immunol* 1984;133:2067–74.
- [19] Gadzinski A, Matz D, Favre E, Léonetti M. Transfer of the ability of HIV-1 Tat to raise an adjuvant-free humoral immune response to unrelated antigens. *Vaccine* 2012;30:2859–68.
- [20] Kittiworakarn J, Lecoq A, Moine G, Thai R, Lajeunesse E, Drevet P, et al. HIV-1 Tat raises an adjuvant-free humoral immune response controlled by its core region and its ability to form cysteine-mediated oligomers. *J Biol Chem* 2006;281:3105–15.
- [21] Lobeck K, Drevet P, Léonetti M, Fromen-Romano C, Ducancel F, Lajeunesse E, et al. Towards a recombinant vaccine against diphtheria toxin. *Infect Immun* 1998;66:418–23.
- [22] Birkholz K, Schwenkert M, Kellner C, Gross S, Fey G, Schuler-Thurner B, et al. Targeting of DEC-205 on human dendritic cells results in efficient MHC class II-restricted antigen presentation. *Blood* 2010;116:2277–85.
- [23] Carayanniotis G, Barber BH. Adjuvant-free IgG responses induced with antigen coupled to antibodies against class II MHC. *Nature* 1987;327:59–61.
- [24] Tacken PJ, de Vries IJM, Torensma R, Figdor CG. Dendritic-cell immunotherapy: from ex vivo loading to in vivo targeting. *Nat Rev Immunol* 2007;7:790–802.
- [25] Tacken PJ, Figdor CG. Targeted antigen delivery and activation of dendritic cells in vivo: steps towards cost effective vaccines. *Semin Immunol* 2011;23:12–20.
- [26] Fadnes B, Husebekk A, Svineng G, Rekdal Ø, Yanagishita M, Kolset SO, et al. The proteoglycan repertoire of lymphoid cells. *Glycoconj J* 2012;29:513–23.

ORIGINAL RESEARCH

Effective antitumor therapy based on a novel antibody-drug conjugate targeting the Tn carbohydrate antigen

Christine Sedlik^{a,b,c}, Adèle Heitzmann^{a,b,c}, Sophie Viel^{a,b}, Rafik Ait Sarkouh^{a,d}, Cornélie Batisse^{a,d}, Frédéric Schmidt^{a,d}, Philippe De La Rochere^{a,b}, Nathalie Amzallag^{a,b,c}, Eduardo Osinaga^{e,f}, Pablo Oppezco^{e,f}, Otto Pritsch^{e,f}, Xavier Sastre-Garau^{g,x}, Pascale Hubert^{a,b,c}, Sebastian Amigorena^{a,b,c,#}, and Eliane Piaggio^{a,b,c,#}

^aInstitut Curie, PSL Research University, Paris, France; ^bINSERM U932, Paris, France; ^cCentre d'Investigation Clinique Biothérapie CICBT 1428, Institut Curie, Paris, France; ^dCNRS UMR3666/INSERM U 1143, Paris, France; ^eDepartamento de Inmunobiología, Facultad de Medicina, Universidad de la República, Montevideo, Uruguay; ^fInstitut Pasteur de Montevideo, Montevideo, Uruguay; ^gDépartement de Biologie des Tumeurs, Institut Curie, Paris, France

ABSTRACT

Antibody-drug conjugates (ADC), combining the specificity of tumor recognition by monoclonal antibodies (mAb) and the powerful cytotoxicity of anticancer drugs, are currently under growing interest and development. Here, we studied the potential of Chi-Tn, a mAb directed to a glyco-peptidic tumor-associated antigen, to be used as an ADC for cancer treatment. First, we demonstrated that Chi-Tn specifically targeted tumor cells *in vivo*. Also, using flow cytometry and deconvolution microscopy, we showed that the Chi-Tn mAb is rapidly internalized – condition necessary to ensure the delivery of conjugated cytotoxic drugs in an active form, and targeted to early and recycling endosomes. When conjugated to saporin (SAP) or to auristatin F, the Chi-Tn ADC exhibited effective cytotoxicity to Tn-positive tumor cells *in vitro*, which correlated with the level of tumoral Tn expression. Furthermore, the Chi-Tn mAb conjugated to auristatin F also exhibited efficient antitumor activity *in vivo*, validating for the first time the use of an anti-Tn antibody as an effective ADC.

ARTICLE HISTORY

Received 9 December 2015
Revised 12 February 2016
Accepted 23 March 2016

KEYWORDS

Biodistribution;
internalization; MMAF;
monoclonal antibody-drug
conjugate; Tn antigen

Introduction

Over the last two decades, monoclonal antibody (mAb) therapy was established as an effective treatment against cancer.^{1,2} Therapeutic mAbs can be used as naked antibodies, inhibiting tumor growth directly by inducing apoptosis upon binding to their specific antigen, and/or indirectly by stimulating the immune system. In addition, antibodies recognizing targets/receptors expressed at the surface of malignant cells can be used as antibody-drug conjugates (ADC) to target potent cytotoxic agents selectively to the tumors without affecting healthy cells. The challenge for ADC strategies is to increase antitumor efficacy with diminished toxicity.³

Antibodies can be conjugated to plant or bacterial toxins (ricin and saporin or diphtheria toxin and pseudomonas exotoxin A, respectively), to radioisotopes (β emitters ⁹⁰Y and ¹³¹I, or α -particles ²¹³Bi and ²¹¹At), to anticancer chemotherapies (doxorubicin, methotrexate or vinblastine), and to toxic drugs or their derivatives, such as calicheamicin (causing double-strand DNA breaks), auristatins and maytansines (inhibitors of microtubule assembly) or α -amanitin (inhibitor of RNA polymerase II).⁴

Several requirements need to be fulfilled for a mAb to be used as an ADC, including high tumor selectivity, high expression of its target cell surface antigen and internalization of antigen-ADC complexes into the cancer cell where the drug will be

active.^{4,5} Upon ligand binding, membrane receptors are internalized within early endosomes. Some receptors are then recycled back to the cell surface, while others are sorted into late endosomes and lysosomes where degradation occurs.⁶

Conjugation of drugs to targeting antibodies is designed, taking into account the subcellular compartment reached by the ADC after internalization into the cell, so that the drug can be released from the carrier under an active form.⁷ Thus, to facilitate the drug release within early endosomes, pH-sensitive linkers (for example acid-labile bonds such as hydrazide) have been incorporated between the drug and the mAb, leading to conjugates stable at pH = 7.4 in the blood, and cleaved at pH = 5 in endosomes.^{5,8} Alternatively, other linkers containing cleavable functions as disulfides, thioethers or dipeptides, have been used that are cleaved inside the lysosomes, while releasing the drug moiety.^{4,5} Drugs can be also attached to the mAb through the non-cleavable maleimidocaproyl linker (mc), which is related to the maleimidocaproyl-Valine-Citrulline (mc-Val-Cit) linker.⁹ The maleimide is designed to react with a thiol function on the antibody and the carboxylic acid end of the linker with the secondary amine of auristatin. Identifying tumor-specific surface proteins that are efficiently internalized and drive their ligands to the appropriate endosomes for drug delivery is a major challenge for the development of effective cancer ADCs.

CONTACT Eliane Piaggio  eliane.piaggio@curie.fr; Sebastian Amigorena  sebastian.amigorena@curie.fr

*Current address: Service de Biopathologie, Institut de Cancérologie de Lorraine, Vandoeuvre-les-Nancy, France.

#These authors contributed equally to this work.

© 2016 Taylor & Francis Group, LLC

Tn (CD175) is a tumor-associated carbohydrate antigen composed of an N-acetyl-galactosamine residue (GalNAc) linked by O-glycosylation to serine or threonine amino acids, mainly found in mucin-type glycoproteins.^{10,11} The Tn antigen is normally cryptic in mucin-type O-glycans and becomes expressed at the surface of tumor cells because of alterations along the O-glycosylation pathways, resulting in defective elongation of carbohydrate chains. Importantly, Tn is highly expressed in various epithelial cancers (primarily ovarian, breast, prostate, colorectal, and lung cancers), and virtually absent in normal tissues.¹²⁻¹⁷ Moreover, the Tn antigen is involved in the adhesion of tumor cells to the lymphatic endothelium, and Tn-antigen expression seems to correlate with metastatic potential and poor prognosis.^{10,15,18} Thus, these data make the Tn-antigen an attractive target for a therapeutic antibody.

Several anti-Tn mAbs with different fine specificities for the Tn antigen have been generated,^{16,18-22} and two of them were reported to increase survival of mice inoculated with a Jurkat tumor cell line¹⁹ or a lung carcinoma cell line.²³ However, none of these antibodies have been validated for their use as an ADC. In a previous work, we demonstrated that naked Chi-Tn mAb, a mouse/human IgG1 chimeric anti-Tn mAb²² was able to induce the rejection of TA3Ha mammary tumor in mice and this effect was dependent on activating FcγRs.¹⁴ In the present study, we further explored the therapeutic potential of the Chi-Tn mAb, but using the antibody as an ADC to selectively target cytotoxic molecules into tumor cells. We showed that the naked Chi-Tn mAb was effectively and rapidly internalized, reaching the early, but not the late, endocytic compartments *in vitro*. Furthermore, *in vivo*, the Chi-Tn mAb selectively accumulated in the solid tumor, but not in healthy tissue. When conjugated to saporin (SAP) or to auristatin F, the Chi-Tn ADC exhibited effective cytotoxicity to Tn-positive tumor cells *in vitro*. Finally, the Chi-Tn mAb conjugated to MMAF also induced a delay of tumor growth *in vivo*, validating for the first time the use of an anti-Tn antibody as an effective ADC.

Results

The chimeric mAb Chi-Tn specifically binds Tn expressed at different levels on various tumor cell lines

The Tn antigen is present in numerous solid and hematologic tumors,^{10,12-17,24-26} but its level of expression varies among the different tumors and Tn can be found on various different peptide sequences. Consequently, to study if the chimeric mAb Chi-Tn can be used as a potential ADC to selectively target cytotoxic molecules into tumor cells, we first confirmed and extended our previous results¹⁴ showing that this mAb recognized Tn at the surface of different tumor cell lines (Fig. 1A). Jurkat cells (human T-ALL) displayed the strongest Tn-specific binding of the Chi-Tn mAb to the cell surface, and the human ovarian cancer cell lines, Shin-3 and OvCar-3, also bound the Chi-Tn mAb, although with a lower intensity. Tn surface expression was also detected by Chi-Tn mAb in breast cancer cell lines, either from human origin, such as MCF7 cells¹⁴ or from murine origin, such as TA3Ha cells (Fig. 1A).

It was previously shown that the ADC activity of therapeutic Abs correlates with the expression level of its cognate tumoral antigen.²⁷⁻²⁹ Thus, we estimated the amount of surface-expressed Tn antigen by quantitative flow cytometry (Fig. 1B).^{27,29} The Jurkat cells expressed the highest number of Tn molecules at the cell surface, approximately 5×10^5 per cell, while Shin-3 or OvCar-3 cells express 6×10^4 molecules per cell. The murine TA3Ha tumor cells express an intermediate level with 1.5×10^5 molecules/cell. This quantification by flow cytometry was strongly correlated with the results obtained by Scatchard analysis using radiolabeled Chi-Tn (unpublished results from F. Davodeau, Nantes).

In vivo, the Chi-Tn mAb specifically targets tumor cells

To study the *in vivo* targeting capacity of the Chi-Tn mAb, we used an experimental tumor model consisting in the subcutaneous (s.c.) injection of the Shin-3 human solid tumor cells to nude mice. By day 12 after the injection, when solid tumors were already palpable, mice were injected intraperitoneal (i.p.) with Chi-Tn mAb or control mAb (Herceptin®, anti-Her2 mAb) and 2 d later, tumor and other organs were analyzed by immunohistochemistry (IHC, Fig. 2A). As shown in Fig. 2B, established solid tumors still highly expressed the Tn antigen, while Tn expression was not detected in other tissues/organs distal to the site of injection of the Shin-3 cells, such as liver, spleen or lungs (data not shown). To evaluate the *in vivo* bio-distribution of the Chi-Tn mAb, we directly labeled the tissue sections with a PE-coupled secondary GaH-Fc Ab F(ab')₂ specific for the human Fc part of the Chi-Tn mAb. As shown in Fig. 2C, the i.p.-injected Chi-Tn mAb was recovered in tumor sections while it was not detected in other organs (liver, spleen, and lungs, Fig. 2D). Moreover, no mAb was detected in tumors from mice injected with the hIgG1 control mAb (data not shown). These data indicate that *in vivo*, the Chi-Tn mAb specifically targets s.c. tumors, whereas it has no detectable binding on normal tissues and suggest that Chi-Tn could be an attractive candidate mAb to deliver radiation, drugs or toxins to tumor sites, without toxicity to normal tissue.

The Chi-Tn mAb is rapidly internalized in cancer cells

To use the Chi-Tn mAb as an ADC, it has to be internalized effectively in its target cells to deliver the cytotoxic compound. We then analyzed the outcome of the Chi-Tn mAb after its binding to cell surface of tumor cells. For that, Jurkat, Shin-3, and TA3Ha cells were first incubated at 4°C with Chi-Tn mAb, then transferred to 37°C, and the membrane-bound Chi-Tn mAb was quantified at different time points by flow cytometry. As shown in Fig. 3A, only 20% of the Chi-Tn mAb initially bound was detected after 5 min at 37°C, at the cell surface of the three different tumor cell lines tested. The percentage of the Chi-Tn mAb remaining at the plasma membrane after 1 h at 37°C reached 15, 4.4, and 10% on Jurkat, Shin-3, and TA3Ha cells, respectively (Fig. 3A). These results showing that the Chi-Tn mAb rapidly disappears from the plasma membrane at 37°C, suggest that the mAb is either internalized into the cells or released into the extracellular medium.

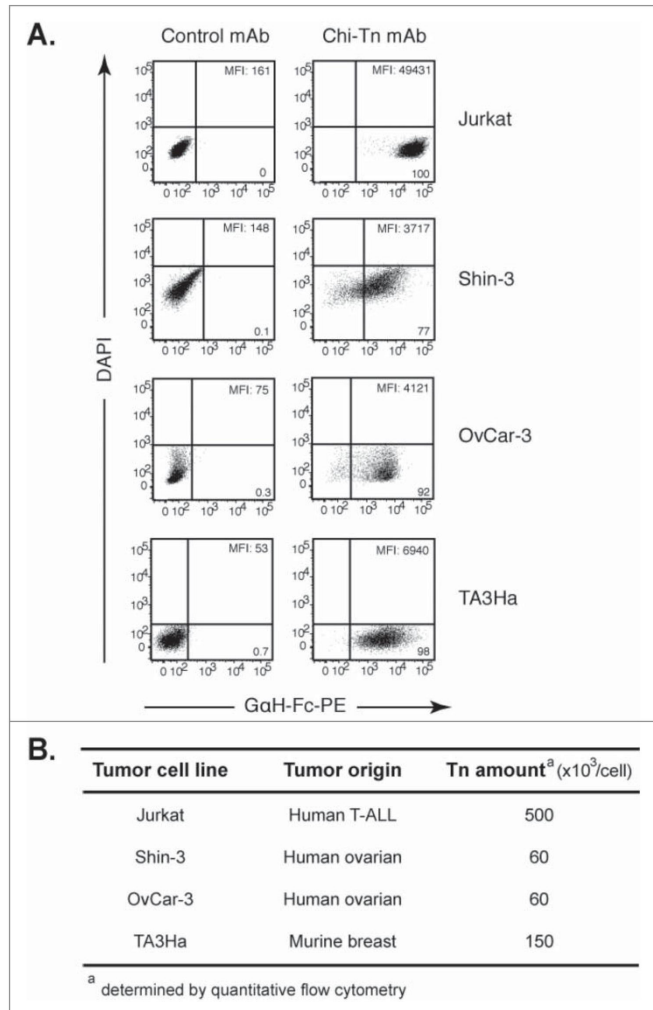


Figure 1. Chi-Tn mAb specifically binds Tn expressed at different levels on various tumor cell lines. (A) Jurkat, Shin-3, OvCar-3 or TA3Ha cells were labeled with the Chi-Tn mAb or a control antibody (Ivlg for human cells or trastuzumab for murine cells) at 20 $\mu\text{g}/\text{mL}$, then with a GaH-Fc-PE secondary antibody. DAPI-negative living cells were acquired by flow cytometry and the PE mean fluorescence intensity (M.F.I.) was determined and is indicated for each sample. Numbers in the quadrants: % of cells. (B) The number of Tn motifs expressed at the cell surface of different tumor cell lines was estimated by quantitative flow cytometry using a murine anti-Tn mAb.

To determine if the Chi-Tn mAb was internalized into tumor cells, the antibody was bound to Jurkat, OvCar-3, Shin-3, or TA3Ha cell surface at 4°C, prior transfer of the cells to 37°C during various times. Analysis by deconvolution microscopy (Fig. 3B) showed that initially, at 4°C, the Chi-Tn mAb was localized at the plasma membrane of the cells. After 5 min incubation at 37°C, the Chi-Tn mAb was observed in

intracellular structures distributed throughout the cytoplasm. Consistent with flow cytometry results, Chi-Tn mAb internalization increased with time and was more noticeable in cells originally displaying higher amounts of the Tn antigen at the plasma membrane (see Fig. 1). After 15 min at 37°C, the Chi-Tn mAb was internalized in about 77, 86, 44, and 79% of Jurkat, OvCar-3, Shin-3, and TA3Ha cells, respectively (data

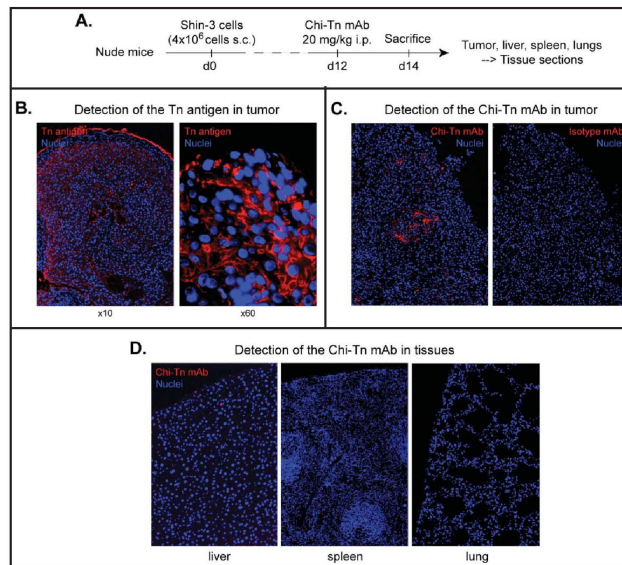


Figure 2. *In vivo* biodistribution of the Chi-Tn mAb. (A) Nude mice were grafted s.c. with 4×10^6 Shin-3 tumor cells, and were injected i.p. on day 12 with the Chi-Tn mAb or the control mAb at 20 mg/kg. On day 14, solid tumor and organs were removed and sectioned for immunofluorescence (IF) studies. (B) To detect Tn-positive cells, tissue sections were labeled with the Chi-Tn mAb, and with GaH-Fc-Biot and Sa-Cy3. (C) and (D) To detect the presence of the Chi-Tn mAb (or control mAb, red), tumor (C) or tissues (D) sections were labeled directly with GaH-Fc-Biot and Sa-Cy3. Nuclei were labeled using DAPI (blue), and images were acquired by microscopy.

not shown). After around 30 min at 37°C, the Chi-Tn mAb-containing vesicles were readily observed forming clusters close to the juxta-nuclear region in all the studied cell lines. We conclude that the Chi-Tn mAb binds to the plasma membrane of tumor cells, and is then rapidly internalized.

The Chi-Tn mAb localizes to early and recycling endosomes

After endocytosis, ligand-receptor complexes are internalized and sorted to early endosomes. Receptors are then either recycled back to the plasma membrane through recycling endosomes, or delivered to late endosomes and lysosomes for degradation.⁶

We investigated the nature of the compartment(s) targeted by the Chi-Tn mAb after internalization using markers of early endosomes, recycling endosomes or late endosome/lysosomes. After internalization in Jurkat cells, Chi-Tn mAb accumulated in transferrin-positive compartments, indicating its presence in early endosomes and/or recycling endosomes.³⁰ (Fig. 4A). Chi-Tn mAb was also present in Rab-11-positive recycling endosomes³⁰ (Fig. 4B), but with a lower proportion of co-localization than in the early endosomes. These co-localizations started as soon as 5 min and lasted for up to 4 h after transfer at 37°C. On the contrary, Chi-Tn mAb could not be detected in late endosomal/lysosomal LAMP-1⁺ compartments, even after 4 h of incubation at 37°C (Fig. 4C). We observed the same pattern of intracellular localization of Chi-Tn in TA3Ha cells, with a co-localization in early endosomes and no detection in LAMP-1-positive compartments (data not shown). Therefore,

internalized Chi-Tn, accumulates in early and recycling endosomes and is delivered inefficiently to late endosomes and lysosomes.

The Chi-Tn mAb coupled to saporin inhibits tumor cell growth *in vitro*

Since Chi-Tn mAb is effectively and rapidly internalized, we evaluated if it could be used as an ADC. To do so, Chi-Tn was coupled to SAP, a ribosome-inactivating protein (RIP) that inhibits protein synthesis and prevents cell proliferation.³¹

We first assessed whether SAP was directly cytotoxic to different cancer cell lines. For that, viability of TA3Ha, Jurkat, OvCar-3, and Shin-3 cells was measured after 3 d of culture in the presence of different concentrations of SAP. Fig. 5A shows that unconjugated SAP, which has limited access to the cell cytoplasm, does not markedly affect the viability of the different cell lines at concentrations lower than 1 nM. However, at higher concentrations, Jurkat and TA3Ha cell growth is inhibited by the drug, indicating that these cells are more sensitive to SAP at higher doses as compared to OvCar-3 and Shin-3 cells.

Conjugation of SAP to the Chi-Tn mAb, importantly increased the drug cytotoxicity, which was not due to the mAb itself because, as previously described,¹⁴ the Ab alone was ineffective at inhibiting *in vitro* cell proliferation of Jurkat, TA3Ha, OvCar-3, and Shin-3 cells (Fig. 5B). SAP-conjugated Chi-Tn mAb (Chi-Tn/SAP, molar ratio: SAP/Chi-Tn = 2.7) induced a dose-dependent inhibition of the growth of the Tn-expressing

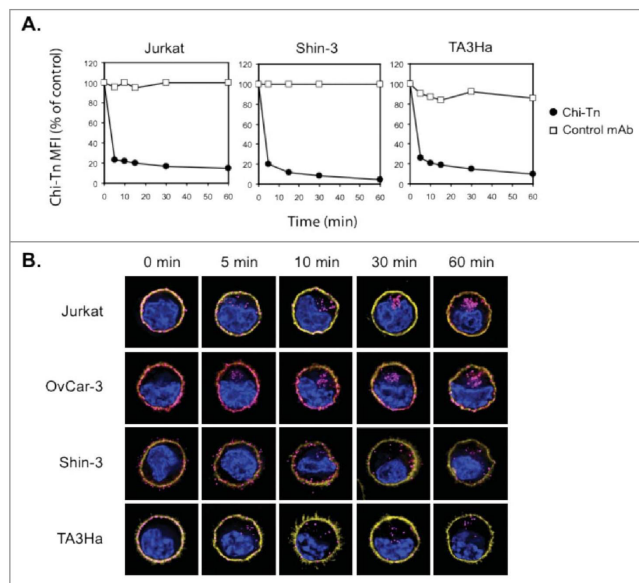


Figure 3. The Chi-Tn mAb is internalized into cancer cells. (A) Jurkat, Shin-3 or TA3Ha cells were incubated for 15 min on ice with the Chi-Tn mAb or with a control antibody (Ivlg for human cells or trastuzumab for murine cells) at $20 \mu\text{g}/\text{mL}$, washed, then transferred to 37°C for the indicated times. Cells were then labeled with GaH-Fc-PE, and the Chi-Tn mAb M.F.I. was determined by flow cytometry in the DAPI-negative living cells gate. For each sample, the Chi-Tn M.F.I. is expressed as a percentage of the Chi-Tn M.F.I. obtained for cells not transferred to 37°C (control cells). (B) Jurkat, OvCar-3, Shin-3 or TA3Ha cells were incubated on ice with the Chi-Tn mAb for 15 min, washed and transferred to 37°C for the indicated period of time. Cells were then fixed to glass coverslips and labeled. Yellow: actin network; pink: membrane-bound or internalized Chi-Tn mAb; blue: DAPI. Arrows indicate examples of internalized Chi-Tn mAb.

tumor cell lines Jurkat and TA3Ha after a 3 d-treatment *in vitro*, but had no apparent effect on OvCar-3 and Shin-3 cells (Fig. 5B). The Chi-Tn/SAP IC_{50} values were 7×10^{-11} M for Jurkat cells and 8×10^{-9} M for TA3Ha cells. Notably, SAP alone only inhibited Jurkat and TA3Ha cell growth at much higher molar concentrations (IC_{50} : $3\text{--}4 \times 10^{-8}$ M) (Fig. 5A). Furthermore, Chi-Tn/SAP conjugates showed no cytotoxic effect on the Tn-negative EL-4 cell line (data not shown), while SAP alone inhibited the growth of these cells at concentrations similar to those inhibiting Jurkat and TA3Ha cell proliferation. Of note, the Chi-Tn/SAP conjugate showed high toxicity when administered to mice (data not shown), even at the low doses previously reported.³²

Collectively, these results demonstrate that Chi-Tn/SAP immunotoxin displays Tn-specific cell cytotoxicity *in vitro*, for concentrations of SAP lower than those required for cell growth inhibition using SAP alone. However, as in our hands the Chi-Tn/SAP conjugate is highly toxic for mice, we abandoned this strategy and conjugated the Chi-Tn mAb to a different cytotoxic drug.

The Chi-Tn mAb coupled to auristatin F inhibits tumor cell growth *in vitro*

Another Chi-Tn ADC was prepared by coupling the mAb to the monomethyl auristatin F drug (MMAF), an antimitotic

agent that inhibits cell division by blocking the polymerization of tubulin.⁹ MMAF is a monomethyl auristatin E (MMAE) analog with a charged C-terminal phenylalanine residue that attenuates the cytotoxic activity compared to the uncharged counterpart MMAE, because it reduces the passive plasma membrane crossing.^{9,33} Since we showed that internalized Chi-Tn mAb accumulates in early and recycling endosomes, while being delivered inefficiently to late endosomes and lysosomes, we chose a protease-independent linker to conjugate the Chi-Tn mAb and the Herceptin[®] control to MMAF. Indeed, the mc linker is stable in the extracellular fluid, but is cleaved once the conjugate has entered a tumor cell, thus releasing the antimitotic compound.^{9,34} We prepared ADC-MMAF that contained an average of five MMAF molecules per antibody (Chi-Tn or Her).

As shown in Fig. 5C, free MMAF is cytotoxic to Tn-positive Jurkat and Her2 positive SKBR3 cells, with IC_{50} values of 4.5×10^2 and 8.3×10^1 nM, respectively indicating that these cells are sensitive to the MMAF drug. Contrary to the Chi-Tn mAb alone, which was ineffective at inhibiting the proliferation of the Tn-expressing tumor cells Jurkat, except at the highest tested dose, the Chi-Tn mAb conjugated to MMAF induced a dose-dependent cytotoxicity on these cells after a 3 d-treatment *in vitro* (Fig. 5D). Although the Chi-Tn/MMAF recognized Tn at the surface of the Shin-3 or OvCar-3 cells Tn-expressing cell lines as effectively as the naked Chi-Tn mAb (data not shown),

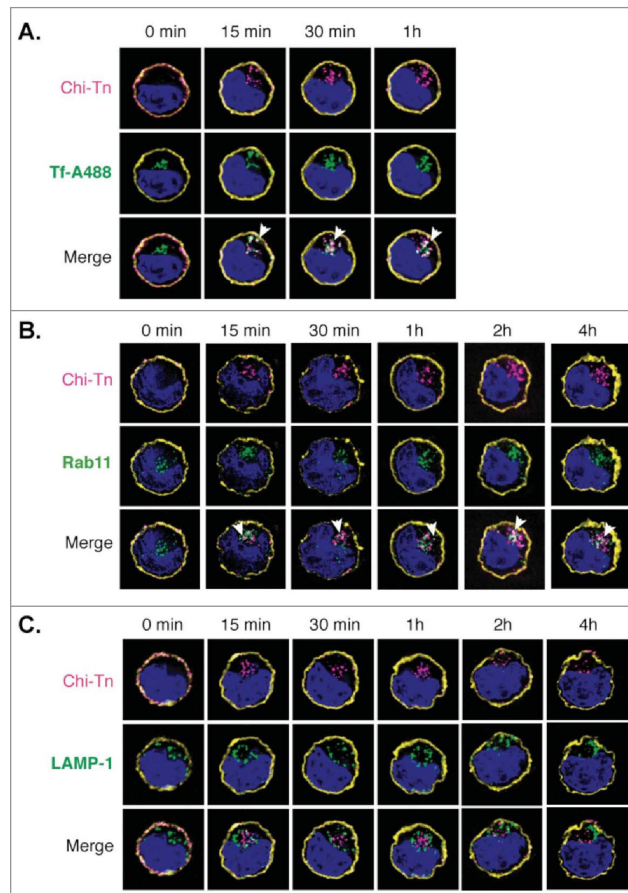


Figure 4. Analysis of the Chi-Tn mAb targeting to endosomal compartments Jurkat cells were labeled with the Chi-Tn mAb, transferred to 37°C for the indicated times, then actin (yellow) and Chi-Tn (pink) were detected in fixed cells. Early endosomes were detected using TF-A488 (green, A), recycling endosomes with Rab11 (green, B), and late endosomes with anti-LAMP-1 mAb (green, C). Blue: DAPI. Images were acquired by deconvolution 3D-microscopy. Examples of co-localization (in white) are indicated by arrows.

the conjugate Chi-Tn/MMAF did not exhibit cytotoxicity toward these cell lines (data not shown). Importantly, the Chi-Tn/MMAF conjugate was specific for Tn expressing tumor cells (Fig. 5D). Indeed, in the same experiment, MMAF conjugated to a non-Tn binding mAb (Her/MMAF) did not have cytotoxic activity to Tn-positive Jurkat cells, indicating that cell killing was subsequent to binding to Tn. In parallel, Her/MMAF conjugate was cytotoxic to Her2-expressing SKBR3 tumor cells (Fig. 5D). These results show that the Chi-Tn/MMAF ADC displays Tn-specific cell cytotoxicity *in vitro*. Therefore, *in vivo* tumor targeting using Chi-Tn/MMAF conjugate should allow the use of lower doses of the cytotoxic MMAF, specifically

delivering it into the Tn positive tumor cells and thus limiting adverse toxic effects.

***In vivo* antitumor efficacy of Chi-Tn/MMAF ADC**

We showed above that Chi-Tn/MMAF ADC exhibited *in vitro* cytotoxicity on Jurkat, but not on OvCar-3 or Shin-3 cells. To evaluate the *in vivo* antitumor activity of the ADC, we grafted Jurkat cells s.c. in Nude mice, but the cells did not grow. Thus, we moved to the LOX melanoma cell line, which expresses a high and stable level of Tn at its surface (Fig. 5E) and forms tumors in Nude mice. We first demonstrated that the

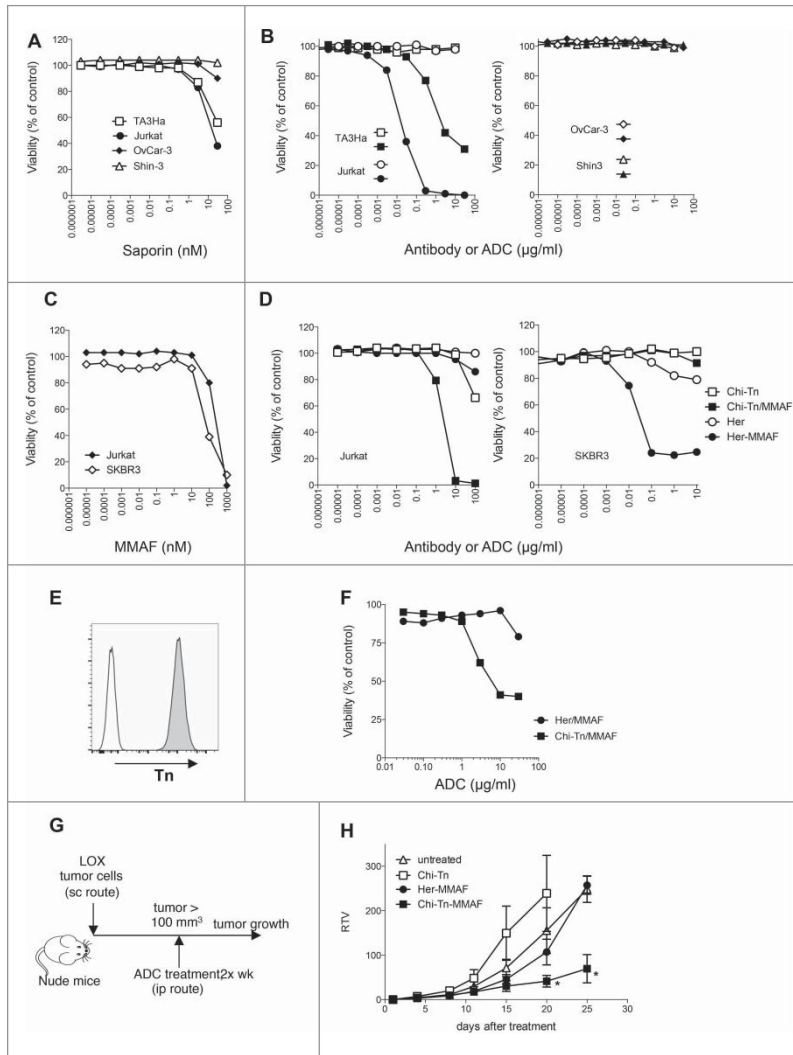


Figure 5. *In vitro* and *in vivo* cytotoxicity of Chi-Tn-ADC on cancer cells (A–D) *In vitro* cytotoxicity of Chi-Tn ADC. (A) TA3Ha, Jurkat, OvCar-3 or Shin-3 cells were cultured with the indicated concentrations of free saporin (SAP). (B) Jurkat, TA3Ha (left panel), and OvCar-3 and Shin-3 cells (right panel) were cultured with the indicated concentrations of Chi-Tn mAb (open symbol) or the Chi-Tn/SAP conjugate (filled symbol). (C) Jurkat and SKBR3 cells were cultured with free MMAF. (D) Jurkat (left panel) and SKBR3 (right panel) cells were cultured with Chi-Tn/MMAF or Her/MMAF conjugate, naked Chi-Tn or Her mAb. Cell viability was assessed after 3 d of culture. Results are expressed as percentage of viable cells compared to untreated cells. (E–H) *In vivo* cytotoxicity of Chi-Tn/MMAF against Tn⁺ LOX tumor cells. (E) LOX cells express a high and stable level of Tn. LOX cells were labeled with the Chi-Tn mAb or a control antibody at 20 μg/mL, then with a GaH-Fc-PE secondary antibody and Tn expression was measured by flow cytometry. (F) LOX cells were cultured with the Chi-Tn/MMAF or Her/MMAF conjugate at the indicated concentrations. Cell viability was then assessed after 3 d at 37°C. Results are expressed as percentage of viable cells compared to untreated cells. (G) Experimental schedule of the *in vivo* antitumor assay. Nude mice were grafted with the LOX Tn⁺ human cell line and then treated twice a week with the Chi-Tn/MMAF (n = 8) or control Her/MMAF (n = 6) conjugates, with the naked Chi-Tn mAb (n = 6), or were left untreated (n = 7). (H) Tumor growth is depicted as Relative Tumor Volume (RTV), as explained in the Materials and Methods section. Statistical significance was calculated with Mann-Whitney test; significant statistical difference was observed on days 20 and 25 between Her-MMAF and Chi-Tn-MMAF treated groups ($p < 0.05$).

Chi-Tn/MMAF conjugate showed cytotoxic activity on the LOX cells *in vitro*, with cytotoxicity increasing with the dose of ADC (Fig. 5F). This effect was specific to Tn binding, since the ADC containing the irrelevant Ab, Her/MMAF, did not exhibit cytotoxicity except at the highest tested dose. Then, the Chi-Tn/MMAF was investigated in the LOX xenograft model in Nude mice (Fig. 5G). After detection of a palpable tumor, mice were treated with the Chi-Tn/MMAF twice a week along the experiment. Mice did not present any overt clinical signs of adverse events associated to the ADC treatment. We observed that the Her/MMAF conjugate and the non-conjugated Chi-Tn treated mice behaved similarly to the untreated mice (no statistical significance). However, tumor-bearing mice treated with

Chi-Tn/MMAF showed an important delay of the tumor growth, highlighting the antitumor activity of the drug-conjugated Chi-Tn antibody (Fig. 5H).

Tn is highly expressed in human cancer tissues, yet at different levels

To further investigate which could be the more adapted clinical setting for the use of anti-Tn drug-conjugate antibodies, we analyzed by IHC the expression level of Tn in paraffin-embedded tumor samples from patients with breast, ovary or endometrium cancers. As shown in Fig. 6, Tn was detected in a great majority of these tumor types, ranging from 80 to 90% of

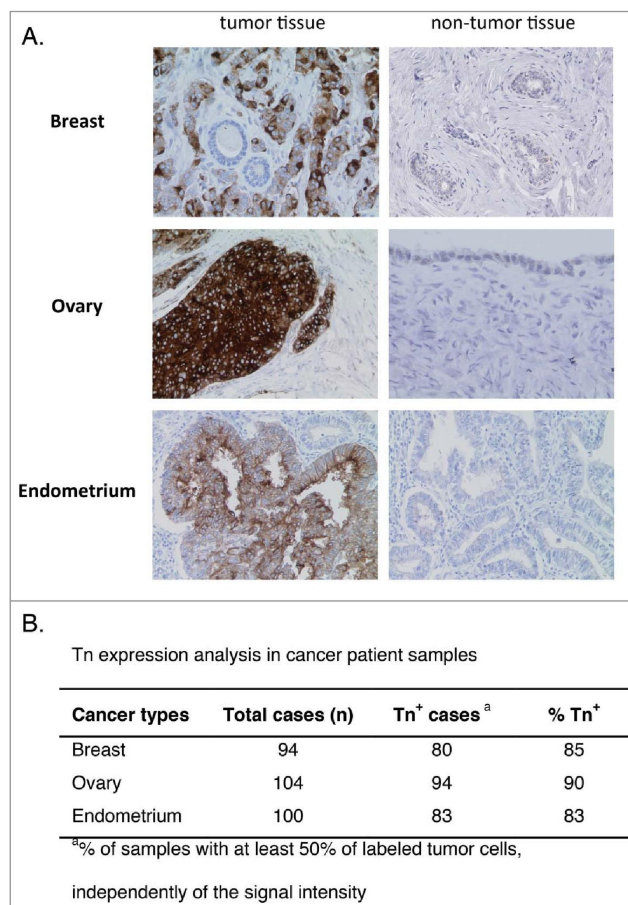


Figure 6. Analysis of Tn expression in cancer samples from patients. Breast, ovary, and endometrium tumor samples were analyzed by IHC. (A) Representative images of Tn expression in tumor and in healthy breast, ovary and endometrium tissues. (B) Quantification of Tn expression in the different tumor samples.

positivity in the tested tumor sections (85% for breast, 90% for ovary, and 83% for endometrium cancers). Although the level of Tn expression was variable among the different samples, we observed that Tn⁺ ovary tumors consistently exhibited the highest intensity of staining. In the tumors, Tn immunostaining was constantly localized in the cytoplasm, with frequent enhancement of the labeling at the plasma membrane. Exclusive staining at the plasma membrane was not observed. Variability in labeling score was related to the number of cells exhibiting significant staining more than variations in staining intensity. Of note, Tn expression could also be detected in non-tumor cells of the epithelium of normal fallopian tubes. The labeling of other non-tumor tissue was always at a distinctly weaker signal compared to tumor cells. These results emphasize that, as observed with the different tumor cell lines, the different tumor types show varying degree of Tn expression that could condition response to anti-Tn drug-conjugated Abs.

Discussion

Ideal antibodies for delivering cytotoxic drugs specifically to tumors should target abundantly expressed tumor-specific surface receptors that are internalized efficiently resulting in effective drug delivery. The Tn antigen (GalNac-O-Ser/Thr) is expressed in a great variety of adenocarcinomas^{10,12,13,15,16} and in some hematologic malignancies,²⁴⁻²⁶ but not in healthy tissue. Each anti-Tn antibody is unique in its recognition pattern and function.³⁵ Here, we show that the Chi-Tn mAb that we have generated recognizes Tn on a variety of solid tumors with high specificity,^{14,36} it is rapidly internalized into Tn-positive tumor cells, and is localized mostly in early endosomes. Given these results indicating that the Chi-Tn mAb is a good candidate to selectively deliver powerful cytotoxic agent to tumor cells, we used an armed antibody approach. Indeed, we show in this study that Chi-Tn mAb inhibits Tn-positive tumor cell growth *in vitro* when coupled to SAP or MMAF cytotoxic drugs, whereas Tn-negative cells remain unaffected. We also describe a unique ADC that inhibits tumor growth *in vivo* by specifically delivering the microtubule disrupting agent auristatin F to Tn-expressing tumors. This constitutes the first evidence that an anti-Tn antibody can be successfully conjugated to a cytotoxic drug to be used as a novel antitumor therapeutic agent.

The chimerization of the original murine anti-Tn 83D4 IgM Ab with human Fc generated the Chi-Tn mAb, which recognizes the Tn Ag on tumor cells with a 10-fold reduced affinity (K_d 2.2×10^{-8} M) as compared to the original IgM (K_d 3.1×10^{-9} M³⁷). The moderate affinity might be correlated to the glycopeptidic nature of the Ag as compared to rituximab or trastuzumab, which are directed against protein (affinity of 10^{-9} – 10^{-10} M), since another IgG1 chimeric anti-Tn mAb was reported to have a low affinity (10^{-7} M).¹⁹ Even though intermediate affinities may be detrimental for binding and internalization, it was shown that low affinity mAbs may penetrate solid tumors more efficiently.³⁸

Usually Abs bound to their ligand enter cells along the endocytic pathway, until they reach the acidic lysosomes where final degradation occurs.³⁹ Of note, in the case of the Chi-Tn mAb, we observed that after binding to the surface-expressed Tn, the

antibody was rapidly internalized and detected mainly in early endosomes and, to a lesser extent, in recycling endosomes. However, although we did not observe the Chi-Tn mAb in lysosomes, even after overnight incubation at 37°C, we cannot exclude that the mAb reaches lysosomes and is too rapidly degraded to be detectable. Nevertheless, the clinically used mAb trastuzumab directed against HER2 has been described as being similarly internalized in early/recycling endosomes and then recycled to the plasma membrane in breast carcinoma cell lines, without reaching lysosomes.⁴⁰ Other Abs were also described to localize in early and/or recycling vesicles^{41,42} and still have antitumor effects, indicating that drug targeting into early endosomes may represent an efficient alternative pathway to obtain antitumor responses with ADC therapy.

Lysosomal compartments are also often the site of cleavage of ADC, especially when the linker contains a dipeptide such as the mc/Val-Cit/PAB used to bind MMAE or MMAF to Abs.^{27,43} Therefore, since the Chi-Tn mAb mainly localized to early endosomes, we chose to couple the Chi-Tn mAb using the protease-independent mc linker. Indeed, this linker has been previously described to appropriately conjugate Abs to auristatin and to be as effective as the dipeptide-based linkers, with the advantage of decreased toxic adverse effects.^{9,44} We first used Chi-Tn mAb conjugated to the plant toxin SAP, a ribosome-inactivating enzyme largely studied recently.⁴⁵ Indeed, SAP is very stable, maintains its enzymatic activity after conjugation, and resists to proteolytic degradation, thus producing very efficient conjugates for the killing of target cells.⁴⁵ We showed that the Chi-Tn mAb can be used as an efficient ADC to induce tumor cytotoxicity, as Chi-Tn/SAP immunotoxin strongly inhibited the proliferation of Tn-positive Jurkat and TA3Ha cells *in vitro*. Unfortunately, we could not evaluate the Chi-Tn/SAP activity *in vivo*, as this conjugate was toxic for mice. Indeed, we tested different Chi-Tn/SAP doses that, in accordance to the existing literature, had been previously used successfully, without toxicity (for review see reference⁴⁵). We have no clear explanations for this unattended experimental observation, which could be due to specificities of this drug-conjugated construct (Ab, linker), mouse genetic background and/or tumor cell type.

We then evaluated auristatin derivatives, and selected MMAF, less toxic as a free drug than the analog MMAE molecule, resulting in reduced adverse effects on healthy tissues in case of release in the extracellular environment before entering the target tumor cell.^{9,43} The optimal drug loading per antibody had already been described for MMAF, with the best therapeutic index (ratio between an effective antitumor activity and the maximal tolerated dose) obtained with four molecules per antibody⁴⁶ as compared to its counterpart with eight drug molecules per antibody. In our hands, our Chi-Tn/MMAF conjugate contained an average of five molecules per antibody – a molar ratio that was previously shown to have antitumor activity with less adverse toxicity⁴⁶ and potently inhibited the proliferation of Tn-positive tumor cell lines *in vitro*. Interestingly, the cytotoxic effect of the Chi-Tn mAb conjugated to MMAF was dependent on the level of expression of Tn. Indeed, we observed that the ADC inhibited proliferation of Jurkat and LOX cells, which express high levels of the target antigen; but not of Shin-3 and OvCar-3, which express low Tn levels,

although these cells were sensitive to the free drug. This suggests that the level of antigen targeted by the ADC is crucial to achieve an effective antitumor effect by the Chi-Tn-drug conjugate, in agreement with previous studies.²⁷⁻²⁹

Our results are the first to show that Chi-Tn-based ADC exhibit antitumor activity in a mice model using the Tn-expressing LOX human tumor xenograft. Along these lines, similar results obtained in *in vivo* models with antibodies targeting other tumor-associated antigens, such as CD22, PMSA, MUC16, and 5T4, conjugated to MMAF or to MMAE,⁴⁷ have supported the clinical development of these antibodies, as illustrated by numerous ongoing clinical trials in various tumor types (<http://www.seattlegenetics.com/pipeline>). Furthermore, an anti-CD30 mAb bound to MMAE (Brentuximab vedotin, SGN-35, Seattle Genetics/Takeda) with high therapeutic efficiency in Hodgkin's lymphoma and anaplastic large cells lymphoma (ALCL), has been recently approved for clinical use in more than 55 countries, including the US and European countries.

Overall, our results documenting the high tumor selectivity of the Chi-Tn mAb, its rapid internalization, and targeting to early and recycling endosomes, as well as its effective *in vitro* and *in vivo* antitumor effect when linked to a cytotoxic drug, establish the proof of concept that an anti-Tn mAb can be used as an ADC. Interestingly, we observed that Tn was highly expressed in different tumor types, such as breast, ovary, and endometrium carcinomas but with variable patterns of distribution and intensity; and also that the antitumor activity of Chi-Tn/MMAF positively correlated with the level of Tn expression by the tumor. Consequently, for clinical application, Tn expression in individual tumors could represent a good predictive biomarker that should be taken into account in order to propose Chi-Tn-ADC to the appropriate patients who might benefit from this treatment, providing better antitumor efficacy with reduced adverse toxicity.

Materials and methods

Cells and mice

TA3Ha (murine breast cancer, kindly given by C. Leclerc, Institut Pasteur, Paris, France), Jurkat (human T-lymphoid leukemia), OvCar-3 and Shin-3 (human ovarian carcinomas), SKBR3 (human breast adenocarcinoma) and LOX (melanoma, kindly given by O. Fodstad, The Norwegian Radium Hospital, Oslo, Norway)⁴⁸ cell lines were cultured in RPMI 1640 (Gibco) containing Glutamax and 10% fetal calf serum (FCS). EL-4 (murine T-lymphoid leukemia) cells were cultured in the same medium supplemented with β -2-mercaptoethanol (Gibco).

Swiss nu/nu female mice (Charles River laboratories, France) were used in agreement with European and National regulations for the Protection of Vertebrate Animals used for Experimental and other Scientific Purposes (facility license No. C75-05-18). Care and use of animals also complied with internationally established principles of replacement, reduction, and refinement in accordance with the Guide for the Care and Use of Laboratory Animals (NRC 2011).

Antibodies

Trastuzumab (Herceptin[®], anti-Her2) was purchased from Hoffman-La Roche. IvIg (Tegeline[®], human immunoglobulins) was obtained from LFB (Courtabouef, France). The Chi-Tn mAb is a mouse/human chimeric IgG1 specific for the Tn-antigen (Oppezzo, 2000), which was produced and purified by RD Biotech (Besançon, France) following our technical indications.

Flow cytometry

To analyze the Chi-Tn mAb binding to tumor cell plasma membrane, Jurkat (10^6), Shin-3, OvCar-3 or TA3Ha (4×10^5) cells were incubated for 15 min on ice with the Chi-Tn mAb or a control antibody (IvIg for human cells or trastuzumab for murine cells) at 20 μ g/mL in PBS containing 0.5% BSA and 0.01% azide (PBS-BSA-azide). After washing, cells were labeled using a secondary F(ab')₂ goat anti-serum specific for the human Fc receptor for IgG (GaH-Fc) coupled to phycoerythrin (PE) (GaH-Fc-PE, Jackson ImmunoResearch Laboratories). DAPI (4',6'-diamidino-2-phenylindole)-negative living cells were acquired using a FACS Canto[™] cytometer (BD Bioscience), and analyzed using the FlowJo software (Tree Star Inc.).

Copy number of Tn antigen was determined by quantitative flow cytometry using a murine anti-Tn mAb kindly provided by R. Lo-Man and C. Leclerc (Institut Pasteur, Paris, France) with the Qifikit (DAKO) following the manufacturer's instructions.

To analyze Chi-Tn mAb internalization, Jurkat (10^6), Shin-3 or TA3Ha (4×10^5) cells were incubated for 15 min on ice with the Chi-Tn mAb or with control antibodies at 20 μ g/mL, washed, then transferred at 37°C in a 5% CO₂ atmosphere for the indicated periods of time. The incubation was stopped using cold PBS-BSA-azide; then the cells were labeled with GaH-Fc-PE. DAPI-negative living cells (10^4) were acquired by flow cytometry and analyzed as above.

Immunohistochemistry

Cancer samples were obtained from surgical specimens removed in patients treated at the Institut Curie (Paris, France). According to French regulation, patients were informed of the research performed and did not express opposition. Tissue sections from formalin fixed paraffin-embedded tumor samples were labeled with the 83D4 murine anti-Tn mAb³⁷ and revealed with a kit containing the biotinylated secondary Ab and the avidin coupled to peroxidase (Vectastain Elite ABC kit, VECTOR Laboratories) following the manufacturer's instructions. Peroxidase was revealed with DAB chromogen (DAKO). Samples were considered as Tn positive when $\geq 50\%$ of tumor cells are labeled.

Biodistribution of the Chi-Tn mAb

Swiss nu/nu female mice were injected s.c. into the flank on day 0 with 4×10^6 Shin-3 ovarian tumor cells. 12 d after tumor xenograft, when solid tumors were grown, mice were injected i.p. with the Chi-Tn mAb or the isotype control mAb

(trastuzumab, Herceptin, Her) at 20 mg/kg in sterile PBS. 2 d after (day 14), mice were euthanized. Solid tumor and organs (liver, spleen, and lung) were removed, paraffin-embedded and sectioned. To detect Tn-positive cells, tissue sections were labeled with the Chi-Tn mAb followed by biotinylated GaH-Fc (GaH-Fc-Biot) and Streptavidin-Cy3 (Sa-Cy3). To detect *in vivo* the presence of the Chi-Tn mAb (or Herceptin), tissue sections were labeled directly with GaH-Fc-Biot and Sa-Cy3. Nuclei were then stained with DAPI, and tissues were mounted on slides.

Images were acquired using a histology microscope Eclipse 90i (Nikon Instruments Europe) equipped with a CDD camera (CoolSNAP HQ2, Roper Scientific), and a dry objective (x10 CFI Plan Apo, NA 0.45).

Three-dimensional deconvolution microscopy

To visualize the Chi-Tn mAb internalization into tumor cells by fluorescence microscopy, Jurkat (10^6), OvCar-3, Shin-3 or TA3Ha (4×10^5) cells were incubated on ice with Chi-Tn at 40 $\mu\text{g}/\text{mL}$ for 15 min, washed with cold medium, and then were incubated at 37°C for the indicated period of time. Internalization was stopped by adding cold PBS-BSA-azide. After washing with PBS containing 0.01% azide (PBS-azide), cells were allowed to adhere for 30 min at room temperature to poly-L-lysine coated glass coverslips, fixed and permeabilized using PBS containing 0.2% BSA and 0.05% saponin (PBS-BSA-saponin). Actin network was labeled using Phalloidin coupled to Alexa Fluor 647 (Phal-A647, Molecular Probes, Invitrogen). The membrane-bound or internalized Chi-Tn mAb was revealed using GaH-Fc-Biot and Sa-Cy3. Cells were then stained with DAPI, and mounted to glass slides with Mowiol.

Early endosomes were detected using Transferrin-Alexa fluor 488 (TF-A488, Molecular Probes), added to the cells at 10 $\mu\text{g}/\text{mL}$ during the internalization period at 37°C. Recycling endosomes or late endosomes were revealed by adding Rab11 or LAMP-1 antibodies, respectively, (BD Biosciences) at 2.5 $\mu\text{g}/\text{mL}$ on fixed cells, then with the corresponding Alexa Fluor 488-conjugated secondary antibody.

Images were acquired using a 3D microscope Eclipse 90i (Nikon) equipped with a CDD camera (CoolSNAP HQ2, Roper Scientific), a piezzo flexure objective scanner (Physik Instrumente), and an oil-immersion objective (x100 CFI Plan Apo VC, NA 1.4). Deconvolutions were performed on stacks of images taken with 0.2 μm plane spacing, using the three-dimensional deconvolution module of MetaMorph[®] software (Universal Imaging Corp.) and the fast iterative constrained PSF-based algorithm.

Antibody-drug conjugates

The Chi-Tn mAb was coupled to SAP toxin through a disulfide linker, by Advanced Targeting Systems (ATS), with a molar ratio SAP/Chi-Tn = 2.7.

The Chi-Tn mAb coupled to MMAF was produced in our lab and also by AGV Discovery. To prepare the conjugates with MMAF, 10 mg of mAb (Chi-Tn or Her) were thiolated for 2 h at room temperature with 40 M excess of Traut's Reagent. The excess of Traut's Reagent was removed by gel filtration (GE

Healthcare) equilibrated in the conjugation buffer. The thiolated antibody was then incubated with a 30 M excess of mc-MMAF diluted in DMSO (Concortis Biosystems) at room temperature overnight. Then, modified antibodies were purified from the excess of the drug by gel filtration after elution with 0.1 M sodium phosphate/0.15 M NaCl/10 mM EDTA (pH 7.6) buffer. The protein concentration was estimated using the BCA protein assay. The molarity of the drug functionality groups after the coupling reaction was determined by Maldi-Tof. The typical overall yield of this antibody modification procedure was five drugs by antibody (Chi-Tn or Herceptin). Modified antibodies were stable for several weeks at 4°C.

Cell viability assay

Jurkat, TA3Ha, OvCar-3 or Shin-3 cells were plated in a 96-W flat bottom tissue culture plates at 10^3 cells/well in triplicate. The mAb conjugated to drug or free drug were added at the indicated concentration, and plates were incubated for 3 d at 37°C. Cell viability was then assessed by adding the CellTiter Blue[®] Cell Viability reagent according to the manufacturer's instructions (Promega) during the last 2 h 30 min of culture for Jurkat cells or the last 4 h for the other tumor cells. The dye reduction was measured on a fluorescent plate reader. Results are expressed as a percentage of viability compared to untreated cells incubated in the same conditions without any treatment during the 3 d.

In vivo tumor therapeutic experiment

Swiss nu/nu female mice (n = 6–8) received a s.c. injection of 0.2×10^6 LOX cells. When the tumor reached a volume approximately of 100 mm³ as calculated according to the following formulae: $V = (L \times l^2)/2$, where L and l are the largest and the smallest perpendicular tumor diameters respectively, mice were injected i.p. with the Abs coupled to the MMAF (4 mg/Kg), twice a week. Growth curves plotted the mean volume of Relative tumor volume (RTV) calculated according to $RTV = (V_x/V_1)$, where V_x is the tumor volume on day X and V_1 is the tumor volume at initiation of the therapy (day 1).

Disclosure of potential conflicts of interest

No potential conflicts of interest were disclosed.

Acknowledgments

We thank the Cytometry Platform, the Nikon Imaging Center, and the Animal facilities of the Institut Curie. We acknowledge the CIC IGR-Curie 1428 (Center Of Clinical Investigation), Institut Curie, Paris; the ECOSud program, Université de Paris, ANR-2010-EMMA-015-01, Medicen Paris Region, SIRIC (Grant INCa-DGOS-4654), ANR-10-IDEX-0001-02 PSL^{*}, and ANR-11-LABX-0043. We also specifically thank André Nicolas from the Platform of Experimental Pathology of the Institut Curie and Virginie Premel for their help in IHC.

Funding

This work was supported by fundings from the Institut National de la Santé et de la Recherche Médicale (INSERM); the Association pour la

Recherche sur le Cancer (ARC); the Institut Curie; the Agence Nationale pour la Recherche (ANR Emergence program), and the Institut National du Cancer (INCa).

References

- Scott AM, Wolchok JD, Old LJ. Antibody therapy of cancer. *Nat Rev Cancer* 2012; 12:278-87; PMID:22437872; <http://dx.doi.org/10.1038/nrc3236>
- Vacchelli E, Eggermont A, Galon J, Sautes-Fridman C, Zitvogel L, Kroemer G, Galluzzi L. Trial watch: monoclonal antibodies in cancer therapy. *Oncoimmunology* 2013; 2:e22789; PMID:23482847; <http://dx.doi.org/10.4161/onci.22789>
- Govindan SV, Goldenberg DM. Designing immunoconjugates for cancer therapy. *Expert Opin Biol Ther* 2012; 12:873-90; PMID:22679911; <http://dx.doi.org/10.1517/14712598.2012.685153>
- Perez HL, Cardarelli PM, Deshpande S, Gangwar S, Schroeder GM, Vite GD, Borzilleri RM. Antibody-drug conjugates: current status and future directions. *Drug Discov Today* 2014; 19:869-81; PMID:24239727; <http://dx.doi.org/10.1016/j.drudis.2013.11.004>
- Chari RV. Targeted cancer therapy: conferring specificity to cytotoxic drugs. *Acc Chem Res* 2008; 41:98-107; PMID:17705444; <http://dx.doi.org/10.1021/ar700108g>
- Maxfield FR, McGraw TE. Endocytic recycling. *Nat Rev Mol Cell Biol* 2004; 5:121-32; PMID:15040445; <http://dx.doi.org/10.1038/nrm1315>
- Bareford LM, Swaan PW. Endocytic mechanisms for targeted drug delivery. *Adv Drug Deliv Rev* 2007; 59:748-58; PMID:17659804; <http://dx.doi.org/10.1016/j.addr.2007.06.008>
- Ulbrich K, Etrych T, Chytil P, Pechar M, Jelinkova M, Rihova B. Polymeric anticancer drugs with pH-controlled activation. *Int J Pharm* 2004; 277:63-72; PMID:15158969; <http://dx.doi.org/10.1016/j.ijpharm.2003.02.001>
- Doronina SO, Mendelsohn BA, Bovee TD, Cervený CG, Alley SC, Meyer DL, Oflazoglu E, Toki BE, Sanderson RJ, Zabinski RF et al. Enhanced activity of monomethylauristatin F through monoclonal antibody delivery: effects of linker technology on efficacy and toxicity. *Bioconjug Chem* 2006; 17:114-24; PMID:16417259; <http://dx.doi.org/10.1021/bc0502917>
- Ju T, Otto VI, Cummings RD. The Tn antigen-structural simplicity and biological complexity. *Angew Chem Int Ed Engl* 2011; 50:1770-91; PMID:21259410; <http://dx.doi.org/10.1002/anie.201002313>
- Springer GF. T and Tn, general carcinoma autoantigens. *Science* 1984; 224:1198-206; PMID:6729450; <http://dx.doi.org/10.1126/science.6729450>
- Beuzelin-Yvraut M, Bourguignat A, Phillips E, Roseto A, Osinaga E. Immunocytological analysis of the Tn associated antigen 83D4 in serous effusions from patients with cancer: comparison with Tn soluble glycoprotein. *J Clin Pathol* 1995; 48:433-7; PMID:7629290; <http://dx.doi.org/10.1136/jcp.48.5.433>
- Croce MV, Rabassa ME, Price MR, Segal-Eiras A. MUC1 mucin and carbohydrate associated antigens as tumor markers in head and neck squamous cell carcinoma. *Pathol Oncol Res* 2001; 7:284-91; PMID:11882908; <http://dx.doi.org/10.1007/BF03032385>
- Hubert P, Heitzmann A, Viel S, Nicolas A, Sastre-Garau X, Oppezio P, Pritsch O, Osinaga E, Amigorena S. Antibody-dependent cell cytotoxicity synapses form in mice during tumor-specific antibody immunotherapy. *Cancer Res* 2011; 71:5134-43; PMID:21697279; <http://dx.doi.org/10.1158/0008-5472.CAN-10-4222>
- Itzkowitz SH, Yuan M, Montgomery CK, Kjeldsen T, Takahashi HK, Bigbee WL, Kim YS. Expression of Tn, sialosyl-Tn, and T antigens in human colon cancer. *Cancer Res* 1989; 49:197-204; PMID:2908846
- Li Q, Anver MR, Butcher DO, Gildersleeve JC. Resolving conflicting data on expression of the Tn antigen and implications for clinical trials with cancer vaccines. *Mol Cancer Ther* 2009; 8:971-9; PMID:19372570; <http://dx.doi.org/10.1158/1535-7163.MCT-08-0934>
- Pancino GF, Osinaga E, Voraueher W, Kakouche A, Mistro D, Charpin C, Roseto A. Production of a monoclonal antibody as immunohistochemical marker on paraffin embedded tissues using a new immunization method. *Hybridoma* 1990; 9:389-95; PMID:2210779; <http://dx.doi.org/10.1089/hyb.1990.9.389>
- Danussi C, Coslovi A, Campa C, Mucignat MT, Spessotto P, Uggeri F, Paoletti S, Colombatti A. A newly generated functional antibody identifies Tn antigen as a novel determinant in the cancer cell-lymphatic endothelium interaction. *Glycobiology* 2009; 19:1056-67; PMID:19528665; <http://dx.doi.org/10.1093/glycob/cwp085>
- Ando H, Matsushita T, Wakitani M, Sato T, Kodama-Nishida S, Shibata K, Shitara K, Ohta S. Mouse-human chimeric anti-Tn IgG1 induced anti-tumor activity against Jurkat cells in vitro and in vivo. *Biol Pharm Bull* 2008; 31:1739-44; PMID:18758069; <http://dx.doi.org/10.1248/bpb.31.1739>
- Avichezer D, Springer GF, Schechter B, Arnon R. Immunoreactivities of polyclonal and monoclonal anti-T and anti-Tn antibodies with human carcinoma cells, grown in vitro and in a xenograft model. *Int J Cancer J Int Du Cancer* 1997; 72:119-27; PMID:9212232; [http://dx.doi.org/10.1002/\(SICI\)1097-0215\(19970703\)72:1<119::AID-IJC17>3.0.CO;2-E](http://dx.doi.org/10.1002/(SICI)1097-0215(19970703)72:1<119::AID-IJC17>3.0.CO;2-E)
- Nakada H, Inoue M, Numata Y, Tanaka N, Funakoshi I, Fukui S, Mellors A, Yamashina I. Epitopic structure of Tn glycophorin A for an anti-Tn antibody (MLS 128). *Proc Natl Acad Sci USA* 1993; 90:2495-9; PMID:7681597; <http://dx.doi.org/10.1073/pnas.90.6.2495>
- Oppezio P, Osinaga E, Tello D, Bay S, Cantacuzene D, Irigoien F, Ferreira A, Roseto A, Cayota A, Alzari P et al. Production and functional characterization of two mouse/human chimeric antibodies with specificity for the tumor-associated Tn-antigen. *Hybridoma* 2000; 19:229-39; PMID:10952411; <http://dx.doi.org/10.1089/02724570050109620>
- Welinder C, Baldetorp B, Borrebaeck C, Fredlund BM, Jansson B. A new murine IgG1 anti-Tn monoclonal antibody with in vivo anti-tumor activity. *Glycobiol* 2011; 21:1097-107; PMID:21470982; <http://dx.doi.org/10.1093/glycob/cwr048>
- Aller CT, Kucuk O, Springer GF, Gilman-Sachs A. Flow cytometric analysis of T and Tn epitopes on chronic lymphocytic leukemia cells. *Am J Hematol* 1996; 52:29-38; PMID:8638608; [http://dx.doi.org/10.1002/\(SICI\)1096-8652\(199605\)52:1<29::AID-AJH5>3.0.CO;2-8](http://dx.doi.org/10.1002/(SICI)1096-8652(199605)52:1<29::AID-AJH5>3.0.CO;2-8)
- Inoue M, Nakada H, Tanaka N, Yamashina I. Tn antigen is expressed on leukosialin from T-lymphoid cells. *Cancer Res* 1994; 54:85-8; PMID:8261467
- Lawrie CH, Marafioti T, Hatton CS, Dirnhofer S, Roncador G, Went P, Tzankov A, Pileri SA, Pulford K, Banham AH. Cancer-associated carbohydrate identification in Hodgkin's lymphoma by carbohydrate array profiling. *Int J Cancer J Int Du Cancer* 2006; 118:3161-6; PMID:16395706; <http://dx.doi.org/10.1002/ijc.21762>
- Asundi J, Reed C, Arca J, McCutcheon K, Ferrando R, Clark S, Luis E, Tien J, Firestein R, Polakis P. An antibody-drug conjugate targeting the endothelin B receptor for the treatment of melanoma. *Clin Cancer Res* 2011; 17:965-75; PMID:21245091; <http://dx.doi.org/10.1158/1078-0432.CCR-10-2340>
- Chen Y, Clark S, Wong T, Chen Y, Chen Y, Dennis MS, Luis E, Zhong F, Bheddah S, Koepfen H et al. Armed antibodies targeting the mucin repeats of the ovarian cancer antigen, MUC16, are highly efficacious in animal tumor models. *Cancer Res* 2007; 67:4924-32; PMID:17510422; <http://dx.doi.org/10.1158/0008-5472.CAN-06-4512>
- Ryan MC, Kostner H, Gordon KA, Duniho S, Sutherland MK, Yu C, Kim KM, Nesterova A, Anderson M, McEarchern JA et al. Targeting pancreatic and ovarian carcinomas using the auristatin-based anti-CD70 antibody-drug conjugate SGN-75. *Br J Cancer* 2010; 103:676-84; PMID:20664585; <http://dx.doi.org/10.1038/sj.bjc.6605816>
- Grant BD, Donaldson JG. Pathways and mechanisms of endocytic recycling. *Nat Rev Mol Cell Biol* 2009; 10:597-608; PMID:19696797; <http://dx.doi.org/10.1038/nrm2755>
- Endo Y, Mitsui K, Motizuki M, Tsurugi K. The mechanism of action of ricin and related toxic lectins on eukaryotic ribosomes. The site and the characteristics of the modification in 28 S ribosomal RNA caused by the toxins. *J Biol Chem* 1987; 262:5908-12; PMID:3571242
- Pastan I, Hassan R, Fitzgerald DJ, Kreitman RJ. Immunotoxin therapy of cancer. *Nat Rev Cancer* 2006; 6:559-65; PMID:16794638; <http://dx.doi.org/10.1038/nrc1891>
- Oflazoglu E, Stone IJ, Gordon K, Wood CG, Repasky EA, Grewal IS, Law CL, Gerber HP. Potent anticarcinoma activity of the humanized

- anti-CD70 antibody h1F6 conjugated to the tubulin inhibitor auristatin via an uncleavable linker. *Clin Cancer Res* 2008; 14:6171-80; PMID:18809969; <http://dx.doi.org/10.1158/1078-0432.CCR-08-0916>
34. Doronina SO, Bovee TD, Meyer DW, Miyamoto JB, Anderson ME, Morris-Tilden CA, Senter PD. Novel peptide linkers for highly potent antibody-auristatin conjugate. *Bioconjug Chem* 2008; 19:1960-3; PMID:18803412; <http://dx.doi.org/10.1021/bc800289a>
 35. Mazal D, Lo-Man R, Bay S, Pritsch O, Deriaud E, Ganneau C, Medeiros A, Ubbilos L, Obal G, Berois N et al. Monoclonal antibodies toward different Tn-amino acid backbones display distinct recognition patterns on human cancer cells. Implications for effective immuno-targeting of cancer. *Cancer Immunol Immunother* 2013; 62:1107-22; PMID:23604173; <http://dx.doi.org/10.1007/s00262-013-1425-7>
 36. Charpin C, Pancino G, Osinaga E, Bonnier P, Lavaut MN, Allasia C, Roseto A. Monoclonal antibody 83D4 immunoreactivity in human tissues: cellular distribution and microcytophotometric analysis of immunoprecipitates on tissue sections. *Anticancer Res* 1992; 12:209-23; PMID:1567169
 37. Osinaga E, Bay S, Tello D, Babino A, Pritsch O, Assemet K, Cantacuzene D, Nakada H, Alzari P. Analysis of the fine specificity of Tn-binding proteins using synthetic glycopeptide epitopes and a biosensor based on surface plasmon resonance spectroscopy. *FEBS Lett* 2000; 469:24-8; PMID:10708749; [http://dx.doi.org/10.1016/S0014-5793\(00\)01248-5](http://dx.doi.org/10.1016/S0014-5793(00)01248-5)
 38. Rudnick SI, Lou J, Shaller CC, Tang Y, Klein-Szanto AJ, Weiner LM, Marks JD, Adams GP. Influence of affinity and antigen internalization on the uptake and penetration of Anti-HER2 antibodies in solid tumors. *Cancer Res* 2011; 71:2250-9; PMID:21406401; <http://dx.doi.org/10.1158/0008-5472.CAN-10-2277>
 39. Lim SH, Vaughan AT, Ashton-Key M, Williams EL, Dixon SV, Chan HT, Beers SA, French RR, Cox KL, Davies AJ et al. Fc gamma receptor IIb on target B cells promotes rituximab internalization and reduces clinical efficacy. *Blood* 2011; 118:2530-40; PMID:21768293; <http://dx.doi.org/10.1182/blood-2011-01-330357>
 40. Austin CD, De Maziere AM, Pisacane PI, van Dijk SM, Eigenbrot C, Sliwkowski MX, Klumperman J, Scheller RH. Endocytosis and sorting of ErbB2 and the site of action of cancer therapeutics trastuzumab and geldanamycin. *Mol Biol Cell* 2004; 15:5268-82; PMID:15385631; <http://dx.doi.org/10.1091/mbc.E04-07-0591>
 41. Iglesias-Bartolome R, Crespo PM, Gomez GA, Daniotti JL. The antibody to GD3 ganglioside, R24, is rapidly endocytosed and recycled to the plasma membrane via the endocytic recycling compartment. Inhibitory effect of brefeldin A and monensin. *FEBS J* 2006; 273:1744-58; PMID:16623710; <http://dx.doi.org/10.1111/j.1742-4658.2006.05194.x>
 42. Perera RM, Zoncu R, Johns TG, Pypaert M, Lee FT, Mellman I, Old LJ, Toomre DK, Scott AM. Internalization, intracellular trafficking, and biodistribution of monoclonal antibody 806: a novel anti-epidermal growth factor receptor antibody. *Neoplasia* 2007; 9:1099-110; PMID:18084617; <http://dx.doi.org/10.1593/neo.07721>
 43. Doronina SO, Toki BE, Torgov MY, Mendelsohn BA, Cerveny CG, Chace DF, DeBlanc RL, Gearing RP, Bovee TD, Siegall CB et al. Development of potent monoclonal antibody auristatin conjugates for cancer therapy. *Nat Biotechnol* 2003; 21:778-84; PMID:12778055; <http://dx.doi.org/10.1038/nbt832>
 44. Jackson D, Gooya J, Mao S, Kinneer K, Xu L, Camara M, Fazanbaker C, Fleming R, Swamynathan S, Meyer D et al. A human antibody-drug conjugate targeting EphA2 inhibits tumor growth in vivo. *Cancer Res* 2008; 68:9367-74; PMID:19010911; <http://dx.doi.org/10.1158/0008-5472.CAN-08-1933>
 45. Polito L, Bortolotti M, Pedrazzi M, Bolognesi A. Immunotoxins and other conjugates containing saporin-s6 for cancer therapy. *Toxins (Basel)* 2011; 3:697-720; PMID:22069735; <http://dx.doi.org/10.3390/toxins3060697>
 46. Hamblett KJ, Senter PD, Chace DF, Sun MM, Lenox J, Cerveny CG, Kissler KM, Bernhardt SX, Kopcha AK, Zabinski RF et al. Effects of drug loading on the antitumor activity of a monoclonal antibody drug conjugate. *Clin Cancer Res* 2004; 10:7063-70; PMID:15501986; <http://dx.doi.org/10.1158/1078-0432.CCR-04-0789>
 47. Bouchard H, Viskov C, Garcia-Echeverria C. Antibody-drug conjugates—a new wave of cancer drugs. *Bioorg Med Chem Lett* 2014; 24:5357-63; PMID:25455482; <http://dx.doi.org/10.1016/j.bmcl.2014.10.021>
 48. Fodstad O, Aamdal S, McMenamin M, Nesland JM, Pihl A. A new experimental metastasis model in athymic nude mice, the human malignant melanoma LOX. *Int J Cancer J Int Du Cancer* 1988; 41:442-9; PMID:3346110; <http://dx.doi.org/10.1002/ijc.2910410322>

Review

Humanized Mice for the Study of Immuno-Oncology

Philippe De La Rochere,¹ Silvia Guil-Luna,² Didier Decaudin,³ Georges Azar,⁴ Sukhvinder S. Sidhu,⁴ and Eliane Piaggio^{1,*}

Immunotherapy is revolutionizing cancer treatment; however, complete responses are achieved in only a small fraction of patients and tumor types. Thus, there is an urgent need for predictive preclinical models to drive rational immunotherapeutic drug development, treatment combinations, and to minimize failures in clinical trials. Humanized mouse models (HIS) have been developed to study and modulate the interactions between immune components and tumors of human origin. In this review, we discuss recent advances in the 'humanization' of mouse models to improve the quality of human immune cell reconstitution. We also highlight new insights into the basic mechanisms, and provide a preclinical evaluation of onco-immunotherapies, as well as the limitations thereof, which constitute drivers for the improvement of the models to increase their translational power.

Immunotherapy in Oncology: The Need for Preclinical Models

Immunotherapies represent a significant leap forward in the successful treatment of cancer, with unprecedented long-term survival rates in different indications [1]. However, many patients still do not benefit from these immunotherapies, leading to increased focus on identifying novel immunotherapies or combinations that can prolong or alter patient responses. To this effect, there is an increasing demand for more predictive preclinical models to drive rational immunotherapeutic drug development, treatment combinations, and to minimize failures in clinical trials.

Rodent models have long been key tools in biomedical research. Given the need for experimental models to recapitulate human biology, mice are one of the most widely used animal models. The four major approaches with mouse models used to assess immunotherapies are: (i) syngeneic mouse tumor models with fully immune-competent hosts; (ii) genetically engineered mouse models (GEMMs); (iii) chemically induced models; and (iv) HIS. While the first three approaches are widely used, one major drawback is that they rely on the murine immune system, which does not always recapitulate the human immune response. Therefore, preclinical models recapitulating a functional human immune system are highly desirable.

HIS for research on cancer immunotherapy comprise three elements: (i) immunodeficient host mice; (ii) human immune cells; and (iii) human tumor cells. In this review, we discuss the advantages and caveats of HIS to study cancer immunotherapy.

Immunodeficient Host Mice

Since the discovery of scid (Table 1) mutant mice during the 1980s [2] and their ability to host human peripheral blood mononuclear cells (PBMC) [3], fetal hematopoietic tissues [4], or hematopoietic stem cells (HSCs) [5], immunodeficient mice have steadily become more sophisticated.

Highlights

Cancer immunotherapy has given impressive clinical responses but only in a minority of patients and only in certain cancer indications. Thus, predictive preclinical models are needed to drive rational immunotherapeutic drug development and minimize failures in clinical trials.

HIS, comprising immunodeficient host mice and human immune and tumor cells, recapitulate the interactions between immune components and tumors of human origin.

Limitations of HIS models include the development of xenograft-versus-host disease and incomplete reconstitution of certain human immune subpopulations.

HIS models have allowed the evaluation of onco-immunotherapies, including cellular and antibody-based immunotherapies.

Understanding the caveats of HIS mice and the increasing genetic optimizations are leading to improved models with heightened translational power.

¹INSERM U932, and SIRIC Translational Immunotherapy Team, Translational Research Department, Institut Curie, PSL Research University, Paris F-75005, France

²Maimónides Institute for Biomedical Research of Córdoba (IMBIC), Córdoba, Spain

³Laboratory of Preclinical Investigation, Translational Research Department, and Department of Medical Oncology, Institut Curie, PSL Research University, Paris F-75005, France

⁴Sanofi Oncology, 1 Impasse des Ateliers, Vitry Sur Seine, France

*Correspondence: eliane.piaggio@curie.fr (E. Piaggio).

Table 1. Different Immunodeficient Host Mice Used for Humanization Protocols

Mouse common or branded name	Strain name	Provider	Refs
NSG B2m, $\beta 2m$ KO NSG	NOD <i>scid</i> <i>Il2r^{tm1}</i> <i>B2m^{tm1}</i>	www.jax.org	[18]
BALB <i>scid</i>	CBySmm.CB17- <i>Prkdc^{scid}</i>	www.jax.org; www.taconic.com; www.horizondiscovery.com	
BRG	BALB/c <i>Rag2^{-/-}</i> <i>IL-2Rg^{c-/-}</i>	www.taconic.com	[13]
BRG hIL-3 hGM-CSF	BALB/c <i>Rag2^{-/-}</i> <i>IL-2Rg^{c-/-}</i> <i>IL3^h</i> <i>CSF2^h</i>	www.taconic.com	[48]
BRGS	BALB/c <i>Rag2^{-/-}</i> <i>IL-2Rg^{c-/-}</i> NOD. <i>sirpa</i>	www.axenis.fr	[13]
BRGSF	BALB/c <i>Rag2^{-/-}</i> <i>IL-2Rg^{c-/-}</i> <i>Flt3^{-/-}</i>	www.axenis.fr	[43,44]
DRAG	NOD.Cg- <i>Rag1^{tm1Mom}</i> <i>Il2rg^{tm1Wj}</i> Tg(HLA-DRA,HLA-DRB1*0401)39-2Kitb/ScasJ	www.jax.org	[56]
HCTLA-4 C57BL/6	C57BL/6 <i>C7LA4^h</i>	www.biocytogen.com	[59]
HUMAMICE	C57BL/6 <i>H2b2m^{-/-}</i> <i>IAb^{-/-}</i> <i>Rag2^{-/-}</i> <i>IL2Rg^{c-/-}</i> <i>per1^{-/-}</i>	Not commercially available	[58]
<i>huPD1</i> gene knock-in mice	C57BL/6 extracellular PD1 ^h	www.crownbio.com www.biocytogen.com	[60]
IL-15-NOG Tg	NOD.Cg- <i>Prkdc^{scid}</i> <i>IL-2Rg^c</i> <i>m1Sug</i> Tg (CMV-IL2/IL15)1-1Jic/JicTac	www.taconic.com	[52]
MISTRG	M-CSF, IL-3, <i>Sirpa</i> , TPO, <i>Rag2^{-/-}</i> <i>IL-2Rg^{c-/-}</i>	www.jax.org	[49]
NOD- <i>scid</i>	NOD.CB17- <i>Prkdc^{scid}</i> /J	www.jax.org www.criver.com; www.janvier-labs.com	[6]
NOG	NOD.Cg- <i>Prkdc^{scid}</i> <i>Il2rg^{tm1Sug}</i> /JicTac	www.taconic.com	[6]
NOG-EXL	NOD.Cg- <i>Prkdc^{scid}</i> <i>Il2rg^{tm1Sug}</i> Tg(SV40/HTLV-IL3,CSF2)10-7Jic/JicTac	www.taconic.com	[47]
NOG-IL2 Tg	NOD.Cg- <i>Prkdc^{scid}</i> <i>IL-2Rg^c</i> <i>m1Sug</i> Tg(CMV-IL2)4-2Jic/JicTac	www.taconic.com	[51]
NRG, NOD Rag gamma	NOD.Cg- <i>Rag1tm1Mom</i> , <i>Il2rgtm1Wj</i> /SzJ	www.jax.org	
NSG TM , NOD <i>scid</i> gamma	NOD.Cg- <i>Prkdc^{scid}</i> <i>Il2rg^{tm1Wj}</i> /SzJ	www.jax.org	[6]
NSG HLA-A2/HDD, NSG TM HLA Class I-A2	NOD.Cg- <i>Prkdc^{scid}</i> <i>Il2rg^{tm1Wj}</i> Tg (HLA-A2/H2-D/B2M) 1Dvs/Sz (NSG-HLA-A2/HHD)	www.jax.org	[55]
NSG HLA-DR	NOG/HLA-DR4/1-A β ^{-/-}	www.jax.org	[57]
NSGS, NOD <i>scid</i> gamma Il3-GM-SF (NSG-SGM3)	NOD.Cg- <i>Prkdc^{scid}</i> <i>Il2rg^{tm1Wj}</i> Tg(CMV-IL3,CSF2,KITLG)1Eav/MloySzJ	www.jax.org	[46]
NSGW41	NOD.Cg- <i>Kit^{W-41J}</i> <i>Prkdc^{scid}</i> <i>Il2rg^{tm1Wj}</i> /WaskJ	www.jax.org	[41]
Nude mouse, athymic nude	<i>Foxn1tm</i>	www.jax.org; www.criver.com; www.janvier-labs.com	[8]
Scid	B6.CB17- <i>Prkdc^{scid}</i> /SzJ	www.jax.org	[2]

The study of hematopoiesis has benefited from models using immunodeficient mice, as has the evaluation of infectious diseases, autoimmunity, and graft-versus-host disease (GvHD) [6,7]. Nevertheless, for cancer immunotherapy, a complication arises, because the models must simultaneously tolerate the transplantation of human tumors and human immune cells.

The first model that allowed human tumor transplantation was the nude mouse, described in 1966, which lacks T cells [8]. However, since then, it has become clear that the more immunodeficient the mice, the better the engraftment efficacy, especially in models lacking natural killer (NK) cell activity [9]. The same applies to the reconstitution of the human immune system. Xenoreactivity towards the human graft, whether tumor cells or HSCs, is due to the

recognition of the human cells as foreign by the mouse innate and adaptive immune systems. The first breakthrough to avoid xenoreactivity was the use of a mouse lacking T and B lymphocytes due to a spontaneous mutation of the protein kinase DNA-activated catalytic polypeptide (*Prkdc*) gene, which affects DNA repair that underlying the *scid* phenotype [2]. Since the initial description of these mice in 1993, genetic engineering of mice has become an important field of research, allowing for the generation of models with improved human immune cell reconstitution. The first genetically engineered mice defective for adaptive murine immunity were generated in 1990 by knocking out the *Rag2* gene [10]. The *Rag* mutations disrupt the V (D)J recombination necessary for T and B receptor generation, blocking T and B cell development and cell survival. These mice allowed human hematopoietic reconstitution, although with low and variable levels of engraftment. In 1995, by comparing human immune reconstitution efficiencies in different mouse backgrounds, crossing the *scid* mutation on the nonobese diabetic (NOD) background showed a clear advantage. The difference observed was driven by accumulated defects in NK cells, macrophage activity, and the complement system, allowing for at least a fivefold improvement in human immune reconstitution as compared to the original CB-17 SCID mice [6]. The next step in significantly improving the quality and levels of human immune system reconstitution was achieved in 2002 by knocking out the common γ -chain of the IL-2 receptor [11,12] (IL-2R γ_c ; shared by the receptors of IL-2, IL-4, IL-7, IL-9, IL-15, and IL-21), leading to the loss of murine NK cells. The combination of the *scid* mutation or *Rag1* and *Rag2* KO with the IL-2R γ_c knockout (KO) gave rise to a 'new generation' of severely immunodeficient mouse models between 2002 and 2005, namely NSG (NOD.Cg-*Prkdc*^{scid}*Il2rg*^{tm1Wjl}/SzJ) [6], NOG (NOD.Cg-*Prkdc*^{scid}*Il2rg*^{tm1Sug}/JicTac) [6], and BRG (BALB/c *Rag2*^{-/-}*IL-2Rg γ_c* ^{-/-}) mice [13].

Interestingly, the C57BL/6 mice carrying the same *Rag* and *g γ_c* KO are still capable of rejecting xenografted human cells [12,14], highlighting the implication of other rejection mechanisms in that particular genetic background. Takenaka *et al.* [14] demonstrated that the genetic background of NOD mice, but not of C57BL/6 mice, encodes an allele of *Sirpa* that strongly interacts with human CD47 molecule, in contrast to other mice strains [13,14]. Indeed, the *Sirpa* gene is essentially expressed on myeloid cells and encodes an inhibitory immunoglobulin superfamily transmembrane protein (CD172a) that acts as a 'do not eat me signal' when interacting with CD47, its ubiquitously expressed cognate ligand.

These findings led to the development of the next generation of HIS mice, in which the transfer of the NOD.*Sirpa* allele (BALB/c *Rag2*^{-/-}*IL-2Rg γ_c* ^{-/-} NOD.*Sirpa*: BRGS) [13], or even a human *Sirpa* (SRG) [15] to other genetic backgrounds, increased their tolerance to human HSC xenografts and justified the noted difference between the C57BL/6 and other mouse genetic backgrounds. These new HIS mice showed more robust reconstitution levels and reproducibility, and allowed initial studies on immuno-oncology therapies, which nevertheless highlighted an important flaw: immune reconstitution is not optimal and the human myeloid compartment is still largely under-represented. Here, we describe the main approaches used for immune cell reconstitution in HIS models, and then discuss the novel developments aiming at improving hematopoietic reconstitution in the host mice.

Mice Humanization

Two major sources of human immune cells are currently used for the establishment of a functional human immune system; (i) PBMCs; and (ii) human CD34+ HSC, which are used in three types of model, with their own advantages and limitations: Hu-PBL (peripheral blood lymphocytes), Hu-CD34+ (also named Hu-SCR for '*scid*-repopulating cell') and BLT mice (bone marrow–liver–thymus), described in detail below (Figure 1A, Key Figure).

Key Figure

Schematic of Hu-PBL, Hu-CD34, and Bone Marrow–Liver–Thymus (BLT) Humanized Mouse Models, and their Use as AVATARS

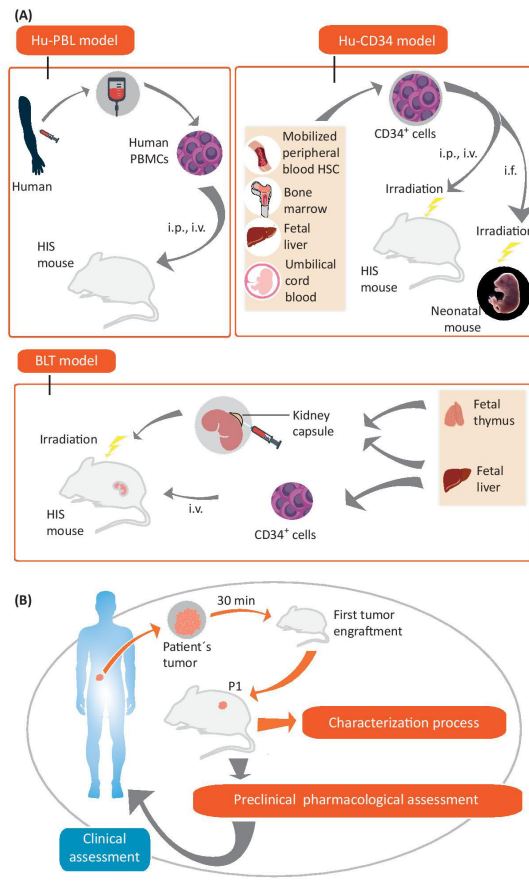


Figure 1. (A) Hu-PBL model: peripheral blood mononuclear cells (PBMCs) are engrafted by intravenous (i.v.) or intraperitoneal (i.p.) injection to an adult immunodeficient mouse. Hu-CD34 model. Hematopoietic stem cells (HSCs) derived from mobilized peripheral blood stem cells, bone marrow, fetal liver or umbilical cord blood are injected into (Figure legend continued on the bottom of the next page.)

PBMCs: Hu-PBL Model

The simplest and most economic version of humanization involves engrafting human leukocytes in immunodeficient mice, known as Hu-PBL. This approach was first described in 1988 using CB17-*scid* mice [3] and has been widely used for the study of human immune responses in autoimmunity and infectious diseases.

Human leukocytes can be obtained from PBMCs, spleen, or lymph nodes. Typically, PBMCs are obtained from healthy donors who are not major histocompatibility complex (MHC) matched with the tumor graft, leading to variations in intrinsic allogenicity. Including in each experimental group mice each reconstituted with a different PBMC donor is an appropriate strategy to compensate for donor variability. PBMCs can be injected intravenously (i.v.), intraperitoneally (i.p.), or intrasplenically into adult mice.

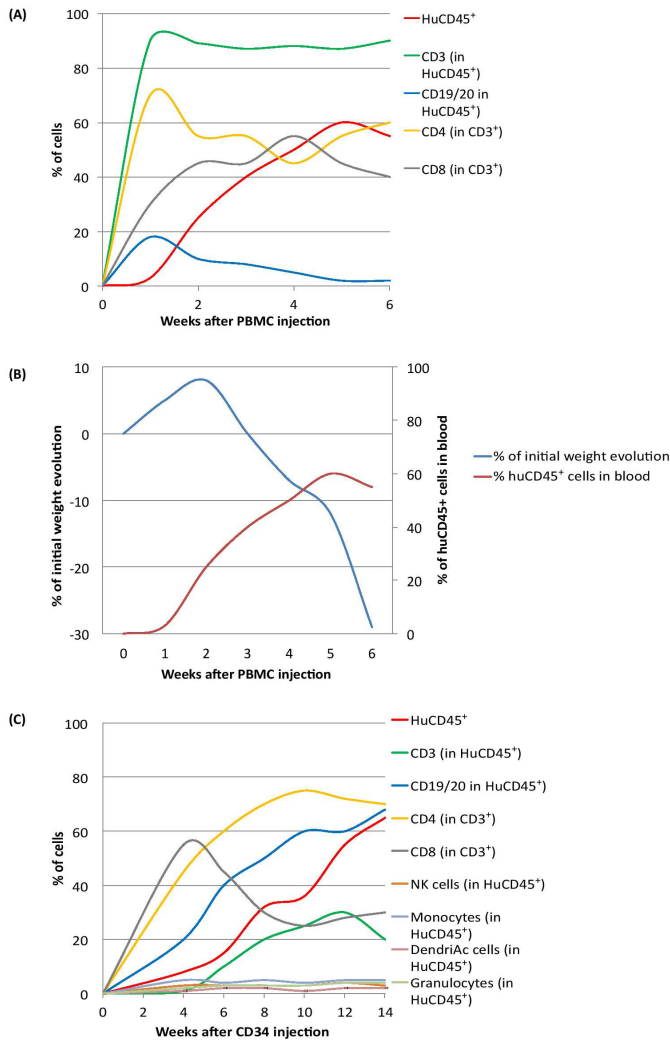
PBMCs are generally isolated by Ficoll-Hypaque gradient centrifugation, in which mainly neutrophils are removed. Among the PBMC inoculum, besides mature human leukocytes, there are a few HSCs which are unable to colonize the murine host due to the lack of a proper microenvironment. Low levels of human B cells and myeloid cells are observed, probably due to the lack of the human cytokines required for their survival [16–18]. Interestingly, low levels of human IL-1 β , GM-CSF, IFN- γ , IL-10, IL-2, and IL-5 have been detected in this model, which may contribute to the survival of the human cells [19].

T cells are the main immune subpopulation that is present and remains functional in the murine host. In our experience, an injection of 20×10^6 PBMCs into NSG mice typically results in ~50% of human CD45⁺ cells in the murine peripheral blood after 4 weeks of engraftment. Approximately 90% of the human CD45⁺ cells are CD3⁺ T cells with an activated and/or memory phenotype and an approximately 1:1 CD4:CD8 ratio, which is maintained for 4–6 weeks after PBMC injection (Figure 2A). The main caveat of this model is that it invariably leads to lethal xeno-GvHD [3,11,18], which can be evaluated by body-weight loss [20] (Figure 2B). The onset of GvHD is directly correlated with the degree of human T cell engraftment, and previous sublethal irradiation accelerates its onset [18]. Thus, the therapeutic observational window is restricted to a few weeks (usually 4–6 weeks after PBMC injection) before evident signs of GvHD [11,18]. Interestingly, CD4⁺ T cells appear to have a major role in the induction of GvHD in Hu-PBL mice, because depletion of CD4⁺ cells from PBMCs before inoculation alleviates clinical symptoms and extends mouse survival [21].

CD34⁺ stem cells: Hu-CD34⁺ and BLT models

Another approach to humanization is the injection of human CD34⁺ HSCs into newborn or adult immunodeficient recipients: the Hu-CD34⁺ model [9] (Figure 1A). The success of engraftment is variable, depending on: (i) HSC source: human umbilical cord blood [11,12], adult bone marrow [22], granulocyte colony-stimulating factor-(G-CSF)-mobilized PBMCs [23], or fetal liver [22]; (ii) route of injection: i.v. (facial or tail vein) or intrafemoral in adult mice, and i.v. (intracardiac or intrahepatic) in newborn mice; and (iii) age, strain and sex of recipient: newborn or young mice (up to 4 weeks of age) allows accelerated T cell development compared with adult mice [24]. This approach requires sublethal γ -irradiation of the host mice to deplete mouse HSCs and

irradiated neonatal or adult immunodeficient mice via i.v., i.p. or intra-femoral (i.f.) route. BLT model. Fetal liver and thymus fragments are implanted under the renal capsule in irradiated adult immunodeficient mice, and hematopoietic stem cells derived from the same fetal liver are injected i.v. (B) The AVATAR approach. Patient-derived xenografts (PDXs) are developed from a fresh piece of a patient's tumor, characterized *in vitro*, and used for pharmacological evaluation of alternative therapies. Results are then applied to propose the most adapted therapy for the individual patient.



Trends in Immunology

(See figure legend on the bottom of the next page.)

facilitate human HSC engraftment. Alternatives to irradiation have been reported, including busulfan [25] and antibody-mediated deletion of mouse progenitor cells [26].

Fetal liver has also been used extensively for making the BLT model (Figure 1A). This model is generated by the transplantation of human fetal liver and thymus tissue into the subrenal capsule, simultaneously with the i.v. injection of autologous CD34⁺ cells from the same fetal liver into adult immunodeficient mice [27]. Cryopreserved fetal thymic tissue can be injected in HIS mice and can be selected to be HLA allele matched to adult HSCs to prevent allogeneic adult rejection. Using this strategy, adult HSCs obtained from patients with immune-related diseases [28], or HSCs genetically modified with tumor-associated mutations [29], recapitulate fundamental traits in the mice associated with the relevant disease. Future engraftment in HIS mice of adult HSCs obtained from patients with cancer should enable the capture of complex immunobiological properties associated with cancer and allow for a more specific assessment of cancer immunotherapies for patients with co-morbidities.

In the Hu-CD34⁺ model, all human hematopoietic lineages are represented, but not all are functionally fully developed [11]. Most of the human B cells are immature CD5⁺ B cells, because the process of B cell differentiation is blocked at the transition phase, with the consequent accumulation of B cell precursors in the spleen [30,31]. CD4⁺ T cells show a memory phenotype, and both T and NK cells display some functional impairment [31,32]. The differentiation of the myelomonocytic lineage is also impaired and monocytes are phenotypically immature [33] (Figure 2C). Although the mouse thymus supports human T cell development, the question of MHC restriction remains unclear. Halkias *et al.* reported that human thymocytes show similar behavior in mouse and human thymic environments and that they serially interact with human HSCs as well as with mouse tissue in HIS mice thymus [34]. Furthermore, Watanabe *et al.* [31] showed that the mouse thymic environment is essential for human T cell development but that the mouse I-A MHC molecule is not, suggesting that the human CD4⁺ TcR repertoire is restricted by HLA class II molecules as well as by murine MHC.

In the BLT model, the transplanted human fetal liver and thymus provide a human thymic microenvironment that supports the development of human T cells and their selection on human MHC molecules. However, a positive selection in the thymus occurs exclusively on human cells, and T cells with affinity for mouse MHC are not eliminated, with the consequence of a higher incidence of GvHD than seen in other CD34⁺ HSC-engrafted models.

Overall, although these models constitute great advancements, some aspects need to be improved, such as the incomplete engraftment of immune cells, xeno-GvHD, and the lack of human cytokines and growth factors. Table 2 compares the different features of Hu-PBMC and Hu-CD34⁺ models.

Tumors of Human Origin: Tumor Cell Lines and PDXs

Both human cell lines and patient-derived xenografts (PDX) represent relevant preclinical tools for immunotherapy assessment (reviewed in [35]). Importantly, various criteria related to the

Figure 2. Kinetics of Human Immune Cell Reconstitution in Peripheral Blood and Graft-versus-Host Disease (GvHD) Development in Humanized Mouse Models (HIS). (A) Reconstitution after intravenous (i.v.) injection of human peripheral blood mononuclear cells (PBMCs) in HIS mice. (B) Hematopoietic reconstitution and GvHD development after PBMC injection in HIS mice. Two to 4 weeks PBMC injection, human CD45⁺ cells begin to be detected in the blood in increasing numbers and, concomitantly, mice develop GvHD, characterized by rapid and severe weight loss. (C) Reconstitution after i.v. injection of human CD34⁺ cells in HIS mice. Data are compiled from different independent studies (Pearson *et al.*, 2008; Notta *et al.*, 2010; Volk *et al.*, 2016).

Table 2. Comparison of PBL and CD34 Humanization of HIS Mice

Feature	Hu-PBL	Hu-CD34
Source of human immune cells	Peripheral blood mononuclear cells	Human umbilical cord blood Adult bone marrow Mobilized peripheral blood cells Fetal liver
Injection routes	i.p./i.v.	i.v. or intraperitoneal (adult); i.v., intracardiac or intrahepatic (newborn)
Strain of mice	NSG/NOG	NSG/NOG
Preconditioning	None	Sublethal γ -irradiation
Immune reconstitution (cell subtypes and quality)	Mature human leukocytes T cells with activated phenotype	All human hematopoietic lineages, to different degrees
GvHD	4-6 weeks	>2 months
Time for reconstitution	Short (3-5 days)	Long (3-4 weeks)
Cost	\$	\$\$\$
Availability of tissues	High	Low
Complexity	Low	Medium

tumor molecular features and to the experimental design should be taken into account when choosing cell lines or PDXs (reviewed in Table 3).

PDXs have been associated with a high predictive value for therapeutic responses to oncology treatments in patients with cancer, including chemotherapy and targeted therapy [36]. Moreover, PDXs have been used for *in vivo* therapeutic screening of targeted therapies using a single-mouse schedule [37]. Such an approach, which decreases the number of mice, and costs, is able to: (i) identify the best treatment or combination of treatments among a panel of PDXs; and (ii) validate the efficacy of tested therapies in selected target-specific tumors. However, such preclinical studies have not yet been developed for immune therapies. Nevertheless, evaluation of radio-, chemo-, and targeted therapies in HIS mice, in the context of a functional immune system, could be of interest.

Table 3. Main Criteria for the Comparison of Human Tumor Cell Lines and PDXs

Criterion		Tumor cell line	PDX
Molecular	Stroma (endothelium, fibroblasts, immune cells . . .)	Mouse	Mouse
	Representativity of human cancers	Intermediate	High
	Tumor cell genetic stability	Low	High
	Evaluation of targeted treatments	Good	Good
	Therapeutic screening (including treatment combinations)	Intermediate	High
	Therapeutic correlation with clinical efficacy	Intermediate	High
Experimental	Route of transplantation (s.c., i.v., orthotopic, intraductal)	Good	Good
	Experimental procedures	Good	Good
	Tumor growth kinetics	Good	Variable
	AVATAR approach	Not relevant	Relevant

One advantage of PDXs is that they can allow personalized therapeutic management of patients with cancer using the so-called 'AVATAR' approach, where a patient's tumor is grafted into immunodeficient mice and, after its *in vivo* growth and molecular characterization, a pharmacological experiment is performed to assess the efficacy of treatments that could be administered to that patient (Figure 1B) [38]. Theoretically, HIS mice could also be used as avatars for the evaluation of immunotherapies. Along this line, Jespersen *et al.* recently showed that adoptively transferred tumor-infiltrating lymphocytes (TILs) were able to kill autologous patient-derived tumor cell lines (provided human IL-2 was continuously supplied) and that, for the few patients tested, eradication of the tumor was correlated with the objective response to adoptive T cell therapy in the clinic [39].

New Developments in HIS Mouse Models

The previously described models are limited in their ability to sustain functional myeloid, NK, and B cell populations, which are required for the evaluation of cancer immunotherapies. Thus, we describe here the different approaches that have been developed to tackle this issue, summarized in Table 4. A summary of commercially available strains is provided in Table 1.

Table 4. Genetic Modification of HIS Mice to Improve HSC and PBMC Engraftment, and to Diminish Xeno-GvHD

Mouse name	Mouse strain	Proteins involved	Effects	Refs
Niches				
NSGW41	NSG	KIT	Improved erythropoiesis, platelet formation, and HSC engraftment	[41]
BRGSF	BRG	FLT3	Increased monocyte and DC development; study of ILCs	[43,44]
Cytokines				
NSG-SGM3	NSG	SCF, GM-CSF, IL-3	Increased differentiation of macrophages and DCs	[46]
NOG-EXL	NOG	GM-CSF, IL-3	Increased differentiation of macrophages and DCs	[47]
BRG hIL-3 hGM-CSF	BRG	GM-CSF, IL-3	Increased differentiation of macrophages and DCs; replacement of alveolar macrophages	[48]
MISTRG	BRG	GM-CSF, IL-3, M-CSF, TPO, Sirp α	Increased differentiation of macrophages and DCs; improved NK development; anemia	[49]
NOG-IL-2 Tg	NOG	IL-2	Development of mature and functional human NK cells	[51]
SRG-15	BRG	IL-15, Sirp α	Improved development of circulating and tissue-resident NK cells; ADCC evaluation	[53]
IL-15 NOG	NOG	IL-15	Improved development of circulating and tissue-resident NK cells; ADCC evaluation	[52]
MHC modifications				
β 2m KO NSG	NSG	β 2m $^{-/-}$	Decreased xeno-GvHD	[18]
NSG HLA-A2	NSG	HLA-A2	Evaluation of HLA-restricted responses	[55]
NSG HLA-DR	NOG I-Ab $^{-/-}$	HLA-DR4	Antibody class-switching	[57]
Humamice	C57BL/6	HLA-A2 *01 ; DR1 *01 ; H-2- β 2m $^{-/-}$ IAB $^{-/-}$ Rag2 $^{-/-}$ IL2ry $_{c}$ $^{-/-}$ Perfl $^{-/-}$	Diminished GvHD. Generation of T and B cell responses against Hepatitis B virus	[58]
Immune checkpoints				
hCTLA-4 C57BL/6	C57BL/6	CTLA-4	Assessment of efficacy and toxicity of antihuman CTLA-4 antibodies in immunocompetent mice	[59]
huPD1 gene knock-in	C57BL/6	PD1		[60]

Niche Preparation for HSC Engraftment

HIS models require myeloablative conditioning of the host mice before transplanting human HSCs [23] to create the required space in the bone marrow niche of the host for human HSC engraftment. Susceptibility to irradiation is strain dependent; the *scid* mutation leads to increased sensitivity to radiation-induced DNA damage compared with the *Rag1^{nu/nl}* or *Rag2^{nu/nl}* mice [40]. Recently, the *c-kit* (CD117) mutant mouse was identified as a suitable host for human HSC engraftment without the need for prior irradiation. Given that *c-kit* is involved in HSC maintenance and differentiation, mice harboring the w41 mutation in *c-kit* (NSGW41 mice) have reduced HSC numbers, which translates into lower competition and better engraftment of human HSCs [41,42]. The NSGW41 mice also sustain more efficient human platelet and erythroid development [41], relevant for the evaluation of platelet activity in the tumor setting.

Dendritic cells (DCs) also show impaired reconstitution in HIS mice. Knocking out FMS-like tyrosine kinase 3 (*Flt3*), which is essential for DC development, leads to improved human DC development at the expense of the murine counterpart [43]. The resulting humanized BRGF (BALB/c *Rag2^{-/-}* *IL-2Rg^{c-/-}* *Flt3^{-/-}*) mouse shows better human monocyte and DC development compared with its parental BRG strain, and improved DC homeostasis results in increased numbers of human NK and T cells [43]. Transferring the *Flt3* KO to the BRGS strain further increases NK cell levels and can even allow limited study of human innate lymphoid cell (ILC) development [44].

Improvement of Myeloid and NK Cell Reconstitution

As mentioned above, human myeloid cells are under-represented or have maturation and functional defects in the current generation of HIS models [33]. One strategy to increase the number and maturation of myeloid cells is the hydrodynamic injection of plasmids encoding human IL-4, GM-CSF, or Flt-3 ligand, or macrophage colony-stimulating factor (M-CSF) [45]. HIS mice of different genetic backgrounds have been genetically engineered to express human *SCF*, *GMCSF*, *IL3*, *TPO*, or *Sirpa*. In the NOD background, NSG mice have been modified to express human *SCF* (*c-kit* ligand), *GMCSF* and *IL3* (NSG SGM3) genes, encoded by cDNA constructs that randomly integrate and are driven by a CMV promoter [46]; and NOG mice have been engineered to ubiquitously express human *GMCSF* and *IL3* (NOG-EXL) genes under control of the $SR\alpha$ promoter [47]. Also, human *IL3* and *GMCSF* have been knocked in in the BRG background [48]. All these strategies induced significant increases in the numbers of myeloid cells and in the function of macrophages [47,48] as compared to parental strains.

In parallel, the BRG mouse has been first knocked in with the human thrombopoietin gene (*TPO*), which resulted in higher human HSC engraftment and better myeloid development, and then with the human *IL3* and *MCSF* genes. Subsequent human *Sirpa* expression was achieved in these mice by BAC transgenesis, giving rise to the MISTRG mice (*MC-SF*, *IL3*, *Sirpa*, *TPO*, *Rag2^{-/-}* *IL2Rg^{c-/-}*) [49].

MISTRG mice support superior levels of myeloid development, increased differentiation of monocytes, DCs, and macrophages, and higher NK development. However, these mice: (i) develop anemia [49]; (ii) have shorter lifespans; and (iii) exhaust the human graft 3–4 months after transplantation.

Supplementation with human IL-2 and/or IL-15 has been attempted to increase NK cell reconstitution. Injection of a DNA vector encoding IL-15 [45] or administration of IL-15/IL-15R α [50] increased human NK cell numbers in immunodeficient mice. Interestingly, Katano and colleagues developed two mice with favored NK cell differentiation: the NOG-IL2 Tg,

expressing human IL-2 [51] and the IL-15-NOG Tg, expressing human IL-15 [52]. Also, Flavell's team generated the BALB/c *Rag2*^{-/-}*IL2Rg*^{-/-} knock-in for human SIRP α and IL-15 (SRG-15) [53], which showed enhanced development and function of NK cells, CD8⁺ T cells, and tissue-resident ILCs.

MHC Manipulation

To avoid xeno-GvHD, which can be acute in Hu-PBL mice, or chronic in Hu-SRC mice, different strategies have been developed based on the genetic manipulation of the MHC molecules. Administration of PBMCs into NSG mice lacking mouse class I and/or class II MHC molecules, such as NSG knocked out for mouse beta-2 microglobulin (β 2m), a structural component of the MHC class I molecule [18], or NOG knocked out for mouse MHC class I and class II molecules [54], led to engraftment of the human immune cells (albeit at poorer rates) and showed limited xeno-GvHD. In the case of Hu-CD34⁺ mice, the mismatch between human and mouse MHCs, besides inducing GvHD, likely underlies defective T cell function. HSC infusion into NSG mice with homozygous expression of HLA class I heavy and light chains (NSG-HLA-A2/HHD) allowed the generation of functional HLA-restricted T cells [55]. Moreover, transplantation of HLA-DR-matched HSC into NOD.*Rag1*KO.*IL2Rg*_cKO mice transgenic for the HLA class II molecule HLA-DR4 (DRAG), highly reconstituted T and B lymphocytes. Furthermore, these mice produced all subclasses of immunoglobulin and antigen-specific IgG upon vaccination, demonstrating the critical role of HLA class II molecules in the development of functional T cells capable of ensuring immunoglobulin class switching [56]. A similar observation was found in NOG mice expressing HLA-DR4 molecules in MHC II-positive cells [57]. More recently, Lone's group generated a mouse combining both murine MHC deficiency and HLA transgene expression named 'HUMAMICE' (*HLAA2*^{+/+}/*DR1*^{+/+}/*H2b2m*^{-/-}/*IAb*^{-/-}/*Rag2*^{-/-}/*IL2Rg*_c^{-/-}/*per1*^{-/-}) [58]. This mouse has no T and B cells due to the *Rag* mutation, no NK cells due to *IL2Rg*_c mutation, and no residual cytolytic activity due to perforin KO. Injection of HLA-matched PBMCs in HUMAMICE reconstituted human immune cells, although at lower levels than in NSG or NOG mice (from 5% to 20% of human CD45⁺ cells in spleen between week 5 and 12 compared with ~50% of human CD45⁺ cells in NSG or NOG), and mice did not present signs of GvHD. The human B and T cells that develop in these mice appear functional, because vaccination with Hepatitis B virus (HBV) induced the production of HBV-specific antibodies.

Humanization of Immune Checkpoints in Immunocompetent Mice

An alternative approach to the use of HIS mice for the study of anti-immune checkpoint antibody-based immunotherapies has been the development of humanized target knock-in mice in immunocompetent C57BL/6 or BALB/c mice. The major advantage of these mice is that a clinical candidate can be evaluated in this model, albeit with a fully murine immune system, and there is no need to generate murine surrogates. A growing number of immunocompetent mice genetically modified to express one or more fully human genes or 'humanized' knock-ins encoding positive and negative immunomodulatory receptors and ligands, such as PD-L1, CD47, BTLA, CD137, TIM3, LAG-3, ICOS, GITR, OX40, OX40L, among others, have been generated and are commercially available. These mice are particularly attractive for the evaluation of immuno-oncology checkpoint combinations. Mice expressing 'humanized' CTLA-4 or PD-1 molecules [59,60] have been useful for characterizing a clinical candidate anti-PD-1 antibody [60] and to dissociate efficacy and autoimmunity induced by anti-CTLA-4 antibodies [59]. Hu-PBL and Hu-CD34⁺ mice models have been described to recapitulate some adverse autoimmune reactions to anti-CTLA-4 administration [61], although they do not allow the uncoupling of anticancer effects from immune-related adverse events.

Preclinical Evaluation of Cancer Immunotherapy in Humanized Models

HIS mice represent one of the most attractive preclinical models for screening of immunotherapeutic approaches, including cellular and antibody-based immunotherapy, immune checkpoint inhibitors, or even gene therapy. A summary of the preclinical evaluation of immune-based therapies performed in HIS mice is presented in Table 5.

Table 5. Preclinical Studies Using HIS Models in Cancer Immunotherapy

Tumor type	Origin of tumor	Origin of human immune cells	Mouse strain	Therapeutic approach	Refs
Mesothelioma	Primary tumor	PBMC	NOD-scid	CAR-T therapy	[62]
Pancreatic cancer	Primary tumor	PBMC	NSG	CAR-T therapy	[63]
Lung cancer	Cell line	PBMC	NSG	CAR-T therapy	[64]
Ovarian cancer	Primary tumor	PBMC	NSG	CAR-T therapy	[65]
B cell aplasia	Cell line	Human stem cells	NSG	CAR-T therapy	[66]
Acute myeloid leukemia	Cell line	Human stem cells	NSG	CAR-T therapy	[67]
	Primary tumor/cell line	Human stem cells	NSG	CAR-T therapy	[69]
Lymphoma	Cell line	Human stem cells	Rag ^{-/-}	CAR-T therapy	[68]
Glioma	Cell line	PBMCs	NSG	CAR-T cells	[70]
Ovarian cancer	Cell line	PBMC	NSG	NK therapy	[72,73]
Glioblastoma	Primary tumor	PBMC	NSG	NK therapy	[74]
Colorectal cancer	Cell line	Human stem cells	BRGS	NK therapy	[75]
Pancreatic cancer	Cell line	PBMC	NSG	NK therapy	[76]
Prostate carcinoma	Cell line	PBMC	NSG	Anti-CD137	[77]
Gastric carcinoma	Primary tumor	PBMC	Rag ^{-/-}	Anti-CD137/Anti-PD1	[21]
Lymphoma/glioblastoma	Cell line	PBMC	NOG	Anti-PD1	[78]
Colon carcinoma	Cell line	PBMC	Rag ^{-/-}	Anti-CD137/PD1	[21]
B cell lymphoma	Cell line	Human stem cells	NSG	Anti-CTLA-4/PD1	[79]
Pleural mesothelioma	Cell line	PBMC	NSG	Anti-PD1 + CAR-T cells	[80]
Leukemia/lymphoma	Primary tumor	PBMC	NOG	Anti-CCR4 mAb	[17]
Hodgkin's lymphoma	Cell line	Human stem cells	NOG	Anti-CCR4 mAb	[51]
Lymphoma	Primary tumor	Human stem cells	NSG	Anti-CD52 mAb	[81]
Leukemia	Primary tumor	Human stem cells	NSG	Anti-CD52-mAb	[82]
Renal cell carcinoma	Cell line	PBMC	NSG	Carbonic anhydrase IX antibody	[83]
Breast cancer	Cell line	Human stem cells	NSG	IL-15 therapy + trastuzumab	[84]
Melanoma	Cell line	Human stem cells	NSG	Anti-GITR mAb	[85]
Colon carcinoma	Cell line	Human stem cells	NSG	EpcAM/CD3 antibody	[86]
Lymphoma	Cell line	PBMC	NSG	Bispecific antibody (REGN1979)	[87]
Ovarian carcinoma	Cell line	PBMC	NSG	Bispecific antibodies (anti-CD3/CLDN6 and anti-CD3/EpcAM)	[88]
Breast cancer	Cell line	PBMC	NSG	Gene therapy	[91]
Leukemia	Cell line	Human stem cells	NSG	IL-15 therapy	[92]
		PBMC	NSG	IL-15 tri-specific engager	[93]

Cell-Based Immunotherapy

Recent progress in the use of humanized mice has provided new developments to assess the efficacy of CAR-T cells. Of note, after several preclinical studies, the US Food and Drug Administration (FDA) approved the first CAR-T treatment for B cell acute lymphoblastic leukemia in 2017. One of the first studies in this area showed that CAR-T cells designed to recognize mesothelin, an antigen highly expressed on mesothelioma cells, exerted potent antitumor effects on malignant mesothelioma of Hu-PBL-mice [62]. The efficacy of other CAR-T cells evaluated in HIS mice is summarized in Table 5 [62–70]. However, CART-T therapy has shown serious adverse events, such as off-tumor toxicity, cytokine release syndrome, or neurotoxicity, which are not reproduced in HIS mice. This is partially due to the lack of the human target expression in normal tissues. The development of more sophisticated HIS models should help to provide safer and more effective CAR-T therapy. For example, transgenic expression of the CAR-T cell targeted human tumor-associated antigen under the mouse endogenous promoter could help identify off-target effects, as already shown for immunocompetent mice [71]. However, a good understanding of the human target expression is required, as is validation that the murine equivalent has a similar expression pattern.

Adoptive NK cell therapy is also a promising cellular immunotherapy for cancer. Recent progress has been obtained in stimulating NK and NKT cell antitumor activity using HIS models in glioblastoma, ovarian, colorectal, and pancreatic cancer [72–76].

Immune Checkpoint Inhibitors

Different human-specific monoclonal antibodies have been evaluated in HIS models, either as mono- or combinatory therapies for different tumor types, including antibodies directed against CD137, PD1-, and/or CTLA-4 [21,77–79] (Table 5). Recently, a combination of PD-1 checkpoint blockade with CAR-T cell infusion was evaluated in an orthotopic mouse model of pleural mesothelioma [80]. However, despite these sporadic successful results for individual models, a variety of responses are seen in HIS mice treated with immune checkpoint Abs, likely attributed to donor-to-donor variability in immune cells used for these reconstituted HIS models.

ADCC Evaluation, Bi-Specific Antibodies and DARPs

HIS models, in which human immune cells mediate the antitumor action of the therapeutic antibodies, allow the study of human antibody-dependent cellular cytotoxicity (ADCC) (Table 5). Thus, HIS mice have been used to evaluate anti-CCR4 and anti-CD52 antibodies that act via NK cell-mediated ADCC in leukemia and lymphoma models [17,51,81,82], as well as antibodies against a surface-expressed protein overexpressed on renal cell carcinoma [83]. Recently, Wege *et al.* evaluated the potential reinforcing effect of trastuzumab in combination with IL-15 in humanized models of breast cancer [84]. Also, Mahne and collaborators observed, in a Hu-CD34+ model treated with an anti-GITR mAb, a reduced frequency of regulatory T cells (Tregs) and an increase in CD8+ T cells that correlated with the inhibition of tumor growth [85].

Bi-specific antibodies targeting T cells to a tumor antigen have been evaluated in humanized preclinical models of colon carcinoma (bi-specific EpCAM/CD3 antibody) [86], lymphoma (bi-specific CD20/CD3 antibody) [87], and ovarian carcinoma (anti-CD3/CLDN6 and anti-CD3/EpCAM) [88,89]. Also, a carcinoembryonic antigen T cell bi-specific antibody (CEA TCB) has been tested in humanized mice, showing potent antitumor activity in poorly infiltrated solid tumors [90] (Table 5).

Interestingly, administration of a recombinant adeno-associated virus (AAV) vector displaying designed ankyrin repeat proteins (DARPs) specific for Her2/neu, reduced breast tumor mass and extended survival longer than trastuzumab [91].

Cytokine-Based Therapy

Administration of proinflammatory cytokines is a commonly used strategy aimed at boosting the antitumor function of effector immune cells. Using HIS mice, IL-15-based immunotherapies stimulated the survival and function of NK cells, leading to significant control of tumor growth, including breast cancer and leukemia [84,92,93]. Wege *et al.* showed that co-administration of trastuzumab and IL-15 induced breast tumor eradication, although it also induced fatal adverse effects associated with T cell hyperactivation [84].

Concluding Remarks and Future Perspectives

In this new exciting era of cancer immunotherapy, the development of HIS models is a promising tool to evaluate novel therapies, to help in the selection and/or ranking of human-specific immunomodulatory agents, to study combinatory treatments, and to guide the design of personalized immunotherapies (see Outstanding Questions). However, although HIS mice recapitulate many aspects of the crosstalk between human cells of the innate and adaptive immune system and tumors, these models still lack key elements of a complete human immune system. Some major hurdles include MHC incompatibility and lack of species-specific growth factors, cytokines, and chemokines to allow the maturation of certain immune subpopulations. Nevertheless, the use of HIS models has already yielded considerable data, not only contributing new insights into basic mechanisms of immunotherapeutics, but also allowing preclinical evaluation of onco-immunotherapies [94]. Understanding the caveats of HIS mice and the increasing genetic optimizations are effectively and actively contributing to the development of improved models with heightened translational power.

Acknowledgments

The authors thank Christine Sedlik and Fariba Nematl for their helpful discussion, and Inmaculada Guil Luna for the illustrations. This work was supported by the Institut Curie (Pic3i, 2015), Institut National de la Santé et de la Recherche Médicale, Institut Carnot, Labex DCBIOL (ANR-10-IDEX-0001-02 PSL and ANR-11-LABX0043), SIRIC INCa-DGOS-Inserm_12554, and Fondation Suisse.

References

- Chen, D.S. and Mellman, I. (2017) Elements of cancer immunity and the cancer-immune set point. *Nature* 541, 321–330
- Bosma, G.C. *et al.* (1983) A severe combined immunodeficiency mutation in the mouse. *Nature* 301, 527–530
- Mosier, D.E. *et al.* (1988) Transfer of a functional human immune system to mice with severe combined immunodeficiency. *Nature* 335, 256–259
- McCune, J.M. *et al.* (1988) The SCID-hu mouse: murine model for the analysis of human hematolymphoid differentiation and function. *Science* 241, 1632–1639
- Lapido, T. *et al.* (1992) Cytokine stimulation of multilineage hematopoiesis from immature human cells engrafted in SCID mice. *Science* 255, 1137–1141
- Shultz, L.D. *et al.* (2007) Humanized mice in translational biomedical research. *Nat. Rev. Immunol.* 7, 118–130
- Pérol, L. *et al.* (2014) Potential limitations of IL-2 administration for the treatment of experimental acute graft-versus-host disease. *Immunol. Lett.* 162, 173–184
- Fogh, J. *et al.* (1977) One hundred and twenty-seven cultured human tumor cell lines producing tumors in nude mice. *J. Natl. Cancer Inst.* 59, 221–226
- Hudson, W.A. *et al.* (1998) Xenotransplantation of human lymphoid malignancies is optimized in mice with multiple immunologic defects. *Leukemia* 12, 2029–2033
- Oettinger, M.A. *et al.* (1990) RAG-1 and RAG-2, adjacent genes that synergistically activate V(D)J recombination. *Science* 248, 1517–1523
- Ito, M. *et al.* (2002) NOD/SCID/gamma(c)(null) mouse: an excellent recipient mouse model for engraftment of human cells. *Blood* 100, 3175–3182
- Treggiani, E. *et al.* (2004) Development of a human adaptive immune system in cord blood cell-transplanted mice. *Science* 304, 104–107
- Legrand, N. *et al.* (2011) Functional CD47/signal regulatory protein alpha (SIRP[alpha]) interaction is required for optimal human T- and natural killer- (NK) cell homeostasis in vivo. *Proc. Natl. Acad. Sci. U. S. A.* 108, 13224–13229
- Takenaka, K. *et al.* (2007) Polymorphism in Sirpa modulates engraftment of human hematopoietic stem cells. *Nat. Immunol.* 8, 1313–1323
- Stowig, T. *et al.* (2011) Transgenic expression of human signal regulatory protein alpha in Rag2^{-/-}gamma(c)^{-/-} mice improves

Outstanding Questions

What are the next steps required for improving immune cell reconstitution, essential for the study of immunology therapies in HIS models? How functional is the reconstituted human immune system?

Can additional genetic engineering of mice allow complete replacement of murine myeloid cells with human ones?

What is the role of the remaining host murine cells in the outcome of preclinical studies?

Will HIS mice represent faithful avatars for the evaluation of immunotherapies?

Will HLA replacement allow the study of response to human vaccines, including neo-epitopes?

Will increased genetic humanization of HIS mice allow for the identification of off-target effects of immunotherapies?

Can humanized mice be manipulated to recapitulate metastatic disease?

Will the high cost and technical difficulties limit the use of these models?

Human immune cell reconstitution is a long, expensive, and laborious process. Can induced pluripotent stem cell-derived immune cells be generated to facilitate the production of HIS mice with syngeneic human tumor and immune cells?

- engraftment of human hematopoietic cells in humanized mice. *Proc. Natl. Acad. Sci. U. S. A.* 108, 13218–13223
16. Shultz, L.D. *et al.* (2007) Humanized NOD/IL2R γ -scid IL2 receptor common gamma chain knockout mice in diabetes research. *Ann. N. Y. Acad. Sci.* 1103, 77–89
 17. Ito, A. *et al.* (2009) Defucosylated anti-CCR4 monoclonal antibody exercises potent ADCC-mediated antitumor effect in the novel tumor-bearing humanized NOD/Shi-scid, IL-2R γ (null) mouse model. *Cancer Immunol. Immunother.* 58, 1195–1206
 18. King, M.A. *et al.* (2009) Human peripheral blood leucocyte non-obese diabetic-severe combined immunodeficiency interleukin-2 receptor gamma chain gene mouse model of xenogeneic graft-versus-host-like disease and the role of host major histocompatibility complex. *Clin. Exp. Immunol.* 157, 104–118
 19. Moser, J. *et al.* (2016) Distinct differences on neointima formation in immunodeficient and humanized mice after carotid or femoral arterial injury. *Sci. Rep.* 6, 35387
 20. Naserian, S. *et al.* (2018) Simple, reproducible, and efficient clinical grading system for murine models of acute graft-versus-host disease. *Front. Immunol.* 9, 10
 21. Sammamed, M.F. *et al.* (2015) Nivolumab and urelumab enhance antitumor activity of human T lymphocytes engrafted in Rag2^{-/-}IL2R γ null immunodeficient mice. *Cancer Res.* 75, 3465–3476
 22. Holyoske, T.L. *et al.* (1999) Functional differences between transplantable human hematopoietic stem cells from fetal liver, cord blood, and adult marrow. *Exp. Hematol.* 27, 1418–1427
 23. Shultz, L.D. *et al.* (2005) Human lymphoid and myeloid cell development in NOD/IL2R γ -scid IL2R γ null mice engrafted with mobilized human hematopoietic stem cells. *J. Immunol. Baltim. Md 1950* 174, 6477–6489
 24. Brehm, M.A. *et al.* (2010) Human immune system development and rejection of human islet allografts in spontaneously diabetic NOD-Fcg γ RIII IL2R γ null Ins2Akita mice. *Diabetes* 59, 2265–2270
 25. Hayakawa, J. *et al.* (2009) Busulfan produces efficient human cell engraftment in NOD/IL2R γ -scid IL2R γ (null) mice. *Stem Cells Dayt. Ohio* 27, 175–182
 26. Czechowicz, A. *et al.* (2007) Efficient transplantation via antibody-based clearance of hematopoietic stem cell niches. *Science* 318, 1296–1299
 27. Lan, P. *et al.* (2006) Reconstitution of a functional human immune system in immunodeficient mice through combined human fetal thymus/liver and CD34+ cell transplantation. *Blood* 108, 487–492
 28. Kalscheuer, H. *et al.* (2012) A model for personalized in vivo analysis of human immune responsiveness. *Sci. Transl. Med.* 4, 125ra30
 29. Xia, J. *et al.* (2016) Modeling human leukemia immunotherapy in humanized mice. *EBioMedicine* 10, 101–108
 30. Rossi, M.J. *et al.* (2001) Relatively normal human lymphopoiesis but rapid turnover of newly formed B cells in transplanted non-obese diabetic/SCID mice. *J. Immunol. Baltim. Md 1950* 167, 3033–3042
 31. Watanabe, Y. *et al.* (2009) The analysis of the functions of human B and T cells in humanized NOD/shi-scid/gammac γ (null) (NOG) mice (hu-HSC NOG mice). *Int. Immunol.* 21, 843–858
 32. André, M.C. *et al.* (2010) Long-term human CD34+ stem cell-engrafted nonobese diabetic/SCID/IL-2R γ (null) mice show impaired CD8+ T cell maintenance and a functional arrest of immature NK cells. *J. Immunol. Baltim. Md 1950* 185, 2710–2720
 33. Gille, C. *et al.* (2012) Monocytes derived from humanized neonatal NOD/SCID/IL2R γ (null) mice are phenotypically immature and exhibit functional impairments. *Hum. Immunol.* 73, 346–354
 34. Halkias, J. *et al.* (2015) Conserved and divergent aspects of human T-cell development and migration in humanized mice. *Immunol. Cell Biol.* 93, 716–726
 35. Wege, A.K. (2018) Humanized mouse models for the preclinical assessment of cancer immunotherapy. *BioDrugs Clin. Immunother. Biopharm. Gene Ther.* 32, 245–266
 36. Izumchenko, E. *et al.* (2017) Patient-derived xenografts effectively capture responses to oncology therapy in a heterogeneous cohort of patients with solid tumors. *Ann. Oncol.* 8, 2595–2605
 37. Gao, H. *et al.* (2015) High-throughput screening using patient-derived tumor xenografts to predict clinical trial drug response. *Nat. Med.* 21, 1318–1325
 38. Calvo, E. *et al.* (2017) A Phase I clinical trial and independent patient-derived xenograft study of combined targeted treatment with dacotinib and figitumumab in advanced solid Tumors. *Clin. Cancer Res.* 23, 1177–1185
 39. Jespersen, H. *et al.* (2017) Clinical responses to adoptive T-cell transfer can be modeled in an autologous immune-humanized mouse model. *Nat. Commun.* 8, 707
 40. Pearson, T. *et al.* (2008) Non-obese diabetic-recombination activating gene-1 (NOD-Rag1 null) interleukin (IL)-2 receptor common gamma chain (IL2r gamma null) null mice: a radioresistant model for human lymphohaematopoietic engraftment. *Clin. Exp. Immunol.* 154, 270–284
 41. Rahmig, S. *et al.* (2016) Improved human erythropoiesis and platelet formation in humanized NSGW41 mice. *Stem Cell Rep.* 7, 591–601
 42. McIntosh, B.E. *et al.* (2015) Nonirradiated NOD.B6. SCID Il2r γ ^{-/-} K1(W41/W41) (NSGW) mice support multilineage engraftment of human hematopoietic cells. *Stem Cell Rep.* 4, 171–180
 43. Li, Y. *et al.* (2016) A novel Flt3-deficient HIS mouse model with selective enhancement of human DC development. *Eur. J. Immunol.* 46, 1291–1299
 44. Lopez-Lastra, S. *et al.* (2017) A functional DC cross talk promotes human IL1C homeostasis in humanized mice. *Blood Adv.* 1, 601–614
 45. Chen, Q. *et al.* (2009) Expression of human cytokines dramatically improves reconstitution of specific human-blood lineage cells in humanized mice. *Proc. Natl. Acad. Sci. U. S. A.* 106, 21783–21788
 46. Billarbeck, E. *et al.* (2011) Development of human CD4+FoxP3+ regulatory T cells in human stem cell factor-, granulocyte-macrophage colony-stimulating factor-, and interleukin-3-expressing NOD-SCID IL2R γ (null) humanized mice. *Blood* 117, 3076–3086
 47. Ito, R. *et al.* (2013) Establishment of a human allergy model using human IL-3/GM-CSF-transgenic NOG mice. *J. Immunol. Baltim. Md 1950* 191, 2890–2899
 48. Willinger, T. *et al.* (2011) Human IL-3/GM-CSF knock-in mice support human alveolar macrophage development and human immune responses in the lung. *Proc. Natl. Acad. Sci. U. S. A.* 108, 2390–2395
 49. Rongvaux, A. *et al.* (2014) Development and function of human innate immune cells in a humanized mouse model. *Nat. Biotechnol.* 32, 364–372
 50. Huntington, N.D. *et al.* (2009) IL-15 trans-presentation promotes human NK cell development and differentiation in vivo. *J. Exp. Med.* 206, 25–34
 51. Katano, I. *et al.* (2015) Predominant development of mature and functional human NK cells in a novel human IL-2-producing transgenic NOG mouse. *J. Immunol. Baltim. Md 1950* 194, 3513–3525
 52. Katano, I. *et al.* (2017) Long-term maintenance of peripheral blood derived human NK cells in a novel human IL-15- transgenic NOG mouse. *Sci. Rep.* 7, 17230
 53. Herndler-Brandstetter, D. *et al.* (2017) Humanized mouse model supports development, function, and tissue residency of human natural killer cells. *Proc. Natl. Acad. Sci. U. S. A.* 114, E9626–E9634
 54. Yaguchi, T. *et al.* (2017) Human PBMC-transferred murine MHC class II β -deficient NOG mice enable long-term evaluation of human immune responses. *Cell Mol. Immunol.* Published online November 20, 2017. <http://dx.doi.org/10.1038/cmi.2017.106>

55. Shultz, L.D. *et al.* (2010) Generation of functional human T-cell subsets with HLA-restricted immune responses in HLA class I expressing NOD/SCID/IL2r gamma(null) humanized mice. *Proc. Natl. Acad. Sci. U. S. A.* 107, 13022–13027
56. Danner, R. *et al.* (2011) Expression of HLA class II molecules in humanized NOD.Rag1KO.IL2RgCKO mice is critical for development and function of human T and B cells. *PLoS One* 6, e19826
57. Suzuki, M. *et al.* (2012) Induction of human humoral immune responses in a novel HLA-DR-expressing transgenic NOD/Shi-scid γ cnul mouse. *Int. Immunol.* 24, 243–252
58. Zeng, Y. *et al.* (2017) Creation of an immunodeficient HLA-transgenic mouse (HJMAMICE) and functional validation of human immunity after transfer of HLA-matched human cells. *PLoS One* 12, e0173754
59. Lute, K.D. *et al.* (2005) Human CTLA4 knock-in mice unravel the quantitative link between tumor immunity and autoimmunity induced by anti-CTLA-4 antibodies. *Blood* 106, 3127–3133
60. Burova, E. *et al.* (2017) Characterization of the anti-PD-1 antibody REGN2810 and its antitumor activity in human PD-1 knock-in mice. *Mol. Cancer Ther.* 16, 861–870
61. Vudattu, N.K. *et al.* (2014) Humanized mice as a model for aberrant responses in human T cell immunotherapy. *J. Immunol. Biot. Med.* 1950 193, 587–596
62. Zhao, Y. *et al.* (2010) Multiple injections of electroporated autologous T cells expressing a chimeric antigen receptor mediate regression of human disseminated tumor. *Cancer Res.* 70, 9053–9061
63. Abate-Daga, D. *et al.* (2014) A novel chimeric antigen receptor against prostate stem cell antigen mediates tumor destruction in a humanized mouse model of pancreatic cancer. *Hum. Gene Ther.* 25, 1003–1012
64. Guedan, S. *et al.* (2014) ICOS-based chimeric antigen receptors program bipolar TH17/TH1 cells. *Blood* 124, 1070–1080
65. Song, D.-G. *et al.* (2012) CD27 costimulation augments the survival and antitumor activity of redirected human T cells in vivo. *Blood* 119, 896–705
66. Diaconu, I. *et al.* (2017) Inducible Caspase-9 selectively modulates the toxicities of CD19-specific chimeric antigen receptor-modified T cells. *Mol. Ther. J. Am. Soc. Gene Ther.* 25, 580–592
67. Gill, S. *et al.* (2014) Preclinical targeting of human acute myeloid leukemia and myeloblastosis using chimeric antigen receptor-modified T cells. *Blood* 123, 2343–2354
68. Hombach, A.A. *et al.* (2016) Superior therapeutic index in lymphoma therapy: CD33(+)/CD34(+) hematopoietic stem cells resist a chimeric antigen receptor T-cell attack. *Mol. Ther. J. Am. Soc. Gene Ther.* 24, 1423–1434
69. Pizotola, J. *et al.* (2014) Chimeric antigen receptors against CD33/CD123 antigens efficiently target primary acute myeloid leukemia cells in vivo. *Leukemia* 28, 1596–1605
70. Brown, C.E. *et al.* (2012) Stem-like tumor-initiating cells isolated from IL13R α 2-expressing gliomas are targeted and killed by IL13-zetakine-redirection T cells. *Clin. Cancer Res.* 18, 2199–2209
71. Gleiberson-Levin, A. *et al.* (2014) Elimination of progressive mammary cancer by repeated administrations of chimeric antigen receptor-modified T cells. *Mol. Ther.* 22, 1029–1038
72. Hoogstad-van Evert, J.S. *et al.* (2017) Umbilical cord blood CD34 $^{+}$ progenitor-derived NK cells efficiently kill ovarian cancer spheroids and intraperitoneal tumors in NOD/SCID/IL2Rgnull mice. *Oncimmunology* 6, e1320630
73. Geller, M.A. *et al.* (2013) Intraperitoneal delivery of human natural killer cells for treatment of ovarian cancer in a mouse xenograft model. *Cytotherapy* 15, 1297–1306
74. Lee, S.J. *et al.* (2015) Natural killer (NK) cells inhibit systemic metastasis of glioblastoma cells and have therapeutic effects against glioblastomas in the brain. *BMC Cancer* 15, 1011
75. Veluchamy, J.P. *et al.* (2017) In vivo efficacy of umbilical cord blood stem cell-derived NK cells in the treatment of metastatic colorectal cancer. *Front. Immunol.* 8, 87
76. Ames, E. *et al.* (2015) NK cells preferentially target tumor cells with a cancer stem cell phenotype. *J. Immunol. Biot. Med.* 1950 195, 4010–4019
77. Fisher, T.S. *et al.* (2012) Targeting of 4-1BB by monoclonal antibody PF-05082566 enhances T-cell function and promotes anti-tumor activity. *Cancer Immunol. Immunother.* 61, 1721–1733
78. Ashizawa, T. *et al.* (2017) Antitumor effect of programmed death-1 (PD-1) blockade in humanized the NOG-MHC double knockout mouse. *Clin. Cancer Res.* 23, 149–158
79. Ma, S.-D. *et al.* (2016) PD-1/CTLA-4 blockade inhibits Epstein-Barr virus-induced lymphoma growth in a cord blood humanized-mouse model. *PLoS Pathog.* 12, e1005642
80. Cherkassky, L. *et al.* (2016) Human CAR T cells with cell-intrinsic PD-1 checkpoint blockade resist tumor-mediated inhibition. *J. Clin. Invest.* 126, 3130–3144
81. Pallasch, C.P. *et al.* (2014) Sensitizing protective tumor microenvironments to antibody-mediated therapy. *Cell* 156, 590–602
82. Leskov, I. *et al.* (2013) Rapid generation of human B-cell lymphomas via combined expression of Myc and Bcl2 and their use as a preclinical model for biological therapies. *Oncogene* 32, 1066–1072
83. Chang, D.-K. *et al.* (2015) Human anti-CAIX antibodies mediate immune cell inhibition of renal cell carcinoma in vitro and in a humanized mouse model in vivo. *Mol. Cancer* 14, 119
84. Wege, A.K. *et al.* (2017) IL-15 enhances the anti-tumor activity of trastuzumab against breast cancer cells but causes fatal side effects in humanized tumor mice (HTM). *Oncotarget* 8, 2731–2744
85. Mahne, A.E. *et al.* (2017) Dual roles for regulatory T-cell depletion and costimulatory signaling in agonistic GITR targeting for tumor immunotherapy. *Cancer Res.* 77, 1108–1118
86. Wuil-Goldenberg, A. *et al.* (2011) Intrahepatically transplanted human cord blood cells reduce SW480 tumor growth in the presence of bispecific EpCAM/CD3 antibody. *Cytotherapy* 13, 109–113
87. Smith, E.J. *et al.* (2015) A novel, native-format bispecific antibody triggering T-cell killing of B-cells is robustly active in mouse tumor models and cynomolgus monkeys. *Sci. Rep.* 5, 17943
88. Stadler, C.R. *et al.* (2016) Characterization of the first-in-class T-cell-engaging bispecific single-chain antibody for targeted immunotherapy of solid tumors expressing the oncofetal protein claudin 6. *Oncimmunology* 5, e1091555
89. McCormack, E. *et al.* (2013) Bi-specific TOR-anti CD3 redirected T-cell targeting of NY-ESO-1- and LAGE-1-positive tumors. *Cancer Immunol. Immunother.* 62, 773–785
90. Bacac, M. *et al.* (2016) CEA TCB: A novel head-to-tail 2:1 T cell bispecific antibody for treatment of CEA-positive solid tumors. *Oncimmunology* 5, e1203498
91. Münch, R.C. *et al.* (2015) Off-target-free gene delivery by affinity-purified receptor-targeted viral vectors. *Nat. Commun.* 6, 6246
92. Carv, J. *et al.* (2013) Natural killer cells generated from cord blood hematopoietic progenitor cells efficiently target bone marrow-residing human leukemia cells in NOD/SCID/IL2Rg(null) mice. *PLoS One* 8, e64384
93. Vallera, D.A. *et al.* (2016) IL15 trispecific killer engagers (TriKE) make natural killer cells specific to CD33+ targets while also inducing persistence, in vivo expansion, and enhanced function. *Clin. Cancer Res.* 22, 3440–3450
94. Sanmamed, M.F. *et al.* (2016) Defining the optimal murine models to investigate immune checkpoint blockers and their combination with other immunotherapies. *Ann. Oncol.* 27, 1190–1198

Philippe DE LA ROCHERE

17 rue Etex
75018 Paris
☎ : 06 76 70 47 82
E-mail : delarocherephilippe@yahoo.fr
38 ans – Permis B
Marié, 2 enfants



Expérience scientifique

- **Octobre 2014 à Septembre 2018** *Institut Curie (Centre d'immunothérapie, INSERM U932)*
Doctorant
Développement de modèles de souris pour l'étude de l'immunothérapie anti-cancer.
- **Juin 2009 à Octobre 2014** *Institut Curie (Département de transfert, INSERM U932)*
Ingénieur d'étude
Développement d'immunothérapie anti-cancer (vaccination ADN, Long peptide...).
- **Mars 2007 à Juin 2009** *Hôpital Saint-Louis (Laboratoire d'immunologie INSERM U662)*
Ingénieur d'étude
Etude sur le vieillissement des cellules souches hématopoïétiques humaines.
- **Décembre 2005 à Juin 2006** *Hôpital Saint-Louis (Laboratoire d'immunologie INSERM U662)*
Stagiaire M2
Etude du rôle de la palmitoylation de la molécule HLA-DR dans sa localisation et sa fonction.

Formation

- **2005-2006** **Master 2** de *Biologie et thérapies des grandes fonctions en immunologie* (mention bien) à l'**Université de Paris XI et Paris XII**
- **2004-2005** **Master 1** de *Biologie moléculaire et cellulaire* (mention assez bien) à l'**Université Paris VI**
- **2003-2004** **Maîtrise** de *Biologie cellulaire et physiologie* à l'**Université Paris V**

Compétences techniques

- **Biologie cellulaire** : culture cellulaire, transfection cellulaire, cytométrie en flux, immunohistochimie, microscopie confocale, FICOLL, purification des précurseurs hématopoïétiques.
- **Biologie moléculaire** : PCR, RT-PCR quantitative en temps réel, préparation ADN, ARN, chromatine.

- **Biochimie** : isolement des radeaux lipidiques sur gradient de sucrose par ultracentrifugation, immunoBlot, dotplot, immunoprécipitation, ELISA, ELISPOT.
- **Expérimentation animale niveau 1 (souris)**: injection (IV, IP, IM, SC), récupération des organes, saignée, électroporation, imagerie (Lumina IVIS)

Compétences complémentaires

- **Informatique**
 - Bonne maîtrise du pack office et de l'environnement Windows
 - Zotero, flowjow, prism, FCAP array, living image.
- **Langues**
 - Anglais : aisance à l'écrit et à l'oral

Bibliographie

Manuscrits en préparation ou soumis

1. A comprehensive analysis of humanized mouse models for the study of cancer immunotherapies

de la Rochere P, Loumagne L, Rathaux M, Dubois M, Nemati F, Sedlik C, Decaudin D, Azar G, Sidhu SS, Piaggio E

2. Inhibition of PI3K increases immune infiltrate in muscle invasive bladder cancer

Borcoman E, de la Rochere P, Richer W, Vacher S, Krucker C, Radvanyi F, Allory Y, Meseure D, Sedlik C, Bieche I, Piaggio E.

3. IL-2/anti-IL-2 antibody complex combined with CTLA-4 -but not PD1- blockade rescues anti-tumor NK function by modulating intra-tumoral regulatory T cells.

Caudana P, Núñez N, de la Rochere P, Pinto A, Denizeau J, Alonso R, Niborski L, Lantz O, Sedlik C, Piaggio E.

4. High dimensional profiling identifies distinct immune patterns in T cells from breast tumors and draining lymph nodes.

Núñez Nicolas Gonzalo, Tosello Jimena, Ramos Rodrigo Nalio, Niborski Leticia Laura, Richer Wilfrid, Bigot Jeremy, Meseure Didier, de la Rochere P, Milder Maud, Viel Sophie, Loirat Delphine, Pérol Louis, Vincent-Salomon Anne, Sastre-Garau Xavier, Lantz O, Burkhard Becher, Sedlik Christine, Amigorena Sebastian and Piaggio Eliane.

5. Peptide-TLR-7/8 agonist conjugate vaccines chemically programmed for nanoparticle self-assembly enhance CD8 T cell immunity to tumor neoantigens.

Lynn G, Sedlik C, Baharom F, Zhu Y, Ramirez-Valdez A, Coble V, Tobin K, Bloble N, Denizeau J, **de la Rochere P**, Francica B, Decker B, Maciejewski M, Cheung J, Yamane H, Smelkinson M, Francica J, Laga R, Bernstock J, Seymour L, Drake C, Lantz O, Piaggio E, Ishizuka A, Seder R.

Manuscripts publiés

1. Humanized mice for the study of immuno-oncology.

de la Rochere P, Guil-Luna S, Decaudin D, Azar G, Sidhu SS, Piaggio E.

Trends Immunology. 2018 Aug 1

2. Effective antitumor therapy based on a novel antibody-drug conjugate targeting the Tn carbohydrate antigen.

Sedlik C, Heitzmann A, Viel S, Ait Sarkouh R, Batisse C, Schmidt F, **de la Rochere P**, Amzallag N, Osinaga E, Oppezzo P, Pritsch O, Sastre-Garau X, Hubert P, Amigorena S, Piaggio E.

Oncoimmunology. 2016 Apr 22;5(7):e1171434.

3. Heparan sulfates targeting increases MHC class I- and MHC class II-restricted antigen presentation and CD8(+) T-cell response.

Knittel D, Gadzinski A, Hua S, Denizeau J, Savatier A, **de la Rochere P**, Boulain JC, Amigorena S, Piaggio E, Sedlik C, Léonetti M.

Vaccine. 2016 Jun 8;34(27):3093-101.

4. Different immunogenicity but similar antitumor efficacy of two DNA vaccines coding for an antigen secreted in different membrane vesicle-associated forms.

Sedlik C, Vigneron J, Torrieri-Dramard L, Pitoiset F, Denizeau J, Chesneau C, **de la Rochere P**, Lantz O, They C, Bellier B.

J Extracell Vesicles. 2014 Aug 27;3.

5. Age-related changes in human hematopoietic stem/progenitor cells.

KurandaK, Vargaftig J, **de la Rochere P**, Dosquet C, Charron D, Bardin F, Tonnelle C, Bonnet D, Goodhardt M.

Aging Cell. 2011 Jun;10(3):542-6.

Communication

- Présentation orale : **Development of novel humanized mice models for the study of cancer immunotherapy 12-13 Mai 2016, Tumor model summit, Bâle, Suisse.**
- Présentation orale : **Development of novel humanized mice models for the study of cancer immunotherapy, 3-5 Octobre 2016, EuroPDX workshop, Weggis, Suisse.**
- Poster : **Development of novel humanized mice models for the study of cancer immunotherapy, 28-30 Novembre 2016, Congrès annuel de la SFI, Paris, France.**